Hydraulic Stability of Geotextile Sand Containers for Coastal Structures

- Effect of Deformations and Stability Formulae –

von der
Fakultät Architektur, Bauingenieurwesen und Umweltwissenschaften
der Technischen Universität Carolo-Wilhelmina
zu Braunschweig

zur Erlangung des Grades eines
Doktor-Ingenieurs (Dr.-Ing.)
genehmigte

Dissertation
von
Juan Antonio Recio Molina
aus Saltillo, Mexiko

Eingereicht am:	8. Juni 2007
Mündliche Prüfung am:	12. Oktober 2007
Berichterstatter:	Prof. Dr.-Ing. H. Oumeraci, Prof. Dr.-Ing. P. L.-F. Liu (Cornell University, Ithaca, USA Prof. Dr.-Ing. G. Heerten (Naue GmbH & Co. KG)

(2008)

Hydraulic Stability of Geotextile Sand Containers for Coastal Structures

- Effect of Deformations and Stability Formulae –

von der
Fakultät Architektur, Bauingenieurwesen und Umweltwissenschaften
der Technischen Universität Carolo-Wilhelmina
zu Braunschweig

zur Erlangung des Grades eines
Doktor-Ingenieurs (Dr.-Ing.)
genehmigte

Dissertation
von
Juan Antonio Recio Molina
aus Saltillo, Mexiko

Eingereicht am:	8. Juni 2007
Mündliche Prüfung am:	12. Oktober 2007
Berichterstatter:	Prof. Dr.-Ing. H. Oumeraci, Prof. Dr.-Ing. P. L.-F. Liu (Cornell University, Ithaca, USA Prof. Dr.-Ing. G. Heerten (Naue GmbH & Co. KG)

(2008)

Foreword

This work was performed with the help and advice of many people. I would like to thank them from the bottom of my heart:

I would like to first thank the institutions that financed this study: (i) the German Academic Exchange Service (DAAD), (ii) the Leichtweiss Institute for Hydraulic Engineering and Water Resources, (iii) Naue Fasertechnik and (iv) the Braunschweigischer Hochschuldbund.

My deep gratitude goes then to Professor Hocine Oumeraci who opened the German doors for me and kindly gave me the opportunity to work in the fantastic environment of Leichtweiss Institute. Apart from being one of the most engaged coastal engineer in the world, he had the patience to explain to me all types of concepts. He was always willing to share his expertise and friendship. Thanks to his constant feedback, this study was completed. Professor Oumeraci's passion for coastal engineering and his constant search for fairness, objectiveness and perfection set a precedent to be followed by me for the rest of my life. No single person has influenced me more than him.

I would also want to thank Gabi Fournier who made smooth my adaptation to the German culture. Gabi helped me to keep my sanity during the tough times of this study. Thanks also to my good friend Markus Brühl who was always willing to help and discuss the issues related to my Thesis and personal life.

I hold a deep gratitude, as well, for Professor Philip Liu, with whom I worked at Braunschweig and at Cornell University. He taught me to view life with respect and humbleness. Without his constant help on numerical and flow dynamics issues, this study would have never been completed.

Thanks to Professor Heerten for making this research possible by financing some of the model tests, by supporting me to attend international conferences and by making possible my stay at Cornell and more important for making believe in geosynthetic solutions.

Moreover, I would like to thank my great friends from Leichtweiss Institute: Andreas Kortenhaus, Hans-Henning Dette, Matthias Kudella, Bernd Ettmer, Peter Geisenhainer, Rainer Kvapil, Herwig Appeltauer, Agnieszka Strusinska, Grzegorz Stanczak, Kai Utschinski, Hans-Joerg Lambrecht, Maiu Castellar and Peter Schley who always motivated me and gave me the support I needed. We worked and spent a fantastic time together.

Thanks also to my parents, my brother Omar, his wife Gaby, my sister Celia and my nieces Gaby, Ale and Ana Lucia who always supported me and despite of the thousand of kilometers that we were apart, made me feel that they were always near to me.

At last, but with my most sincere love and gratitude, I would like to thank my beautiful wife Cecilia who unconditionally supported me through the duration of this study. Her patience and support have made our family stronger and more prepared for the future challenges that this life will present. She motivated me, kept me focused and scared away all my thoughts of failure. Her love and comprehension are the most valuable treasures in my life.

Juan Recio

Juan Antonio Recio Molina

ABSTRACT

Hydraulic Stability of Geotextile Sand Containers for Coastal Structures

- Effect of Deformations and Stability Formulae -

New shore protection structures such as seawalls, groins, breakwaters, revetments and artificial reefs are increasingly being developed. Softer and low cost protection alternatives, such as structures made of geotextile sand containers (GSC) are often used instead of more expensive and hard coastal structures made of concrete or rubble material.

Although the effect of the deformations of the sand containers on the hydraulic stability is significant, no stability formula is available to account for those deformations and the associated processes leading to the observed failures. Therefore, the primary objective of the thesis is the hydraulic stability of coastal GSC-structures, taking into account the effect of those deformations and associated processes.

To achieve a better understanding of the processes that affect the stability of GSC-structures several types of hydraulic model experiments and analyses were performed. Among the processes investigated, the following are worth mentioning: (i) permeability of GSC-structures and its influence on the stability, (ii) wave-induced loads on the sand containers, (iii) wave induced flow on GSC-structures, (iv) internal movement of sand in the containers and its effect on the stability, (v) variation of contact areas among neighbouring GSCs during wave action, (vi) types of displacement of GSCs within a coastal structure and finally (vii) the effect of the deformations on the stability of GSC-structures.

In addition, a flow model and two structural dynamic models were further developed, validated and applied to extend the range of the hydraulic model tests towards a better understanding of the processes involved in the wave structure interaction. The wave-induced forces on the GSCs are calculated by using a RANS-VOF type model, initially developed at Cornell University, USA. The stresses and deformations for each sand container are simulated by using a finite element model (FEM) and finally, the displacement of containers is simulated by a discrete element model (DEM).

Based on the experimental and numerical results, analytical stability formulae that account for the deformation of the individual GSCs for each type of observed displacement are developed and the required drag, inertia and lift coefficients are determined experimentally. Stability formulae for each type of coastal structures made of geotextile sand containers such as breakwaters, revetments, dune reinforcement and scour protection systems are proposed.

Moreover, recommendations for the application of the stability formulae and for the construction of GSC-structures are outlined.

Based on the results of several experimental, numerical and theoretical studies performed in this thesis, a much better understanding of the hydro-geotechnical processes which affect the stability of the coastal GSC-structures has been achieved. Moreover, reliable stability formulae for GSC-structures which account for the deformation effect of the GSCs have been derived.

Juan Antonio Recio Molina

Kurzfassung

Hydraulische Stabilität von geotextilen Sandcontainern für Küstenschutzwerke

-Verformungseinfluß und Stabilitätsformeln-

Für den Schutz sandiger Küsten wird verstärkt nach Alternativen zu den herkömmlichen harten Küstenschutzmaßnahmen wie z.B. Deckwerken aus Beton und Steinmaterial gesucht, da diese häufig als Verfelsung der Küste empfunden werden.

Ein Konzept, die Dünenerosion und somit deren Funktionsverlust zu verhindern, stellt die Dünenverstärkung durch Geotextilien dar. Neben dem lagenweisen Einbau des Geotextils besteht die Möglichkeit, den lokal vorhandenen Sand in geotextilen Containern zu verpacken, die den Kern der Düne bilden. Derartige Container können ebenfalls als Ufermauer, Deckwerke, künstliche Riffe und Buhnen eingesetzt werden. Dadurch werden Transportkosten und die mit dem Transport verbundenen Umweltbelastungen erheblich reduziert. Eine erhöhte Aufmerksamkeit ist demzufolge der Bemessung dieses Bauwerkstyps zu widmen. Haupthindernis für den verstärkten Einsatz geotextiler Sandcontainer (GSC) bildet dabei das Fehlen zuverlässiger Bemessungsgrundlagen, die die Verformung der Sandcontainer und die hydraulischen Prozesse, welche die Stabilität beeinflussen, berücksichtigen. Numerische und experimentelle Untersuchungen waren daher unverzichtbar, um physikalisch begründete Bemessungsansätze zu entwickeln.

Am LWI wurden Modellversuche durchgeführt, um die auftretenden hydraulischen Prozesse, die die Stabilität beeinflussen, zu untersuchen. Besonderes Augenmerk wurde dabei auf folgende Aspekte gelegt: (i) Durchlässigkeit der Küstenbauwerke aus geotextilen Sandcontainern; (ii) Interaktion von Welle und GSC-Struktur; (iii) welleninduzierte Kräfte auf die GSC; (iv) Bewegungen des Sandkerns im Inneren der GSC; (v) Versagensformen der GSC infolge welleninduzierter Kräfte und (vi) Einfluss der Verformung des Containers auf die Stabilität.

Zusätzlich wurden alle physikalischen Prozesse durch numerische Modelle simuliert, um die Interaktion der verschiedenen Prozesse zu untersuchen. Zwei numerische Modelle wurden benutzt: (i) ein RANS-VOF-Modell (**R**eynolds **A**verage **N**avier **S**tokes and **V**olume of **F**luid), um den Seegang, die dadurch induzierte Strömung und Belastung zu bestimmen und (ii) ein struktur-dynamisches gekoppeltes FEM-DEM-Modell (Finite and Discrete Element Method), um die Interaktion zwischen den Strukturelementen sowie die Stabilität der Struktur zu simulieren.

Die Ergebnisse der Modellversuche und der numerischen Simulationen haben beigetragen, das Verständnis des Gesamtbildes der physikalischen Prozesse, die die Stabilität beeinflussen, maßgeblich zu verbessern und zuverlässige Stabilitätsformeln für Strukturen aus geotextilen Sandcontainern unter Berücksichtigung der Verformung der Container zu entwickeln. Zusätzlich wurden die benötigten empirischen Kraft- und Verformungsbeiwerte anhand hierfür speziell konzipierter experimenteller Untersuchungen ermittelt.

Die Stabilitätsformeln können für die konstruktive Bemessung von Küstenschutzwerken wie zum Beispiel Wellenbrechern, Deckwerken, künstlichen Riffen und Buhnen sowie für den Kolkschutz aus geotextilien Sandcontainern verwendet werden. Die Möglichkeiten und Grenzen der Anwendbarkeit der neuen Formeln für die Ingenieurpraxis werden aufgezeigt.

Table of Contents

CHAPTER 4: PROCESS AFFECTING THE HYDRAULIC STABILITY OF GSC-STRUCTURES: EXPERIMENTAL STUDIES AND RESULTS

CHAPTER 5: PROCESS AFFECTING THE HYDRAULIC STABILITY OF GSC-STRUCTURES: NUMERICAL STUDIES AND RESULTS

CHAPTER 6: NEW HYDRAULIC STABILITY FORMULAE

Chapter 1

Introduction

1.1 Motivation

People have been drawn to the coast since the beginning of history, and today, about half of the world's population is said to live within 100 kilometres of the coastline. Protecting coastal areas has been an important factor for most of human societies. The United States Survey Program (IPCC 1996) estimates that every year more than 150,000 people die due to natural hazards and damage cost raise to more than 100 billion dollars (25% of these figures correspond to coastal associated disasters). On the other hand, coastal zones belong to the most valuable and sensitive ecosystems, suggesting that hard protection measures should be minimized (Oumeraci 2004). This illustrates why new shore protection structures are increasingly being developed and alternative systems, such as **g**eotextile **s**and **c**ontainers (GSC) are often replacing more traditional materials/solutions such as concrete or rock material. In addition, in recent years the importance of visual harmony with the coast as well as the reversibility of engineering measures has increased in the search for sustainable solutions for coastal protection.

Coastal structures built with geotextile sand containers are obtained by substituting rocks or concrete units by containers made of geotextile and filled with locally available sand. A range of successful coastal protection structures using GSCs have been constructed in many parts of the world, especially in Australia and Germany (Heerten 2000, and Restall and Saathof 2002 and 2004) (Figure 1- 1).

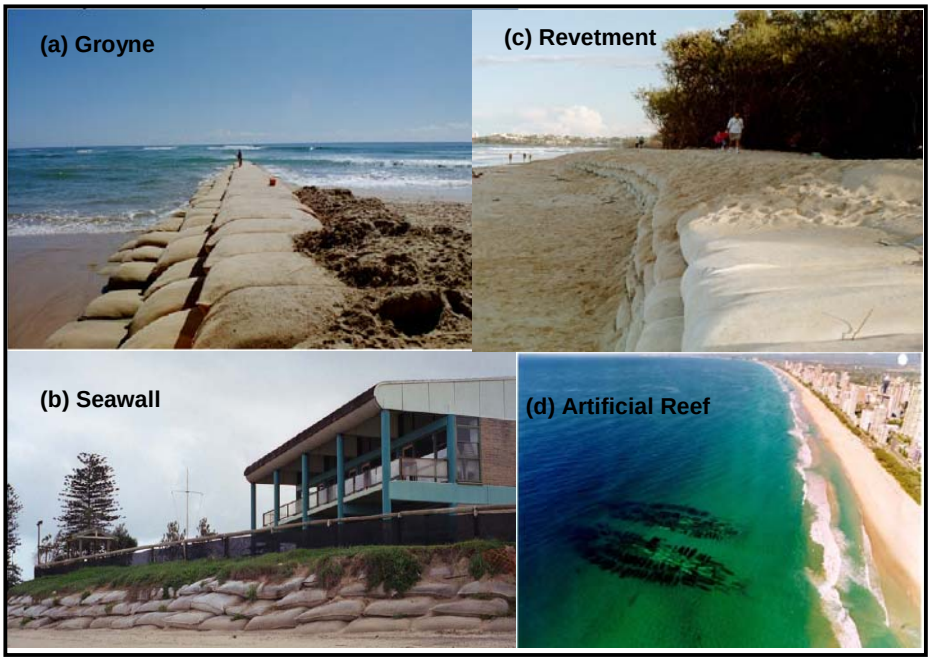

Figure 1- 1: Coastal Structures Made of Geotextile Sand Containers (after Restall and Saathof 2002)

Geotextile sand containers have been used as permanent construction elements in coastal works for more than 20 years. With the increasing costs of "conventional" construction materials and environmental awareness of coastal engineering activities, the use of geotextile

sand containers has proven to be environmentally and economically advantageous as shown in Table 1.1

Table 1.1: Advantages and Disadvantages of GSC-Structures

Advantages
➢ GSCs can be successfully used as coastal structures to solve conventional coastal problems.
➢ GSC-structures are resistant against wave action and coastal related natural hazards.
➢ GSCs adapt and conform readily to changing site conditions and morphological foundation changes.
➢ Total construction and life cycle costs are often considerably less than traditional materials due to reduction in work volume, non-sophisticated equipment requirement, low-skilled labour requirement and the possibility of using locally available sand.
➢ GSC-structures are flexible and behave advantageously under cyclic hydrodynamic loads.
➢ GSC-structures are usually covered with sand or with marine or coastal flora, giving the structure a pleasant and "natural" appearance.
➢ GSC can be easily removed, if engineering measures did not prove successful.
Disadvantages
➢ Design and construction requires consideration of site specific conditions
➢ Lack of deep understanding of the hydraulic processes affecting the stability of GSC-structures
➢ Lack of reliable design tools which can compromise the safety under different conditions.
➢ Long term effect of marine growth on the structural durability of the GSCs is still not fully understood.

1.2 **Objectives**

The primary objective of this study is to develop hydraulic stability formulae for the design of structures built with geotextile sand containers. This development should be process oriented and should consider all the hydro-geotechnical processes affecting the hydraulic stability of GSCs.

1.3 **Methodology**

The methodology adopted in this research is briefly illustrated in Figure 1-2. First, the state of knowledge related to different aspects of the hydraulic stability of GSC-structures is systematically reviewed and analyzed with the objective of identifying the most relevant physical processes and hydraulic properties of the GSC-structures which may affect the stability of the geotextile sand containers.

Second, a variety of laboratory experiments are conducted in order to identify, understand and possibly quantify the afore-mentioned processes, particularly focusing on those affecting the deformations of the GSCs and the effect of the latter on the stability.

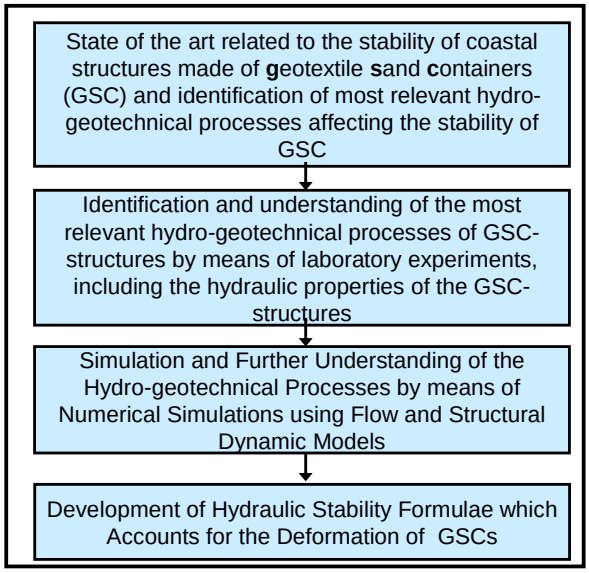

Figure 1- 2: Methodology of this Thesis

Third, available hydrodynamic models for the prediction of the wave loads and structural dynamic models for the prediction of stresses and deformations of the GSCs are further developed, validated and applied to extend the knowledge gained from the laboratory experiments.

Finally, analytical hydraulic stability formulae which account for the effect of the deformations of the GSCs are developed and the force coefficients (drag, inertia and lift) which cannot be determined analytically, are obtained from additional laboratory experiments designed only for this purpose.

Chapter 2

State of the Art Review

The present state of the knowledge related to the hydraulic stability of **g**eotextile **s**and **c**ontainers (GSCs) used for coastal structures is addressed with the main objective of specifying in more detail the objectives and methodology formulated in Chapter 1.

This chapter is divided in six sections: (i) first, the mechanical properties of GSCs relevant for the hydraulic stability are described; (ii) followed by the description of the hydraulic processes relevant for the hydraulic stability of GSCs; then, (iii) available relevant experiments on the hydraulic stability of GSCs are presented; (iv) available hydraulic stability formulae for GSC-structures are discussed; (v) identification of most appropriate numerical codes for the numerical simulations of GSC-structures are outlined and (vi) the detailed specifications for the objectives and methodology of this thesis are presented.

GSC-structures are structures built with geotextile sand containers. The geotextile containers have enough tensile strength, UV-, abrasion and damage resistance to withstand a coastal environment up to 40 years (Restall and Saathoff 2002). Geotextiles can be manufactured with the required characteristics which depend on site specific conditions. Some examples of GSC-structures for coastal applications are: seawalls, revetments, submerged-reefs, groins, dune-reinforcement, breakwaters, and scour-protection-systems. In principle, any type of coastal structure made of rocks or concrete material can also be built with geotextile sand containers. A significant number of GSC-structures have been constructed over the last 20 years. In Australia, where stones are scarce, more than 17 projects have been documented by Restall et al (2004). In Germany, prototype GSC-revetments were constructed both in the North and Baltic Sea coasts (Heerten et al 2000 and Oumeraci et al, 2002).

2.1 Mechanical Properties of GSCs and GSC-Structures Relevant to the Hydraulic Stability

The mechanical properties of GSCs, relevant to the hydraulic stability are briefly described. Analyses are focused on the mechanical properties of GSCs that are relevant to the hydraulic stability of GSCs.

2.1.1 Friction at Interface of Geotextile-Geotextile and Sand-Geotextile

Interfaces of geotextile-geotextile and geotextile-sand are investigated by means of direct shear stress. The results provide the friction coefficient of the interface between geotextile-geotextile and geotextile-sand which are required to quantify the effect of the friction between GSCs on the hydraulic stability (see also Section 5.5.8).

To date, there are only few information on the friction between two geotextiles surfaces. Grett (1984), Kim and Yoo (2004), and Naue (2004) performed direct shear tests on two geotextiles using the standard large direct shear stress test on a shear box with dimensions of 0.30m x 0.30m.

Grett (1984) systematically tested woven and nonwoven geotextiles and found that the friction angle among geotextile varies from 16^o to 18^o for woven geotextile, 20^o to 26^o for mechanical-nonwoven geotextiles and 23^o to 30^o for thermal-nonwoven geotextiles (Figure

2-1). Kim and Yoo (2004), on the other hand, tested non-woven geotextile and obtained a friction angle of approx 35°. Finally, Naue (2004) found a friction angle for nonwoven geotextile between 20° and 26° (Table 2.1).

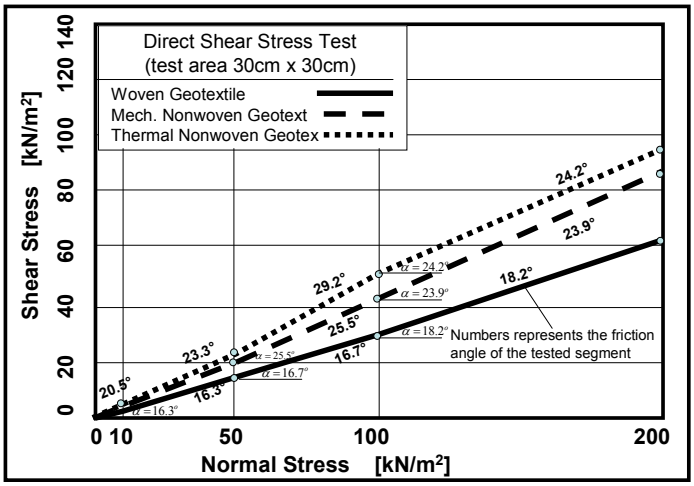

Figure 2-1: Direct Shear Stress Test Results (after Grett 1984)

Table 2.1: Friction Angles and Friction Factors (after Naue 2004)

	Interface Materials	Friction Angle ϕ	Friction Factor $\tan\phi$
Nonwoven Geotextile	Terrafix 1200R (mechanical nonwoven) vs. Sand	30.11	0.57
	Terrafix 1200R (mechanical nonwoven) vs. Terrafix 1200RP	25.97	0.48
	Terrafix 1200RP (mechanical nonwoven) vs. Terrafix 1200RP	22.53	0.41
Woven Geotextile	Geolon PP120S (woven) vs. Geolon PP120S	20.38	0.37
	Mirafi GT1000 (woven) vs. Mirafi GT1000	14.80	0.26
	Mirafi GT500 (woven) vs. Mirafi GT500	11.91	0.21

Note: Friction angle between woven and sand is not available

2.1.2 Deformability and Stress-Strain Relation of GSCs

The deformability and stress-strain relation of geotextile sand containers which is relevant to the stability of GSCs is briefly outlined (see also Section 5.5.5).
Results are based on the work of Matsuoka et al (2001), who performed analyses and tests (unconfined/confined biaxial test) on sand containers.

Figure 2-2 shows a two dimensional sand container subjected to the principal stresses, σ_1 and σ_3. Under the application of σ_1 and σ_3, the total perimeter of the container usually extends and produces additional stresses that act on the sand particles inside the container, whose components are expressed as:

$$\sigma_1 = 2T_{tension} / B \text{ and } \sigma_3 = 2T_{tension} / h_{soilcont} \qquad (2.1)$$

where B and $h_{soilcont}$ are the width and height of the sand container, respectively. Thus, the stresses acting on the sand particles inside the container are the combined result of the externally applied stresses and the additionally generated stresses by $T_{tension}$ which is the tension of the geotextile under load, as shown in Figure 2-2. At failure, the following equation was derived by Matsuoka (2001):

$$\sigma_1 + \frac{2T_{tension}}{B} = K_p(\sigma_3 + \frac{2T_{tension}}{h_{soilcont}}) \qquad (2.2)$$

$$\text{where } K_p = \frac{1+\sin\phi}{1-\sin\phi} \qquad (2.3)$$

where ϕ is the friction angle of the sand. By comparing equation (2.3) with the strength expression for a cohesive-frictional material, an equation to describe the apparent cohesion c of sand containers due to their tension $T_{tension}$ can be obtained:

$$c = \frac{T_{tension}}{B\sqrt{K_p}}\left(\frac{B}{h_{soilcont}}K_p - 1\right) \qquad (2.4)$$

Equation 2.4 means that a sand container has "cohesion" due to the effect of the container on the sand particles inside the container (Figure 2-3).

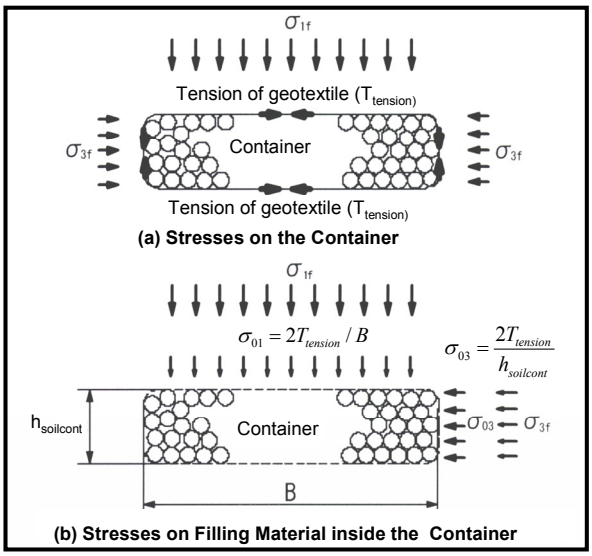

Figure 2-2: Stresses on Two Dimensional Sand Container and on the Sand inside the Container (after Matsuoka 2001)

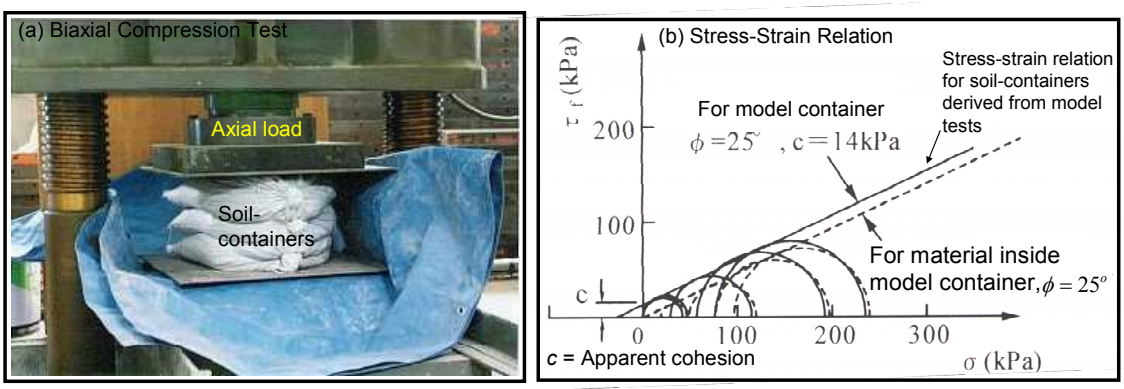

Figure 2-3: Results of Biaxial Compression Tests on Sand Containers (after Matsuoka 2001)

Matsuoka validated his results by biaxial compression tests and unconfined compression tests on sand containers. Results showed that the critical load to induce the failure a sand container (tearing of textile) is about 42 times larger than the tensile strength of the container material itself. Therefore, the sand container has an extremely higher tensile strength than that originating from the tension of the container alone (without filling).

2.1.3 Other Mechanical Properties of Sand Containers and GSC-Structures

Extensive research was performed on the mechanical properties of sand containers such as durability, permeability, impact resistance and tensile strength Naue (2003) and Mirafi (2004), Grett (1984). Detailed information can also be found in the volumes of the Geotextile and Geomembrane Journal published by Elsevier.

Results related to the permeability of GSCs (Grett 1984, Mirafi 2004) have shown that the permeability of the geotextile is usually similar to the permeability of sand; therefore, the permeability of a GSC is normally considered to be in the range of the sand fill.

The only available research results on the permeability of GSC-structures are those presented by Bourzaev (2003).
Bourzaev, assuming that the permeability of the geotextile is the same as the sand inside the container used the results from the large scale model tests conducted in the Large Wave Flume (GWK) by Oumeraci et al (2002) to determine the permeability coefficient of the tested GSC-revetment. The sand used in the tests inside the GSC had a permeability coefficient of $k = 1.6 \times 10^{-4}$ m/s, while the permeability of the cover layer made of 150 litre sand containers was found to be around $k = 1 \times 10^{-2}$ m/s. Bourzaev (2003) concluded that the permeability of a GSC-structure is eventually governed by the gaps between the GSCs.

A further important fact related to the permeability of a GSC-structure is the result presented by Pilarczyk (1998) regarding the introduction of a geotextile filter behind armour layers of stone revetments. He showed that if a geotextile filter is placed directly under the cover layer it will drastically reduce the permeability of the structure. The same principle may also apply to GSC-revetments: if a geotextile filter is placed under the GSC-revetment (Figure 2-4) it will be pressed against the GSCs by the out flowing water of the receding wave. It should thus, be treated as a part of the cover layer. Subsequently, the water-flow through the GSCs is concentrated at the gaps between the elements, reaching very high flow velocities and resulting in large pressure heads over the geotextile. The presence of a geotextile filter may reduce considerably the permeability of the overall revetment.

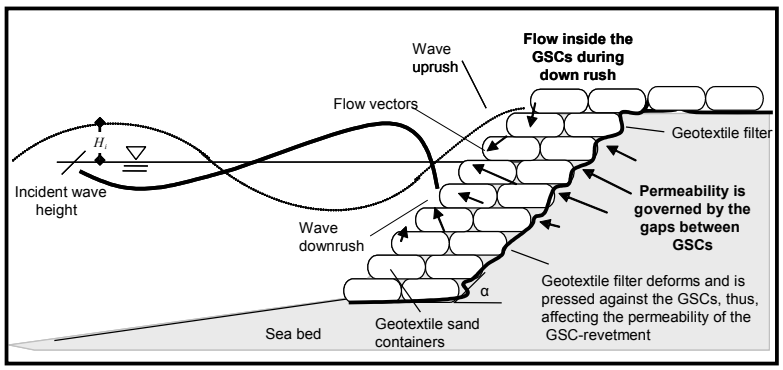

Figure 2-4: Permeability of a GSC-Revetment Affected by a Geotextile Filter

2.2 Hydraulic Processes Relevant for the Hydraulic Stability of GSC-Structures

The present stage of knowledge on the hydraulic processes affecting the hydraulic stability of GSCs is briefly reviewed. To date, only Oumeraci et al (2002) and Bourzaev (2003) performed process-oriented investigations on the stability of GSC-structures. Therefore, this section is focused mainly on wave reflection, wave overtopping and wave up/down rush.

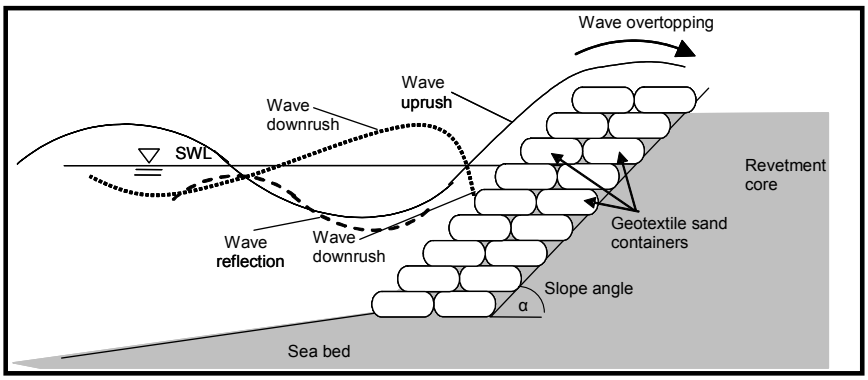

Figure 2-5: Main Hydraulic Processes Acting on a GSC-Revetment

2.2.1 Wave Reflection of GSC-Structures

Waves on a solid obstacle are very often partially reflected. In the case of a vertical, impermeable structure, the fraction of wave energy reflected can be very large (up to 80%). For permeable structures like GSC-structures, the reflection will be less. In general, incident wave energy E_i can be partly dissipated E_d by wave breaking and surface roughness; partly transmitted E_t by wave overtopping and through the structure; and partly reflected E_r back to the sea, thus:

$$E_i = E_r + E_t + E_d \qquad (2.5)$$

Reflection can be quantified by the bulk reflection coefficient,

$$k_r = \frac{H_r}{H_i} = \sqrt{\frac{E_r}{E_i}} \qquad (2.6)$$

where H_i and H_r are the significant wave heights of incident and reflected waves, respectively. Transmission coefficient and dissipation coefficient can be defined by: $k_t = \frac{H_t}{H_i}$, and $k_d = \frac{H_d}{H_i}$, where H_d and H_t are the height of the dissipated wave and transmitted wave, respectively (Figure 2-6):

$$k_r^2 + k_d^2 + k_t^2 = 1 \qquad (2.7)$$

Reflections coefficient for GSC-structures were obtained from small and large-scale model tests (Oumeraci et al, 2002). With the geometry shown in Figure 2-7 and plotting the results against the surf similarity parameter (ξ_o) which is defined as:

$$\xi_o = \tan\alpha \Big/ \sqrt{\frac{H_o}{L_o}} \qquad (2.8)$$

where α is the slope angle of the revetment, H_o / L_o the deepwater wave steepness, H_o is the deepwater wave height, L_o is the deepwater wavelength ($gT^2/2\pi$), T is the wave period and g is the acceleration due to gravity), Oumeraci et al (2002) found that the reflection coefficient

for GSC-revetments (with 45° slope angle) varies between k_r=*0.5* and k_r=*0.7* for surf similarity number of $\xi_o = 5 \square 14$ (Figure 2-7).

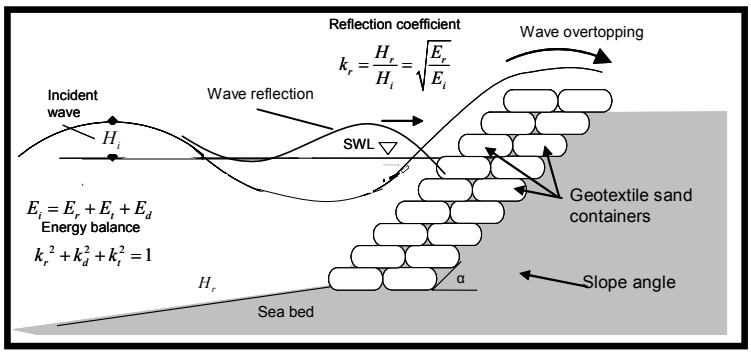

Figure 2-6: Wave Reflection on a GSC-Revetment

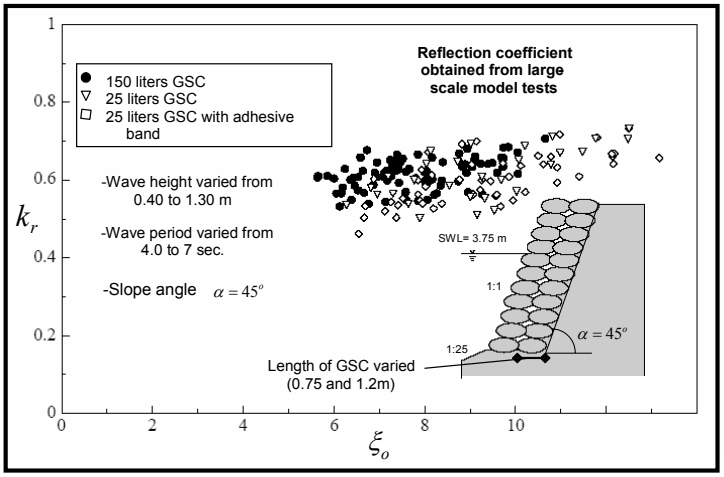

Figure 2-7: Reflection Coefficient k_r from Large-Scale Model Tests (after Oumeraci et al, 2002)

2.2.2 Wave Overtopping of GSC-Structures

Overtopping is mainly governed by the crest elevation of the revetment in relation to the heights of individual waves (relative freeboard). The degree of overtopping is measured by the amount of overtopped water, either as the amount per wave per unit length of the structure or as the mean rate of overtopping of volume per unit length and time. The mean rate of overtopping is averaged over the duration of the storm waves (Figure 2-8).

Overtopping occurs only if the run-up level exceeds the freeboard R_c of the structure (Figure 2-9). The relative freeboard, R_c /H_s (being H_s the significant wave height) represent one of the most important dimensionless parameter for the prediction of overtopping. However, the wave period or wave steepness, surface roughness and hydraulic permeability also represent significant influencing parameters.

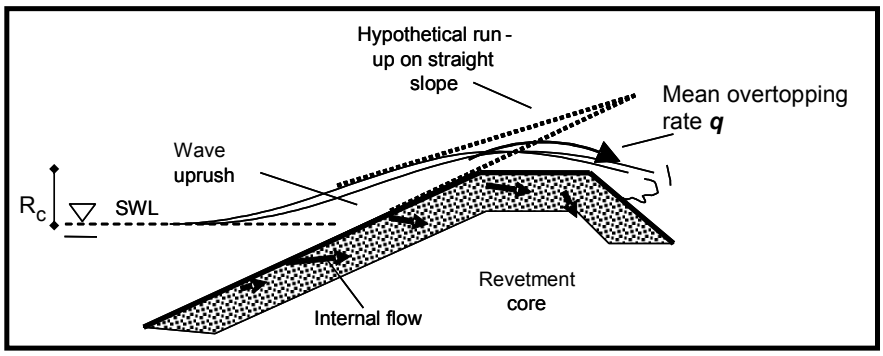

Figure 2-8: Overtopping on a Permeable Revetment

Formulae for wave overtopping of sloping structures are empirical; they are fitted to results from hydraulic model tests for specific geometries. In general, the average overtopping discharge per unit length of structure q is a function of the standard parameters: (H_s, T, σ, β, Rc, d, g, structure geometry), where σ is the spreading of short-crested waves, β the angle of wave incidence and d is the water depth in front of structure.

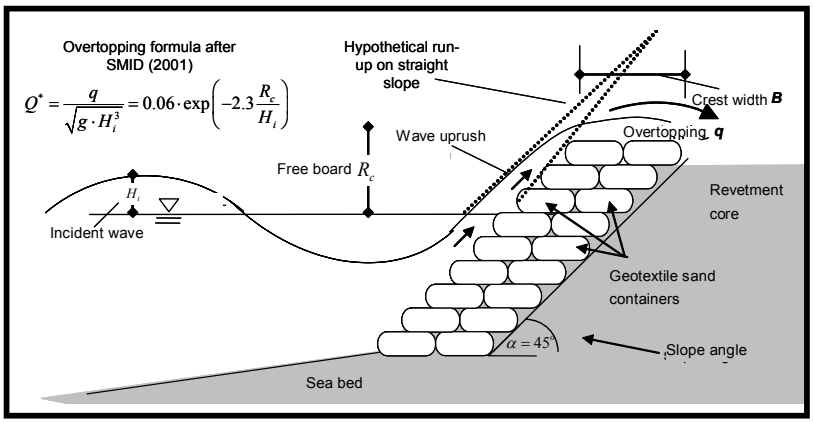

Figure 2-9: Wave Overtopping on a GSC-Revetment

There are many overtopping formulae for sloping structures and seawalls (i.e. Van der Meer 1987). Oumeraci et al (2002) proposed the following overtopping formulae based on large-scale model tests results and the analyses by Smid (2001):

$$Q^* = \frac{q}{\sqrt{g \cdot H_i^3}} = 0.06 \cdot \exp\left(-2.3 \frac{R_c}{H_i}\right) \qquad (2.\ 9)$$

$$q = 0.188 H_s^{3/2} \exp\left(-2.3 \frac{R_c}{H_s}\right) \qquad (2.\ 10)$$

where Q^* (relative overtopping rate) is a dimensionless average discharge per meter and R_c/H_s is the dimensionless freeboard.

Oumeraci et al (2002) also found that small and large-scale model tests showed similar relative overtopping rates and that scale effects were within the range of the uncertainties of the measurements (Figure 2-10).

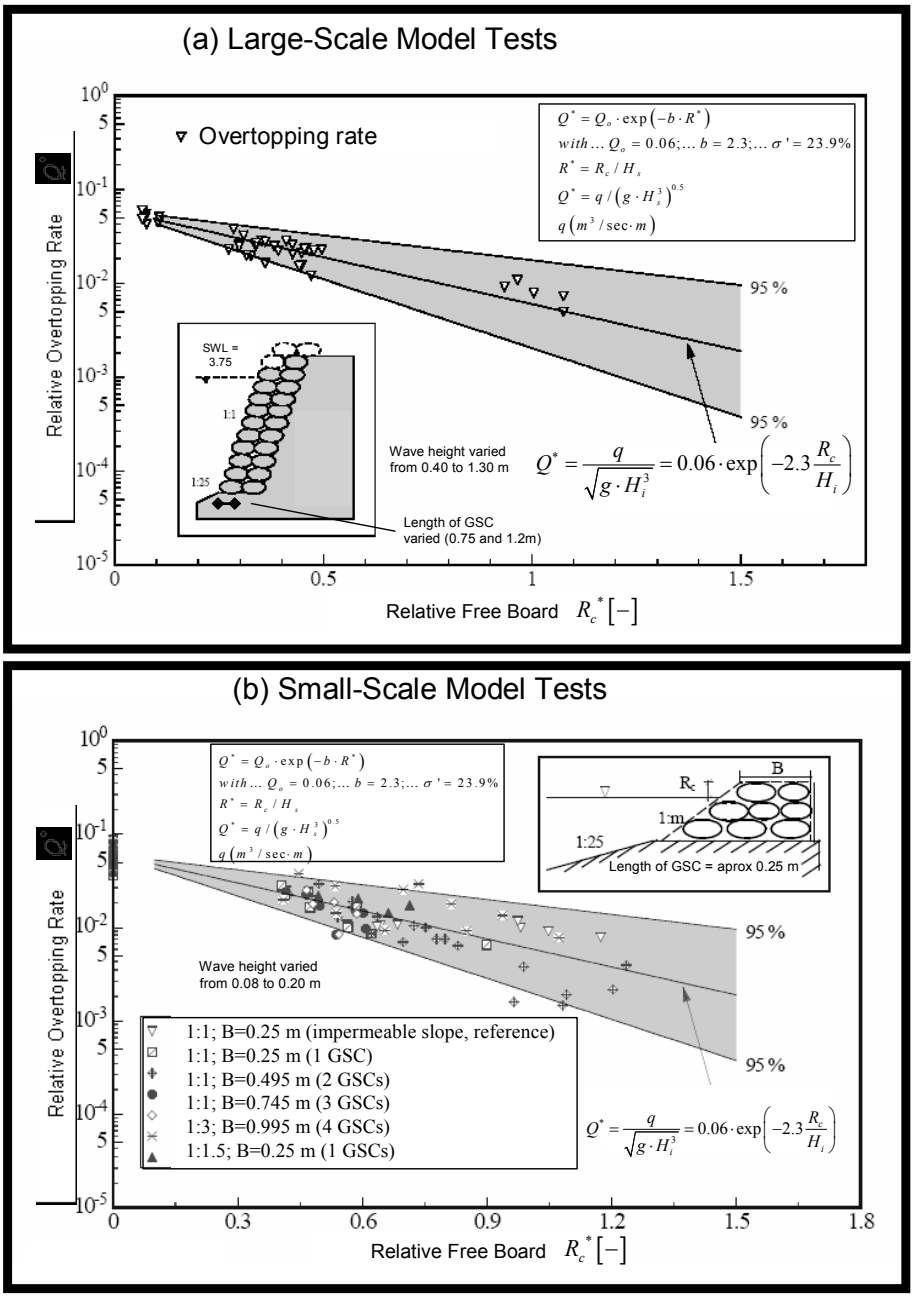

Figure 2-10: Relative Overtopping Rate Obtained from Large and Small-Scale Model Tests (after Oumeraci et al, 2002)

2.2.3 Wave Runup on GSC-Structures

Runup is the maximum elevation of wave uprush above still-water level. Waves have periods which trigger wave breaking on almost all sloping structures. The wave breaking causes runup, R_u, and rundown, R_d, defined as the maximum and minimum water-surface elevation measured vertically from the still water level (Figure 2-11).

R_u and R_d depend on the height and steepness of the incident wave and its interaction with the preceding reflected wave, as well as the slope angle, the surface roughness, and the permeability and porosity of the slope. Maximum values of flow velocities and values of R_u and R_d for a given sea state and slope angle are reached on smooth impermeable slopes.
Surface roughness affects the run-up. Roughness reduction factors for many kinds of materials were measured experimentally; however, there is no reduction factor available for GSC-structures.

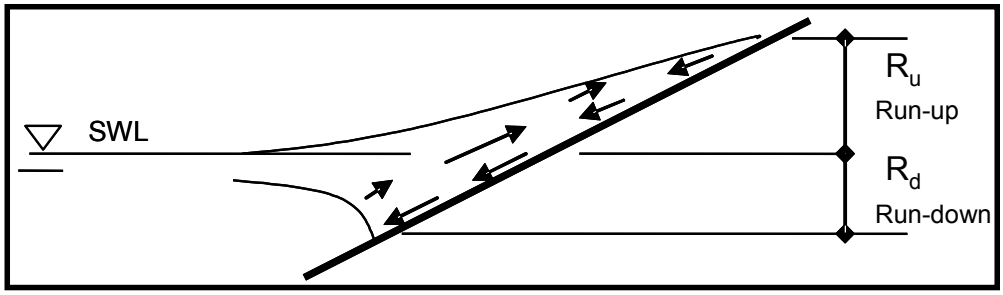

Figure 2-11: Runup and Rundown on an Impermeable Revetment (definition sketch)

Wave run-up is often described by the statistical value $R_{u2\%}$. This is the run-up level, vertically measured with respect to the still water level, which is exceeded by two per cent of the incident waves. The relative run-up is given by $R_{u2\%}/H_s$. The relative run-up is usually given as a function of the surf similarity parameter (equation 2.8). The general design formula for wave run-up for revetments is (Pilarczyk 1998):
$R_{u2\%} / H_s = 1.6\gamma_b\gamma_f\gamma_\beta\xi_o$ with a maximum of 3.2 $\gamma_f\gamma_\beta$
with γ_b being the reduction factor for a berm, γ_f the reduction factor for slope roughness and γ_β is the reduction factor for oblique wave attack.
Since no results are yet available to asses the reduction factor for GSC-structures, Pilarczyk, proposed to use γ_{fGSC} = 0.8. This value needs to be treated with caution since it was assessed in the basis of analogy with other materials, thus lacking any experimental verification.

2.2.4 Wave Uprush and Downrush for GSC-Structures.

Unlike parametric investigations, there is limited information regarding the hydraulic processes associated with the hydraulic stability of GSC-structures. However, present stage of the knowledge related to stone revetments is briefly reviewed since some of the processes are similar (CEM 2004). A typical cross section of a permeable revetment with up and downrush is shown in Figure 2-12. The arrows indicate the velocity vectors of the flow inside the revetment. These vectors govern the stability of the revetment which is subject to a complex flow over and through the permeable structure.

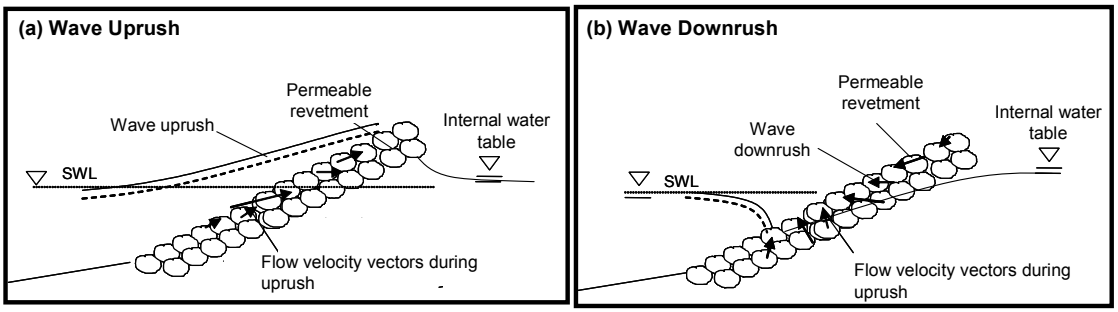

Figure 2-12: Hydraulic Flow in a Permeable Revetment During Uprush and Downrush

During wave run-up the resulting wave forces will be directed opposite to the gravity forces. Therefore, wave run-up is less hazardous than wave run-down. Wave run-down will exert a pulling force on the cover layer and the decreasing phreatic level will coincide with a downward flow gradient.
The mobilizing and resisting forces on individual elements, on the other hand, are extremely important for the stability of GSC-revetments, but can hardly be derived analytically. Therefore, stability formulae were derived experimentally as a function of the incident wave and wave period. Scaled model test results (Oumeraci et al 2002) showed that the most critical containers within a GSC-revetment are those placed in the area around the still water level and the containers at the crest of the revetment (Figure 2-13).

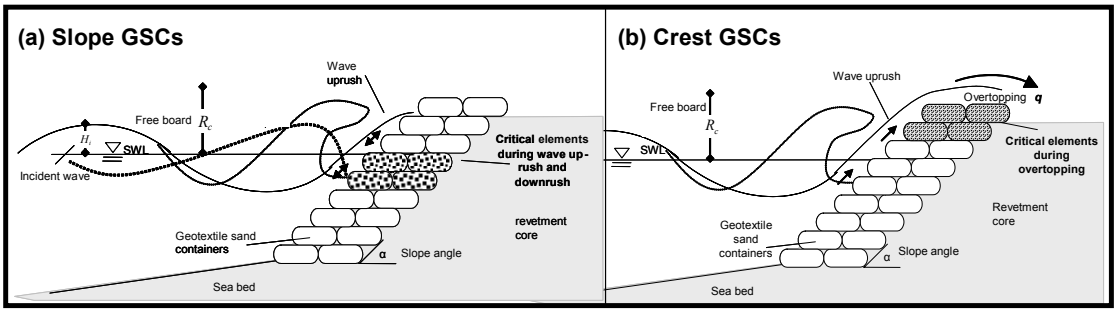

Figure 2-13: Critical Locations for Sand Containers in the Structure

2.2.5 Concluding Remarks on the Hydraulic Processes on GSC-Structures

To date, only very few process-oriented investigations have been performed on the stability of GSC-structures. Many of the processes associated with the instability of these structures are still not well understood. Identifying and understanding the hydraulic processes and their interactions which are associated with the stability of GSC-structures, are extremely important to develop reliable stability formulae. Detailed investigations of the processes associated with the hydraulic stability of GSC-structures are addressed in Chapters 4 and 5.

2.3 Available Laboratory Experiments on the Hydraulic Stability of GSCs

Over the past decades several hydraulic model tests related to the stability of GSC-structures were conducted worldwide. Most of the previous model tests focused on the stability of GSC-revetments and GSC-breakwaters. The results of a comparative analysis of the results of previous hydraulic model tests are briefly outlined (Figure 2-14 and Table 2.2).

Detailed information of these laboratory tests (Figure 2-14) are given by Bouyze (1990), Hudson (1956), Jacobs and Kobayashi (1983 and 1985), Kübler (2002), Porraz (1979), Ray (1977), US-CEM (2004), Tekmarine (1982), Venis (1967), Oumeraci et al (2002), and Pilarczyk (2000). The cross sections of the model structures investigated are comparatively shown in Figure 2-14, including more detailed information and the contribution of each study to the advance of knowledge on the hydraulic stability (Table 2.2).

Overall, the results show that overlapping of GSCs, filling ratio of the containers, wave conditions acting on the structure, steepness of the slope and orientation of the container with respect to the wave direction represent important factors affecting the hydraulic stability.

Previous scale-model investigations, however, did not consider the effect of important factors such as the permeability of the structure, the deformability of the container, the internal movement of sand inside the containers and the friction between containers.

Table 2.2. Comparative Analysis of Previous Model Tests Related to the Hydraulic Stability of GSC-Structures

Author and Year	Type of Structure	Scale	Wave-flume dimensions (m)	Wave Type	Container Material	Container Dimensions	Filling Material	Filling ratio	Over-lapping	Stability Criteria	Contribution
VENIS (1967) :	Submerged breakwater (1:n=1:15)	1:5; 1:20	U/3.0/0.6	Unknown	Jute	Wwithout filling (1:5) 0.4 x 0.4 m	Dry sand ρ_s= 1600 kg/m3 wet sand 1900 kg/m3	50%-90%	--	--	Recommendation of a sand fill ratio of 80%. lower filling ratio reduces the stability
DELFT Hydraulics (1975)	Revetment, sand tubes, (1:n=1=3)	01:25	Unknown	Spectra	Jute and linen	Tube diam. 0.9m and 1.5m	Sand	90%-100%	--	Movement starts H/(ΔD_n) = 2.0 Damage =4.5	No consideration of wave period, tubes more stable than containers. Stability proportional to tube diameter. Larger mattresses give higher stability. Sand fill ratio does not influence the stability of mattresses
RAY (1977) :	Breakwater and submerged breakwater	1:1	Unknown	Regular waves	Nylon	Without filling 2.44 x 1.52m full 2.15x1.2x0.33	Wet sand, ρ_s= 2000 kg/m3	75%	--	From H/(ΔD_n) = 3.0 to = 5	Steep waves induce reduction in stability (specially on submerged breakwaters).
PORRAZ (1979) :	Breakwater (1:n:1:1 and 1:n=1:2)	1:60	70/0.6/1.2	Regular waves	Polyethylene	Full 5.6x2.3x0.5cm	Mortar ρ_s=2140 kg/m3	Un known	--	For 1:n=1:1 and H_{crit}=6cm H/(ΔDn)=2.0 for 1:n=1.2 and H_{crit}=9cm H/(ΔDn)=2.0	Steepness of slope, higher overlapping induces higher stability, higher loads are on the top of the slope. Recommendations for a larger crest element. Higher stability with containers perpendicular to the structure axis
TEKMARINE (1982) :	Revetment slope (1:n=1:3)	1:60	107/3.7/4.6	Regular waves and Spectra	Unknown	Without filling 0,61 x 0.33m; full 0.54 x 0.26 x0.14m	Gravel ρ=1923 kg/m3 (cement)	Un known	50%	50% overlapping H/(ΔDn)=2.1 without overlapping 1.8 combination2.1	Overlapping length increases the K factor to 1.5, Elements near the SWL are critical for the stability, Recommendations for maximum possible overlapping
JACOBS & KOBAYASHI (1983/1985) :	Revetment slope (1:n=1:3)	Unknown	24.4/0.61/1.4	Regular waves	Geotextile	Without filling 12.7x8.9cm; full 12.4x6.2x3.3cm	dry sand ρ_s= 1699 kg/m3 wet sand 1955 kg/m3	Un known	50%	50% overlapping H/(ΔDn)=2.4	Increase in the overlapping increases the stability, Introduction of a empirical constant, Formulation of the relation between the stability number Ns and the surf similarity parameter ξ
BOUYZE & SCHRAM (1990)	Submerged breakwater (1:1)	Unknown	8/1/0.35/	Current	Geotextile	1m x 0.36 m full	Sand	Un known	50%	$\frac{u_{cr}}{\sqrt{g\Delta_i D}} = 0.5 \cdot to \cdot 1.0$	Critical velocity before movement of the elements. No particular contribution.
DELFT Hydraulics (1994) :	3 Layers of containers in a submerged breakwater (1:n=1:1)	1:20	55/1.0/1.2	Pierson Moscowitz Spectra	Geotextile	Full 1.0x0.42x0.09	Sand	Un known	--	Movement starts H/(ΔDn)=1.83. Displacement H/(ΔDn)=2.33	Description of the dependency of the stability with the experiment parameters. No particular contribution
WOUTERS (1998) :	--	Develop stability formula from the experimental data of Porraz (1978), Tekmarine (1982) and Jacobs &Kobayashi (1983, 1985)								H/(ΔDn) =2.5/√(ξ_o)	Develop of a function for describing the stability number with the surf similarity parameter
OUMERACI et al (2002) (small scale)	Dune protection, slope revetment and submerged breakwater (1:n=1:1; 1:1.5 and 1:3)	1:8	100/2.0/1.2	Jonswap Spectra	Geotextile and linen	Without filling 0.31x0.15 full 0.25x0.1x0.06m	Sand	80%	<=50%	H/(ΔDn) =2.0/√(ξ_o)	High influence in the stability by the overlapping,
OUMERACI et al (2002) (large scale)	Revetment (1:1)	1:6	300/5.0/7	Jonswap Spectra	Geotextile	150lt and 25lt	Sand	80%	<=50%	H/(ΔDn) =2.7/√(ξ_o)	Some scale effects observed. Stability increased by the use of adhesive stips among elements. New stability formulae based on the Wouters formula. Formulas for crest and slope elements

$\xi_o = \frac{\tan\alpha}{\sqrt{H_0 / L_0}}$; D = equivalent diameter of the unit $\rho_s =$ density of sand; $\rho_w =$ density of water; $\Delta = \frac{\rho_s}{\rho_w} - 1$ *k*= permeability coefficient; u_{cr} = critical flow velocity

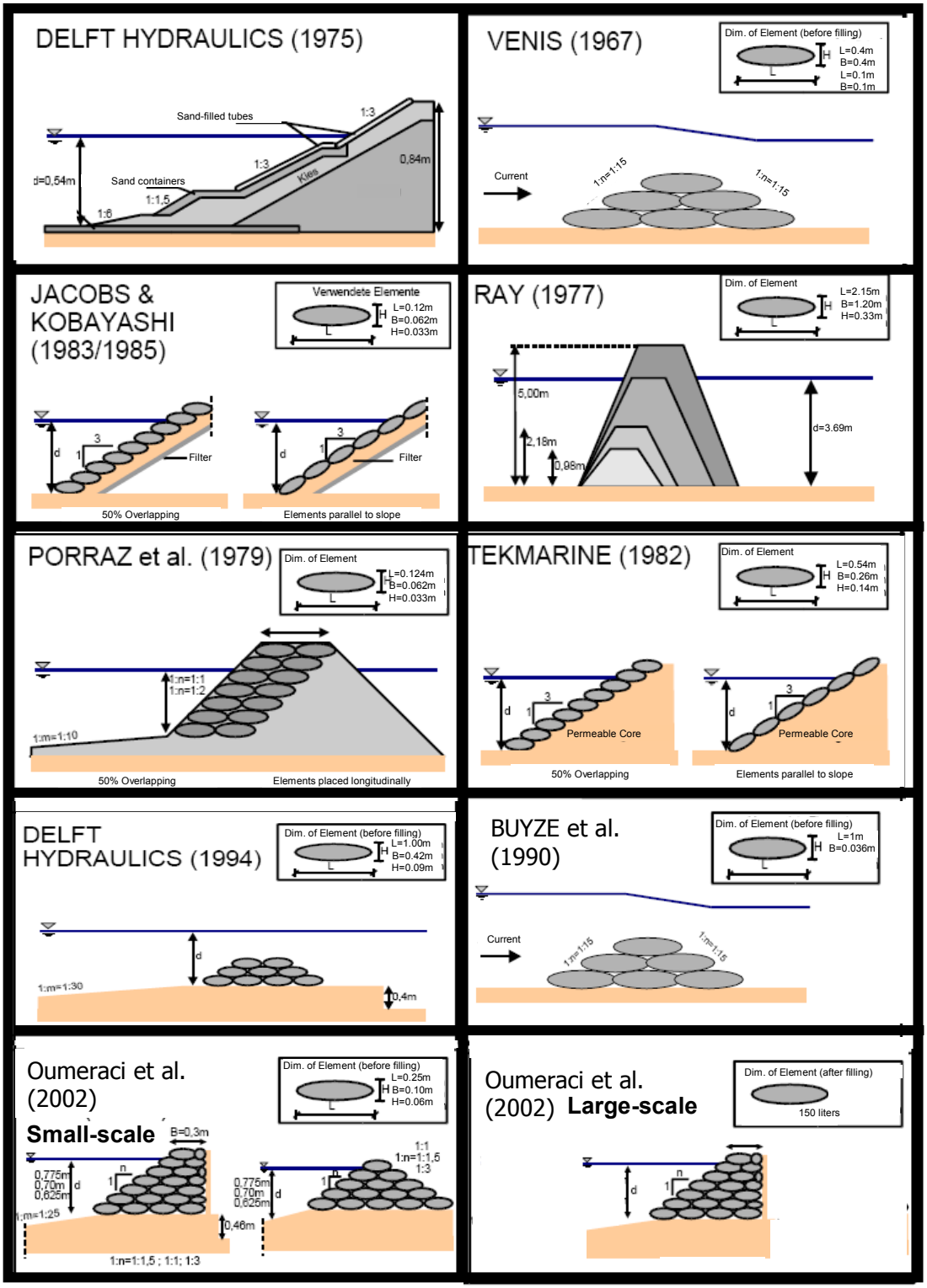

Figure 2-14 Comparative Cross Section of Previous Model Tests of GSC-Structures (Modified from Oumeraci et al 2002)

2.4 Available Hydraulic Stability Formulae for GSC-Structures

GSC-structures have been traditionally designed using stability formulae for stone-armour layers and mainly based in Hudson's formula (1956).

Available formulae are based in the stability number concept and in the balance of wave-induced forces. The wave-induced forces on armour units might be expressed as a sum of a drag force F_D, a lift force F_L and an inertia force F_M. The stabilizing force is the gravitational force F_G. Assuming that at the stage of instability, drag and lift force dominates the inertia force, a stability ratio can be approximately formulated as the drag force plus the lift force divided by the gravity force (Figure 2-15)

$$\frac{F_D + F_L}{F_G} \approx \frac{\rho_W D_n^2 v^2}{g(\rho_S - \rho_W) D_n^3} = \frac{v^2}{g \Delta D_n} \qquad (2.11)$$

where D_n is the equivalent cube length $D_n = \left(\frac{W}{\rho_s}\right)^{1/3}$, W is the weight and ρ_s and ρ_w are the mass densities of armour units and water, respectively; and v is a characteristic flow velocity. By inserting $v \approx (gH)^{1/2}$ for a wave height of H_s and g for the gravity acceleration in equation 2.11, the stability number, N_s, is obtained:

$$N_s = \frac{H}{\Delta D_n} \qquad (2.12)$$

$$\text{with } \Delta = \left(\frac{\rho_s}{\rho_w} - 1\right) \qquad (2.13)$$

2.4.1 Stability Formula of Hudson (1956)

Based on geometrical considerations of the balance of forces acting on an armour stone (Figure 2-15) and considering the wave-induced forces on armour units, Hudson (1956) proposed the following formula:

$$N_s = \frac{H}{\Delta D_n} = (K \cot \alpha)^{1/3} \qquad (2.14)$$

where α is the slope angle and K is a stability coefficient taking into account all other variables.

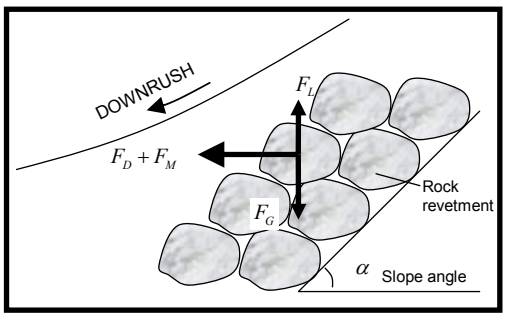

Figure 2-15: Forces on Armour Unit (definition sketch by Hudson, 1956)

Values of K for different types of materials/shapes are obtained experimentally. The required averaged weight of the armour unit is obtained by re-writing equation 2.14 as:

$$W_{50} = \frac{\rho_s g H^3}{K\left(\frac{\rho_s}{\rho_w} - 1\right)^3 \cot\alpha} \qquad (2.15)$$

where K is an empirical parameter which depends on the roughness, shape and interlocking properties of the armour unit.

The main advantages of the Hudson formula are its simplicity and the wide range of armour units and configurations for which K-values have been derived. The major limitations are: wave period, inertia force and storm duration are not explicitly considered, although they can implicitly be taken into account in the K-value derived from the experiment (refer to Section 2.4.5 for further discussions).

2.4.2 Stability Formula of Bouyze and Schram (1990)

Based on scale model tests as well as the Hudson and Isbash formula (Isbash 1976); Bouyze and Schram (1990) proposed a stability formula for GSC-structures. Bouyze and Schram performed model tests on geotextile tubes filled with sand and subjected to unidirectional flow (Figure 2-16). Based on the critical velocity u_{cr} that induced incipient movement of the geotextile tubes, they proposed the following formula:

$$\frac{u_{cr}}{(g\Delta D)^{0.5}} = 0.5 \cdot to \cdot 1.0 \qquad (2.16)$$

where u_{cr} is the critical velocity (averaged over the water column), g the gravity acceleration, Δ is the relative density of the geotextile tube (defined in equation 2.13) and D is the diameter of the geotextile tube.

The advantage of the Bouyze-formula is its simplicity. The major limitations are: (i) the empirical value is obtained from a unidirectional flow instead of waves and (ii) only tests using geotextile tubes, thus, it cannot be used for geotextile containers with finite length.

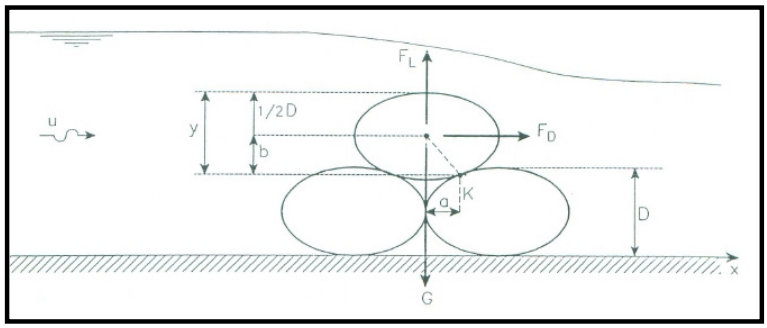

Figure 2-16: Definition Sketch by Bouyze and Schram (1990)

2.4.3 Stability Formula of Wouters (1998)

Based on the Hudson formula and the experimental data from Porraz (1979), Tekmarine (1982) and Jacobs & Kobayashi (1983); Wouters proposed a stability formula considering balance of moments of the lift force F_L, the drag force F_D and the stabilizing gravitational force F_G. Instead of the required weight of the armour unit, the thickness D of the cover layer defined by the relationship $D = l \sin\alpha$ (2.17) is calculated.

The next adaptation was the inclusion of the porosity *n*, to obtain a more realistic density of the GSC:

$$\rho_E = (1-n)\cdot\rho_s + \rho_w \cdot n \qquad (2.18)$$

where *n* is the porosity of the filling material (sand). The stability number can then be obtained with (Wouters 1998):

$$N_S = \frac{H_S}{\left(\frac{\rho_E}{\rho_W}-1\right)\cdot D} = \frac{C_W}{\sqrt{\xi_0}} \qquad (2.19)$$

where ρ_w is the density of water, ρ_E is the density of GSC, C_w is an empirical parameter derived from the experiments, ξ_0 is the surf similarity parameter defined in equation 2.8. For GSC-revetments, based on experimental data, Wouters (1998) proposed a value for C_w = 2.0

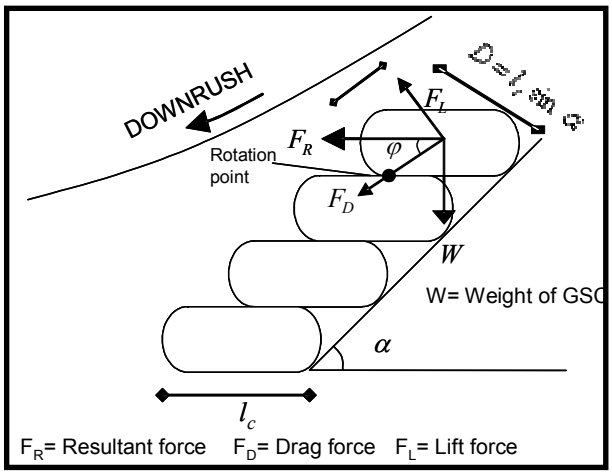

Figure 2-17: Definition Sketch of the Parameters Used by Wouters (1998)

The advantages of this formula consist in the consideration of the porosity of the filling material and consideration of wave period. The limitations are due to parameter C_w which can only be obtained experimentally and to the inertia force which is not considered (further discussions in Section 2.4.5).

2.4.4 Stability Formulae of Oumeraci et al (2002)

Based on data from large-scale model tests and the formula of Wouters (1998), Oumeraci et al (2002) proposed a modified formula for GSC-revetments. The main differences from the Wouters formula were the distinction between slope and crest elements and the introduction of a more accurate value for the empirical parameter C_w. For slope elements, Oumeraci et al (2002) proposed:

$$N_{s,slope} = \frac{H_S}{\left(\rho_E/\rho_W - 1\right)\cdot D} < \frac{2.75}{\sqrt{\xi_0}} \qquad (2.20)$$

where N_S is the stability number for slope elements. For crest elements:

$$N_{s,crest} = \frac{H_S}{\left(\rho_E/\rho_W - 1\right)\cdot D} < 0.79 + 0.09\frac{R_c}{H} \qquad (2.21)$$

where R_c is the freeboard of the revetment.

The advantages of this formula are that crest and slope elements can be designed independently. Oumeraci et al (2002) identified for the first time the difference in boundary conditions and acting forces on GSCs placed on the crest and slope of the structure (these differences are again addressed in Section 5.5.7).

2.4.5 Discussion and Implications

Available stability formulae have contributed to the increase of GSC-structures worldwide. However, none of the formulae is based on a deep understanding of the processes affecting the stability of GSCs. Hudson's formula (1956) is derived for rocks and thus based on non-deformable rock material. Bouyze's formula (1990) is valid only for GSCs with infinite lengths, thus unrealistic for sand containers. Wouters' formula (1998) does not account for the contact areas or possible sliding of the elements. The validity of the formula by Oumeraci et al (2002) might be limited to the tested conditions.

A reliable stability formula should be based on the understanding of the involved hydro-geotechnical processes. None of the available formulae satisfies this requirement. Therefore, development of new more reliable stability formula is necessary (see Chapter 6 for details).

2.5 Conclusions Drawn from the Present Knowledge on the Stability of GSCs

Figure 2-18 shows a summary of the state of knowledge available related to the hydro-geotechnical processes associated with the hydraulic stability of GSCs. The most critical processes have been identified: (i) wave-induced pressures on GSCs, (ii) internal movement of sand inside GSCs, (iii) permeability of the structure and (iv) wave-induced deformations of GSCs. However, many uncertainties are still present (Table 2.3) and thus, clarification of the afore-mentioned processes and their interaction is still necessary (refer to Section 2.7).

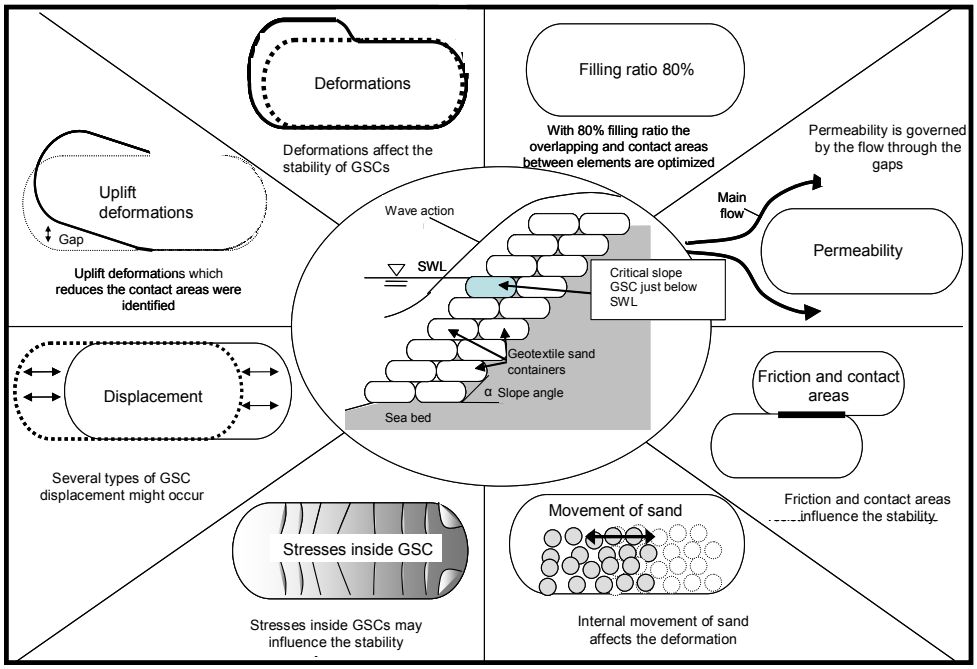

Figure 2-18: Conclusions Drawn from the State of the Art Review Related to the Stability of GSC-Structures

Table 2.3: Conclusions Drawn from Previous Analyses

Process	Conclusions Drawn	Unsolved Issues and Uncertainties
Critical GSCs	Among the slope containers, critical elements are containers lying just below the still water level. Elements at the bottom are the most stable.	Why are containers just below the SWL critical?
Deformation of GSC	Affects the contact area between containers and therefore the hydraulic stability of GSC-revetments	How and when do deformations occur? How do they influence the stability?
Displacement of Slope-GSCs	Displacement is gradual and depends on the amount of deformation of each element. Displacement depends mainly on the wave height acting on the revetment.	How and when do displacements occur? Which are the most relevant types of displacement?
Overlapping and Friction between GSCs	Specifically affect the stability of GSC. Larger overlapping is associated with higher stability of the structure. A filling ratio of 80% provides optimal overlapping. Higher friction between containers also increases the hydraulic stability.	How do the contact areas and overlapping influence the hydraulic stability of the GSCs?
Stresses Inside the GSC	Stresses induced by the loading of the GSCs influence the deformation of the containers during wave action	Do stresses inside the container also substantially influence the stability? Do they also affect the displacement of GSCs?
Internal Movement of Sand Inside the GSC	Internal movement of sand influence the deformation process	How does the internal movement of sand inside the container influence the stability?
Wave Forces on GSC-Structures	Wave induced forces are impossible to obtain accurately from existing formulae for revetments.	How can the wave induced-forces on the GSC be predicted?
Resisting Forces of GSC-Revetments	Resisting forces are mainly determined by the contact area between GSCs and the total normal force acting on this area	How does the interaction between resisting forces among GSCs affect the stability?
Permeability of GSC	The permeability is assumed to be governed by gaps between GSCs.	How can this assumption be verified? How does permeability affect the stability?

2.6 Numerical Models for the Hydraulic Stability of GSCs

Given the complexity of the forces on GSC-structures and considering all the processes affecting the stability, numerical modelling represent appropriate complementary means to cope with all the involved processes and their interactions, so that the laboratory experimental tests can be extended to include further conditions which are impossible to simulate experimentally. For this purpose an extensive investigation on the available numerical models has been performed. As a result, a RANS-VOF model to simulate the wave-induced flow on the GSC-structure and two coupled structural dynamic models (FEM-DEM) were selected as the most appropriate and practical tools to be used.

Developing the numerical models from scratch, considering the time frame of this thesis is not feasible; therefore, available models were analyzed with respect to their appropriateness for GSC-structures, then modified, extended and validated by experimental data.

2.6.1 Hydrodynamic Flow Model

The most appropriate and feasible way to obtain the temporal and spatial distribution of the wave-induced pressures on GSCs is by using the two dimensional RANS-VOF model called "Cobras", which has been developed by the research team of Professor Dr. Philip L F Liu in Cornell University, Ithaca, New York, USA (Lin and Liu 1997, 1998, 1999, 2002 and 2004). However, the flow model (RANS-VOF) cannot simulate the flow through the gaps between GSCs. Therefore, modifications are needed to simulate the flow inside the GSC-structure (see Chapter 5).

2.6.2 Structural Dynamic Model

A coupled **F**inite **E**lement and **D**istinct **E**lement **M**odel (FEM-DEM) represents the most appropriate feasible tool to simulate the stress-deformation and stability of GSC-structures. This can be explained by the fact that large deformations and displacements of the GSCs may occur. Therefore, the FEM simulates the deformations and stresses while the DEM, simulates the displacement and contact identification between GSCs.
The most suitable and affordable coupled FEM-DEM software environment for this purpose was found to be the two dimensional UDEC model (**U**niversal **D**istinct **E**lement **C**ode). However, it needs to be modified, extended and adapted to tackle the specific problem of the deformation and stability of GSC-structures (see Chapter 5)

2.7 Implications for the Objectives and Methodology to be Adopted in this Study

Considering the results which have been achieved in previous sections, additional laboratory and numerical studies are required to clarify the geo-hydraulic processes associated with the stability of GSCs.

2.7.1 Required Laboratory Experiments

The best way to clarify the processes affecting the stability of GSC-structure is by means of well designed process-oriented laboratory experiments and numerical simulations. Table 2.4 shows the experiments needed to clarify the hydro-geotechnical processes that affect the stability of GSC-structures. Several types of model tests with different measurements are being performed with the following main objectives: (i) better understand the flow field and its interaction with a GSC-structure, (ii) quantify the wave-induced pressures and forces on GSCs and (iii) quantify and understand the wave-induced deformation and displacements of GSCs.

Table 2.4: New Model Tests Needed to Furhter Clarify the Hydraulic Processes of GSC-Structures

Experiment Designation	Experimental Facility	Description of the Experiment	Objectives of the Experiment
Wave-induced pressures on GSCs	Wave-flume of Leichtweiß Institute	A container instrumented with pressure gauges well distributed around its surface: built in the wave-flume and subject to wave action	- Derivation of wave-induced pressures around the container - Quantify the influence of wave parameters and wave-induced pressures on stability of GSCs
Internal movement of sand and contact areas	Wave-flume of Leichtweiß Institute	A transparent container with coloured sand as fill material: built in the wave-flume and subject to wave action	- Clarification of influence of movement of sand inside the GSCs on the stability
Interaction between wave induced flow and structure	Wave-flume of Leichtweiß Institute	**P**article **I**mage **V**elocimetry (PIV) technique for visualization and quantification of the flow: implemented at the wave-flume with a GSC-structure	- Clarification of the interaction between wave-induced flow and structures -Acquisition of reliable data for future numerical simulations

Contact areas between GSCs subject to wave action	Wave-flume at Leichtweiß Institute	Uplift and displacements of GSCs in a GSC-structure induced by wave-action: recorded by video techniques	- Quantification of the variation of the contact areas between GSCs during wave action
Effect of breaking wave impact	Wave-flume at Leichtweiß Institute	Instrumented GSC-structure to measure pressures and pressure propagation into the structure as a result of breaking waves	- Quantify the influence of breaking wave impact on the stability of GSCs
Permeability of GSC-structures	Permeability tank and wave-flume at Leichtweiß Institute	GSC-structure subject to steady flow to measure the hydraulic permeability	- Verification of the assumption that the permeability of GSC-structures is governed by the gaps. -Investigate the influence of further parameters such as the GSC-size on the permeability

2.7.2 Required Numerical Simulations

Laboratory investigations are not capable to fully clarify all the involved geo-hydraulic processes and their interaction that are associated with the stability of GSC-structures. Therefore, the laboratory experiments are extended by means of numerical simulations.
Considering that the RANS-VOF model provides the wave-induced pressures on GSCs, the additional processes will be simulated by the coupled FEM-DEM model as shown in Table 2.5. The internal movement of sand inside GSCs, the interface between sand-geotextile and the filling ratio cannot be implemented and simulated within the time frame of this PhD (see Table 2.5). Assumptions, modifications and improvements of the codes were performed to tackle these limitations (see Chapter 5 for details).

Therefore, the models selected in Section 2.6 are coupled to extend the range of the conditions tested in the laboratory.
Coupling of the RANS-VOF model with the FEM-DEM code presents considerable difficulties which cannot be solved within the time frame of this PhD. Therefore, only a "partial coupling" of the models was performed. A detailed description of the models is given in Chapter 5, while the procedure for coupling as shown in Figure 2-19 can be summarized as follows:

(i) The wave-induced pressures and resulting forces on the GSCs as well as further hydraulic boundary conditions are provided by the RANS-VOF model, which are then used as input values for the FEM-DEM codes.

(ii) If the wave-induced forces are large enough to induce change in the shape and/or displacements, the FEM-DEM model will compute the deformations and movement of the containers.

(iii) The initial conditions for the flow model are updated and the wave-induced forces on the elements for the next time step are provided again by the RANS-VOF model.

(iv) The procedure described in steps (i) to (iii) will continue until the GSC is pulled out from its location within the overall GSC-structure.

Table 2.5: Capabilities and Limitations of an FEM-DEM Code for GSC-Structures.

Item/Process	Definition Sketch	FEM MODEL	DEM MODEL
Stress-strain behaviour of geotextile material	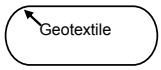	FEM could simulate it by considering a series of "beam" elements with only tensile strength. **Difficult to Implement**	DEM can only simulate homogeneous blocks, but not composite materials. **Not Feasible**
Sand inside the container	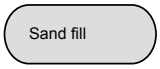	FEM could use an isoparametric quadratic element, which will have same properties as sand. **Feasible**	It would be necessary to create a block with similar soil characteristics of a sand-bag. **Difficult to Implement**
Interface sand-geotextile inside GSC	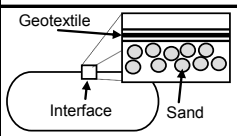	FEM could use a special interface element (unilateral and tangential springs). **Difficult to Implement**	DEM can only simulate homogeneous blocks,but not composite materials. **Not Feasible**
Movement of sand inside the GSC	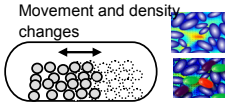	Sand movement and density distribution cannot be simulated. **Not Feasible**	A special feature of DEM can simulate movement of particles, but not inside a GSC. **Not Feasible**
Flow inside the GSC	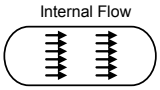	FEM can calculate pore pressures and flow through a porous media. **Feasible**	Can be simulated (even gap-flow) using the special flow-particle scheme of DEM. **Feasible**
Stresses inside the GSC	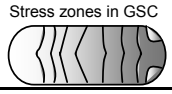	Main advantage of FEM is its stress calculation capability **Feasible**	Can simulate stresses, strain and porosity. **Feasible**
Filling ratio of GSC	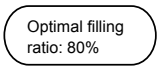	FEM can only simulate continuous media, therefore only filling ratio of 100% can be properly simulated. **Not Feasible**	Variable filling ratio cannot be simulated. **Not Feasible**
Change in shape of GSC (Deformations)	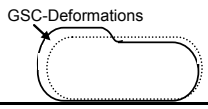	Deformations represent on of the main capabilities of FEM. **Feasible**	Proper simulation but only by supposing a uniform homogeneous GSC. **Limited Feasibility**
Uplift and downlift of GSC during wave action	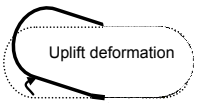	Cannot be properly simulated due to large displacements of the GSCs inducing very large gaps. **Not Feasible**	Can simulate large displacements in various directions of a discontinuous media. **Feasible**
Lateral displacement	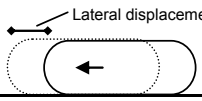	FEM could partially simulate a one direction displacement. **Limited Feasibility**	Very appropriate for small and large displacements. **Feasible**
Simultaneous simulation of multiple elements	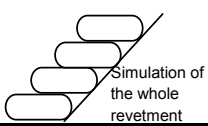	FEM can only simulate one or two discontinuos areas, never a whole structure. **Not Feasible**	Very appropriate, discontinuous medium treated as an assemblage of stiff blocks. **Feasible**
Time step analysis	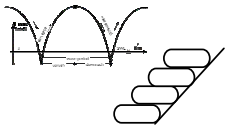	FEM is a structural dynamic model, so time step analysis is easily implemented. **Feasible**	DEM represents a structural dynamic model, so time step analysis is easily implemented. **Feasible**

Note: The feasibility or non-feasibility is related essentially to the time frame of this PhD thesis

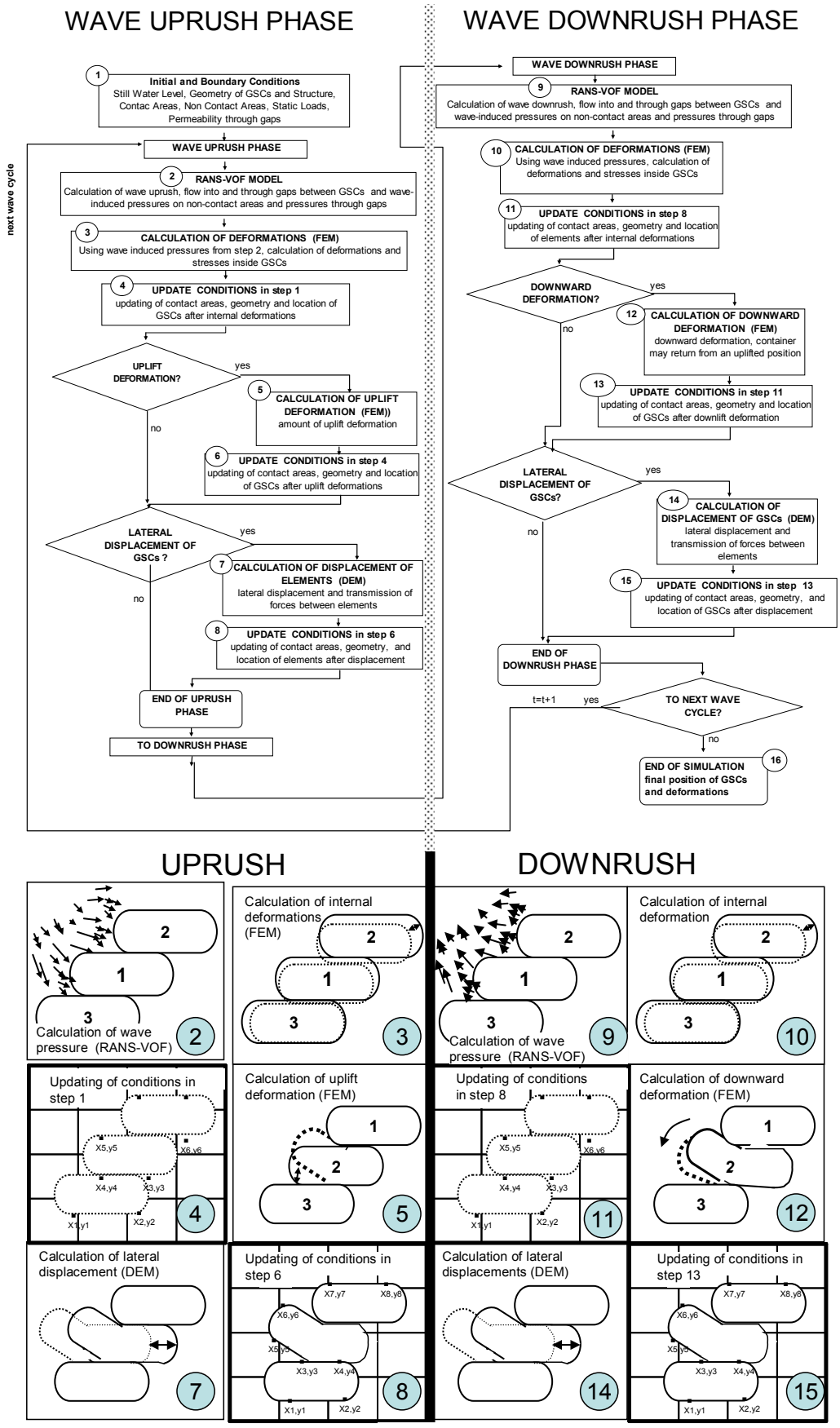

Figure 2-19: Definition Sketch of the Numerical Simulation of GSC-Structures

2.7.3 Specification of Objectives and Methodology

After the review of the state of the knowledge related to the hydraulic stability of GSCs, the objectives and methodology presented in Chapter 1 have been confirmed and specified more precisely as shown in Figure 2-20 and can be summarized as:

(i) Identify, understand and quantify the effect of GSC-deformations and associated processes which affect the hydraulic stability by means of appropriate laboratory experiments.

(ii) Extend the knowledge gained from the laboratory experiments through numerical simulations by using improved validated hydrodynamic and structural dynamic models.

(iii) Develop semi-analytically hydraulic stability formulae that can account for the deformation effects, including the experimental determination of empirical coefficients which cannot be addressed theoretically.

Therefore, this study is divided in the following work packages:

State of the Art Review. Analyses of the specific processes and previous works related to the stability of GSC-structures focusing on: (i) previous GSC-structures constructed worldwide, (ii) analyses on the mechanical properties of geotextile sand containers, (iii) hydraulic processes related to GSC-structures, (iv) available model tests on the stability of GSC-structures, (v) available design formulae for these structures and (vi) identification of most appropriate numerical codes to reproduce and extend the geo-hydraulic processes associated with the stability of GSCs (Chapter 2).

Performance of New Process-Oriented Laboratory Experiments. New experiments consist on: (i) instrumented GSC subjected to wave action to record its wave-induced pressures, (ii) transparent GSC with coloured sand to investigate internal movement of sand inside GSC, (iii) video techniques to visualize the flow field and to quantify the deformations and variation of contact areas of neighbouring GSCs under wave action, (iv) instrumented GSC-structure to measure the propagation of wave-induced pressure under breaking waves, and (v) permeability tests of GSC-structures to quantify the influence of the permeability on the hydraulic stability of GSCs (Chapters 3 and 4).

Flow Model. To further understand the hydraulic processes affecting the stability of GSC-structures, a numerical hydrodynamic model is further developed and validated: (i) adaptation of the flow model to a GSC-structure, (ii) modifications to account for multiple elements in a structure and finally, (iii) the model is adapted to simulate wave-induced flow through the GSCs and through the gaps between neighbouring containers (Chpater 5).

Structural Dynamic Models. A coupled FEM-DEM model is used to simulate the stability of GSC-structures: (i) adaptation of the model to GSC-structures, this includes adapting the model to simulate accurately a complex element as the sand container, where two materials (a geotextile and a sand fill) exist, (ii) modification of the code to account for the deformation of the container as observed in model tests.

"Coupling" of the Two Models. The flow and structural dynamic models are "partially coupled": (i) by synchronizing of the time steps among models and (ii) by sharing information among the models at optimized previously defined time steps (Chapter 5).

Development of Design Formulae for GSC-Structures. Based on both experimental and numerical results, generic stability formulae for GSCs are derived (Chapter 6).

Performance of Model Tests to Derive the Empirical Coefficients for Stability Formulae. Performance of model tests to validate the stability formulae and to derive empirical coefficients needed for the formulae (Chapter 6).

Modifications to the Formulae to Account for the Effect of the Deformations on the Hydraulic Stability. Based on both experimental and numerical results and on the

generic formulae, the formulae are modified to account for the effect of the deformations (Chapter 6).

Conclusions and Future Work. Finally, conclusions of the study, recommendations for the engineering practice and for future research work are presented (Chapter 7).

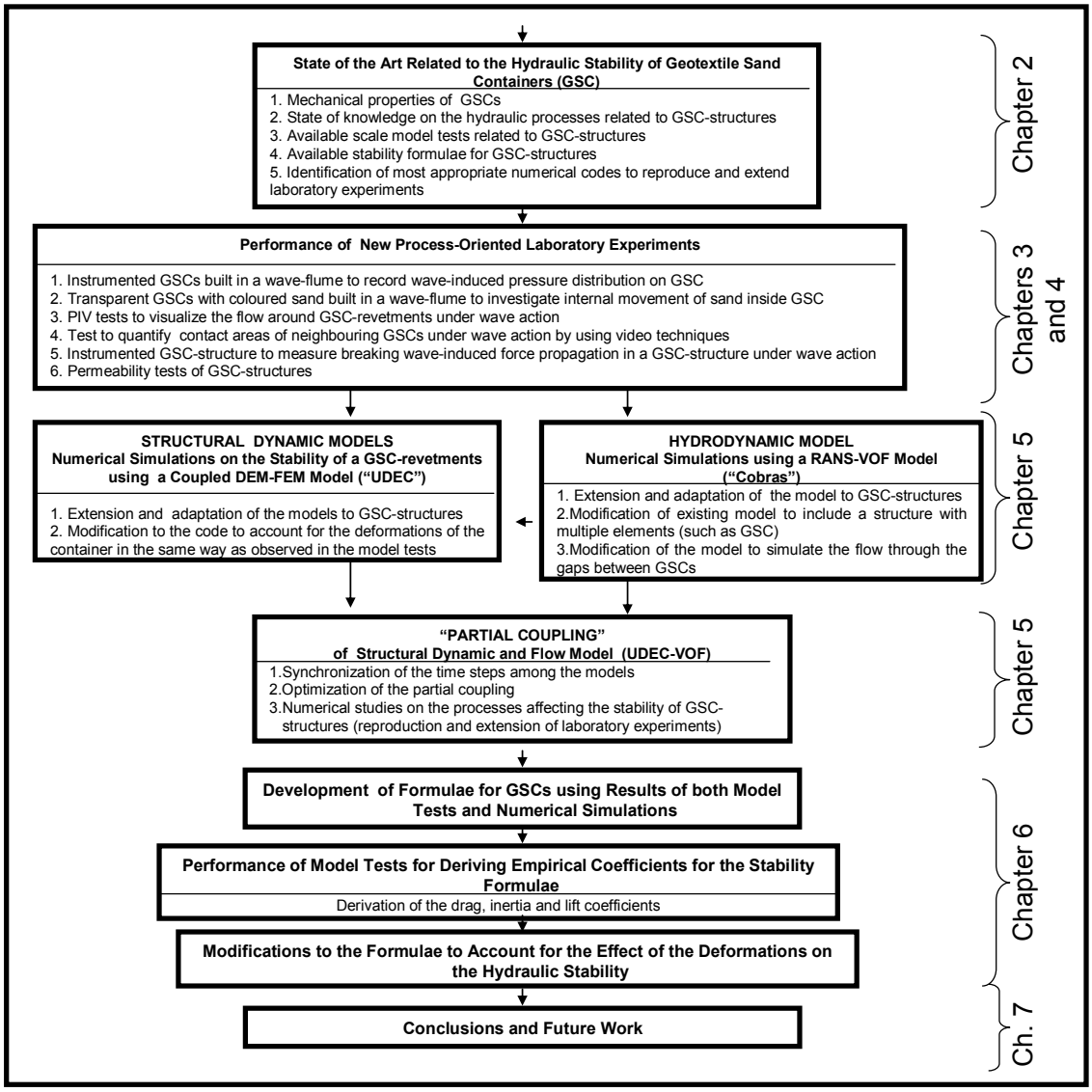

Figure 2-20: Methodology and Work Packages

Chapter 3

Hydraulic Permeability of GSC-Structures: Laboratory Tests and Results

The hydraulic permeability of coastal structures such as revetments, seawalls, breakwaters, etc. significantly affects their hydraulic stability when subject to wave loads (e. g. Hendar 1960, Hudson 1956 and 1961, Pilarcyzck 1998). The higher the permeability of a revetment, the higher its stability. Higher permeability reduces the seepage forces and pressure "build-up" in the structure. Permeability also strongly affects wave transmission and other processes associated with wave-structure interaction (Chao-Lung, 2004; and Muttray and Oumeraci, 2002). In addition, permeability is extremely important for GSC-structures used as flood defences (e.g. dune reinforcement, seawalls, etc.), since it substantially affects the inundation rate. Despite the importance of the permeability for both functional design and hydraulic stability, no information is available for the assessment of the permeability of GSC-structures.

Therefore, comprehensive hydraulic model tests have been performed for the first time to determine the permeability of several types of GSC-structures. Moreover, the stability of GSC-structures with different permeability and different arrangements of the sand containers but with the same geometry is investigated under wave action in the wave-flume of Leichtweiss Institute (LWI). Finally, a conceptual model for the permeability of GSC-structures is proposed.

3.1 Theoretical Background

The two most common approaches to describe the flow through porous structures are those proposed by Darcy and Forchheimer.

If the flow through the structure is **steady and laminar,** Darcy's formula (Lambe 1979) can be used (Figure 3-1):

$$Q = k\, i\, A \qquad (3.\ 1)$$

where Q is the flow rate; k the Darcy's coefficient of permeability (depends on the soil and viscosity of the pore fluid); A is the total cross area of filter sample normal to the flow and i is the hydraulic gradient:

$$i = \frac{\Delta h}{\Delta l} = const \qquad (3.\ 2)$$

with Δh is water head difference, before and after the filter sample ($\Delta h = h_1 - h_2$) and Δl is the length of filter sample.

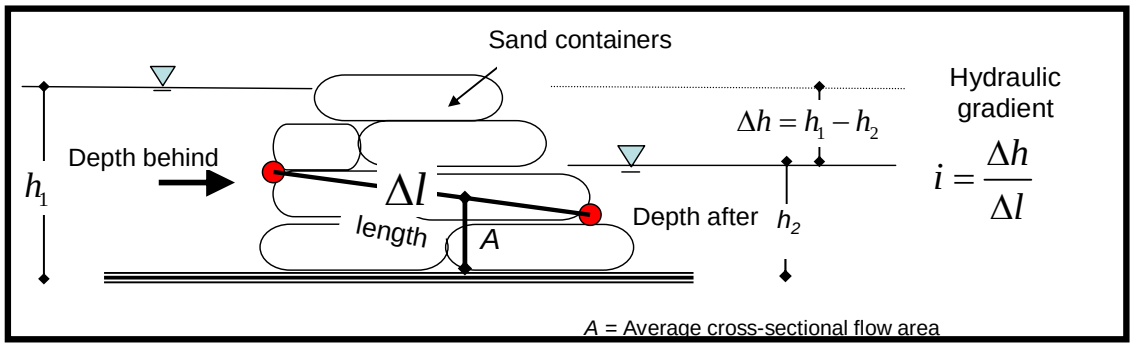

Figure 3-1: Flow through GSC-Structures

If the flow through the structure is **unsteady and turbulent**, i. e. when the Reynolds number *Re* and the inertia of the fluid on the grain particles become important, the Darcy relation can no longer be expressed in a linear form. For these cases the approach suggested by Forcheimer would rather apply (Engelund 1953):

$$i = au + bu^2 \qquad (3.\ 3)$$

where *a* and *b* are two empirical coefficients which can be expressed as:

$$a = \alpha \frac{(1-n)^3}{n^2} \frac{v}{gD^2} \qquad (3.\ 4)$$

$$b = \beta \frac{(1-n)}{n^3} \frac{1}{gD} \qquad (3.\ 5)$$

where *n* is the porosity of the material, *g* is the acceleration of gravity, *D* the diameter of the grain, *v* is the kinematics viscosity of water and α and β are empirical coefficients.

The flow through a GSC-structure is not homogeneous. Turbulent flow is expected to occur in the gaps between containers while laminar flow is expected through the containers. Despite the in-homogeneity of the flow and its unsteadiness, the permeability of GSC-structure will preferably be described by the Darcy permeability coefficient *k*.

3.2. Basic Permeability Tests for GSC-Structures.

Permeability tests were performed to obtain the permeability of various types of GSC-structures and to quantify the influence of parameters such as the size of the containers, the gap size and the mode of placement of GSCs on the permeability.

3.2.1 Experimental Set-Up

The permeability tests were performed by constructing a GSC-structure in a tank (2m wide, 5m long and 1.5m high). The height of GSC-structure is 1.3m, width 2m and variable length depending on the model. The water head difference was kept constant during each test in order to ensure steady flow conditions (Figure 3-2). Several structure geometries and two sizes of sand containers were tested under at least three different hydraulic gradients.

The **measurements** during the model tests focused on the in-outflow (Figure 3-2). These were obtained by means of ADV-devices (**A**coustic **D**oppler **V**elocimeters). The ADVs were located 0.11m from the structure, exactly faced to a gap between containers (closest possible location). The water depths at both side of the structure and the steady flow were also recorded.

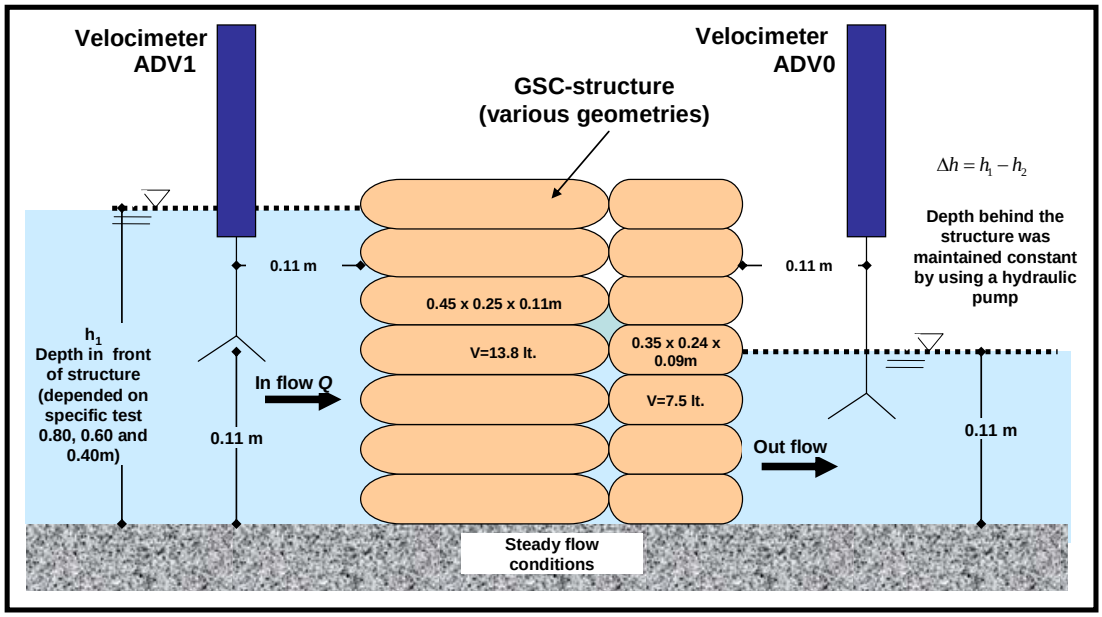

Figure 3-2: Experimental Set-Up for Basic Permeability Tests

The sand containers used in the model tests were made of a nonwoven geotextile with a permeability coefficient of k= 1.1 x 10^{-1} m/s and sand with a median grain size of D_{50}= 0.2mm, density of ρ_s =1800 kg/m^3 and permeability coefficient of approx k= 1.1 x 10^{-4} m/s.

The sand containers have a filling ratio of 80%. Two sizes of sand containers were used (Figure 3-3): (i) 0.45m x 0.28m x 0.11m and (ii) 0.35m x 0.24m x 0.09m.

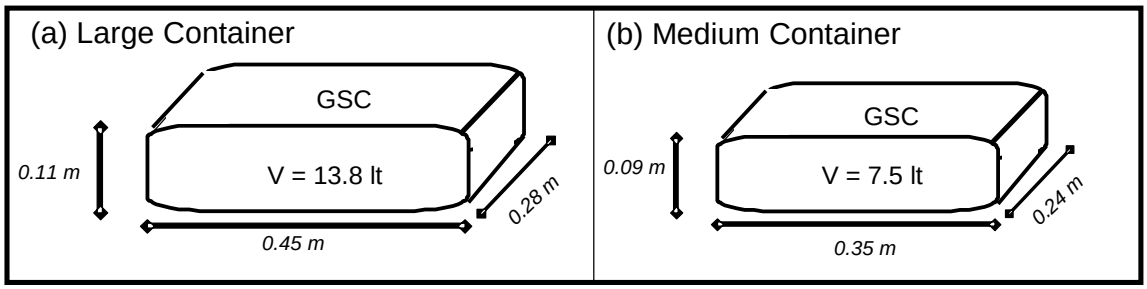

Figure 3-3: Sizes of Containers Used in the Permeability Model Tests

A total of 11 model alternatives were tested (Figure 3-4), which differ from each other by the following items: (i) lay-out of the containers in the arrangement of the structure, (ii) size of containers and (iii) length of the structure.

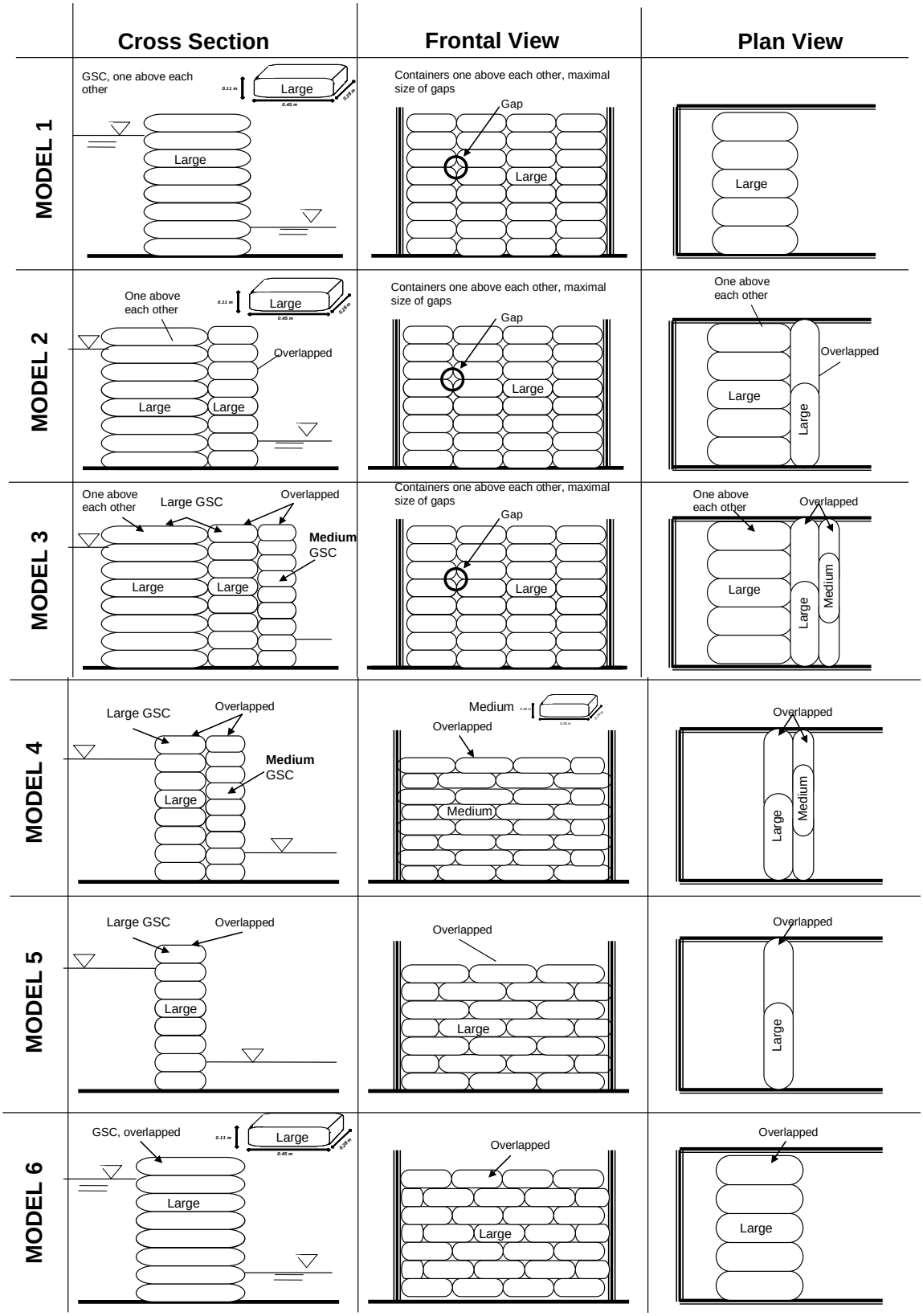

Figure 3-4: Model Alternatives Considered in Basic Permeability Tests (continues on next page)

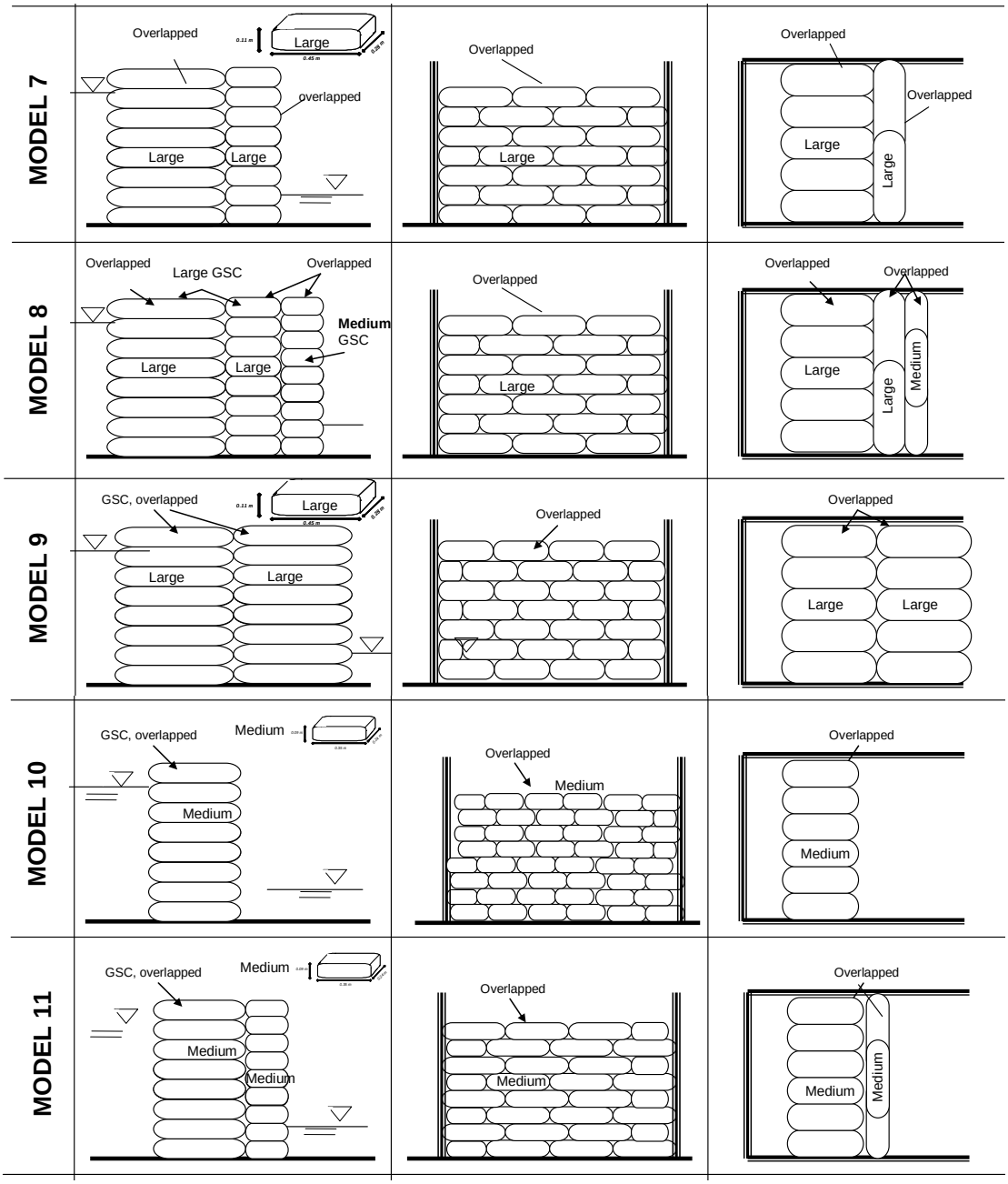

Figure 3-4: Model Alternatives Considered in Basic Permeability Tests (continued from previous page)

Table 3.1: Results of Basic Permeability Tests (see Figure 3-1 for definition of parameters)

Nr	Cross Section	Test No.	Model	h_1 (m)	h_2 (m)	L (m)	Δl (m)	i	A (m2)	Q (m3/s)	Q (l/s)	ADV vel (cm/s)	k (m/s)	**k** AVG (m/s)
1		1a	1	0.47	0.11	0.50	0.59	0.61	0.35	0.0113	11.25	17.23	0.0531	0.050
		1b	1	0.47	0.11	0.50	0.59	0.61	0.35	0.0107	10.74	18.02	0.0507	
		1c	1	0.52	0.11	0.50	0.58	0.71	0.38	0.0139	13.94	xx	0.0520	
2		2a	2	0.43	0.11	0.80	0.87	0.37	0.32	0.0021	2.07	1.79	0.0173	0.020
		2b	2	0.50	0.11	0.80	0.85	0.46	0.37	0.0039	3.88	3.45	0.0232	
		2c	2	0.47	0.11	0.80	0.86	0.42	0.35	0.0032	3.21	3.72	0.0220	
		2d	2	0.42	0.11	0.80	0.87	0.36	0.32	0.0046	4.61	2.77	0.0407	
3	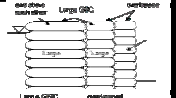	3a	3	0.57	0.11	1.15	1.18	0.39	0.41	0.0018	1.81	2.69	0.0114	0.013
		3b	3	0.42	0.11	1.15	1.20	0.26	0.32	0.0013	1.34	xx	0.0164	
		3c	3	0.45	0.11	1.15	1.20	0.28	0.34	0.0012	1.19	xx	0.0125	
4		4a	4	0.52	0.11	0.56	0.63	0.65	0.38	0.0014	1.37	1.05	0.0056	0.005
		4b	4	0.47	0.11	0.56	0.64	0.56	0.35	0.0013	1.25	1.90	0.0064	
		4c	4	0.40	0.11	0.56	0.66	0.44	0.31	0.0010	1.00	xx	0.0055	
		4d	4	0.54	0.11	0.56	0.63	0.69	0.39	0.0016	1.55	1.29	0.0058	
5	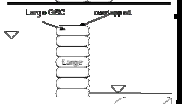	5a	5	0.52	0.11	0.32	0.43	0.95	0.38	0.0029	2.91	7.47	0.0081	0.008
		5b	5	0.46	0.11	0.32	0.45	0.77	0.34	0.0022	2.15	3.29	0.0081	
		5c	5	0.39	0.11	0.32	0.48	0.59	0.30	0.0014	1.39	xx	0.0079	
6	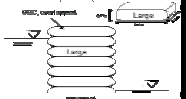	6a	6	0.43	0.11	0.50	0.60	0.53	0.32	0.0028	2.80	5.42	0.0163	0.015
		6b	6	0.52	0.11	0.50	0.58	0.71	0.38	0.0038	3.85	6.15	0.0144	
		6c	6	0.47	0.11	0.50	0.59	0.61	0.35	0.0029	2.93	4.86	0.0138	
7		7a	7	0.55	0.11	0.80	0.85	0.52	0.40	0.0020	1.98	2.51	0.0096	0.009
		7b	7	0.42	0.11	0.80	0.87	0.36	0.32	0.0011	1.09	2.02	0.0096	
		7c	7	0.48	0.11	0.80	0.86	0.43	0.35	0.0023	2.29	2.42	0.0150	
8	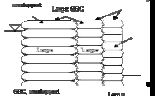	8a	8	0.46	0.11	1.10	1.15	0.31	0.34	0.0011	1.12	xx	0.0107	0.010
		8b	8	0.43	0.11	1.10	1.15	0.28	0.32	0.0009	0.93	1.54	0.0103	
		8c	8	0.48	0.11	1.10	1.14	0.32	0.35	0.0011	1.08	xx	0.0094	
9	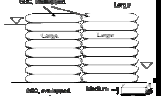	9a	9	0.48	0.11	1.00	1.05	0.35	0.35	0.0019	1.92	3.52	0.0153	0.014
		9b	9	0.42	0.11	1.00	1.06	0.29	0.32	0.0014	1.37	4.69	0.0147	
		9c	9	0.45	0.11	1.00	1.05	0.32	0.34	0.0015	1.54	xx	0.0142	
10	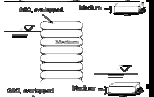	10a	10	0.47	0.11	0.45	0.55	0.66	0.35	0.0019	1.87	xx	0.0082	0.008
		10b	10	0.39	0.11	0.45	0.57	0.49	0.30	0.0012	1.21	2.84	0.0082	
		10c	10	0.52	0.11	0.45	0.54	0.77	0.38	0.0024	2.37	3.01	0.0082	
11	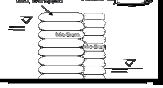	11a	11	0.51	0.11	0.75	0.81	0.50	0.37	0.0013	1.35	3.49	0.0073	0.007
		11b	11	0.48	0.11	0.75	0.81	0.46	0.35	0.0012	1.16	2.87	0.0072	
		11c	11	0.44	0.11	0.75	0.82	0.40	0.33	0.0010	0.98	2.56	0.0074	

AVG= average xx= value not measured

3.2.2 Results of Basic Permeability Tests

The definition of the parameters used and the results of the permeability tests are summarized in Figure 3-1 and Table 3.1, respectively.

To investigate the influence of the size of the gaps between GSCs and other parameters such as the size of container and arrangement of GSCs, a comparative analysis of the results was performed. Detailed information on the analysis is provided by Recio and Oumeraci (2007a).

The main results of the analysis may be summarized as follows:

(i) The flow through GSC-structures essentially reduces to the flow through the size of the gaps; i. e. the size of the gap governs the overall permeability of the GSC-structure.
(ii) The smaller the container, the smaller the permeability coefficient of the structure. This can be explained by the size and distribution of the gaps between containers. A structure made with smaller containers will have more and smaller gaps, subsequently the friction losses of the gap flow will be higher.
(iii) If only the permeability performance of the structure is important, then either longitudinal or transversal GSC-arrangements will provide similar total flows through the structure. However, the hydraulic stability of sand containers under wave action is lower for transversally placed containers than for longitudinally placed GSCs (Oumeraci et al, 2002; Porraz, 1979 and Tekmarine, 1982).
(iv) The permeability of a GSC-structure (and thus the total flow through the structure) is considerably reduced, if there is a second layer of overlapped containers that obstructs the flow coming out of the gaps of the first layer (see Figure 3-4, model 7).
(v) The permeability coefficient of GSC-structures with elements parallel to the flow as commonly used for coastal structures (e. g. Island of Sylt, Germany and Australia in Oumeraci et al, 2002 and Restal et al 2004) may vary from 8×10^{-3} m/s (medium containers) to 1.5×10^{-2} m/s (large containers).

3.3. Further Permeability Tests and Effect of Permeability on Hydraulic Stability of GSC-Structures

After the permeability tests, further tests on the permeability and its effect on the hydraulic stability of coastal structures such as breakwaters and revetments were performed. The geometry of the GSC-structure was the same as used in prototype GSC-structures. However, before starting with new tests, the data derived from the model test by Oumeraci et al (2002) performed in the Large Wave Flume at Hannover (GWK) were first analyzed with respect to the permeability of the tested GSC-structure.

3.3.1 Permeability of GSC-Structure Tested in the Large Wave Flume (GWK)

Model tests were conducted at the large wave flume at Hannover (GWK) in order to investigate the hydraulic stability of GSC-revetments. After the model tests, the time required for the water to flow from behind the structure and the variation of water level before the structure versus time were recorded (Figure 3-5). The entire structure consists of a structure made of 150 litre GSCs founded on a sand slope. The sand slope was covered with a nonwoven geotextile (Figure 3-5). Since the GSC-structure is placed on a sand slope that is also protecting the coastal area, the permeability was calculated for both GSC-structure and sand slope. More details can be found in Recio and Oumeraci (2007a). For this GSC-structure the derived permeability coefficient is $k = 2x10^{-2}$ *m/s* (Figure 3-5).

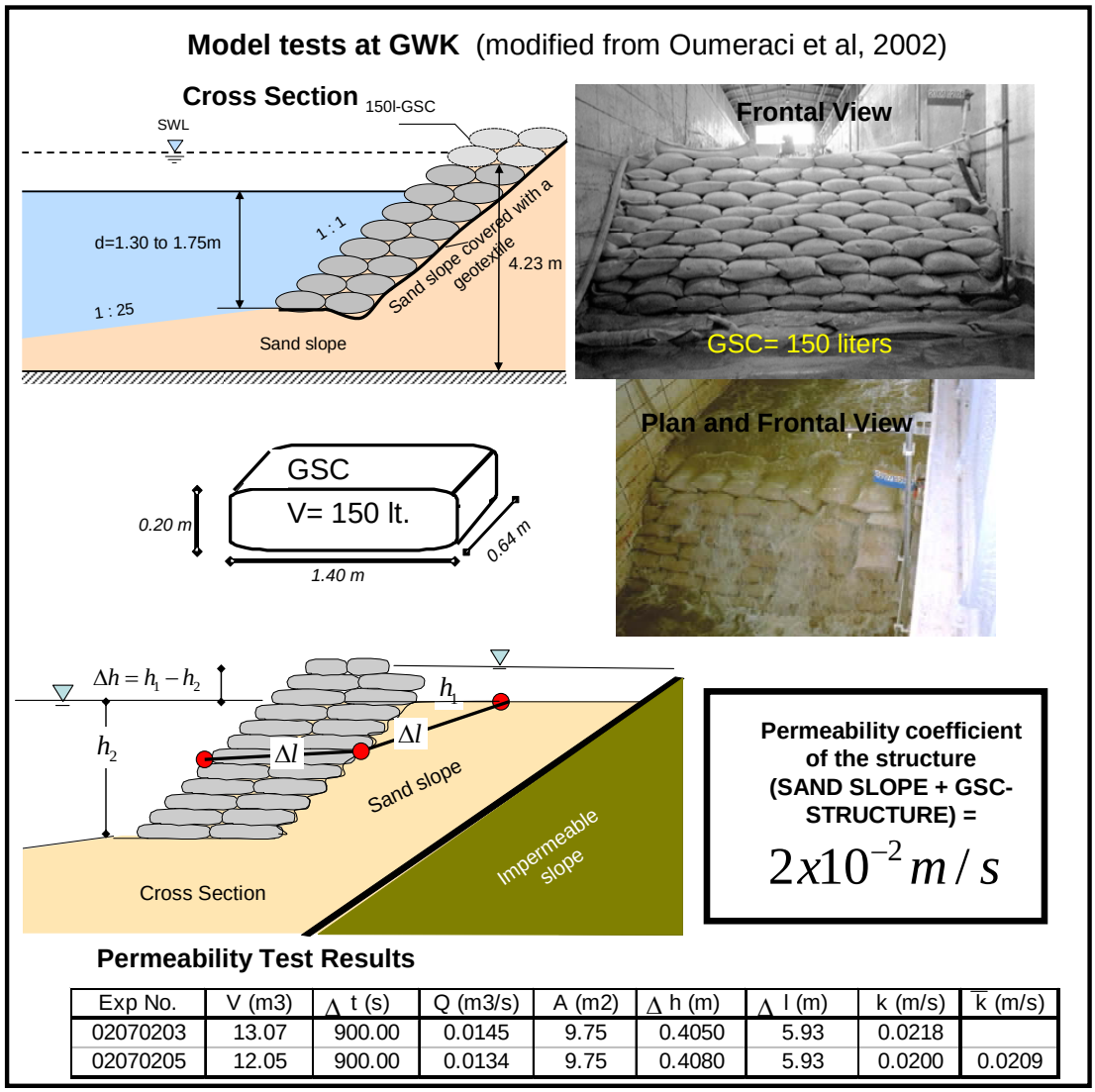

Permeability Test Results

Exp No.	V (m3)	Δ t (s)	Q (m3/s)	A (m2)	Δ h (m)	Δ l (m)	k (m/s)	$\overline{k}$ (m/s)
02070203	13.07	900.00	0.0145	9.75	0.4050	5.93	0.0218	
02070205	12.05	900.00	0.0134	9.75	0.4080	5.93	0.0200	0.0209

Figure 3-5: Results of Permeability Tests of a GSC-Revetment in the Large Wave Flume of GWK (modified from Oumeraci et al, 2002)

3.3.2 Permeability of GSC-Structures in the Wave-Flume of Leichtweiss-Institute

The model set-up was designed in the same way as in the basic permeability tests (see Figures 3-1 and 3-2), with the difference that the tests were performed in the wave flume of LWI (Figure 3-6).

The revetment was made of large sand containers (0.45m x 0.28m x 0.09m), which were also used in the basic permeability tests (Section 3.2). The permeability coefficient is around $k=1.4 \times 10^{-2} m/s$ and is almost the same as the coefficient obtained in models 6 and 9 (Table 3.1).

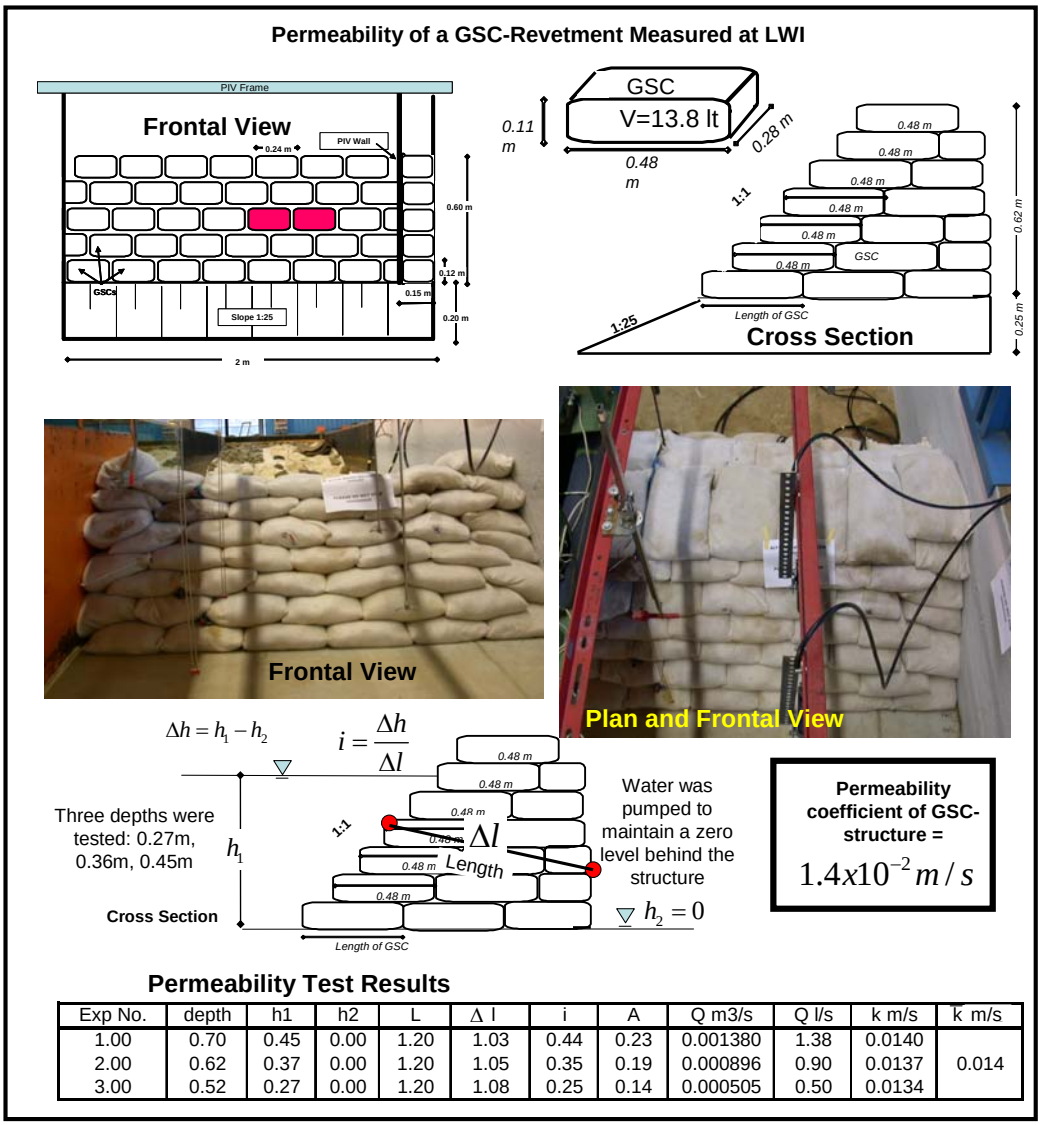

Permeability Test Results

Exp No.	depth	h1	h2	L	Δ l	i	A	Q m3/s	Q l/s	k m/s	k̄ m/s
1.00	0.70	0.45	0.00	1.20	1.03	0.44	0.23	0.001380	1.38	0.0140	
2.00	0.62	0.37	0.00	1.20	1.05	0.35	0.19	0.000896	0.90	0.0137	0.014
3.00	0.52	0.27	0.00	1.20	1.08	0.25	0.14	0.000505	0.50	0.0134	

Figure 3-6: Results of Permeability Tests of a GSC-Revetment Tested at the Wave-Flume of Leichtweiss Institute (LWI)

3.3.3 Effect of the Mode of Placement on the Permeability of GSC-Structures

(a) Experimental Set-Up

The configurations tested in the LWI-wave-flume during the second stage of model tests are shown in Figure 3-7b. A smaller size of containers is used for this purpose (Figure 3-7a). The primary objective of these tests is to investigate the influence of the mode of placement of GSCs on the permeability of the entire GSC-structure.

The structure has a height of approximately 0.81m, and was built with sand containers with the following dimensions: 0.26m length, 0.13m width and 0.052m height (Figure 3-7a). With this size of container, three types of arrangements were tested (Figure 3-7b):

(i) **Model A:** GSC-structure with containers placed longitudinally in the wave-flume.

(ii) **Model B:** GSC-structure with containers placed both longitudinally and transversally (interlaid) in the wave flume in order to block the gaps of the previous layer.

(iii) **Model C:** GSC-structure with the containers placed randomly by dropping them from an elevation of about 1m in the wave-flume.

(iv) **Model D:** A gravel structure with the same geometry as the GSC-structure was also tested for comparison. The gravel structure is made of stones with a diameter of D_{50} = 2.3cm, D_{max}=2.9cm, D_{85}/D_{15}=1.4.

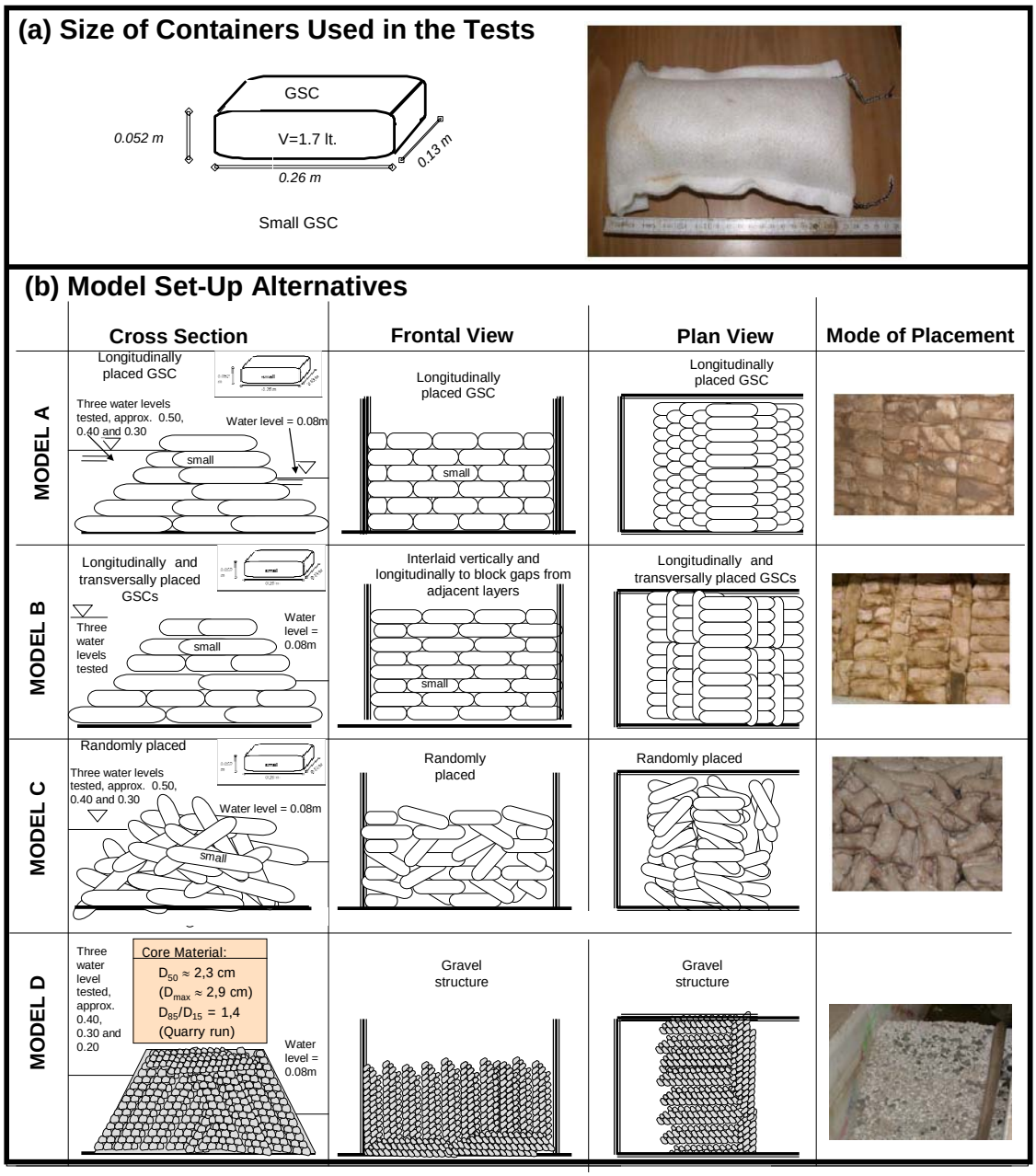

Figure 3-7: Configurations Tested to Investigate the Effect of the Mode of Placement on the Permeability

(b) Experimental Results

The results of the permeability tests are summarized in Figure 3-8. For more details refer to Recio and Oumeraci (2007a).

The structure made of randomly placed containers has the higher permeability coefficient of the three tested GSC-structures, because the probability of the water flowing through the

structure of finding a "direct" way (with large gap size) across the structure is higher than in the other two configurations. The smallest permeability coefficient is expectedly obtained for the containers placed interlaid in a way that the second layer blocks the gaps of the first layer of containers.
Further interesting results is the comparison among the obtained permeability coefficients: the permeability of the sand material ($k=10^{-3}m/s$) is approximately ten times smaller than the permeability of the GSC-structure ($k=10^{-2}m/s$); moreover, the permeability of the GSC-structure ($k=10^{-2}m/s$) is approximately ten times smaller than the coefficient of a gravel structure ($k=10^{-1}m/s$).

Finally, randomly placed sand containers and longitudinally placed containers have similar permeability (randomly placed slightly higher than longitudinally). This can be explained because in the longitudinal containers, the water-flow has a direct way across the structure through the longitudinal gaps. However, these gaps are smaller than the gaps that appear between randomly placed containers.

Model Structure	Description	Darcy's Permeability Coefficient k (m/s)
	Structure made of geotextile sand containers **placed interlaid** blocking the gaps of the previous layer	1.244×10^{-2}
	Structure made of geotextile sand containers **placed longitudinally** to the flow	2.274×10^{-2}
	Structure made of geotextile sand containers **placed randomly**	2.412×10^{-2}
	Structure made of **gravel** (D_{50} = 2.3 cm, D_{max}=2.9cm, D_{85}/D_{15}=1.4).	3.881×10^{-1}

Remark: Permeability of gravel is normally higher than 10^{-2}m/s and permeability of sand is between $1x10^{-3}$ and $3x10^{-3}$m/s.

Figure 3-8: Comparison of Permeability Coefficients with Different Mode of Placement

3.4. Effect of Permeability on the Hydraulic Stability of GSC-Structures

The mode of placement may significantly affect the permeability of a GSC-structure. In the wave-flume of LWI, the same GSC-structures as in Section 3.3. (small containers with same geometry and same size but with different mode of placement and thus different permeability) are tested under wave action to investigate the influence of the permeability and mode of placement on the hydraulic stability.

In the wave-flume each of the three configurations as shown in Figure 3-8 were subject to increasing regular wave heights until the structure collapsed. The wave period was maintained constant (T=2s). Thus, if one structure resisted 100 regular waves of a specific wave height, wave generation will stop, and after 20 minutes the structure was subject to wave action with

another series of higher 100 waves. In the same way, the wave height was increased until the structure collapsed. After collapse, the structure was rebuilt and the experiment with the same wave height was repeated for verification.

Mode of Placement of GSCs	Wave Height (H) (m)	Wave Period (T) (sec)	Water Depth (d) (m)	Hydraulic Stability	GSCs Displaced after Wave Action
Longitudinal 	H = 0.08	T = 2	d =0.50	Stable	0
	H = 0.12	T = 2	d =0.50	Stable	0
	H = 0.16	T = 2	d =0.50	Stable	0
	H = 0.20	T = 2	d =0.50	Stable	0
	H = 0.24	T = 2	d =0.50	UNSTABLE	9
Interlaid 	H = 0.08	T = 2	d =0.50	Stable	0
	H = 0.12	T = 2	d =0.50	Stable	0
	H = 0.16	T = 2	d =0.50	UNSTABLE	38
Random 	H = 0.08	T = 2	d =0.50	Stable	0
	H = 0.12	T = 2	d =0.50	Stable	0
	H = 0.16	T = 2	d =0.50	UNSTABLE	23

Figure 3- 9: Effect of Permeability and Mode of Placement on the Stability of GSC-Structures

The results of the model tests of structures with different mode of placement under wave action are shown in Figure 3- 9. As expected, the structure with the lower permeability showed the lower resistance against wave action. The higher permeability behind the first layer dissipates the pressures behind the structure, thus, providing higher hydraulic stability.

The comparison between containers placed randomly and longitudinally shows that the latter have a higher stability than the randomly placed containers. This is obvious, since only surface piercing structures were tested. Therefore, the displacements started at the slope where the contact areas and the contribution of the weight of neighbouring containers contribute to the hydraulic stability of the GSCs (Figure 3- 10).

This result on the higher stability of longitudinal containers applies only for surface piercing structures, since Grüne et al (2007) and Recio and Oumeraci (2007c), showed that with submerged structures made of GSCs, the critical container is the one placed at the crown of the structure (which has reduced contact areas and no weight contribution from neighbouring containers). More details of these analyses, including the failure mechanisms of randomly placed GSCs, can be found in Recio and Oumeraci (2007a).

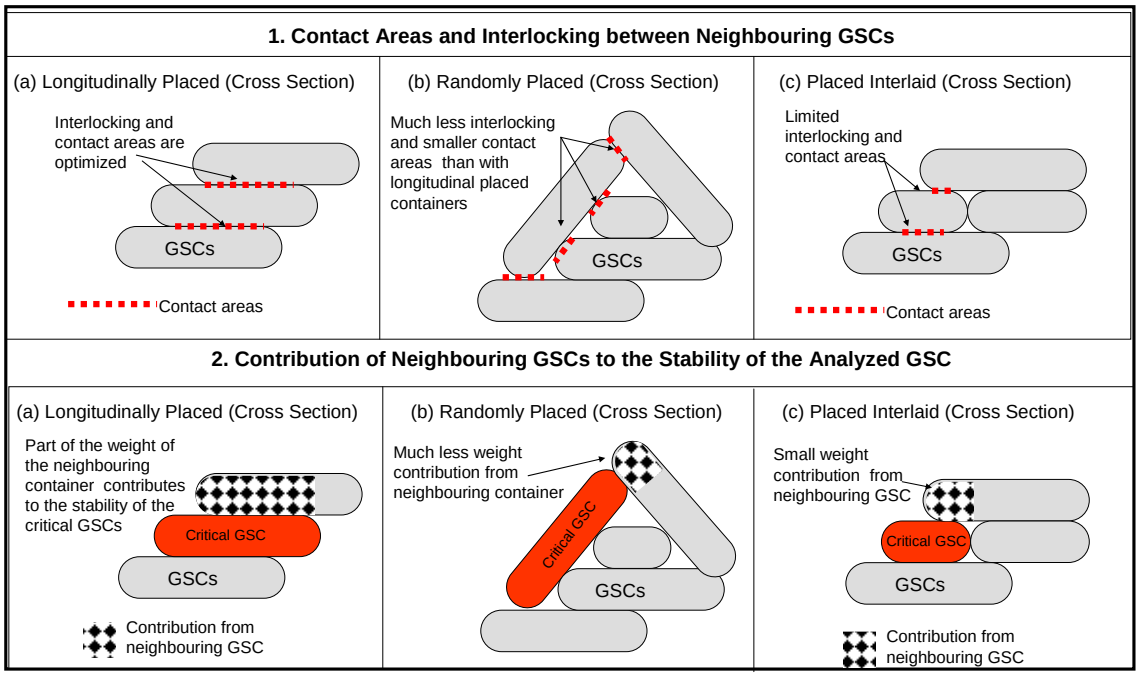

Figure 3- 10: Comparison of Contact Areas and Contribution of Neighbouring GSCs on the Hydraulic Stability between Tested GSC-Structures

3.5. Overall Summary of Permeability Tests

The most important results obtained from the permeability tests described in Section 3.2 to 3.4 are summarized in Figure 3-11, showing that:

a) The permeability of a GSC-structure depends mainly on the size of the gaps. The flow through a GSC-structure is governed by flow through the gaps and thus, the flow through the sand container can be neglected.

b) If no reliable data are available, a permeability coefficient for GSC-structures of $k = 10^{-2}$ m/s would be appropriate.

c) The optimal arrangement to reduce the permeability of a GSC-structure is by blocking the gaps of the fist layer with transversal containers of a second layer (see models 7 and 11 in Figure 3-4 and Table 3.1). With this mode of placement the permeability coefficient is approximately 5×10^{-3} m/s.

d) The mode of placement of the sand containers in a GSC-structure considerably affects the permeability of the structure. Random placing has the highest permeability, but smaller hydraulic stability for surface piercing structures than longitudinally placed containers.

	Cross Section	Size GSC	Permeability k (m/s)	Remarks
MODEL 5	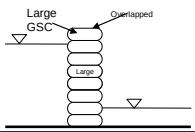	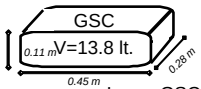 Large GSC	$0.8x10^{-2}$	-Transversal GSC-structures have smaller permeability.
MODEL 6	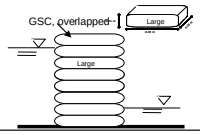	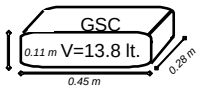 Large GSC	$1.5x10^{-2}$	- One typical structure used for GSC-revetments.
MODEL 7	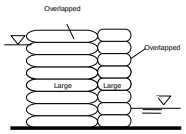	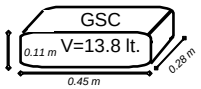 Large GSC	$0.9x10^{-2}$	- Optimal structure if minimal permeability is needed.
MODEL 9	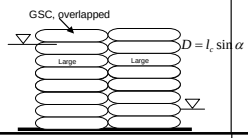	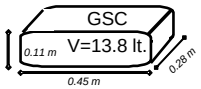 Large GSC	$1.4x10^{-2}$	- Most typical structure used as GSC-revetment.
MODEL 10	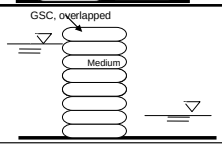	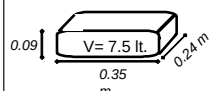 Medium GSC	$0.8x10^{-2}$	-Small containers induce lower permeability.
MODEL 11	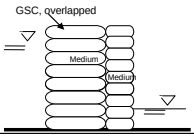	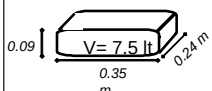 Medium GSC	$0.7x10^{-2}$	-Blocking directly the gaps reduces considerably the permeability.
LWI	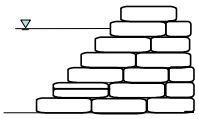	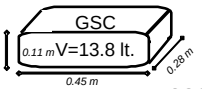 Large GSC	$1.4x10^{-2}$	- GSC-revetments built only with sand containers.
GWK	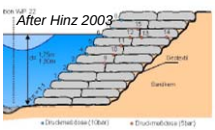	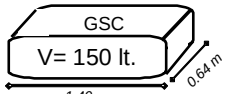 GWK-GSC	$2x10^{-2}$	- This permeability coefficient is for a GSC-structure with a sand slope. Based on data from Hinz and Oumeraci (2002).
MODEL A	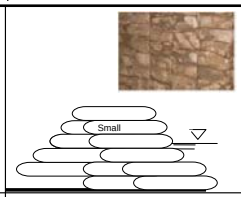	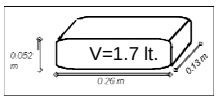 Small GSC	$2.2x10^{-2}$	-Small containers placed longitudinally, higher hydraulic stability than randomly placed for surface piercing structures.
MODEL B	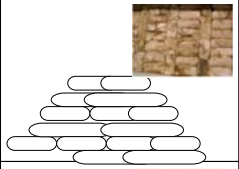	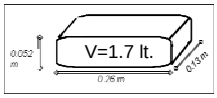 Small GSC	$1.2x10^{-2}$	-Small containers placed longitudinally and transversally, each layer blocking the gaps from previous layer. Lowest stability.
MODEL C		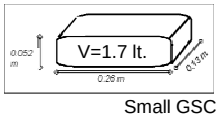 Small GSC	$2.4x10^{-2}$	- Small containers placed randomly, higher permeability but smaller stability compare with longitudinal containers.

Figure 3-11: Summary of Laboratory Results

3.6. Conceptual Model for the Permeability of GSC-Structures

The permeability of GSC-structures has shown to be governed by the gaps between sand containers. Based on this conclusion a conceptual model including the size and shape of the gaps is first proposed. Recommendations are then provided to derive the permeability of GSC-structures based on simple parameters such as the dimensions of the container. More details of the conceptual model and a detailed study of the state of the art on the permeability of porous structures can be found in Recio and Oumeraci (2007a). This study has shown that to date, there is no conceptual model that can be applied directly to the permeability of GSC-structures. The peculiarities of a GSC-structure are, that it has: (i) inhomogeneous materials (GSCs consist of sand and geotextile) and (ii) well defined gaps between GSCs, which govern the flow through the structure.

(a) Assumptions

The following assumptions (Figure 3- 12) are made to derive the conceptual model:

i. The flow through the sand container itself is neglected (impermeable GSCs), so that the permeability of the structure is solely determined by the flow through the gaps.
ii. The gaps among neighbouring containers are considered as triangular pipes which may then be transformed to a hydraulically equivalent diameter.
iii. The Reynolds number of the gap flow is directly related to the size of the gaps.
iv. The size of the gaps is considered constant (in reality, the size of the gaps varies slightly depending on their location in the structure).
v. Flow resistance along the gap (water-geotextile-interface) is constant.
vi. Flow velocities upstream of the structure can be neglected ($v_\infty = 0$). Flow in gaps is only induced by difference of water levels in front and behind the structure.
vii. Only the friction losses along the gap (triangular pipe) are considered, inflow and outflow losses are neglected.

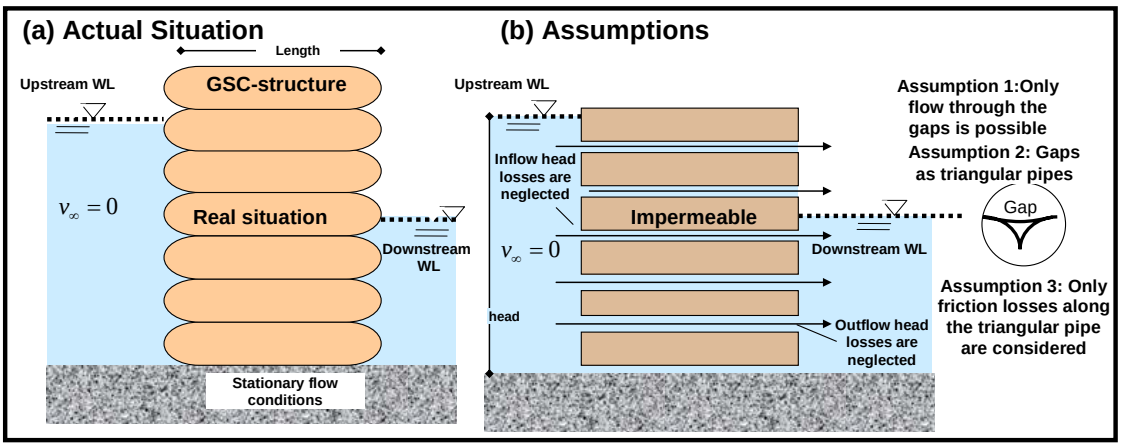

Figure 3- 12: Assumptions of the Conceptual Model

(b) Conceptual Model

Moreover, the GSC-structure is considered two dimensional and divided in three regions (Figure 3-13c) in which energy conservation is maintained:

Zone A: Interface between the upstream flow and the GSC-structure (Figure 3-13c):
The interface between structure and upstream flow where the latter suddenly converges from the open flow to the triangular pipe (gap along the GSC-structure).
The initial velocities at the entrance of each gap of the structure are obtained by assuming that the flow transition is analogous to a sudden pipe contraction, thus, the velocity at the entrance of the gap is induced by the hydraulic gradient at the gap minus the local losses induced by the contraction.
Zone B: Flow through the structure along each of the individual gaps:
Zone B compromises the length of the flow channel from the beginning of the gap to the end of the gap (Figure 3-13c). In this zone, the velocity at the beginning of the gap is equal to the velocity at the end of the gap minus friction losses due to the roughness along the gap.
Zone C: Interface between the structure and the downstream flow:
The interface between the end of the gap and the downstream flow where the flow diverges from the triangular gap-pipe to the open flow downstream (Figure 3-13c). The interface between the GSC-structure and the downstream flow is treated as a simple wave discharge problem where the velocity after the end of the gap is equal as the velocity at the beginning of the gap plus losses.

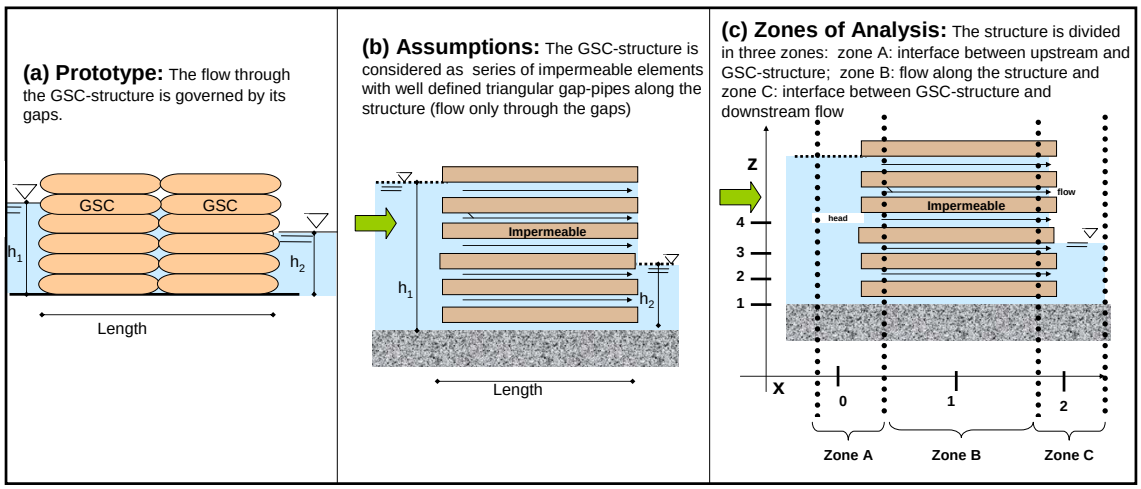

Figure 3- 13: Principle of the Conceptual Model

Thus, considering the afore-mentioned zones, the flow through the gap can be described as:

$$\frac{v_0^2}{2g}+\frac{p_0}{\rho_w g}+z_0-h_0=\frac{v_1^2}{2g}+\frac{p_1}{\rho_w g}+z_1-h_r=\frac{v_2^2}{2g}+\frac{p_2}{\rho_w g}+z_2-h_0=const. \qquad (3.\ 6)$$

where v_i is the velocity at point i (Figure 3-13c), p_i is the pressure at point i, ρ_w is the density of water, h_r is the friction head losses along the gap, h_0 is the inflow and outflow head losses, g is gravity acceleration and z_i (Figure 3-13c) is the height of the measurement point in the direction of gravity.

Recalling the assumptions of the study, where the local losses are neglected, then, equation 3.6 can be re-written as follows:

$$\frac{v_0^2}{2g}+\frac{p_0}{\rho_w g}+z_0=\frac{v_1^2}{2g}+\frac{p_1}{\rho_w g}+z_1-h_r=\frac{v_2^2}{2g}+\frac{p_2}{\rho_w g}+z_2=const. \qquad (3.\ 7)$$

where h_r can be defined as:

$$h_r = \lambda \frac{L}{D_{eq}} \frac{v^2}{2g} \quad (3.\ 8)$$

where L is the length of the gap, D_{eq} is the equivalent diameter of the gap-pipe, v is the velocity in the gap, g is the gravity acceleration and hr is the friction head loss.

The friction factor λ is a function of the Reynolds number Re and influenced by the relative roughness of the pipe k_{fric} / D_{eq}, where k_{fric} is the roughness of the material used in the pipe (in this case, the roughness of the geotextile). The roughness of each material is determined experimentally (refer to Recio and Oumeraci 2007a for typical values of k_{fric}). Reynolds number can be defined as:

$$\mathrm{Re} = \frac{v D_{eq}}{\nu} \quad (3.\ 9)$$

where v is the velocity in the pipe, ν is the kinematic viscosity of water and D_{eq} is the equivalent diameter of the pipe. For a triangular pipe, like the gaps in a GSC-structure, D_{eq} can be defined as:

$$D_{eq} = 4R_h \quad (3.\ 10)$$

where the hydraulic radius R_h can be defined as:

$$R_h = \frac{A}{P} \quad (3.\ 11)$$

where A is the cross area and P is the wet perimeter of the pipe.

(c) Pipe Friction of GSC-Gaps

Equation 3.7 describes the flow of each gap in the GSC-structure. The total flow through the structure is obtained by summing up the flow through individual gaps. However, to solve equation 3.7, the friction factor λ needs to be accurately determined as a function of the flow regime:

(i) For laminar pipe-flow, Poiseuille's equation is applied (Re<2320):

$$\lambda = \frac{64}{\mathrm{Re}} \quad (3.\ 12)$$

(ii) For turbulent flow three equations are proposed, depending on how developed the turbulent flow is (Oumeraci 1999):

For hydraulic smooth regime $\left(\mathrm{Re} \frac{k_{fric}}{D_{eq}} < 65 \right)$:

$$\lambda \approx \frac{0.309}{(\lg \mathrm{Re} - 0.845)^2} \quad (3.\ 13)$$

For the transition regime ($65 < \mathrm{Re} \frac{k_{fric}}{D_{eq}} < 1300$):

$$\frac{1}{\sqrt{\lambda}} = 2.0 \cdot \log\left(\frac{2.51}{\mathrm{Re}\sqrt{\lambda}} + \frac{k_{fric} / D_{eq}}{3.71} \right) \qquad (3.\ 14)$$

and for fully turbulent flow ($\mathrm{Re}\frac{k_{fric}}{D_{eq}} > 1300$):

$$\lambda \approx \left(\frac{1}{2 \cdot \log\left(\frac{3.71}{k_{fric} / D_{eq}} \right)} \right)^2 \qquad (3.\ 15)$$

The only unknown for determining the flow through each gap in a GSC-structure and thus, through the whole GSC-structure is the pipe friction factor λ, which for turbulent flows requires the knowledge of the roughness of the gap-pipe k_{fric} (roughness of geotextile).
The roughness k_{fric} can be derived from the data obtained from the basic permeability tests (Section 3.1). In this way, the roughness k_{fric} of the gap-pipe will implicitly account for other effects that are not considered in the conceptual model such as variations of the pipe-gap, flow through the containers itself, etc.

Using the permeability test results, the relative-roughness of GSC-gaps k_{fric}/D_{eq} and thus, the pipe friction factor λ are determined iteratively (Figure 3-14). For turbulent flows, the relative roughness of GSC-gaps is found to be around k_{fric}= 0.6mm. The value is plausible, if compared with the values of known materials. More details on the derivation of the roughness and typical roughness values of other materials can be found in Recio and Oumeraci (2007a).

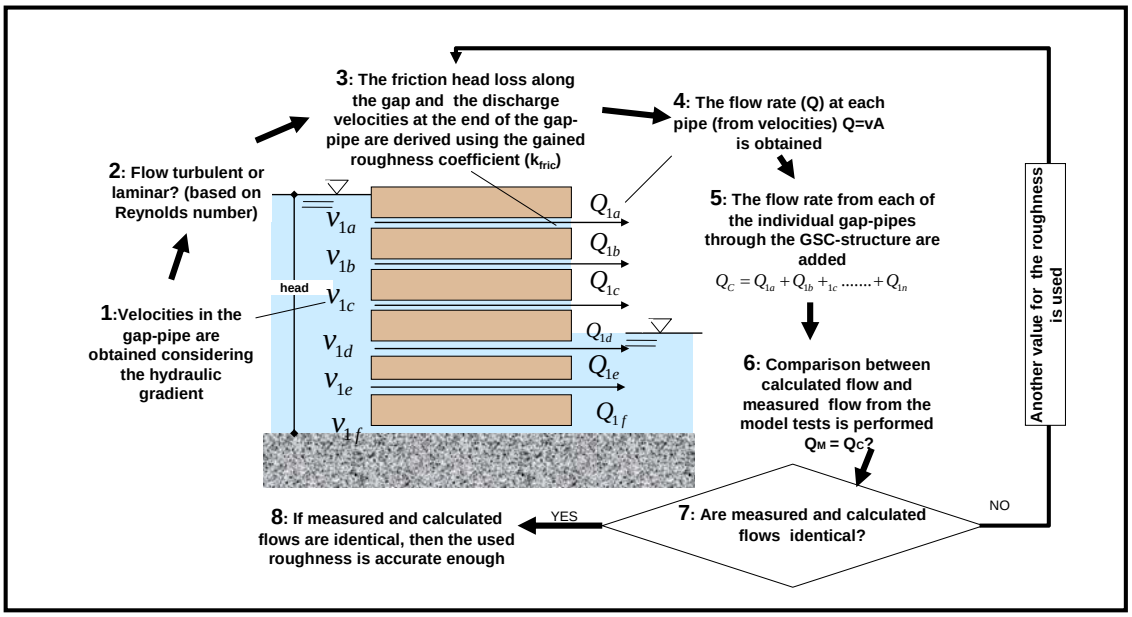

Figure 3- 14: Iterative Procedure to Determine the Roughness k_{fric} of Gap-Pipes in GSC-Structures

d) Validation of the Conceptual Model

To validate the proposed conceptual model and the derived roughness k_{fric} for GSC-pipe-gaps, the results of the permeability tests of Sections 3.2 and 3.3 are compared with calculated results obtained by using the conceptual model (Table 3.2).

The difference between calculated and measured results depends on the type of structure being compared: (i) for longitudinal placed containers, measured and calculated results vary from 1% to 48%; (ii) for interlaid containers from 0% to 33%; (iii) for GSC-structures the variation depend on the size of the container. For large containers, the agreement is within 32%. Moreover, for small containers (1.7 lt.) (randomly and longitudinal placed GSCs) the agreement is not good, however, results are always in the same order of magnitude. The reason for the large disagreement between measured and calculated results for small containers might be due to the very small size of the gaps between small containers (less than 1cm). With such a small gap-size, the difference of flow velocities along the gap and velocity through the container itself are not so large. Therefore, the assumption that the flow is governed only by the gaps is no longer valid.

Table 3.2: Comparison between Measured and Calculated Permeability Coefficients (see also Table 3.1)

Nr.	Structure	Test No.	Model	h1	h2	MEASURED		CALCULATED		Mes/Cal	
			Model	(m)	(m)	k m/s	k AVG	k m/s	k AVG		AVG
4	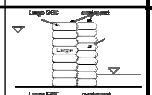	4a	4	0.52	0.11	0.0056		0.0068		0.820	
		4b	4	0.47	0.11	0.0064	0.005	0.0064	0.007	1.005	0.769
		4c	4	0.40	0.11	0.0055		0.0063		0.873	
		4d	4	0.54	0.11	0.0058		0.0061		0.949	
5	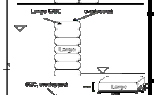	5a	5	0.52	0.11	0.0081		0.0052		1.560	
		5b	5	0.46	0.11	0.0081	0.008	0.0048	0.005	1.693	1.529
		5c	5	0.39	0.11	0.0079		0.0057		1.386	
6	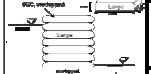	6a	6	0.43	0.11	0.0163		0.0143		1.137	
		6b	6	0.52	0.11	0.0144	0.015	0.0146	0.014	0.983	1.059
		6c	6	0.47	0.11	0.0138		0.0136		1.017	
7	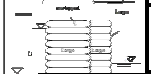	7a	7	0.55	0.11	0.0096		0.0081		1.185	
		7b	7	0.42	0.11	0.0096	0.009	0.0101	0.009	0.953	1.000
		7c	7	0.48	0.11	0.0150		0.0088		1.705	
8	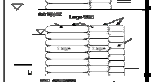	8a	8	0.46	0.11	0.0107		0.0071		1.512	
		8b	8	0.43	0.11	0.0103	0.010	0.0085	0.008	1.210	1.333
		8c	8	0.48	0.11	0.0094		0.0069		1.362	
9	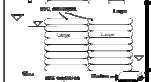	9a	9	0.48	0.11	0.0153		0.0193		0.794	
		9b	9	0.42	0.11	0.0147	0.014	0.0196	0.020	0.748	0.718
		9c	9	0.45	0.11	0.0142		0.0196		0.724	
10		10a	10	0.47	0.11	0.0082		0.0045		1.823	
		10b	10	0.39	0.11	0.0082	0.008	0.0053	0.005	1.554	1.633
		10c	10	0.52	0.11	0.0082		0.0049		1.673	
11		11a	11	0.51	0.11	0.0073		0.0079		0.923	
		11b	11	0.48	0.11	0.0072	0.007	0.0070	0.007	1.024	0.938
		11c	11	0.44	0.11	0.0074		0.0075		0.984	
GSC		GSC1	gsc	0.45	0.00	0.0140		0.0198		0.707	
		GSC2	gsc	0.36	0.00	0.0137	0.014	0.0200	0.020	0.685	0.687
		GSC3	gsc	0.27	0.00	0.0134		0.0200		0.670	
Ran	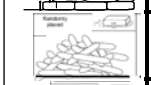	Random1	ran	0.36	0.08	0.0245		0.0788		0.311	
		Random2	ran	0.50	0.08	0.0266	0.024	0.0788	0.079	0.338	0.309
		Random3	ran	0.65	0.70	0.0219		0.0788		0.278	
Int	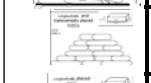	Interlaid1	inter	0.63	0.06	0.0110		0.0450		0.244	
		Interlaid2	inter	0.68	0.06	0.0123	0.011	0.0480	0.047	0.256	0.243
		Interlaid3	inter	0.50	0.05	0.0110		0.0480		0.229	
Lon	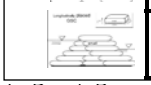	Longitu1	lon	0.50	0.05	0.0148		0.0788		0.188	
		Longitu2	lon	0.64	0.05	0.0192	0.019	0.0788	0.079	0.244	0.240
		Longitu3	lon	0.36	0.05	0.0228		0.0788		0.289	

k= Darcy's Permeability Coeff; Measured = Permability Tests; Calculated= Conceptual Model; AVG=average

Remark: For structures made of interlaid GSCs (i. e. models 7, 8, 11), the conceptual model considered the number and size of gaps of the smallest layer (in plan-view)

3.7 Procedure for the Assessment of the Permeability of GSC-Structures

A procedure to determine the Darcy's permeability coefficient of GSC-structures is proposed according to the following steps (Figure 3-15):

i. Count the number of gaps, measure its size and measure its position in the structure (hydraulic head on each of the gaps). If this information is not available, the procedure explained in Recio and Oumeraci (2007a) can be used, in which the size and number of gaps per square meter of the GSC-structure (in front view) can be derived. Two gaps per container. The hydraulic diameter of each gap is equal to $0.16h_{GSC}$, where h_{GSC} is the height of the filled container.

ii. Calculate the hydraulic head at the entrance of each gap and consider the gap as a triangular pipe. Since the head is the difference between the water level behind and after the structure, and the water level up and down stream of the structure is unknown, the head can be calculated by assuming that the water level downstream is zero. This assumption might over predict slightly the permeability of the structure.
iii. Determine the velocity at the entrance of the gap (Bernoulli's equation).
iv. Determine, whether the flow in the gap is turbulent or laminar.
v. For laminar flow, calculate the pipe-friction factor λ using equation 3.8.
vi. For turbulent flow, calculate the friction factor λ using a roughness value of k_{frc}=0.6mm (k_{fric}=0.0006m) and equation 3.13, 3.14 or 3.15 depending on the flow regime.
vii. Calculate the total friction head loss at each of the individual gap-pipes, using equation 3.8.
viii. Obtain the velocities at the end of the pipe-gap (Bernoulli's equation) and thus, the total flow in each pipe.
ix. Sum up the flow in each of the pipe-gaps to obtain the total flow through the structure.
x. Calculate the permeability coefficient of the structure by using equation 3.1

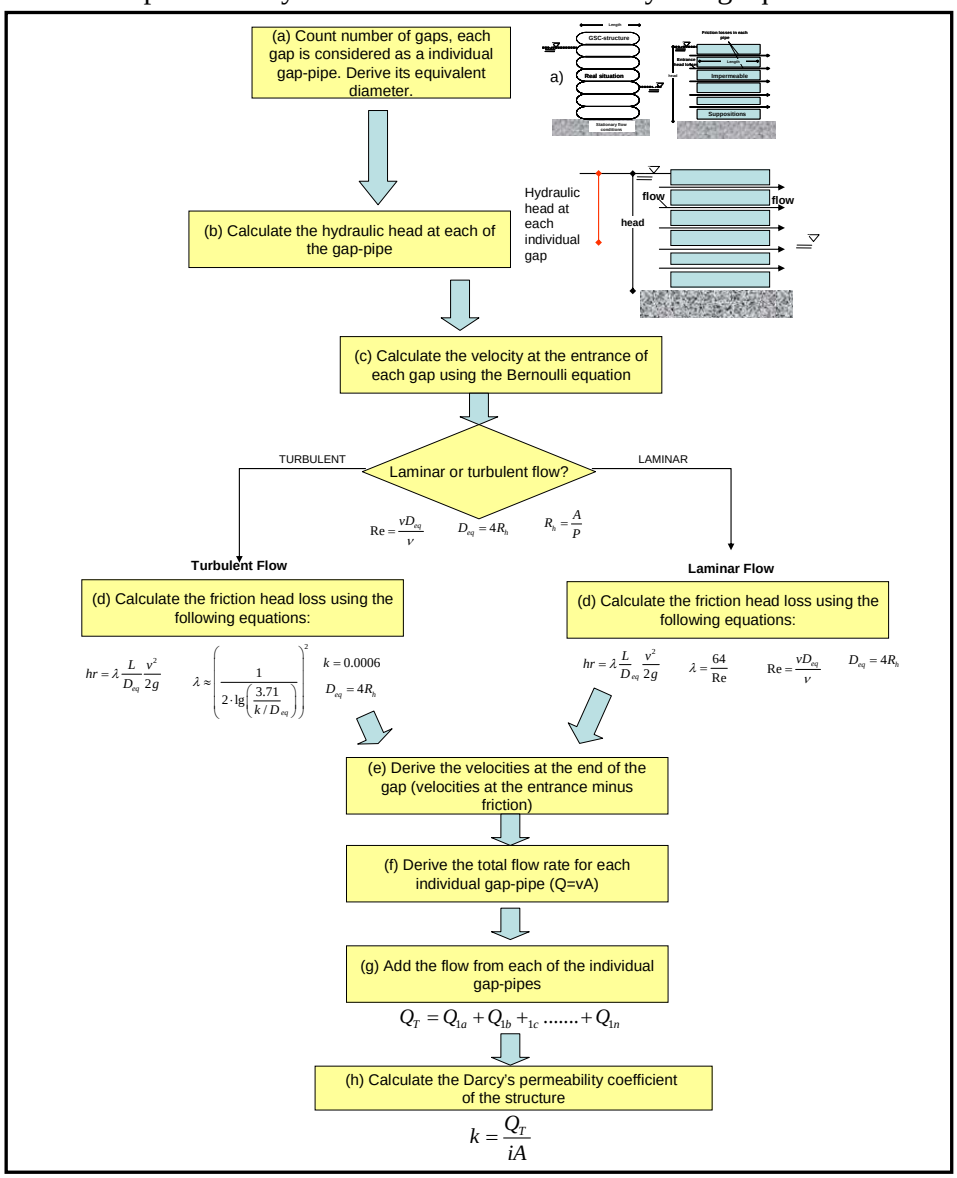

Figure 3- 15: Procedure for the Determination of the Darcy's Permeability Coefficient for GSC-Structures

A “MatLab” programme, which allows to determine the permeability of a GSC-structure based on parameters such as the size of the container, the water level upstream and dimensions of the structure, is given in Recio and Oumeraci (2007a).

Limitations of the Conceptual Model:

(i) Due to the limitations of the model tests, only Reynolds numbers between $10^4<Re<10^5$ were used. Therefore, higher Reynolds numbers might affect the accuracy of the conceptual model.

(ii) This procedure should be used for preliminary assessment only, permeability tests should be performed when very accurate permeability coefficients are needed.

3.8. Summary and Concluding Remarks

Recalling that the filling ratio inside the sand containers was always around 80%, the main results achieved in this Chapter can be summarized as follows:

(i) The permeability of a GSC-structure depends mainly on the size of the gaps. The flow through a GSC-structure is governed by the flow through the gaps and thus, the flow through the sand container can be neglected.

(ii) If no reliable data are available, a permeability coefficient for GSC-structures of $k=10^{-2}$ *m/s* would be appropriate.

(iii) The optimal arrangement to reduce the permeability of a GSC-structure is by blocking the gaps of the first layer with transversal containers of a second layer (see models 7 and 11 in Figure 3-4 and Table 3.1). With this mode of placement the permeability coefficient is approximately $k=5 \times 10^{-3}$ *m/s*.

(iv) The mode of placement of the sand containers in a GSC-structure considerably affects the permeability of the structure. Random placing has the highest permeability, but smaller hydraulic stability for surface piercing structures than longitudinally placed containers.

(v) A simple conceptual model is proposed (Section 3.5), which can be used to approximately estimate the permeability of GSC-structures.

(vi) The pipe-friction roughness was derived from the experiments and found to be around k_{fric}=0.6mm.

Chapter 4

Processes Affecting the Hydraulic Stability of GSC-Structures: Experimental Studies and Results

The processes that affect the deformations and stability of GSC-structures are experimentally investigated by means of several types of hydraulic model tests.
The primary objective of this chapter is to summarize the results obtained from these tests. A detailed description of the experimental results and analyses can be found in Recio and Oumeraci (2005b, 2005c, and 2006b), Gemme (2005) and Burg (2006). The following processes were investigated: (i) wave-induced loads on the sand containers, (ii) wave induced flow on GSC-structures, (iii) internal movement of sand in the containers and its effect on the stability, (iv) variation of contact areas among neighbouring GSCs under wave action, (v) types of displacement of GSCs in a GSC-structure and finally (vi) the effect of the deformation on the stability of GSC-structures.
Based on the experimental results a better understanding of the processes which affect the hydraulic stability of the structure has been achieved, including the effect of the deformations of the sand containers and their interaction.

4.1 Experimental Set-Up and Procedure

The model tests were performed in the wave flume of Leichtweiss Institute. At one end regular and irregular waves were generated. At the other end a structure made with geotextile sand containers was built (Figure 4-1a).
The 2m-wide flume was divided in two sections (Figure 4-1b). In the first section at the glass window, PIV measurements of the wave-induced flow are performed, using the large-scale PIV system proposed by Bleck and Oumeraci (2004). The main characteristics of the PIV set-up are summarized in Figure 4-2. The general PIV characteristics consisted in a measurement flow area of 2 x 1 meters, ("PIV-section") lighted with halogen lamps and using seeding particles having approximately the same density as water. The common commercially available PIV-system with laser-light could not be used because, a "PIV-section" of only $0.25m^2$ section (instead of the $2m^2$ with white light) was possible.
Inside the "PIV-section", a single column GSC-structure was installed (Figure 4-1c) and subject to different wave conditions. Over the "PIV-section" two vibrating trays were constructed, from where the amount of seeding particles in the flow was controlled. To visualize the flow, the "PIV-section" was illuminated using halogen lamps and the flow was recorded using a CCD-chip-camera (DMP-60-H13). This camera and the PIV section were covered with a black textile "tent" to avoid disturbance from other light (and noise) sources. After the images were recorded, the "DaVis PIV-software" (DaVis 1999) was applied to process velocity vectors (Figure 4-2).
In addition, a permeable transparent container was filled with coloured sand and placed in the structure to investigate the sand movements inside the container (Figure 4-1a). The sand movements were recorded using digital video cameras.
In the other section, adjacent to the "PIV section", pressure measurements on instrumented container are performed to record wave-induced loads (Figure 4-3). This instrumented container was placed at different elevations in the structure to investigate the influence of the

location of the GSC with respect of the still water level on the wave-induced pressures. Then, by integrating the pressures around the containers, the total wave-induced forces and moments were derived (Figure 4-3).

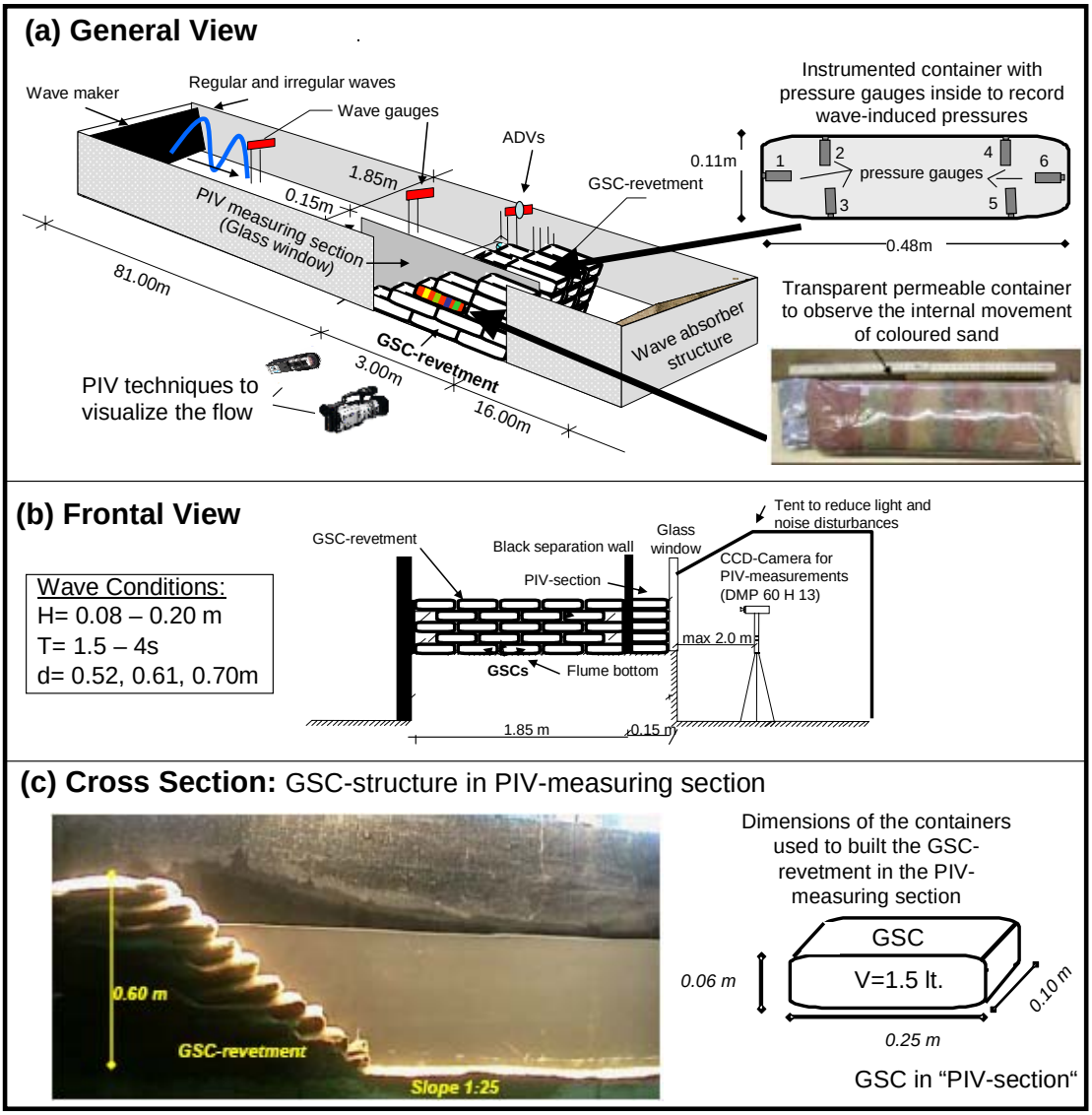

Figure 4-1: Experimental Set-Up in the LWI-Wave-Flume

Surface elevations are recorded in front of the structure and along the flume using common resistance type wave gauges (Figure 4-4). The wave gauges directly in front of the structure are combined with pressure cells and ADV-probes (Acoustic Doppler Velocimeters) in order to measure the different energy components simultaneously. In addition, ADV-probes have been used to validate PIV-measurements (Figure 4-11). The structure is also instrumented with four additional pressure gauges on its seaward face to record wave-induced pressure distribution (Figure 4-4).

The GSC-structure was subject to both regular and irregular wave trains with wave heights varying from 0.08m to 0.20m and wave periods from 1.5s to 4s by using three constant water depths (0.52m, 0.61m and 0.70m).

More details on the experimental set-up can be found in Recio and Oumeraci (2005b, and 2006b).

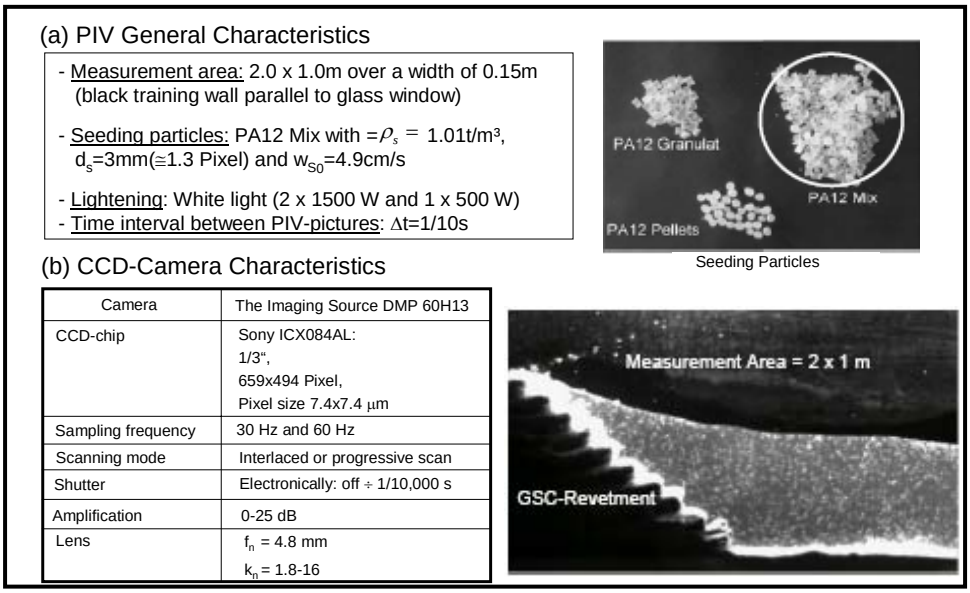

Figure 4-2: Main Characteristics of PIV-Set-Up (modified from Bleck and Oumeraci, 2004)

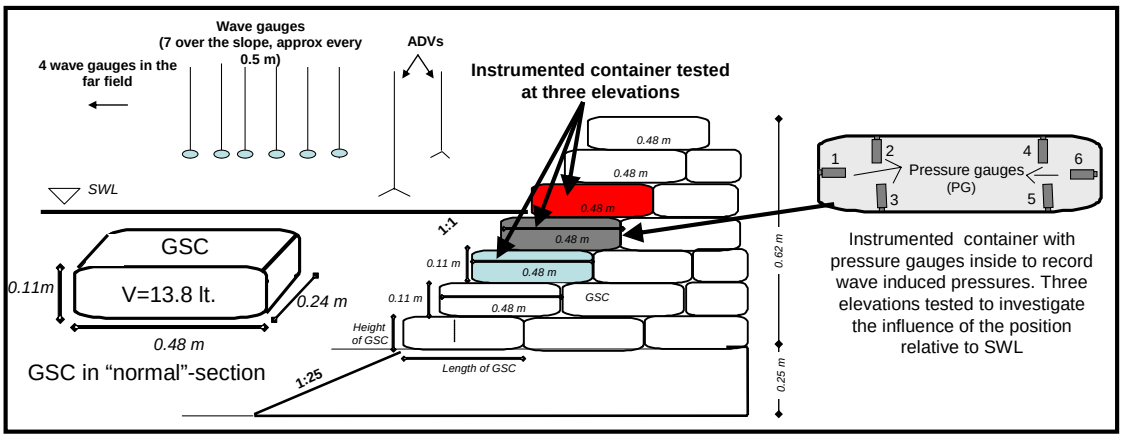

Figure 4-3: GSC-Structure in the Wave-flume (adjacent to PIV-measuring section)

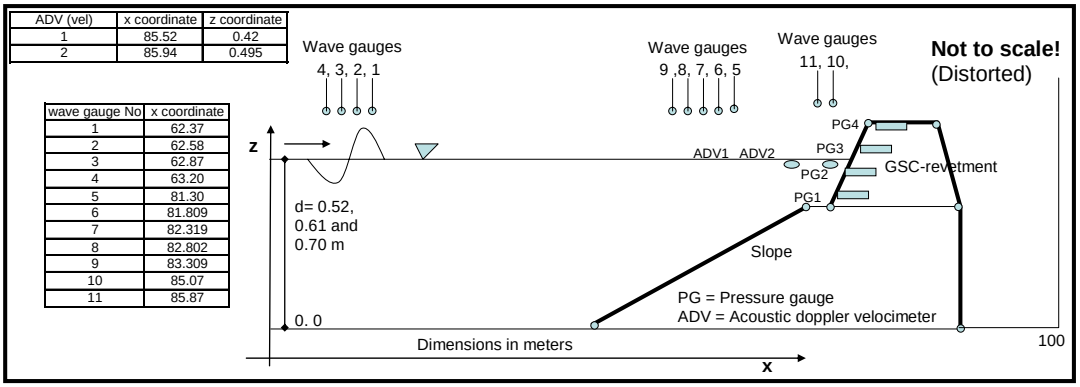

Figure 4-4: Location of the Measurement Devices

4.2 Wave Load on Instrumented Sand Container and on GSC-Structure

4.2.1 Wave-Induced Pressures and Forces on Instrumented Container

Among the three tested elevations of the instrumented container, the largest wave-induced pressures are recorded at the container placed just below the still water level (SWL). For all three locations, the temporal development over each wave cycle of the pressure distribution around the container as well as the resulting wave-induced force and overturning moment have been determined (Recio and Oumeraci, 2005b, and Burg, 2006), showing that the most critical situation for the hydraulic stability of the structure clearly occurs during wave downrush. Most critical is the GSC that is placed just below the still water level (Position 2 in Figure 4-5).

The critical area for the stability of surface piercing GSC-structure is just below SWL. This is due to the fact that wave up and downrush velocities in front and inside the GSC-structure are different, thus, inducing a "build-up" of the hydraulic gradient inside the structure which has a maximum value at the beginning of downrush at the area just below SWL (Figure 4-6). More details on the interaction of wave-induced forces and critical area in a GSC-structure are discussed again in Chapter 5 (Section 5.5.4).

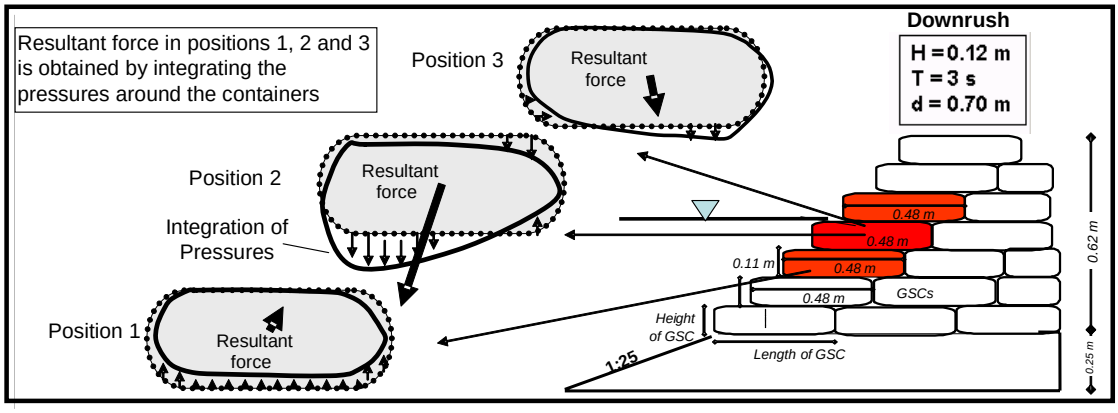

Figure 4-5: Wave-Induced Loads on Instrumented Sand Container

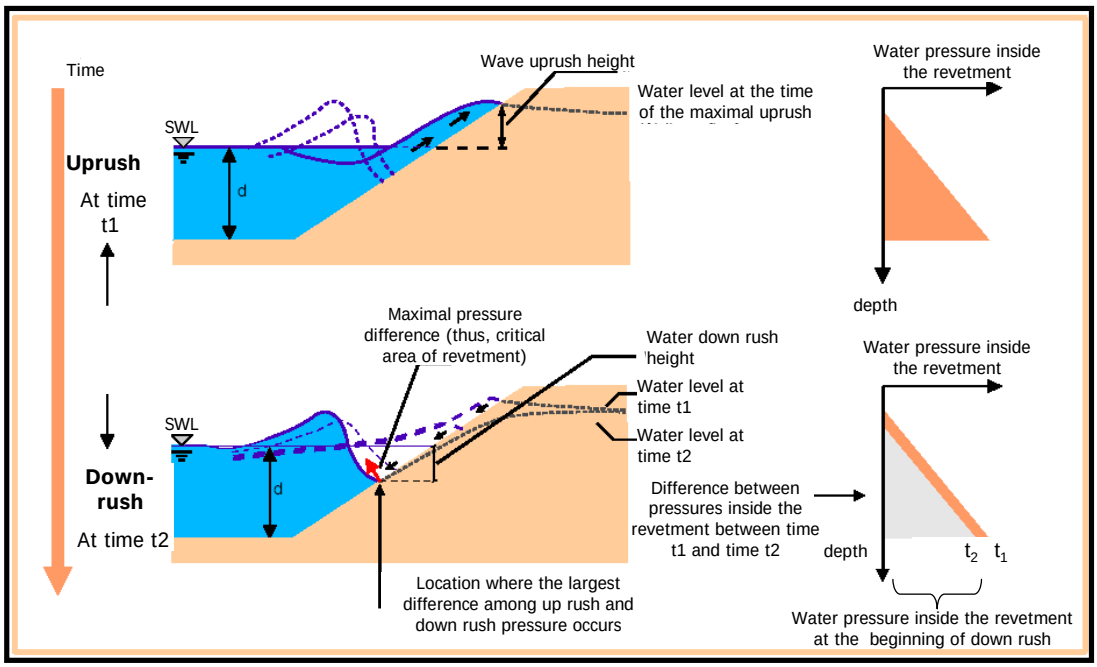

Figure 4-6: Wave-Induced Pressures in Front and inside a GSC-Structure (modified from Oumeraci et al, 2002)

4.2.2 Breaking Wave Loads on GSC-Structures

The hydraulic processes on a coastal structure are different when subject to breaking waves or non-breaking waves (Oumeraci 2003). Therefore, an investigation on the forces induced by breaking waves in front of a GSC-structure was performed (Figure 4-7). The detailed analysis of the wave-induced loads on GSC-structures can be found in Recio and Oumeraci (2006b).

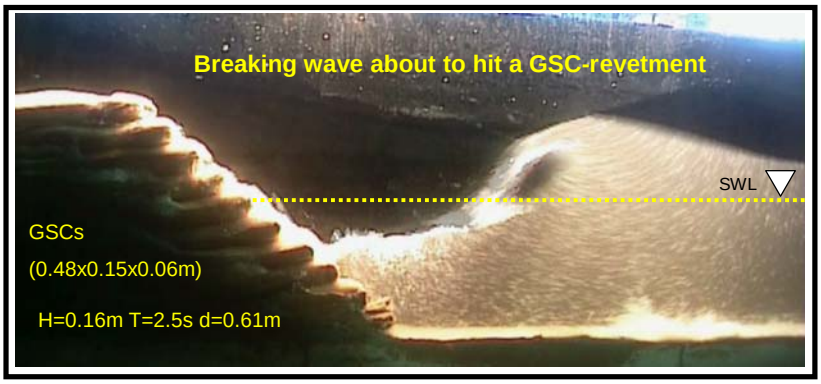

Figure 4-7: Breaking Wave on a GSC-Structure in the LWI-Flume

Breaking and broken waves are known to induce the most destructive loads affecting coastal structures. In the case of structures with gaps (like in a GSC-structure) the combination of horizontal and uplift forces which are generated inside the horizontal gaps, might cause the collapse of a coastal structure.

High pressures at the entrance of the gap usually lead to high pressures inside the gap. The pressure propagation inside the gap will determine, how critical the total pressures on the constitutive elements of the structure may be (Marth 2005).

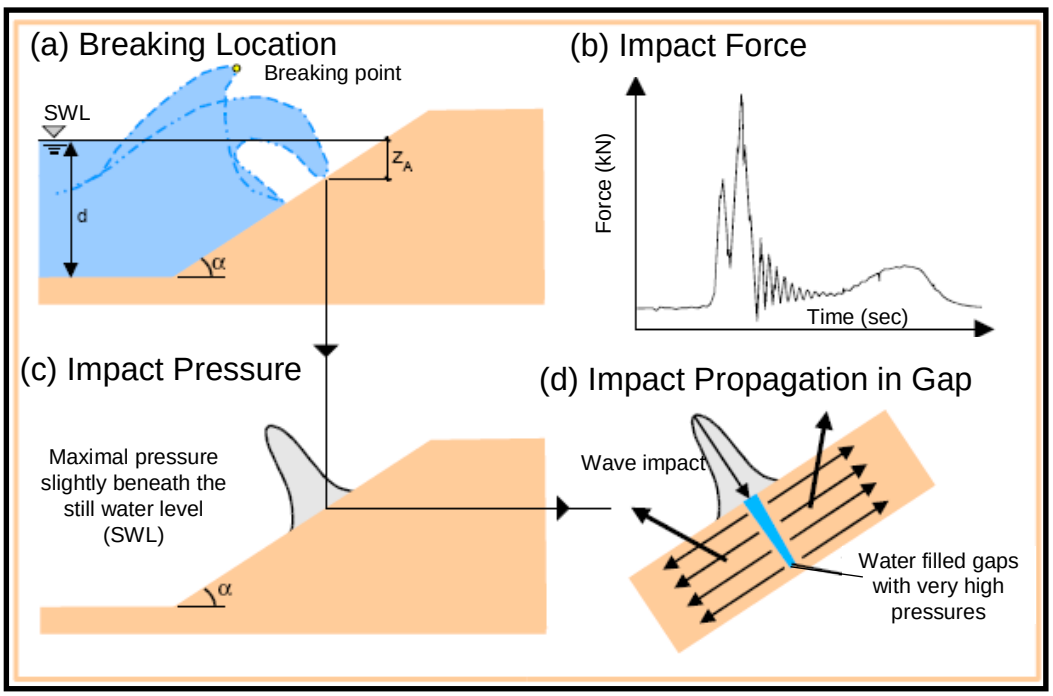

Figure 4-8: Breaking Wave Load on Dike Slope (principle sketches, modified from Oumeraci et al, 2002)

However, there is no information available about the stability of GSC-structures subject to breaking waves and about the pressure propagation within the gaps between sand containers. Therefore, a detailed analysis of the wave-induced pressures inside the gaps between the containers was performed.

Führböter (1991) showed that a breaking wave induces a maximum pressure slightly beneath the still water level (SWL) (Figure 4-8a). The resulting impact force is characterized by a very high peak and a short duration (Figure 4-8b). The impact pressures propagate through the gaps into the structure, where they are redistributed and possibly amplified or damped, depending on the boundary conditions within the gap (Marth, 2005) (Figure 4-8d).

The same phenomenon, as schematically illustrated in Figure 4-8, was also recorded by the pressure gauges in the gaps between geotextile sand containers. The precise time, when the breaking wave hits the structure, was also recorded (Figure 4-9b). When a breaking wave hits the area just above the SWL, the instrumented container located in the impact zone, recorded higher pressures on its front. At the impact time the resulting forces will cause a separation of the two containers (Figure 4-9c). The upper container moves upwards and rotates in clockwise direction (Figure 4-9d), while the container below the impact point moves downward and rotate in opposite direction. In order to decide, whether this breaking wave-induced pressure inside the gaps, and thus, on the container, is critical for the stability of the structure, a detailed analysis of the pressure propagation inside the gap is performed.

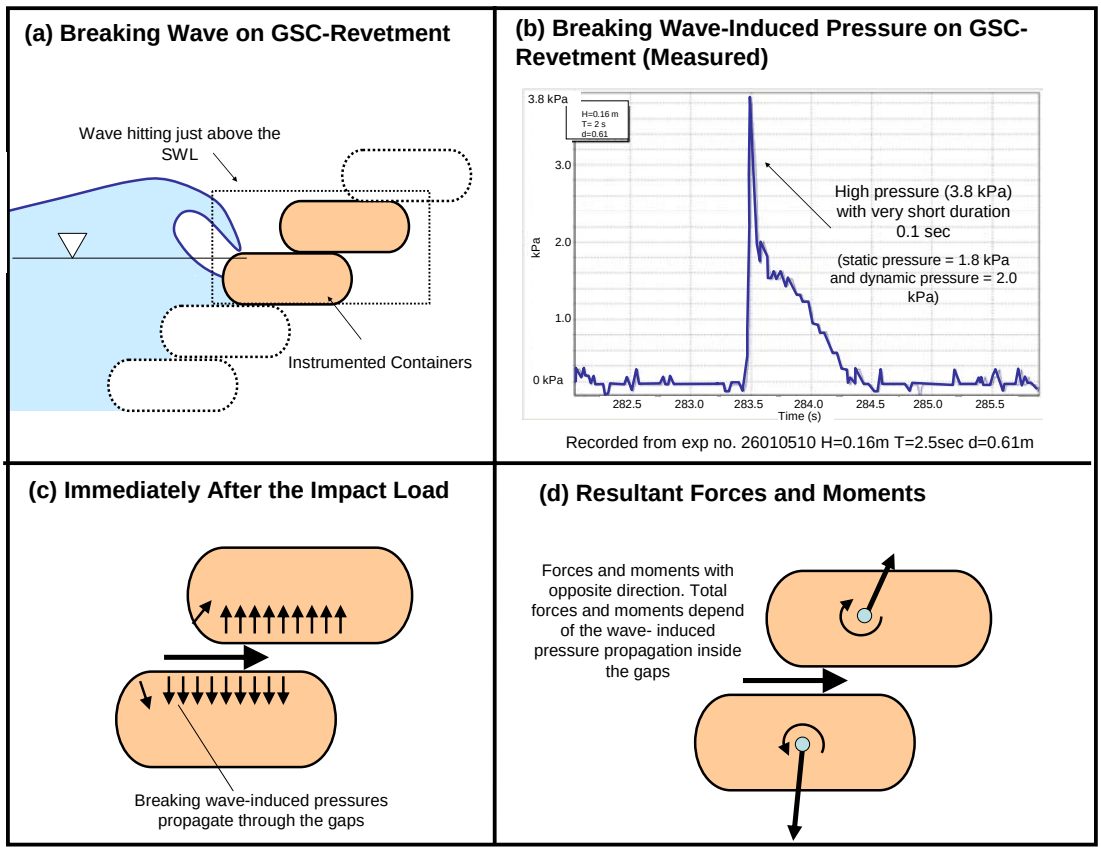

Figure 4-9: Breaking Wave Impact Loads on a GSC-Structure

Marth (2005) showed that the pressure impulse which enters a gap with rigid impermeable boundaries is damped while propagating through the gap. However, at the end of the gap the incoming pressures are reflected. Therefore, the pressures will be approximately doubled as a result of the superposition of the incoming and the outgoing compression wave. This superposition of the incoming pressure and reflected pressure signals could generate a seaward displacement of the elements of the coastal structure. Moreover, if the gaps are open at the end, the wave-induced pressures in the gap will be considerably smaller than those with "closed end".

Using the results from the pressure measurements within the gap, it is observed that the pressure along the gap between the containers do not increase (Figure 4-10b). Moreover, at the end of the gap (just behind the instrumented container), the wave-induced pressure is lower than in the middle of the gap (Figure 4-10c). This clearly shows that due to the flexibility and porosity of the containers, there is a decrease of pressure as it propagates along the gap. Recio and Oumeraci (2005b) also compared the loads induced by breaking and non-breaking waves on GSC-structures (Table 4.1) and found that forces induced by both types of waves are similar (higher instantaneous load for breaking wave). However, since the duration of the non-breaking waves is longer, Recio and Oumeraci (2005b) concluded that breaking waves are less critical for the stability of GSC-structures than non-breaking waves. This is probably due to the flexibility of the GSCs which contributes to damp the pressure propagation along the structure.

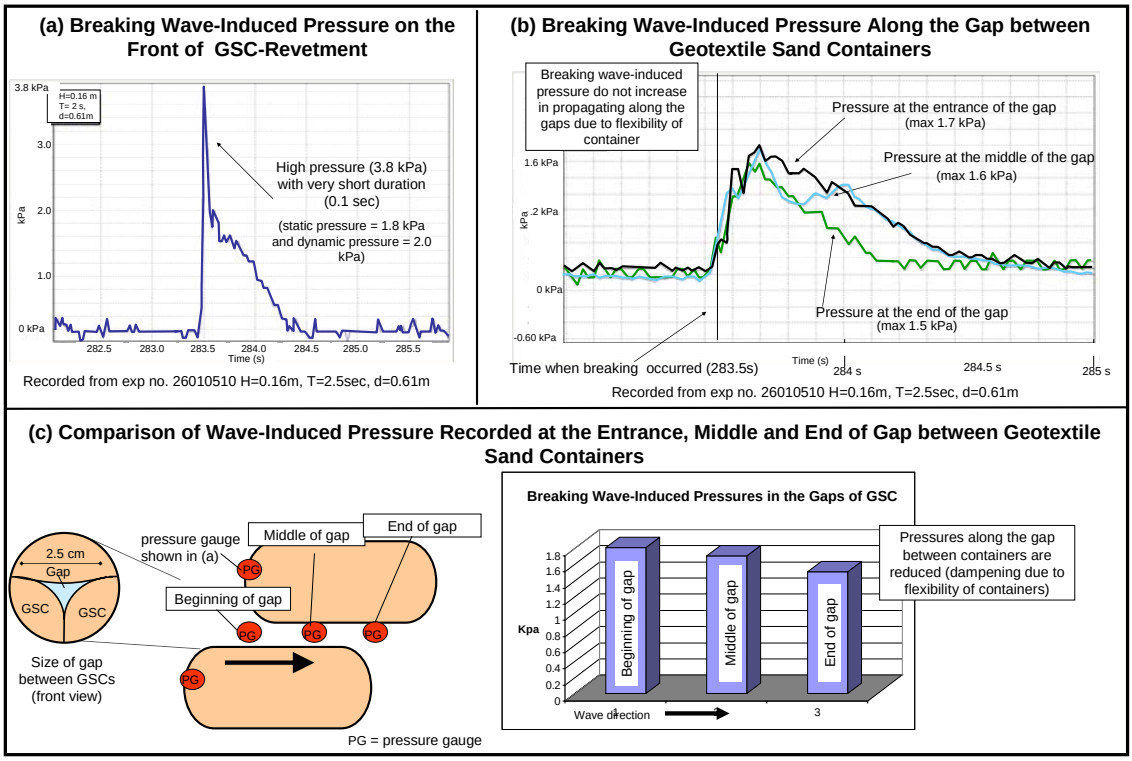

Figure 4-10: Pressure Propagation along a Gap between Geotextile Sand Containers

Table 4.1: Comparison between Wave-Induced Pressures by Breaking / Non-Breaking Waves

	Breaking Wave	Non- Breaking Wave
Maximal wave-induced pressure (kPa)	3.8 (quasi static + impact =1.8+2.0=3.8)	1.8
Duration of maximal wave-induced pressure (sec)	0.1	1.2
Maximal total force (integration of pressures) (N)	33.49	55.87
Duration of maximal total force (sec)	≈ 0.40	≈ 0.60

4.3 Wave-Induced Flow on GSC-Structure

To get an insight into the coherent structure of the flow next to the structure and to obtain consistent data for validation of the RANS-VOF-model which is used in Chapter 5, PIV-measurements were performed.

The images obtained from the CCD camera were processed to get flow velocity vectors and based on the images and the flow velocity vectors, the global and local effects were determined.

The PIV-data are compared with common measurement devices such as ADVs (Acoustic Doppler Velocimeters), showing a relatively good agreement (Figure 4-11). More details on the PIV-analyses can be found in Recio and Oumeraci (2005b) and Gemme (2005), including the run-up friction coefficient which was derived for GSC-structures.

PIV-results have the advantage that the whole wave-induced flow on a GSC-structure can be analyzed at every time step (Figure 4-12). The entire wave breaking process (Figure 4-13) was recorded by PIV-techniques. However, accurate velocity vectors could hardly be obtained during the post-breaking process due to the extremely strong vortices and turbulence.

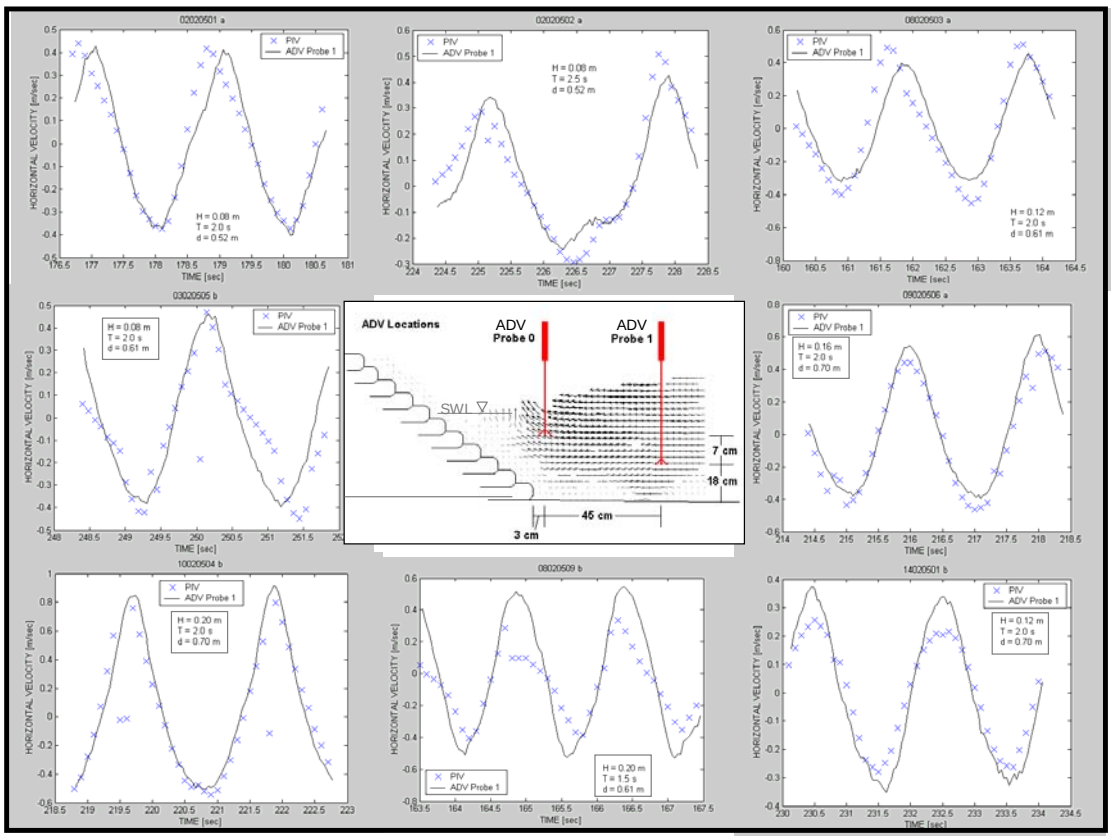

Figure 4-11: Comparison between Wave-Induced Velocities Measured by PIV and ADV Techniques

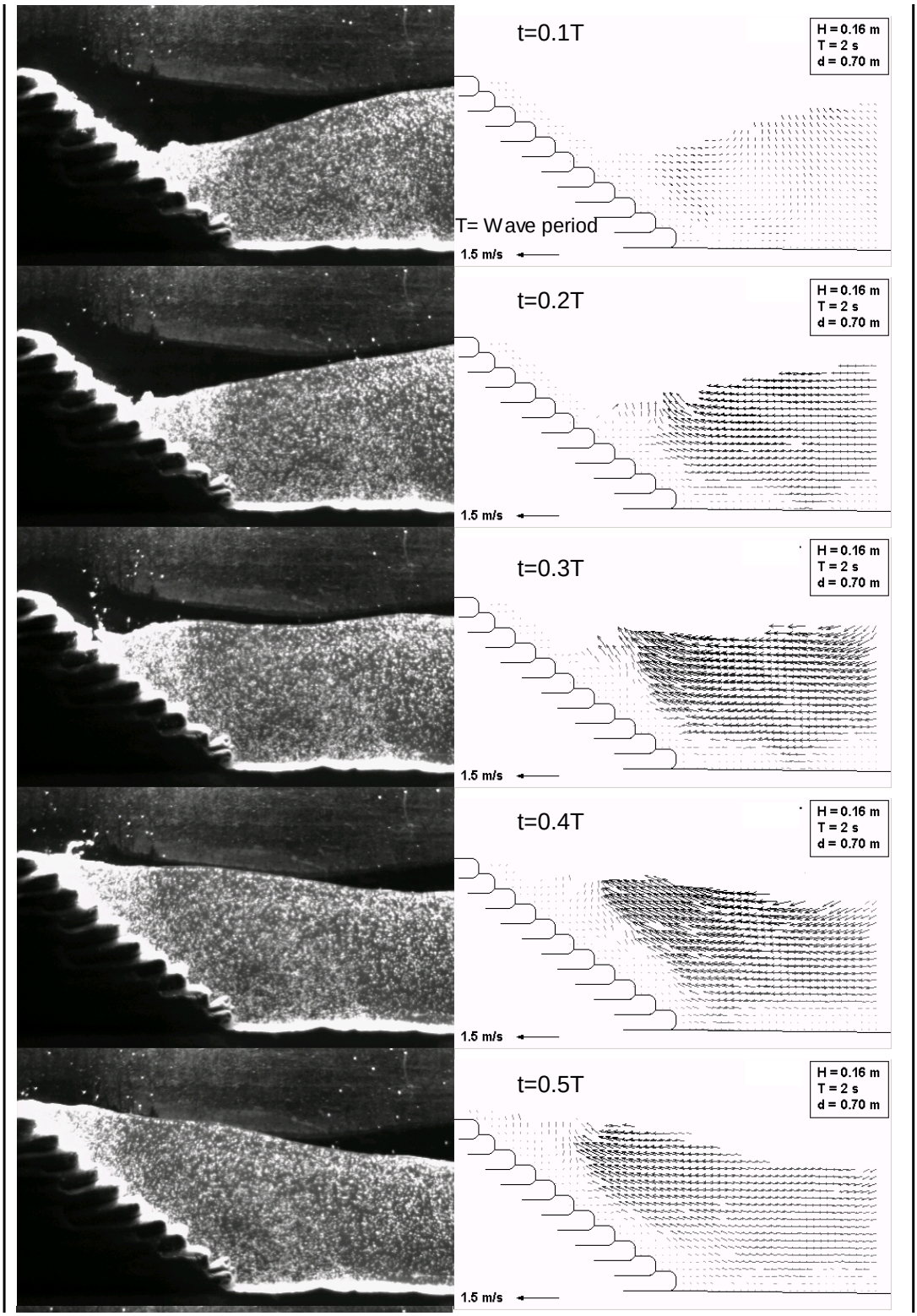

Figure 4-12: Flow Visualization over a Wave Cycle by Means of PIV-Techniques (continues on next page)

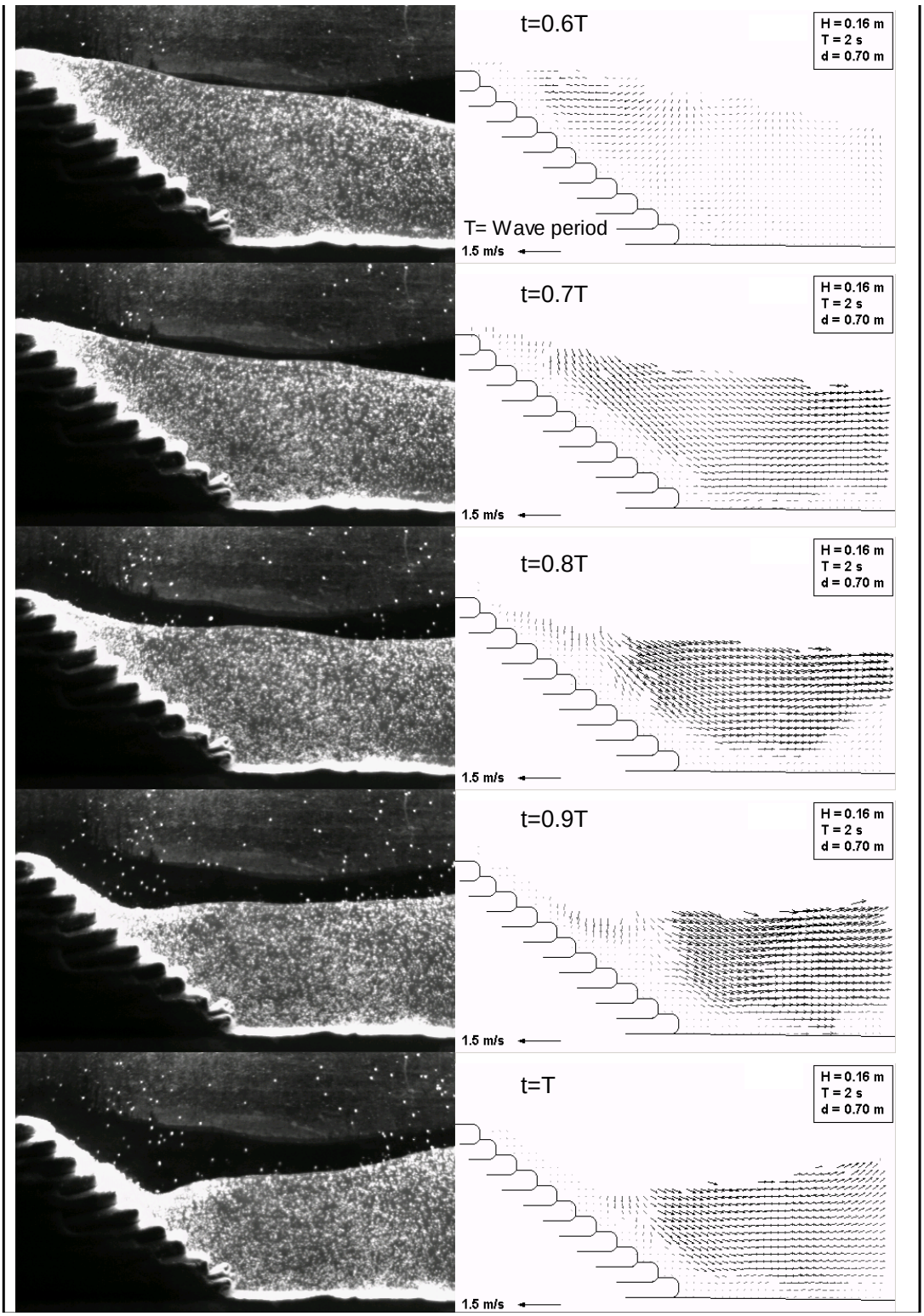

Figure 4-12: Flow Visualization over a Wave Cycle by Means of PIV-Techniques (continued from previous page; refer to Recio and Oumeraci, 2005b; and Gemme, 2005 for more details)

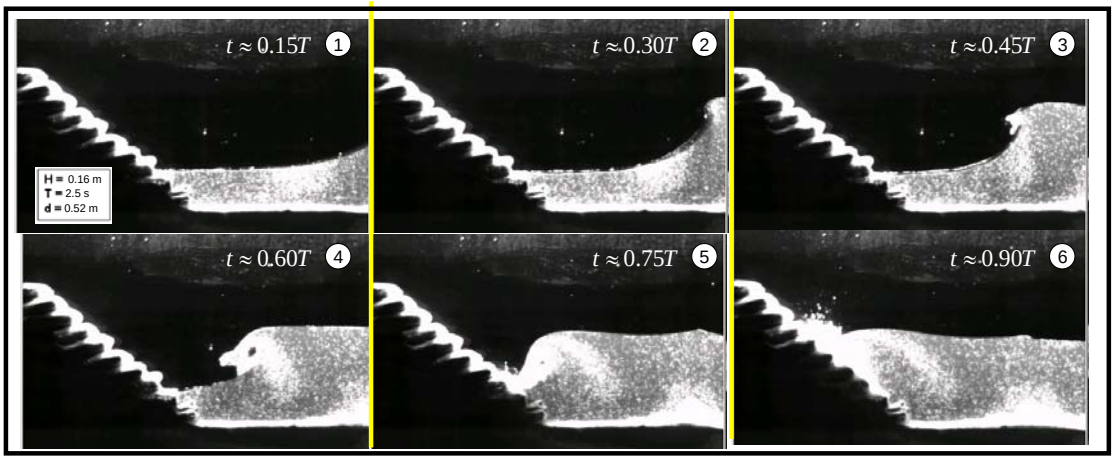

Figure 4-13: Breaking Wave on a GSC-Structure

For each model test, several waves are recorded and the associated velocity fields are obtained. The latter, together with the visualization of the seeding particles, help to clarify the flow processes on the structures. A better insight in these processes is achieved when the images are observed in rapid succession. However, the photographs and PIV-vectors show clearly how the flow varies at every phase of the wave cycle (Figure 4-12). It is found that the flow in front of the structure is initially orbital (Figure 4-14). During wave up and downrush, it was observed that the flow consists in a main flow running up/down and in local flows that are "trapped" between the containers (Figure 4-14). The velocity vectors of the main flow are approximately parallel to the structure slope. During uprush an "uplift" deformation of the containers is induced. During downrush, the velocity vectors of the main flow will reinforce the return process of the up-lifted part to a "normal" position and will also induce a seaward directed force on the containers ("pull-out effect").

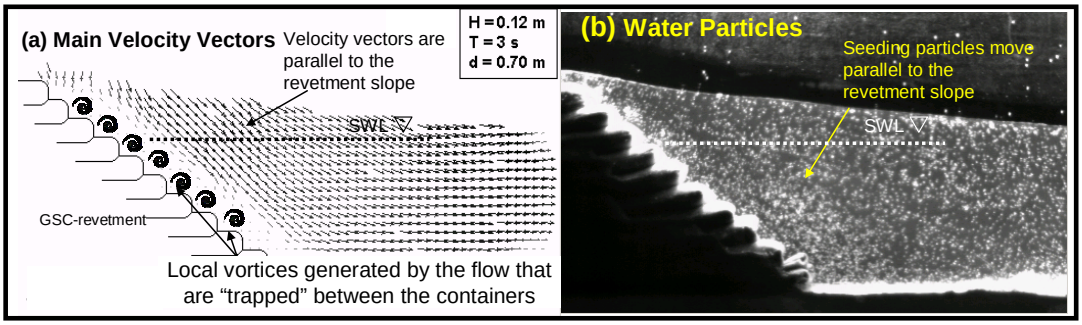

Figure 4-14: Global and Local Effects on a GSC-Structure

Among the local effects at the structure, vortex generation is also investigated. During wave action two different types of vortices are observed:

(i) Well-structured vortices: The motion is characterized by the separation of the fluid particles around each step along the structure which form vortices. These vortices are generated during up and downrush, and occur in the areas between containers (vortices have clockwise direction during downrush and vice versa). These vortices may affect the stability of the structure by applying a small rotational force on the container (Figure 4- 15a).

(ii) Non-structured vortices: They occur during uprush induced by higher waves (higher than 0.12m) (Figure 4- 15b).

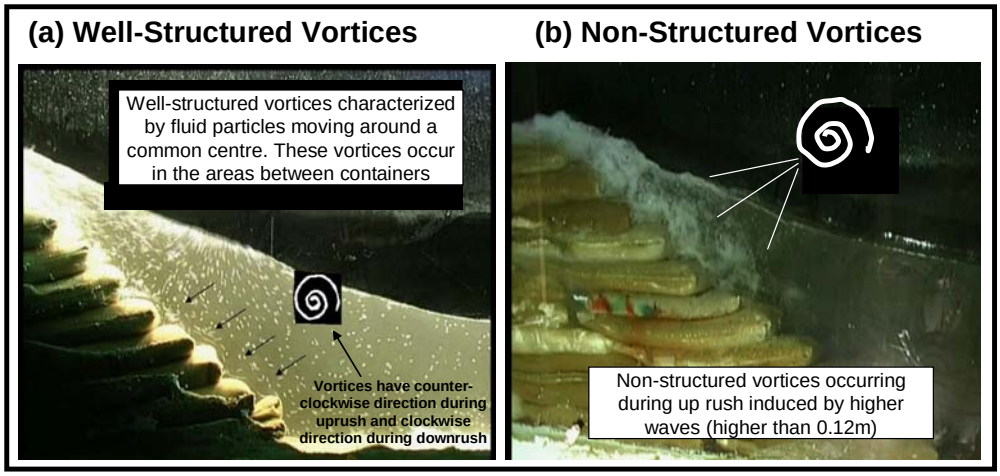

Figure 4- 15: Local Effects on a GSC-Structure

4.4 Internal Sand Movement in the Container

The internal movement of sand inside the containers, based on the analysis of the video records of the coloured sand inside a transparent container, is also investigated (Figure 4-1 and Figure 4-16). The observations of the coloured sand in the transparent permeable container subject to wave attack have shown that (Figure 4-17):

(i) Similar pattern of the sand motion occur for different wave conditions. As expected, noticeable movements of sand are only induced by larger incident waves.

(ii) The largest sand movements occur during the first 30 wave cycles, which then rapidly decrease. This means that the sand fill re-accommodates due to the wave-induced forces on the container.

(iii) During wave uprush the dominant sand movement is rather rotational and directed upward (Figure 4-17a).

(iv) During wave downrush the movement is essentially directed seaward (Figure 4-17b). At this stage, displacement of the container occurs as soon as a given critical wave height is exceeded.

(v) After few wave cycles, the sand accumulates at the seaward end of the container, causing a deformation of the latter and reducing the contact areas with neighbouring containers (Figure 4-17c).

(vi) Conditions prevail (v) as long as no further horizontal displacement of the container occurs, internal movements of sand are triggered by any incremental horizontal displacement of the container. These movements of sand occur, because the contact areas of the GSC with the neighbouring containers are reduced. As a result, the entire process of sand movement will again repeat itself in a similar way as during the first wave cycles. (Figure 4-17d).

The clarification of the internal movement of sand inside GSCs indicates that the deformation of a GSC will indeed affect the stability of GSC-structures. On the other hand, this conclusion has very important implications for the construction of GSC-structures. As explained in Figure 4-17, the displacement of each GSC depends on the internal movement of the contained sand, thus, the sand fill ratio of each GSC is critical for the stability. A GSC with a very low sand fill ratio will be much more unstable as a GSC with an optimal filling ratio (balance between flexibility and small movement of sand).

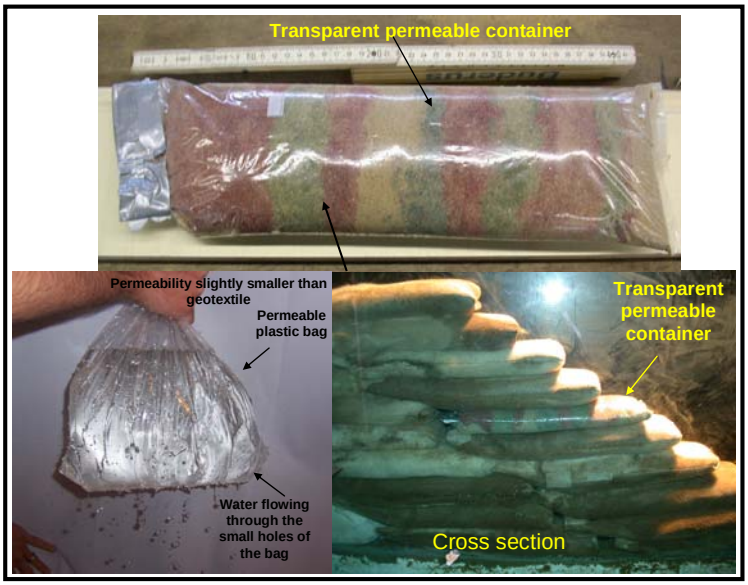

Figure 4-16: Permeable Transparent GSC Used to Investigate the Internal Movement of Sand

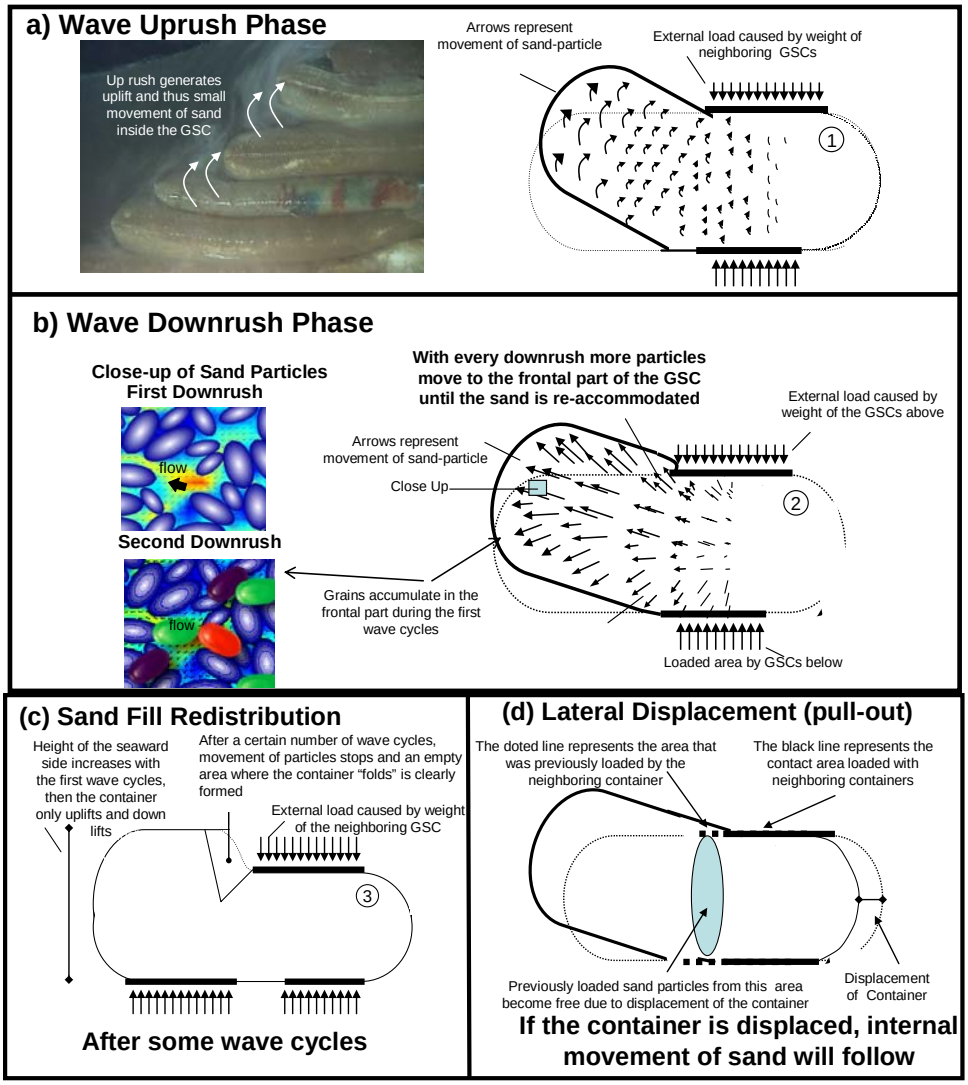

Figure 4-17: Internal Movement of Sand inside the Transparent Container

Moreover, video observations of the GSC-structure are performed from the beginning of its construction until the end of the model tests to identify variations that the GSC-structure may suffer due to changing conditions.
Expectedly, it is observed that the height of the GSCs and thus, also the height of the GSC-structure is reduced due to the saturation of the sand material inside the container. For the tested GSC-structure, the height of both containers and GSC-structure was reduced approximately by 4% from dry to wet conditions (Figure 4- 18). A further reduction of approximately 6% of the height occurred during wave action, leading to a total reduction of about 10% as compared with dry conditions prior to wave attack. Thus, it was confirmed that wave action induces compaction of sand fill (Recio and Yasuhara, 2001). However, after analyzing the movement of sand inside the GSC, it was observed that the reduction of the height of the GSC (and thus the GSC-structure) is also induced by the internal movement of sand inside the GSCs to the frontal part of the containers (Figure 4-17b).

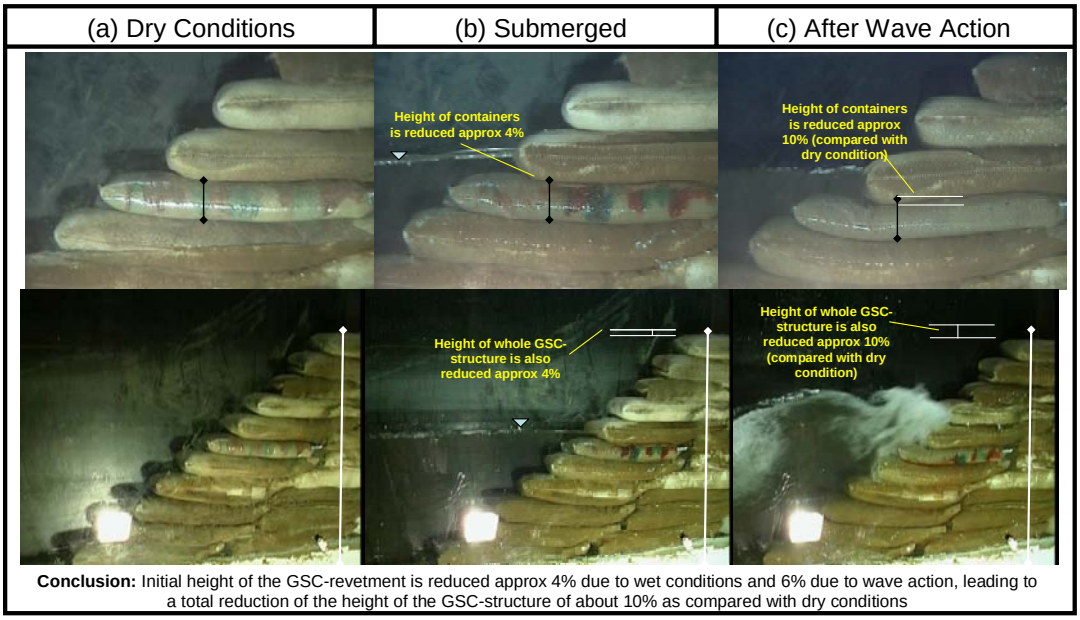

Figure 4- 18: Reduction of the Height of a GSC-Structure Due to Internal Movement of Sand

4.5 Variation of "Effective" Contact Areas between GSCs under Wave Action

During wave action, the variation of the contact areas among neighbouring containers was monitored by means of video observations (Figure 4-19).

The contact areas among neighbouring containers are reduced due to the uplifting of containers. Considering that the resisting force of GSC is a function of its weight projected on the contact area, a reduction on these contact areas will reduce the stability of the structure (Figure 4-19). The "effective" resisting contact areas between neighbouring GSCs are a function of the slope of the structure (Figure 4-19d). The larger the slope angle of the GSC-structure, the larger the contact areas between neighbouring containers (see Recio and Oumeraci, 2005b for more details). This means that the uplift deformation of the GSCs is directly influenced by the slope angle of the GSC-structure.

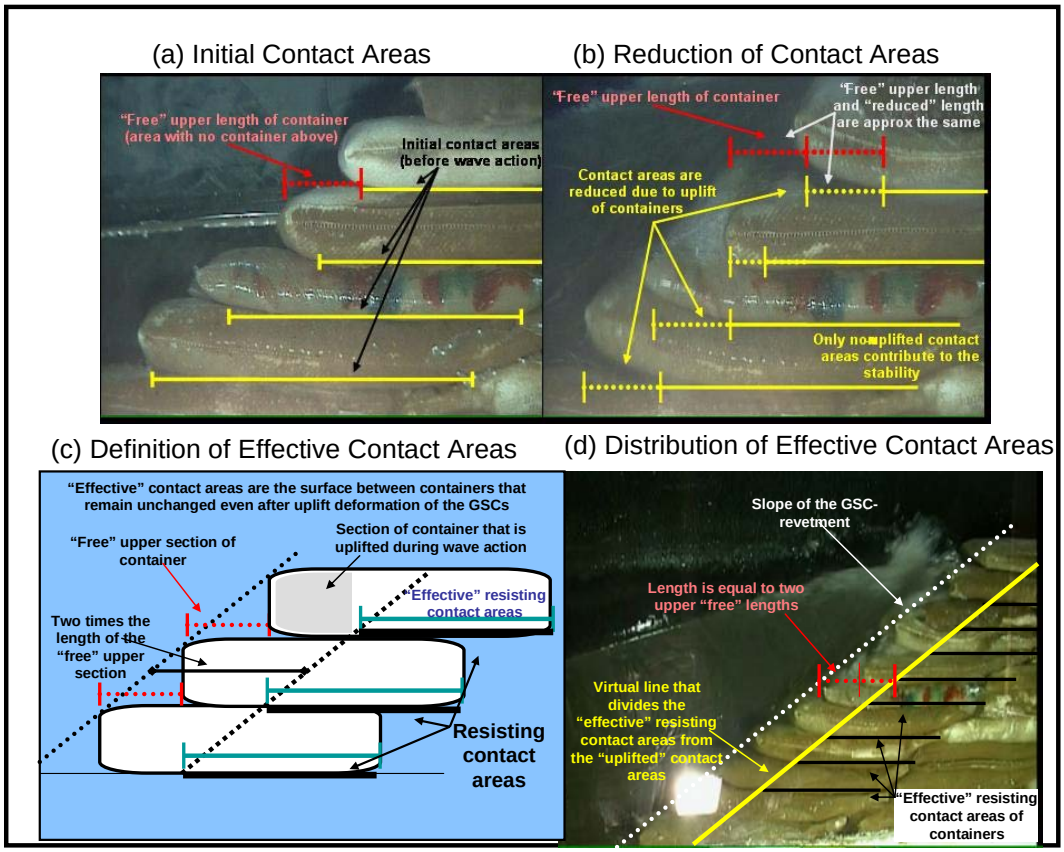

Figure 4-19: Variation of the Contact Areas between GSCs During Wave Action

4.6 Failure Modes of GSCs in a GSC-Structure under Wave Action

From the model tests performed in this study and from the analysis presented by Oumeraci et al (2002) (Figure 4- 23), two main types of displacements of GSCs are identifed: sliding and overturning.

4.6.1 Sliding

Sliding represents the most common hydraulic failure mode of GSC. It occurs when the container progressively slides either in a seaward (slope and crest containers) or landward (crest containers only) direction.

During **wave uprush** (Figure 4-20a), the wave-induced flow uplifts the frontal part of the containers. Moreover, the local vortex flow between the containers may contribute to sliding by inducing an additional overturning moment force on the container. Uplift of the containers reduces the contact areas and thus the stabilizing forces.

During **wave downrush** (Figure 4-20b), the uplifted container returns down, its contact areas are still reduced: (i) due to the uplift deformation and (ii) due to the internal movement of sand. The return flow behind the container induces seaward directed forces. When the seaward forces are higher than the resisting forces a sliding displacement of the GSC will occur ("pull-out effect", Figure 4-20). This displacement is normally progressive and only becomes noticeable after several wave cycles (for example, with a wave height of 0.12m and period of 3 seconds, a sliding in the range of few of centimetres is recorded after approx. 100 wave cycles).

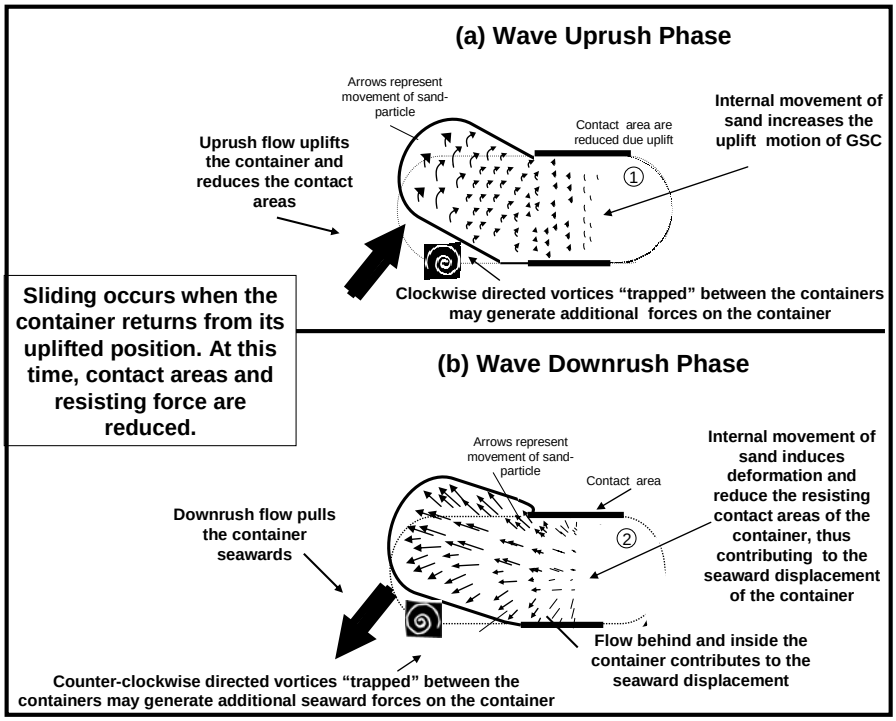

Figure 4-20: Sliding Process of Slope-GSC

4.6.2 Overturning

Overturning occurs when the displacement of the GSC is rotational. Two types of overturning are observed depending of the location of the GSC on the structure: (a) container in the slope of the structure and (b) container on the crest.

(a) Overturning on the Structure Slope: this displacement occurs for GSCs that are located near SWL when the incident wave height is large enough to induce displacement of the container. The displacement of the container is rather rotational in the upward direction. The wave load on the container is so large, that during the wave uprush phase, the container is uplifted and detached seaward in a rotationally way from the GSC-structure. This type of displacement occurs only, if the wave-induced load on the containers is much larger than the resisting force (Figure 4-21).

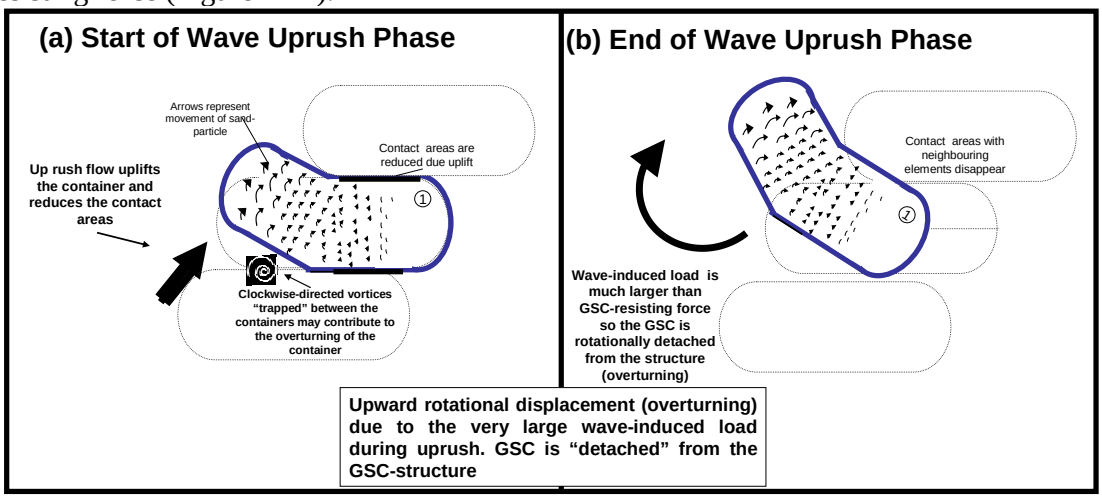

Figure 4-21: Overturning of Containers on the Slope of the Structure (see also Figure 6-32)

(b) Overturning on Structure Crest: this displacement occurs during the wave uprush or downrush phase for GSCs that are placed at the top of the structure when the wave-induced force on the element induces uplift followed by a rotational seaward or landward displacement of the container (Figure 4-22). Landward displacement occurs when the wave-induced uprush load in the container is large enough to induce uplift and overturning of the container (Figure 4-22a).
Seaward displacement occurs when the container is returning from uplift deformation and the downrush induced loads on the GSC generate seaward overturning (Figure 4-22b).

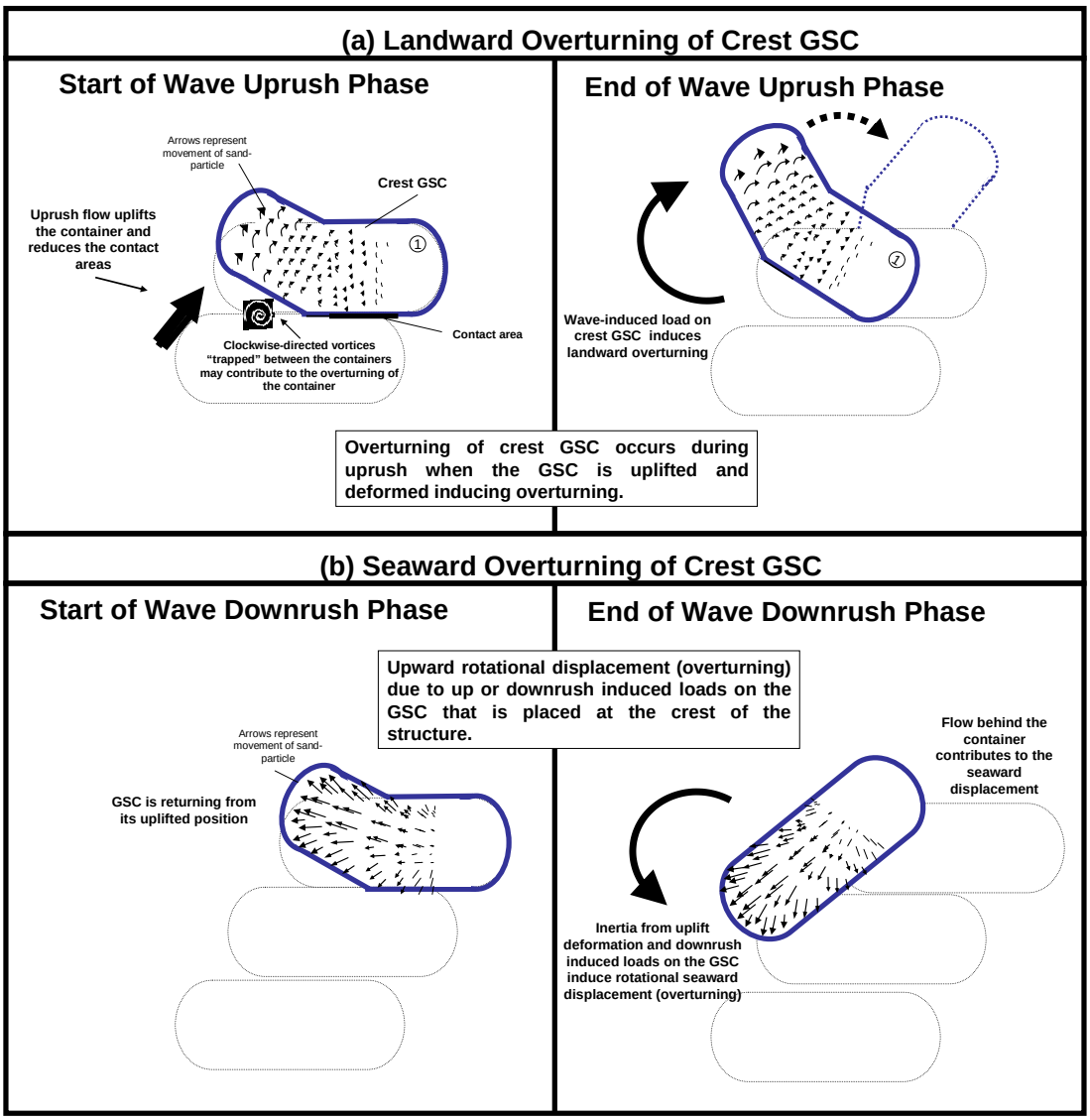

Figure 4-22: Overturning Containers at the Crest of the GSC-Structure

Sliding and overturning of GSCs were recorded during the model tests performed by Oumeraci et al (2002) (Figure 4- 23a). After the tests (Figure 4- 23b) several containers showed seaward deformation of their frontal part due to sliding and internal movement of sand inside the container.

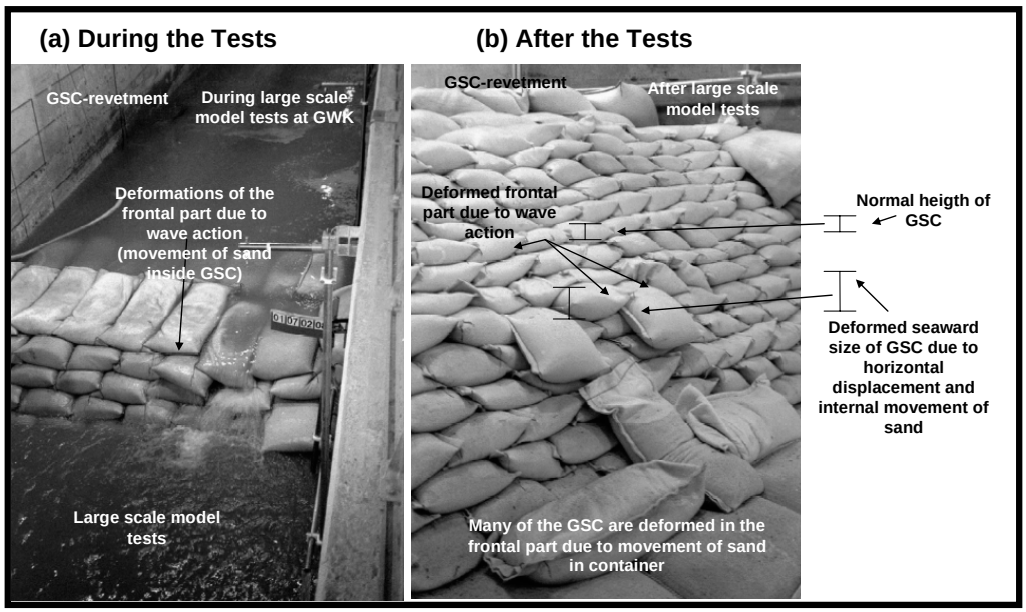

Figure 4- 23: Displacements Observed after the Model Tests at the Large Wave Flume (modified from Oumeraci et al, 2002)

4.7 Effect of Container Deformations on the Stability of GSC-Structures

The experimental results have shown that the deformation of the constitutive containers under wave action strongly affects the hydraulic stability of GSC-structures. In this section, an attempt is made to examine analytically why the deformation affects the stability of GSC-structures. To understand, how the deformation of GSCs (uplift deformation and internal movement of sand) affects the hydraulic stability, it is necessary to consider the balance of forces on a sand container (Figure 4- 24).

(a) Definition Sketch	(b) Mobilizing Forces	(c) Resisting Force
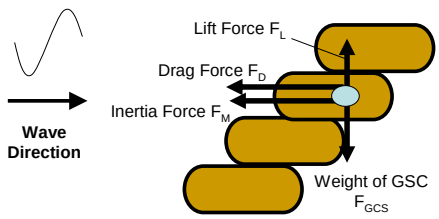	$F_D = 0.5 C_D \rho_w A_S u^2$ $F = C_M \rho_w V \frac{\partial u}{\partial t}$ $F_L = 0.5 C_L \rho_w A_T u^2$	$F_{GSC} = \rho_{GSC} g V$ $\rho_{GSC} = (\rho_s - \rho_w)$

Figure 4- 24: Force Balance on a GSC

The wave loads (mobilizing forces) on the structure can be defined as:

Drag force $F_D = 0.5 C_D \rho_w A_s u^2$ (4. 1)

Inertia force $F_M = C_D \rho_w V \frac{\partial u}{\partial t}$ (4. 2)

Lift force $F_L = 0.5 C_L \rho_w A_T u^2$ (4. 3)

where ρ_W is the density of water, C_D, C_L and C_M are empirical force coefficients, u is the wave-induced horizontal particle velocity, $\frac{\partial u}{\partial t}$ is the associated horizontal particle acceleration, V is the volume of the sand container, A_S the projected area of the containers normal to the wave direction while A_T is the projected area in wave direction (Figure 4-25).

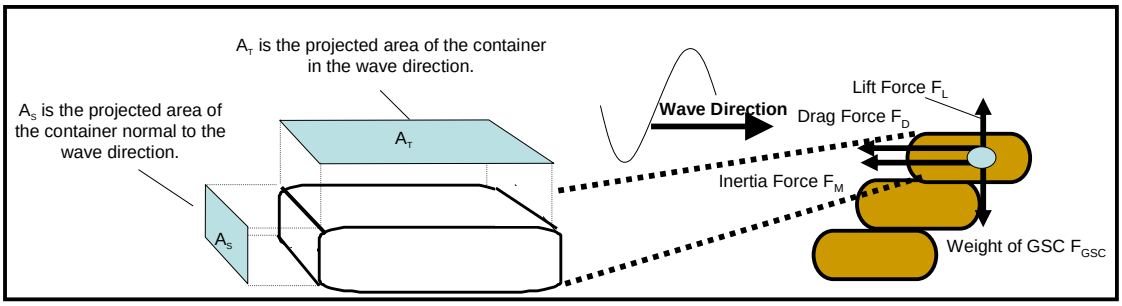

Figure 4- 25: Projected Areas A_S and A_T of a Sand Container (definition sketch)

The resisting force on the submerged container can be defined as:

Resisting Force: $F_{GSC} = \rho_{GSC} g V$ (4. 4)

where $\rho_{GSC} = (\rho_s - \rho_w)$ is the submerged density of the sand containers and g is the gravity acceleration.

Depending on the way the containers are placed to build a coastal structure, on the geometry and on the hydrodynamic processes involved, two main types of displacements may occur: (a) sliding and (b) overturning.

(a) Sliding

The stability against sliding of the container can be described as follows (Figure 4-26):
Resisting horizontal force > Mobilising horizontal force.

$$\mu\left[F_{GSC} - F_L\right] \geq F_D + F_M \quad (4.5)$$

where μ is the friction coefficient between geotextile sand containers.

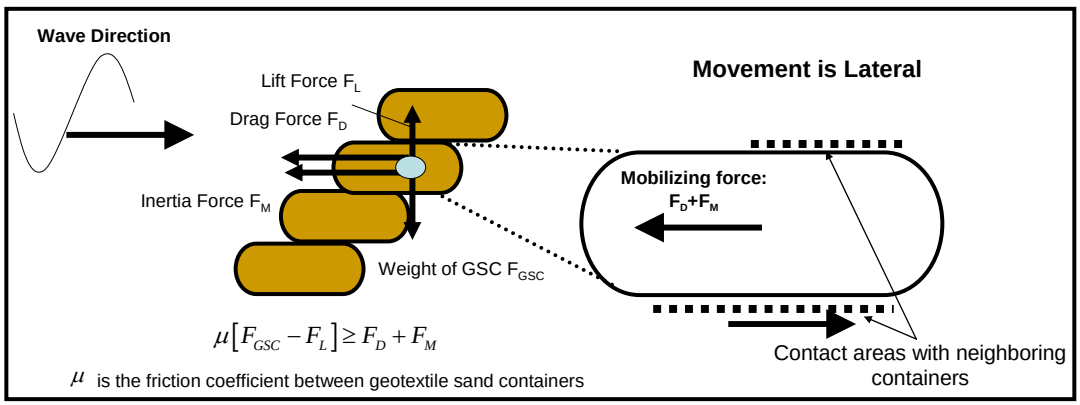

Figure 4-26: Hydraulic Stability of a Sand Container against Sliding

When internal movement of sand inside the container occurs, the frontal part of the container will be enlarged and the rear part reduced. This means that the projected areas A_S and A_T will change, because in equation (4.1) and (4.2) the mobilizing forces F_D and F_L are a function of the projected areas A_S and A_T, respectively, thus, F_D and F_L will both increase accordingly.

Now, if the deformed container is uplifted, the contact areas with neighbouring containers are smaller than before sand movements leading to a reduction of the resisting forces. Therefore, the sliding stability of the container is reduced due to the internal movement of sand (Figure 4-27).

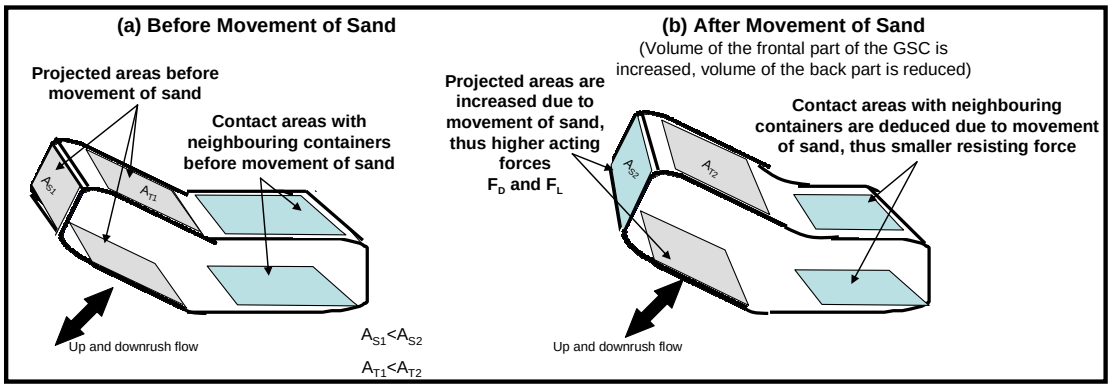

Figure 4- 27: Effect of the Internal Movement of Sand on the Sliding Stability of a Sand Container

b) Overturning

The stability against overturning of the container can be described as (Figure 4-22 and 4-28): Resisting moments ≥ Mobilising moments.

$$F_{GSC} \cdot r \geq (F_D + F_M) m_s + F_L \cdot r_s \qquad (4.\ 6)$$

where r_s is the horizontal projection of the distance between the centre of gravity of the container G and the rotation point O. O is defined as a virtual point located at the edge of the contact area of the container opposite to the acting direction of the wave forces (refer also to Wouters 1998). m_s is the vertical projection of the distance between the centre of gravity of the container and the rotation point (Figure 4- 28).

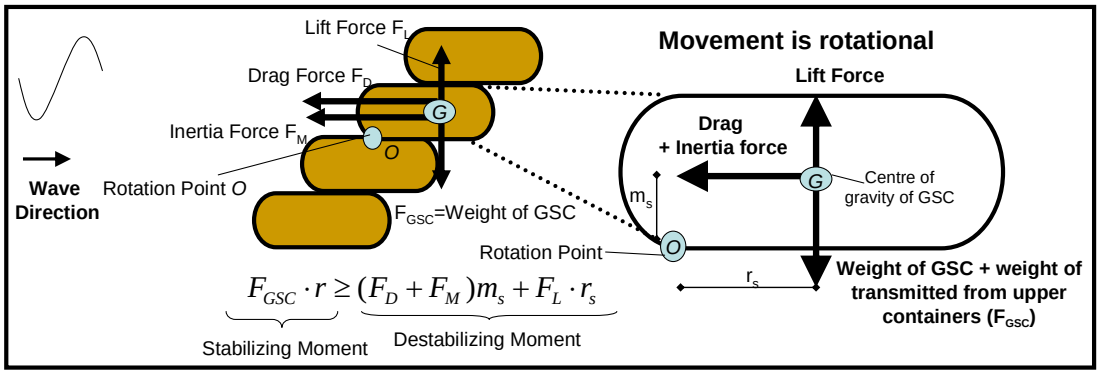

Figure 4- 28: Stability of a GSC against Overturning

When the sand inside the container has moved seaward and accumulated at the frontal part, the centre of gravity G of the container also moves seaward to a different location since the frontal part of the container has suffered deformations. Thus, the resisting moment on the container decreases (due to the fact that the centre of gravity G has moved a distance δ to G'), but mobilizing moment on the right side ($F_L \cdot r_s$) increased; however the increase rate is less than that of the resisting moment on the left size because $F_{GSC} > F_L$. Therefore, the stability of the container decreases (Figure 4- 29).

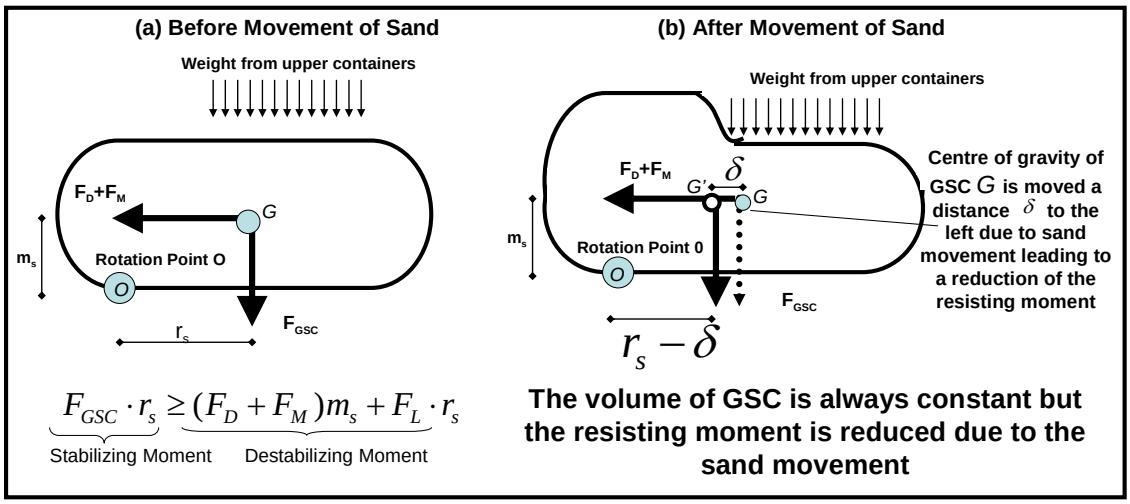

Figure 4- 29: Effect of the Internal Movement of Sand on the Overturning Stability of a Sand Container

4.8 Summary and Practical Implications of the Results

Based on: (i) the detailed measurements of wave-induced loads on the instrumented sand container, (ii) on the PIV-measurements of the flow field in front of the GSC-structure, and (iii) the video observations of the internal movement of coloured sand in a transparent container, an improved understanding of the processes, which affect the stability of GSC-structures, has been achieved, including the effect of the deformation of the sand containers and their interaction.

The main results and their practical implications for the hydraulic stability may be summarized as follows:

i) The most critical location on the seaward slope with respect to the hydraulic stability is for the containers placed just below the still water level.

ii) The most critical phase for the stability of slope containers is expected during wave downrush.

iii) The deformations of the container strongly affect the stability of GSC-structures. Deformations contribute to reduce the resisting contact areas between the containers and thus, the resisting forces on the containers

iv) The internal movement of sand inside the container induces deformation of the container and may, therefore, substantially affects the stability of the GSC-structure. Internal movement of sand depends on the fill ratio of the container and thus, has to be strictly controlled to assure the stability of any GSC-structure.

v) Breaking waves are not as critical as originally expected for the hydraulic stability of GSC-structures due to the flexibility and damping properties of the GSCs that attenuate the propagation of pressure inside the GSC-structure.

Chapter 5

Process Affecting the Hydraulic Stability of GSC-Structures: Numerical Studies and Results

A computational fluid dynamic model and two computational structural dynamic models are further developed and validated to extend the range of the conditions tested in the hydraulic scale-model tests performed (see Chapter 4) towards an improved understanding of the processes that affect the stability of structures made of **g**eotextile **s**and **c**ontainers (GSCs). The wave-induced forces on the GSCs are calculated by the "COBRAS"-model, a RANS-VOF type model, which is based on the **R**eynolds-**A**veraged **N**avier-**S**tokes equations and the **V**olume **O**f **F**luid concept. The stability of the GSC-structure is examined by the available "UDEC" code in which: (i) the stresses and deformations for each GSC are simulated by using a Finite Element model (FEM) and (ii) the displacement of each GSC is simulated in "UDEC" by a Discrete Element model (DEM) which has been extended/adopted for this study. The numerical models (RANS-VOF/FEM-DEM) are further improved and validated using own experimental data, and then further applied to extend the knowledge on the involved processes, which has been gained from the experiments (see Chapter 4). Therefore, the chapter focuses on the following issues: (i) brief description of the models, (ii) coupling of the models, (iii) adaptation of the models to GSC-structures, (iv) validation of the models and (v) analysis of the processes that affect the stability of GSC-structures by means of numerical simulations.

5.1 Brief Description of the Models

5.1.1 Computational Fluid Dynamic Model "COBRAS"

COBRAS ("**Co**rnell **Br**eaking Waves **a**nd **S**tructures") is a numerical model, which can describe particularly the evolution of a breaking waves and their interaction with structures. The model is based on the code "Ripple", which was originally developed at "Los Alamos National Laboratory", USA. "COBRAS" simulates two dimensional incompressible fluid flow with free surfaces of general topology. Finite difference solutions to the incompressible Reynolds equations for the mean flow field and the k-ε equations for the turbulent field are obtained on a non-uniform mesh. The free surface locations are represented by the Volume of Fluid (VOF) data on the mesh. A two step projection method is used for the mean flow solutions, aided by the incomplete Cholesky conjugate gradient technique solving the Poisson equation for the mean pressure and dissipation rate in the k-ε equations are estimated by the combination of the upwind method and the central difference method.

The governing equations and more detailed information on "COBRAS" can be found in Recio and Oumeraci (2006a) and Lin and Liu (1997 and 1998)

"COBRAS" has been modified and extended to simulate: (i) the flow through the gaps between elements and (ii) the induced pressures inside the gaps. In addition, the code was adapted to simulate the flow through the porous media inside the sand containers (for details refer to Recio and Oumeraci 2006a).

5.1.2 Computational Structural Dynamic Models "UDEC"

The **U**niversal **D**istinct **E**lement **C**ode (UDEC) is a two-dimensional numerical code which is based on the Finite and Discrete element methods for deformations and discontinue modelling. "UDEC" can simulate the response of discontinuous media subjected to either static or dynamic loading. The discontinuous medium is represented as an assemblage of discrete blocks or elements (FEM in UDEC). The discontinuities are treated as boundary conditions between blocks (DEM in UDEC); large displacements along discontinuities and rotations of blocks are allowed (DEM). Individual blocks behave either as rigid or deformable material (FEM). Deformable blocks are subdivided into a mesh of finite-difference elements, and each element responds according to a prescribed linear or non-linear stress-strain law (FEM). The relative motion of the discontinuities is also governed by linear or non-linear force-displacement relations for movement in both the normal and shear directions.
There are six constitutive models provided in UDEC to describe the deformation of blocks (FEM): (i) elastic, isotropic model, (ii) Drucker-Prager model, (iii) Mohr-Coulomb model, (iv) ubiquitous-joint model, (v) strain-softening model and (vi) double-yield model. "UDEC" uses the "Coulomb frictional behaviour" and refers to the capability of the model to simulate displacement of each block (element) in all directions where a discontinuity (gap) exists (DEM). The displacement model of UDEC is intended to simulate the individual displacement of blocks under shear (refer to Itasca, 2004, for more details).

Dynamic analysis in UDEC permits two-dimensional, plane-strain or plane-stress, fully dynamic analysis. The calculation is based on the explicit finite difference scheme to solve the full equations of motion. In UDEC, the dynamic input can be applied in one of the following ways: (i) a velocity history, (ii) a stress history, (iii) a force history and iv) a fluid pressure history.
Details of the coupling between the FEM and DEM in UDEC can be found in Itasca (2004, Volume 1).

The UDEC model is modified in the following ways: (i) the model was extended to allow different zones with different properties inside an element (for example, an element (GSC) may be subdivided in two or more zones with completely different properties) and (ii) the model was modified to read output files generated by "COBRAS".

5.2. "Partial Coupling" of the Fluid Dynamic and Structural Models (COBRAS-UDEC),

Due to time limitations and feasibility aspects, only a "partial coupling" of "COBRAS" and "UDEC" was required within the framework of this PhD-study. "COBRAS" and "UDEC" have been run independently, only sharing input and output information among them. Ideally, the models (fluid and structural dynamic models) should run simultaneously, sharing continuously and instantaneously information. Therefore, partial coupling might represent serious limitations only in the following cases: (i) a detached element is "floating" away from the structure, (ii) displacement of several elements occur simultaneously, and (iii) deformations during a time step are large enough to affect considerably and immediately the boundary conditions of neighbouring elements.

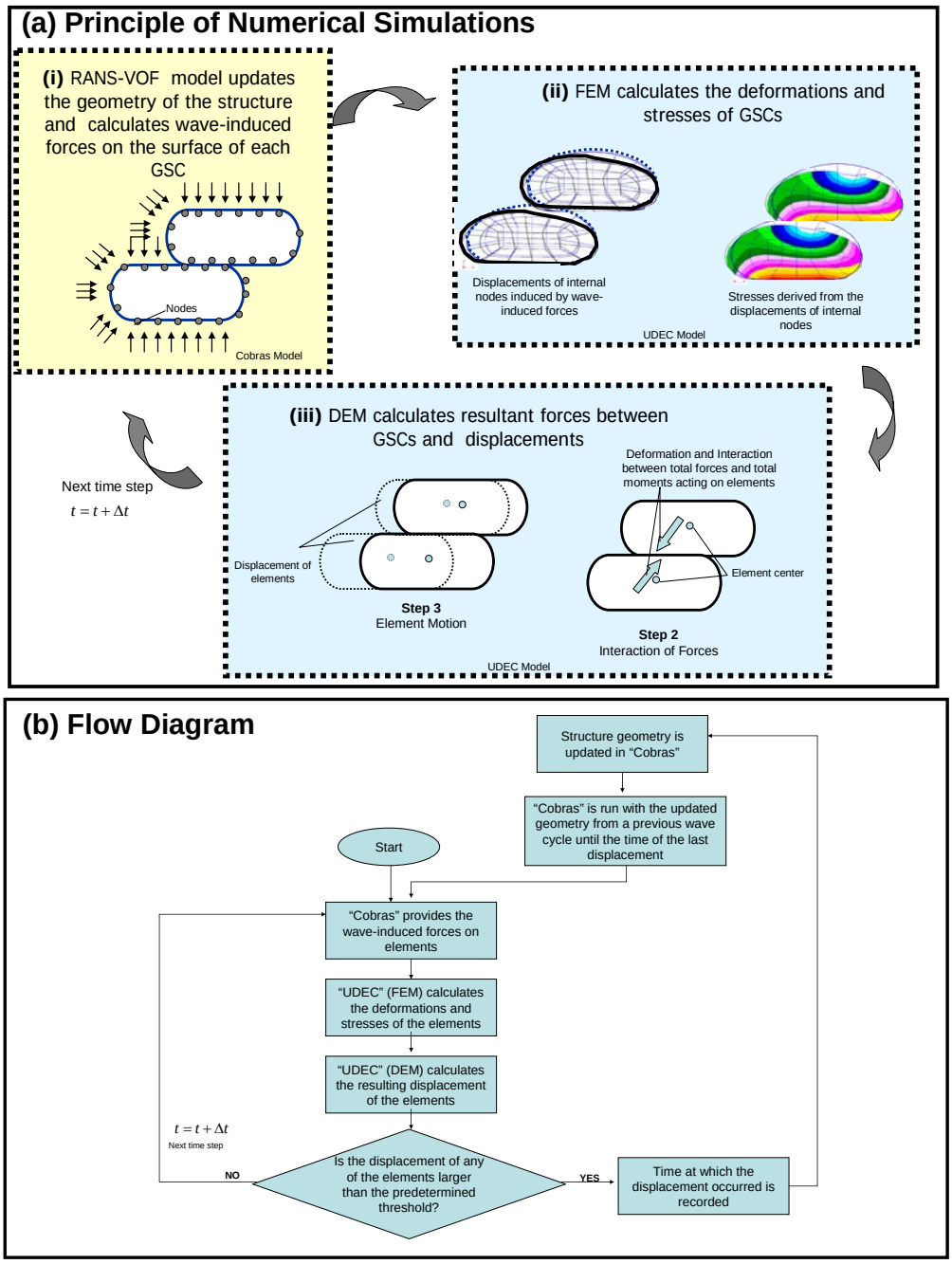

Figure 5-1: "Partial Coupling" of the Flow Model and the Structural Models

The "partial coupling" of the models is performed as follows (Figure 5-1):

(i) The flow model "COBRAS" calculates the wave-induced pressures along the surface of each element (pressures are integrated into forces at each nodal point of the perimeter of the finite element mesh in each GSC, see Figure 5-1a).

(ii) The structural dynamic model (FEM in UDEC) calculates the displacements of each node of the GSC (deformations). From the GSC-deformations, the model (FEM) derives the stresses (Figure 5-1b).

(iii) From the displacements of the nodes that are in the surface of each element that interact with the neighbouring elements, the structural dynamic model (DEM in UDEC) calculates the resultant forces among each of the GSCs in the structure. The displacement of each element is then calculated by considering the shear properties of the discontinuities and the derived resultant forces (Figure 5-1c).
(iv) Finally, the model proceeds to the next time step with an updated geometry (if required) for the calculation of the wave-force by "COBRAS".

Since only a "partial coupling" is performed the two main factors that control the accuracy of the simulations are:

(i) **The magnitude of the time step:** Ideally the time step should be as small as practicable, especially for the DEM model. The time step in DEM is critical, since a large time step could induce large indentation between elements and thus, displacement could be unrealistic (see Recio and Oumeraci, 2007b and Itasca, 2004 for more details). On the other hand, a very small time step will increase considerably the computational time. The optimal time step is determined by "trial and error" and depends on the required accuracy of the simulation.
(ii) **Tolerance for updating the structure geometry in "COBRAS":** Every deformation or displacement of the elements will disturb the wave-induced flow and thus, the wave-induced forces on the elements in the next time step. With a fully coupled model, the geometry is updated and the subsequent disturbance of the flow considered at every time step. However, with the "partially coupling" as described in Figure 5-1, updating the geometry of the structure at every time step will not be practicable, so that a more feasible option is to update the geometry of the structure in "COBRAS" only after a tolerance has been exceeded (threshold displacement of a GSC higher than a predetermined value) (see Recio and Oumeraci 2007b for details). The value of the threshold for triggering the update in "COBRAS" should be as small as computationally possible. A threshold of 5cm ($1/8^{th}$ of the length of the element) showed reliable results. For a preliminary rough analysis, the threshold can be set very high to speed the computation. Another option is to stop the simulation when the displacement is larger than the threshold. In this case, the results will show where the critical displacement occurred and at which rate. Using this information, it may be predicted, whether the structure will be stable or not.

5.3 Modifications and Adaptation of the Models to GSC-Structures

Based on the knowledge obtained from various model tests and analyses of coastal structures made of sand containers (Chapter 4 and Recio and Oumeraci, 2005b and 2006b), the models were adapted to represent accurately the hydraulic processes responsible for the instability of GSC-revetments.

5.3.1 Fluid Dynamic Model "COBRAS"

(a) 2-D Assumption for Gap Flow

The flow in/on the GSC-structure is three dimensional while "COBRAS" can simulate only two dimensional flow.
Therefore, assumptions are made to convert the 3D flow into a 2D situation (Figure 5-2). The size of the containers is reduced to create a continuous gap between containers,

while their frontal part is prescribed as vertical to maintain the wave-reflection coefficient of the structure (see Recio and Oumeraci, 2006a for more details).

(b) Computational Domain and Discretization

Aside from the aforementioned 2D-flow assumptions, further numerical assumptions are made to achieve a practicable computational domain. Since most of the numerical simulations are intended to reproduce the previous model tests at LWI, the geometry of the computational domain was adapted to account for the dimensions of the LWI-wave flume (Figures 5-2 and 5-3). However, to reduce the computational time, the length of the wave flume was reduced from 100m to 44m as shown in Figure 5-3. The length of the domain is 44m length and 1m height. The domain is divided in three sub-domains (meshes) to save computational time and to increase accuracy in the area around the containers.

The size of the cells in the first domain varies from 5cm to 1cm. Largest cells are at the left-end boundary where accuracy is irrelevant.

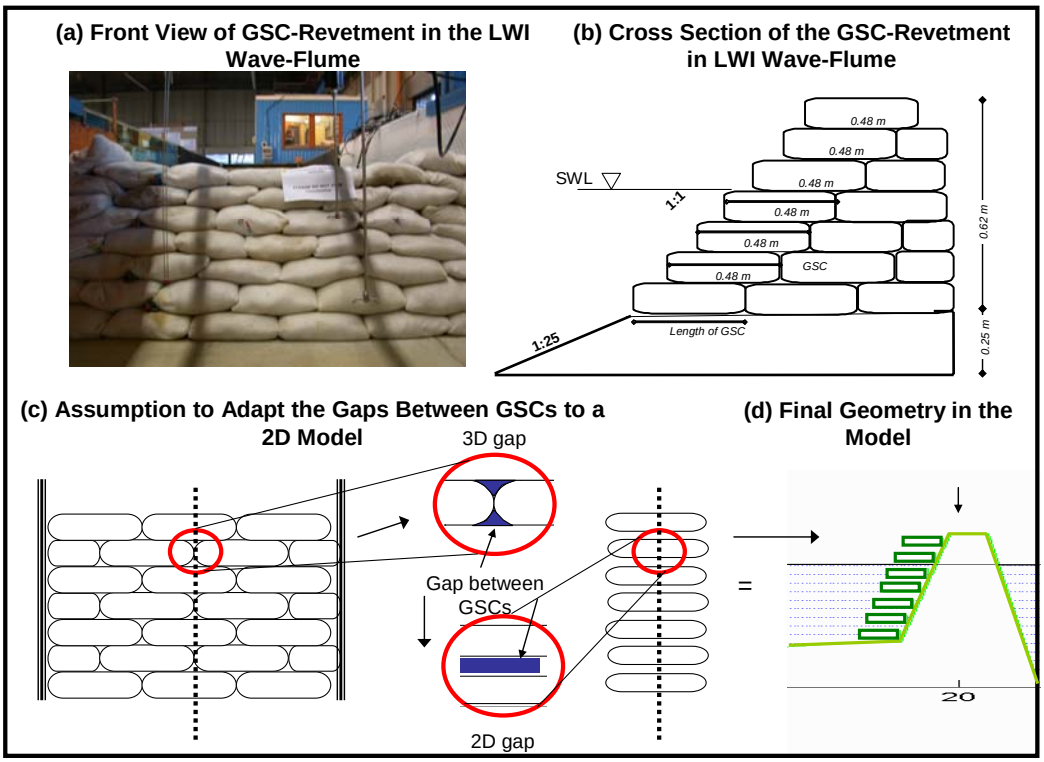

Figure 5- 2: Conversion of a 3D-Flow into a 2D-Flow Problem

The size of the cells in the area around the containers (sub-domain 2 in Figure 5-3) is 1cm x 1cm. The gaps between containers were always simulated with at least 3 cells in the vertical direction to provide accurate results (see Recio and Oumeraci 2006a for more details). Finally, the size of the cells of the third domain varies from 1cm to 5cm at the right-end boundary.

In addition, an internal wave maker and a “sponge layer” that damps the energy behind the wave maker are implemented near the left boundary of the computational domain (Figure 5-3).

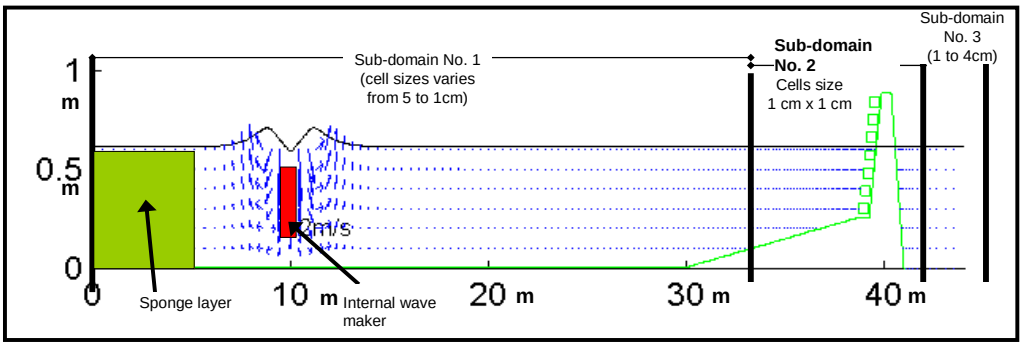

Figure 5- 3: Computational Domain Considered in the Simulations

5.3.2 Structural Dynamic Models "UDEC"

(a) Idealization of Geotextile Sand Container

Due to the complexity as well as to the stochastic and 3D nature of the stability problem, it is not practicable to simulate all the processes and interactions that may affect the stability of the GSCs. Moreover, a geotextile sand container (GSC) is a very complex composite element which consists of three components with different properties: (i) the surface of the GSC made of the geotextile, (ii) the interface between the geotextile and the sand and, (iii) the sand fill itself (Figure 5- 4). Recalling that one of the limitations of the "UDEC" model is associated with the requirement that each element is made of a continuous material (no discontinuities inside element), some assumptions to change the composite material of GSC to a homogeneous-continuous material were performed. Thus, for the simulations, the properties of the homogeneous material in the block have "average properties" of the three components of the GSC (Figure 5- 4).

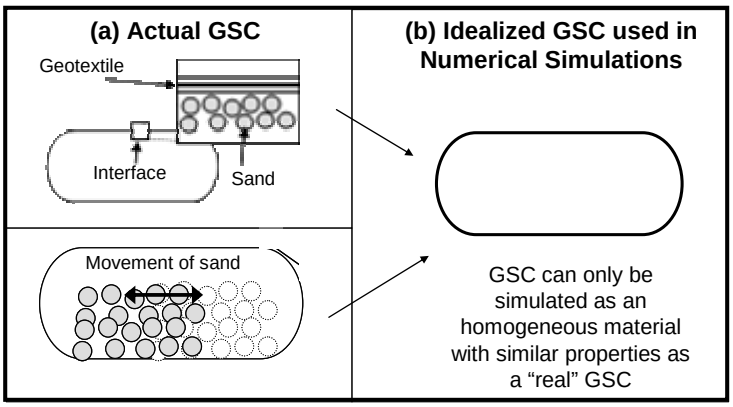

Figure 5- 4: Idealization of a Geotextile Sand Container for Structural Dynamic Computations

Matsuoka (2001) performed model tests on the properties of geotextile sand (and other types of soil) containers (see Recio and Oumeraci, 2007b and Section 2.1.2). The properties for the simulations were taken from the results obtained by Matsuoka and are described in Section 2.1. Based on biaxial-load tests a relation for the stress-strain behaviour of sand containers and "cohesion" values for sand containers were obtained and implemented in the structural model (see Figure 2-5, Matsuoka, 2001 and Recio and Oumeraci, 2007b for more details).

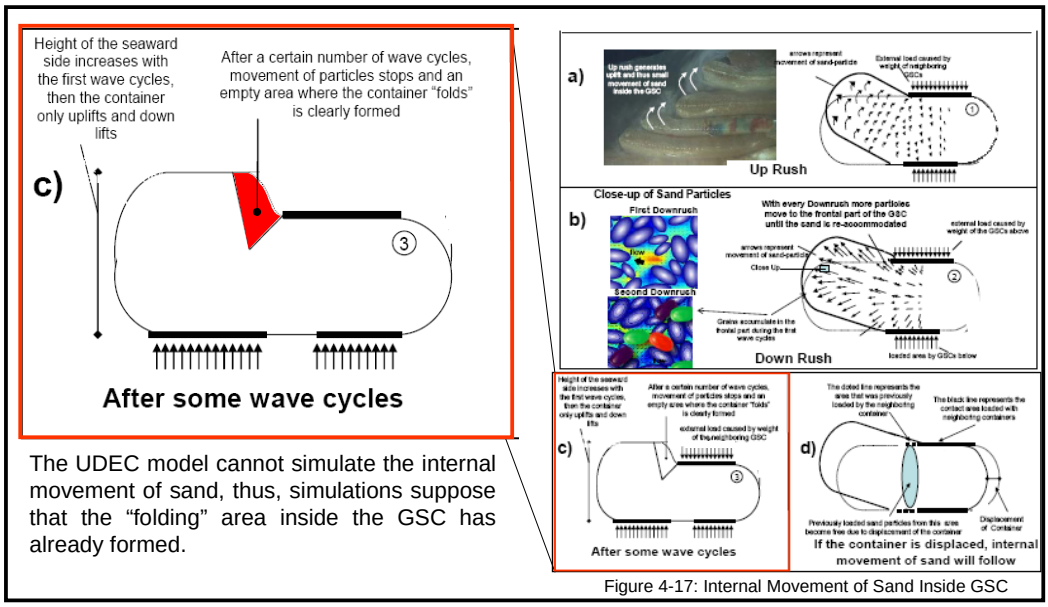

Figure 5- 5: Internal Movement of Sand inside a GSC and "Empty" Area Where the GSC "Folds" During Uprush (see also Figure 4-17)

(b) Computational Domain and Discretization

The computational domain of "UDEC" is shown in Figure 5- 6. The structure follows the typical geometry of the GSC-structure with the addition of three fixed blocks at the bottom and right boundaries to make the computational domain more stable. The GSC-structure was divided in two finite triangular meshes: (i) one small mesh for the GSCs (triangular elements in the mesh are approx. 2cm x 2cm) and (ii) one larger mesh for the rest of the structure (triangular elements in the mesh approx. 8cm x 8cm). As with the flow model, the smaller mesh is implemented in the areas where more accuracy is required (Figure 5- 6).

In addition, the internal movement of sand inside a GSC significantly affects the stability of the structure (Figure 5-5), Recio and Oumeraci, 2005b and Section 4.4). After the initial wave cycles, an empty area inside the GSC where the latter "folds" during uprush is formed (Figure 5-5c). Since the internal movement of sand inside the GSC is not simulated, it was assumed during the simulations that the initial arrangement of sand inside the GSC has already occurred and that the "folding" area is already formed.

The "folding" area is created by reducing the values of the stiffness matrix that correspond to the elements that are in this area (Figure 5-7). For more details on the "stiffness" matrix refer to Recio and Oumeraci (2007b), Abaqus (2000), and Itasca (2004). The values of the "folding" area considerably affect the stability of the GSC-structure. The "folding" area absorbs energy that is no longer transmitted to the neighbouring containers, thus the deformation values of this area are decided to represent accurately the stability of the GSC-structure (values of the folding area are critical for the validation of the models). The optimal values of the folding area remain constant during all the simulations (see Table 5.1 for details).

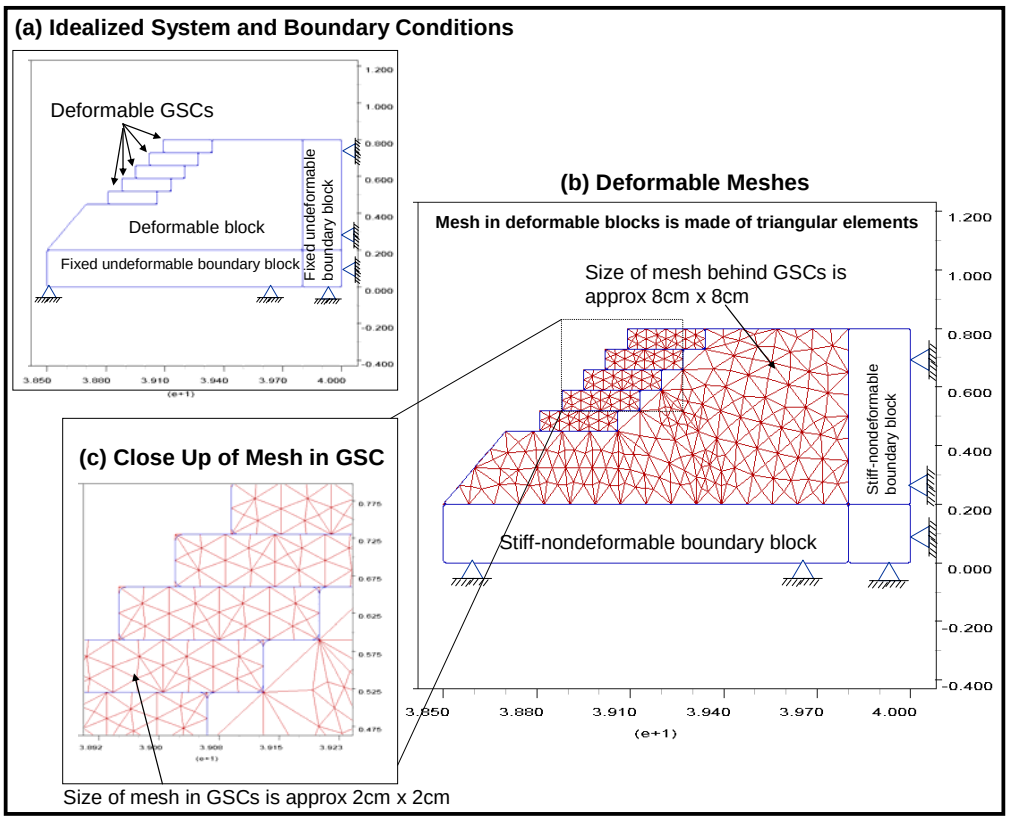

Figure 5- 6: Computational Domain and Discretization in the Structural Dynamic Model ("UDEC")

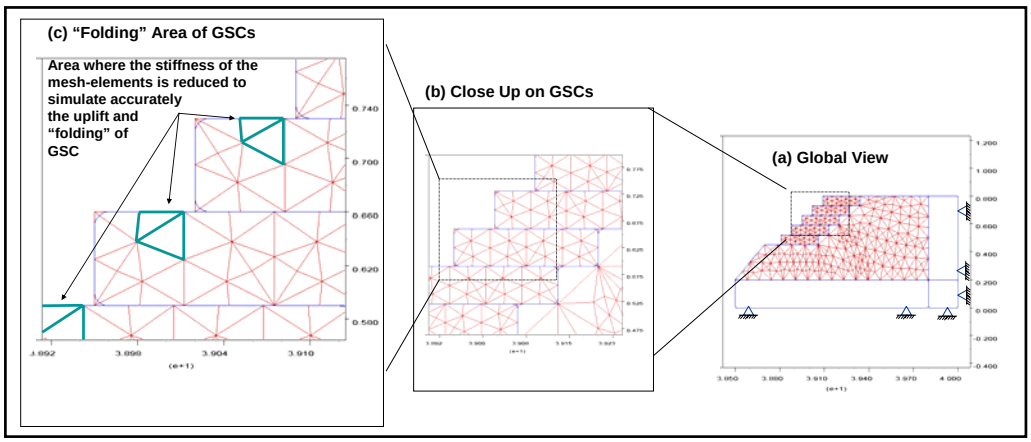

Figure 5- 7: Implementation of the "Folding" Area inside the GSCs in the Numerical Simulations (see also Figure 5- 5)

5.4 Model Validation

5.4.1 Validation of "COBRAS"

Results from "COBRAS" were compared with the experimental data obtained from the model tests described in terms of surface elevation, wave pressure and particle velocity described in Chapter 4. A comparison between computational results and experimental data is shown in Figure 5-8. More results are given in Recio and

Oumeraci (2006a). The agreement for the free surface elevation, velocities and wave-induced pressures is relatively good (scatter normally within 20% in terms of the peak amplitude and 8% in terms of the phases).

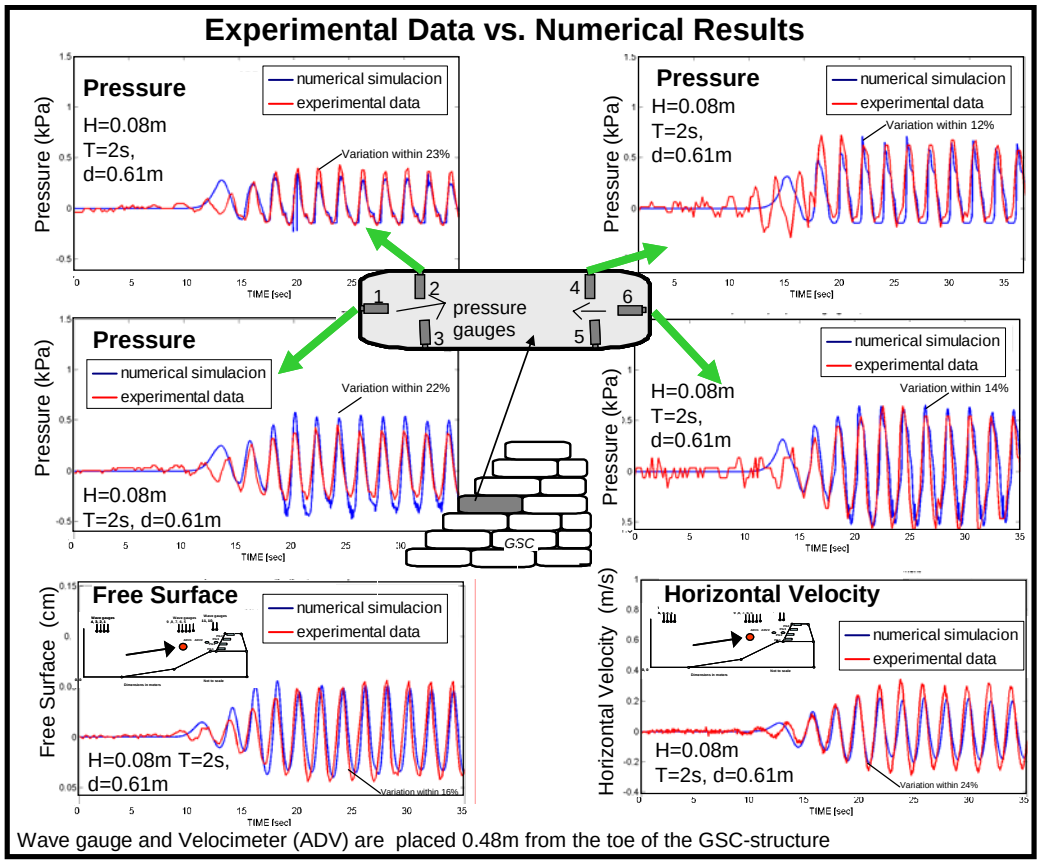

Note: For comparisons involving all the pressure gauges and more wave conditions refer to Recio and Oumeraci (2006a)

Figure 5- 8: Measured and Computed Wave-Induced Pressures, Free Surface Elevation and Particle Velocities

5.4.2 Validation of the "Partially Coupled" Model System "COBRAS-UDEC"

(a) Experiments Used for Validation

Since "UDEC" uses wave-induced forces computed by "COBRAS" as input, it is not practicable to validate "UDEC" without performing "partially coupled" COBRAS-UDEC simulations. Therefore, to validate the "partially coupled" model system and to check its feasibility to simulate the hydraulic stability of GSC-structures, the COBRAS-UDEC system was applied to the GSC-structure tested by Oumeraci et al (2002) in the LWI wave-flume (Figures 5-9 and 5-10). The main reasons for the selection of these tests among other available model tests (e.g. Recio and Oumeraci 2006b) are:

(i) The size of the GSC-structure tested by Oumeraci et al (2002) is very small compared with other available tests; thus, computational times are substantially reduced.

(ii) Oumeraci et al (2002) performed stability tests and found a stability threshold which depends on the wave conditions (see next section for more details). This stability threshold is used to calibrate the threshold between

"movement" and "no movement" of GSCs in the numerical simulations and finally to validate the model system.

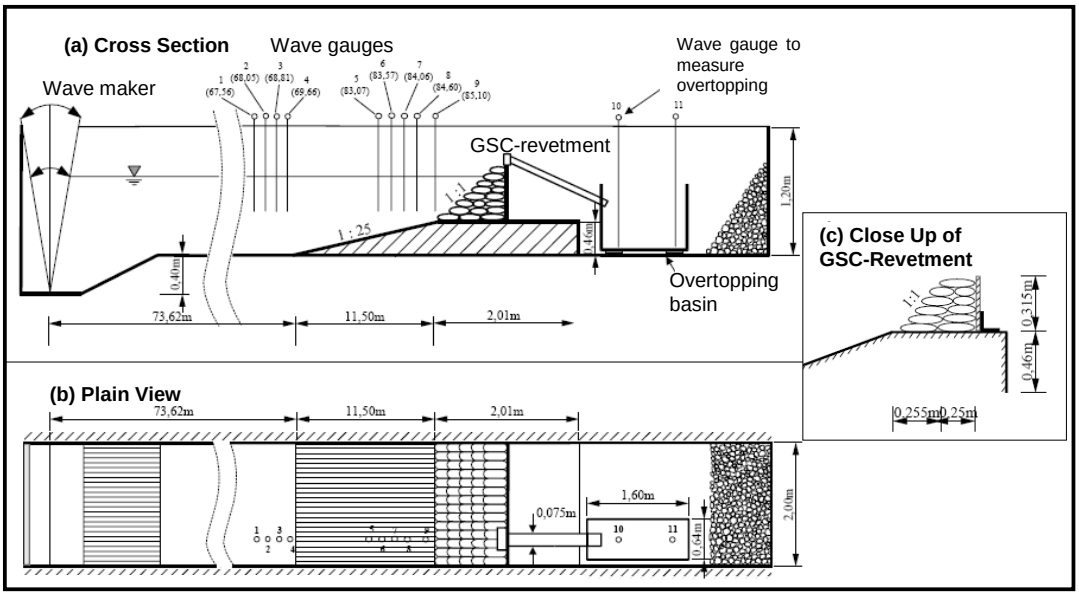

Figure 5- 9: Experimental Set-Up of the Model Tests Performed in the LWI-Wave-Flume by Oumeraci et al (2002)

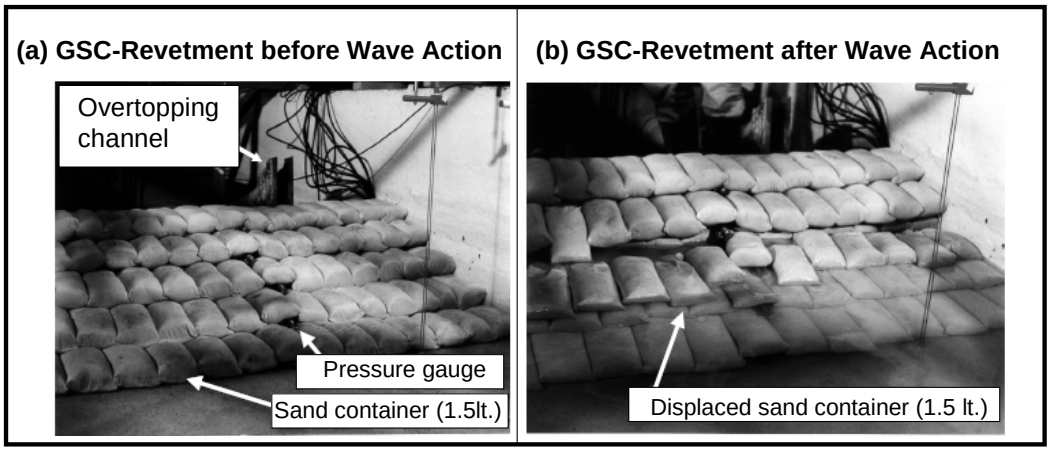

Figure 5- 10: Model Tests Performed in the LWI-Wave-Flume by Oumeraci et al (2002)

For these tests a GSC-structure was constructed in the wave flume of LWI using sand filled containers of 0.25m x 0.1m x 0.06m, with a slope of 1:1 ($\alpha = 45^o$). The structure was subject to regular and irregular waves varying from 0.08m to 0.20m with wave periods varying from 1.5s to 4s. The water depth was varied from 0.61m to 0.77m (Figure 5-9).

(b) Input Parameters for the Numerical Simulations

The main input values used for the "coupled" simulations are summarized in Table 5.1. The values for the fluid dynamic model are selected following the experience gained within the research team of Professor Philip L F Liu of Cornell University. The values for the structural dynamic model were selected, following the results by

Matsuoka (2001) and the values for the "folding" area inside the GSCs were determined iteratively. The friction angle between GSCs was selected, considering the values obtained from large scale shear-box tests performed by Naue (2004) (Table 2.2).

Table 5.1: Main Input Parameter and Assumptions Used in the Numerical Simulations

"COBRAS" PARAMETERS		"UDEC" PARAMETERS	
Description	**Input Values**	**Description**	**Input Values**
Time step	0.02 s	Time step	0.02 s
Density of water	1000 kg/m^3	Density of all non-submerged deformable GSCs	1800 kg/m^3
Type of wave	Stokes V, Internal wave maker	Density of all submerged deformable GSCs	800 kg/m^3
Kinematic viscosity of water	1x10^{-6} m^2/s	Bulk modulus of GSCs	2.5x10^6 Pa
Turbulence model	$k-\varepsilon$ (nonlinear eddy viscosity)	Shear modulus of GSCs	1.1x10^6 Pa
Turbulence seed parameter	0.5	Cohesion of all GSCs	1.4x10^4 Pa
Eddy viscosity behaviour parameter	5	Bulk modulus of "folding" area inside GSCs	9x10^4 Pa
Max Courant Number	0.3	Shear modulus of "folding" area inside GSCs	4x10^4 Pa
Wave heights	0.08- 0.20m	Friction angle between GSCs	28^o
Wave period	1.5-3 s	Cohesion of "folding" area inside GSCs	1.4x10^4 Pa
Water depth	0.61 m	Maximal displacement of GSC before updating the geometry in "COBRAS"	0.05 m
Mesh in domain	1600 x 100	Constitutive model for the deformation of GSCs	Mohr-Coulomb

Using the "partially coupled" model system, several numerical simulations with the same geometry and conditions as tested by Oumeraci et al (2002) were performed. Coupled simulations are shown in the DVD attached to this thesis.

(c) Comparisons between Numerical and Experimental Results

First, the comparison between the simulated and observed deformation of sand containers and the reduction of contact areas is briefly discussed before embarking into the more quantitative validation with respect to the hydraulic stability.

The comparison of the uplift deformation between experimental data and numerical results is shown in Figure 5- 11. As found in Chapter 4 and Recio and Oumeraci (2005b and 2006b), the uplift of the GSC depends on the slope angle of the structure. The differences between experimental and numerical results vary from 29% for uplift

deformation of the critical container and to 12% for the reduction of contact areas during wave action (Figure 5- 11).

Regarding the frontal deformation reported by Recio and Oumeraci (2005b) (Figure 4-23), it is seen that the numerical model cannot perform exactly in the same way as observed in the model tests, because this deformation is directly induced by the internal movement of sand inside the GSC, which cannot be simulated by the "partially coupled" model COBRAS-UDEC.

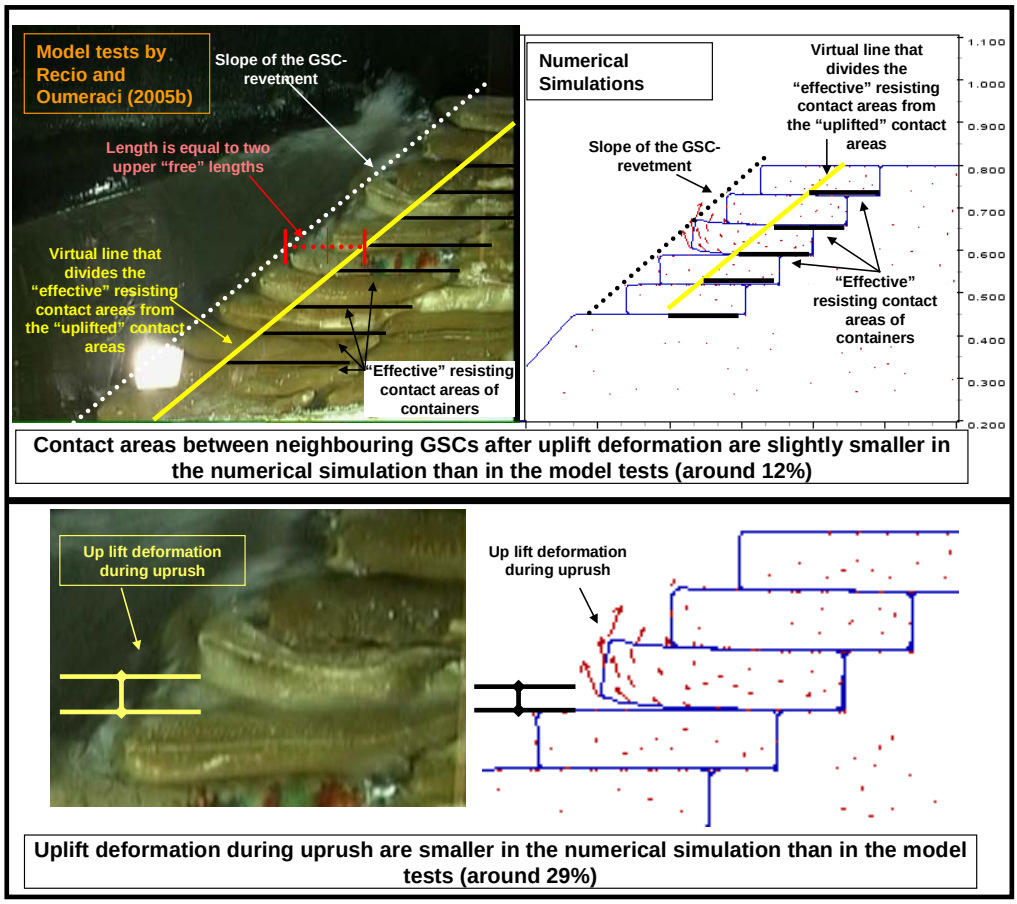

Figure 5- 11: Qualitative Comparison of Computed and Observed Uplift Deformation

All numerical simulations were compared with the experimental data obtained by Oumeraci et al (2002) (for more details see Recio and Oumeraci, 2007b). As a result of the experiments Oumeraci et al derived stability formulae for the slope and crest containers (Figure 5- 12 and refer to Section 2.4.4 for details on the formulae).

For the slope containers, the stability number N_s is plotted as a function of the surf similarity parameter ξ_0 (refer to equations 2.8 and 2.12 for definition of the parameters).

The results of the simulations are shown in Figure 5- 13. GSC-structures are stable for a wave height of 0.08m (except the simulation with H=0.08m, T=3s) and for a wave period of 1.5s (except the simulation with H=0.20m, T=1.5s).

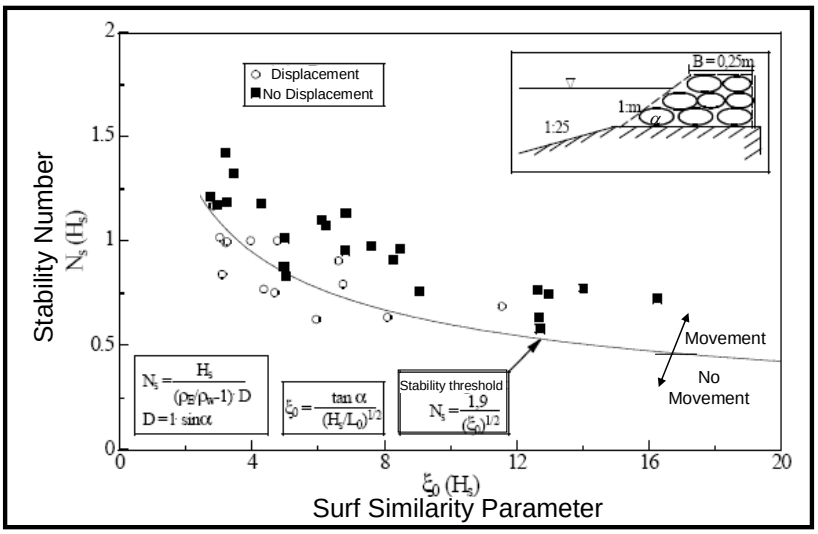

Figure 5- 12: Experimental Results for Slope Containers (after Oumeraci et al, 2002)

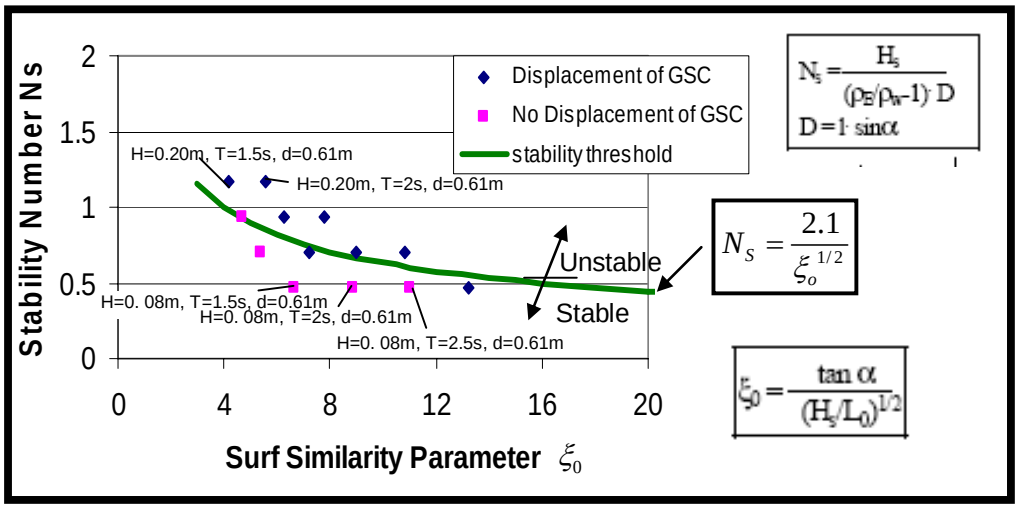

Figure 5- 13: Computed Results for GSCs on the Slope

In order to reduce computational time, the GSC-structure was considered unstable, if the displacement of one of the GSCs was observed to increase incrementally with every wave cycle as illustrated in Figure 5- 14b, showing that the displacement rate within one wave cycle provides a clear indication on the instability of the GSC-structure. For example, if the displacement of one GSC occurs stepwise with every wave cycle, the structure can be considered as unstable. In fact, this assumption is reasonable, since Oumeraci et al (2002) and Recio and Oumeraci (2006b) found that if the displacement of GSCs starts to occur incrementally, it will continue with every wave cycle until the container will be pulled out from the structure (see also Chapter 4).

The stability threshold of the numerical results is plotted and compared with the stability threshold obtained by Oumeraci et al (2002) (Figure 5- 15). The agreement between numerical and experimental results shows qualitative differences as a function of ξ_o of about 10% for the range of $\xi_0 = 4 to 13$.

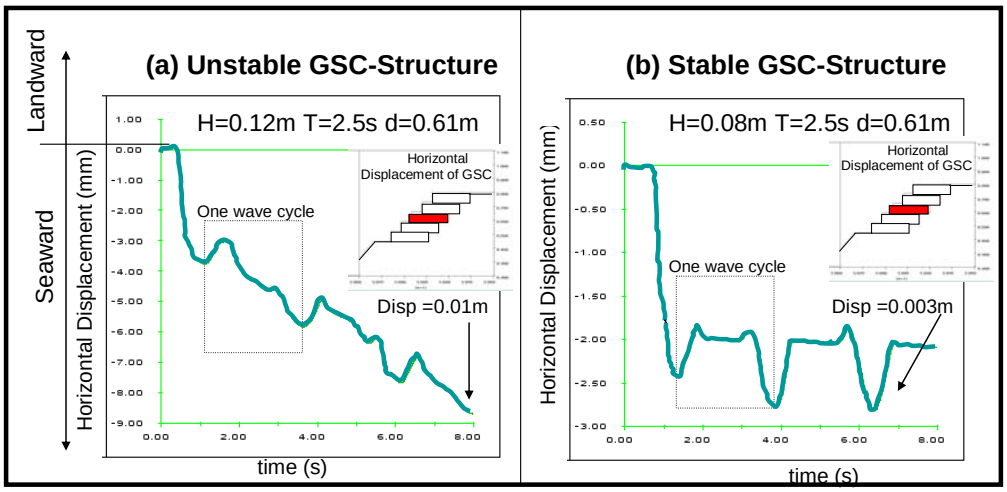

Figure 5- 14: Horizontal Displacement of GSC in a GSC-Structure under Wave Action

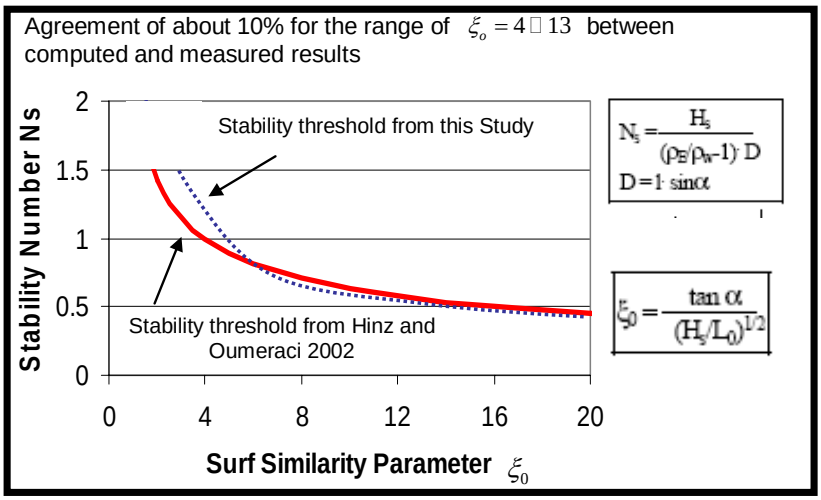

Figure 5- 15: Numerical Results of this Study vs. Stability Threshold Derived by Oumeraci et al (2002)

5.5. Numerical Simulations and Analysis of the Stability of GSC-Structures

Using the validated "COBRAS-UDEC" model system, numerical simulations are performed to achieve an improved understanding of the following processes that are associated with the instability of GSC-structures. Only the most important results are reported here, for the results of all analyses refer to Recio and Oumeraci (2006a and 2007b).

5.5.1 Up and Downrush Velocities on and in a GSC-Structures

The flow velocity field during downrush is shown in Figure 5-16. The same results were observed during the model tests (see attached DVD for more details). The water particle follows an orbital trajectory before reaching the revetment. In addition, the same flow separation and small vortices as in the laboratory experiments are observed at the "steps" in front of the structure (see animated videos attached to this thesis for details).

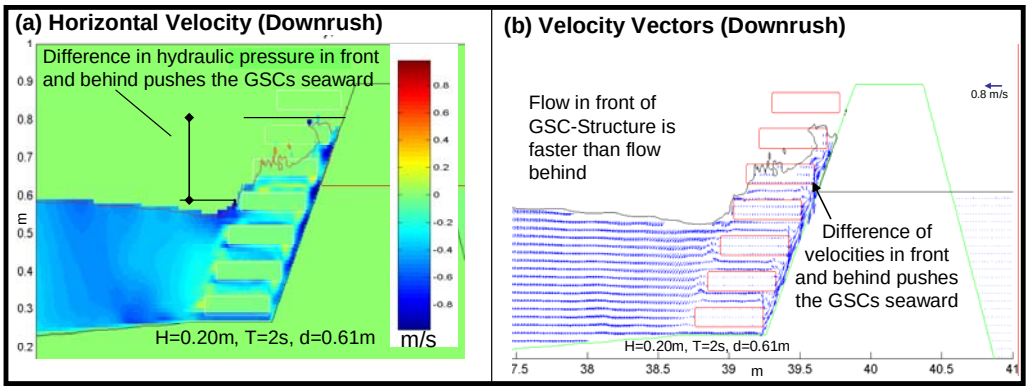

Figure 5- 16: Downrush Velocities inside the Revetment

Results from the simulations of the up and downrush velocities have shown that:

(i) In average, the wave-induced velocities behind the containers are smaller than in front of the structure. However, larger individual particle velocities appear behind the first GSC-layer where the gap between the rear of the container and the slope behind becomes very narrow.

(ii) Downrush velocities behind the containers last longer time compared with downrush velocities in front of the structure. This supports the conclusion drawn in Chapter 4, stating that the critical area is below SWL. The averaged velocity inside the GSC-structure is smaller than outside. As a result, a pressure gradient that pushes the GSC seaward, which is maximal at the area just below the SWL, is generated (see also Figure 5- 21).

5.5.2 Wave-Induced Velocities inside the Sand Fill of the Containers

Further advantages of using a permeable container in the numerical simulations are associated with the possibility to investigate the flow inside the containers. Recalling that the velocities inside the containers (velocities through the sand fill) obtained from the numerical model are averaged velocities, it is observed that the maximal velocities inside the containers are more than 18 times smaller than the maximal velocities outside the containers (Figure 5- 17), thus, supporting the conclusion drawn in Chapter 3, stating that the flow within a GSC-revetment is essentially governed by the gaps between the containers and that the flow through the sand fill of the containers themselves is negligibly small.

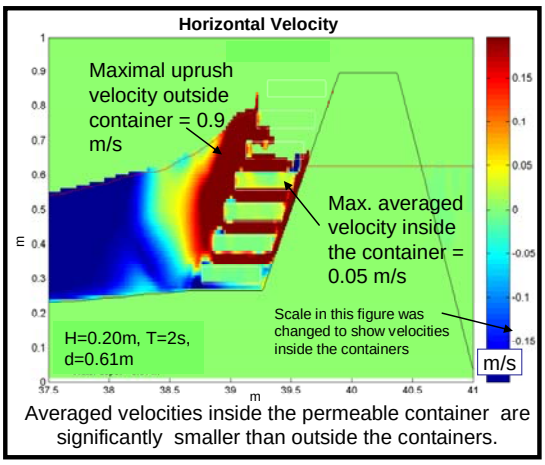

Figure 5- 17: Wave-Induced Velocities inside and outside the Container

5.5.3. Wave-Induced Pressure and Turbulence on and in the GSC-Structure

Numerical results also provide an insight of the turbulence intensity and wave-induced pressures in and on the GSC-revetment.

Pressure analyses have shown that:

- The maximal pressure on the revetment occurs just at the end of the uprush phase (Figure 5- 18a).The water remains longer behind the containers than in front generating a pressure gradient that pushes the GSCs seaward (for more details refer to Recio and Oumeraci 2006a).

Turbulence analyses have shown that:

- There is a high turbulence intensity at the toe of the structure (Figure 5- 18b), indicating where potential wave-induced scour erosion and at which rate it may occur.
- There is also a moderate intensity under the wave crest extending from the bottom to the top. This indicates where mixing and sediment movement due to wave action might occur (Figure 5- 18b)

For more details refer to Recio and Oumeraci 2006a.

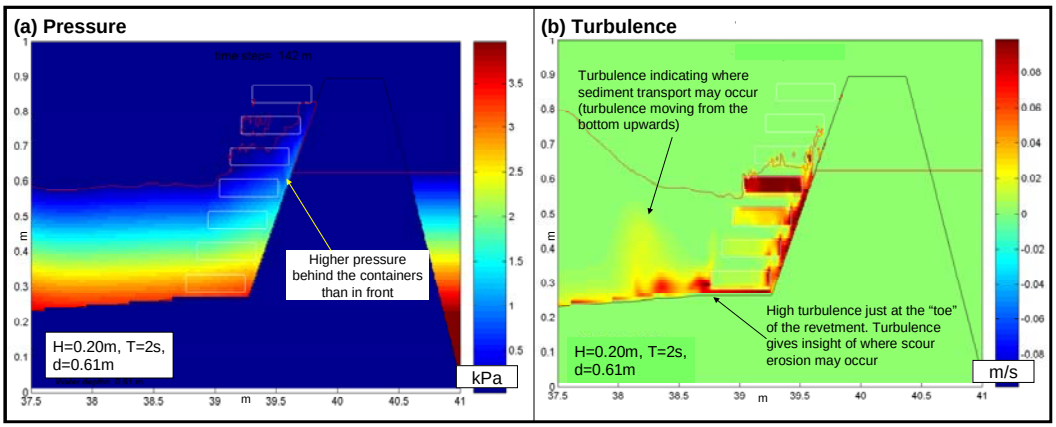

Figure 5- 18: Wave-Induced Turbulence and Pressures on and in the GSC-Revetment During Downrush

5.5.4. Wave-Induced Forces on Containers and Interactions

Using the validated models, the wave-induced forces on each container are investigated to provide a further insight into the interaction between the wave loading of neighbouring containers.

The numerical results are found to be very similar to the ones recorded during the model tests and support that the critical container for the stability of a revetment is the container placed just below the SWL (Figure 5-19).

The most interesting benefit of the numerical simulations is the possibility to analyze the interaction of wave-induced forces on neighbouring containers (see also attached videos). The total wave-induced forces on the containers have the same frequency, but a phase shift is observed, especially for the horizontal forces (Figure 5-20).

The "phase shift" depends on the wave period and the slope angle of the structure (see Recio and Oumeraci, 2006a for more details). The main reason for this "phase shift" is that during wave action each GSC is located at a different elevation and is thus, subject to different wave-induced forces. As illustrated in Figure 5- 21, when the first wave reaches the two lower containers, the upper container has no wave-induced pressure. With the progression of the wave on the structure, each GSC that is reached by the crest of the wave will experience an increase of the loading, while the

containers underneath experience a decrease. This indicates that the resultant forces between neighbouring GSCs are different and influenced by the position of the GSC with respect to the SWL.

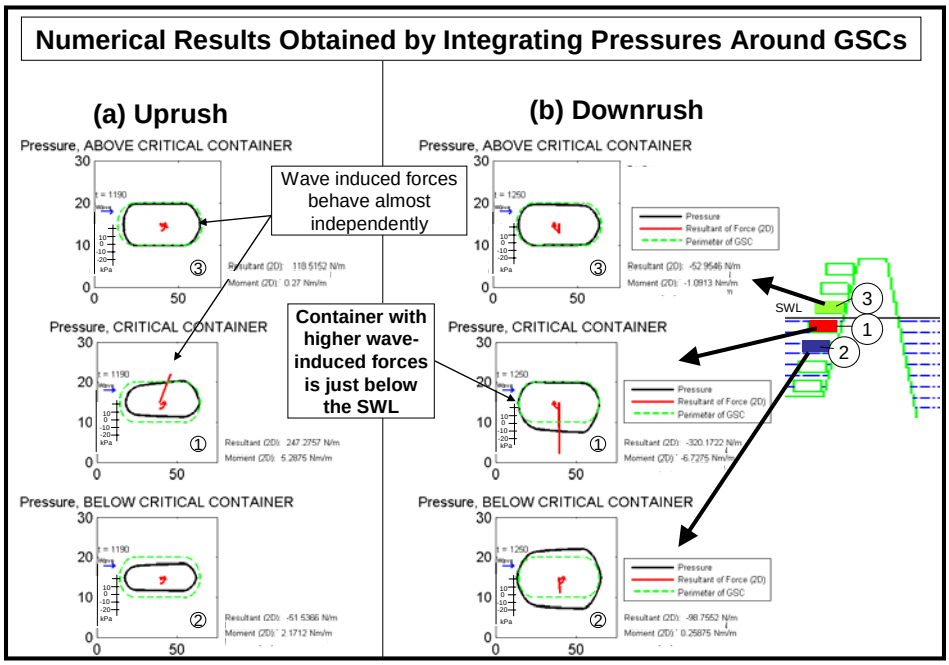

Figure 5- 19: Interaction of Wave-Induced Forces on Neighbouring Containers (H=0.2m T=2s d=0.61m)

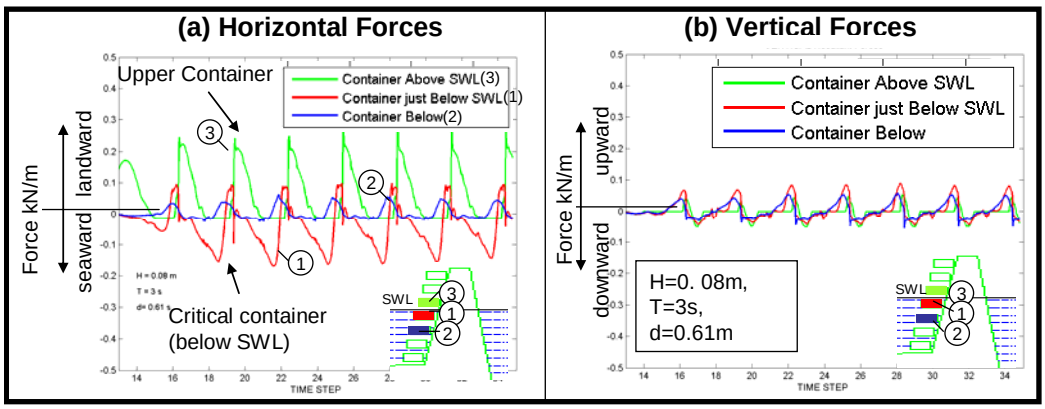

Figure 5- 20: Analysis of Wave-Induced Forces on Sand Containers

5.5.5 Wave-Induced Deformations of Sand Containers

The deformations of GSCs induced by wave action is illustrated by Figure 5- 22. The vectors show the displacement of the nodes in the UDEC-model. The container just below still water level suffers the largest uplift deformation. However, as also observed in the laboratory tests, the deformations of other containers which reduce its contact areas, are also present (see attached videos for more details). There is a qualitatively good agreement with the laboratory tests:

(i) The critical GSC is the container located below the still water level (SWL).
(ii) The uplift deformation of the frontal part of the GSC occurs during uprush
(iii) The displacement of the GSC is incremental (stepwise) and occurs mainly during the downrush phase.

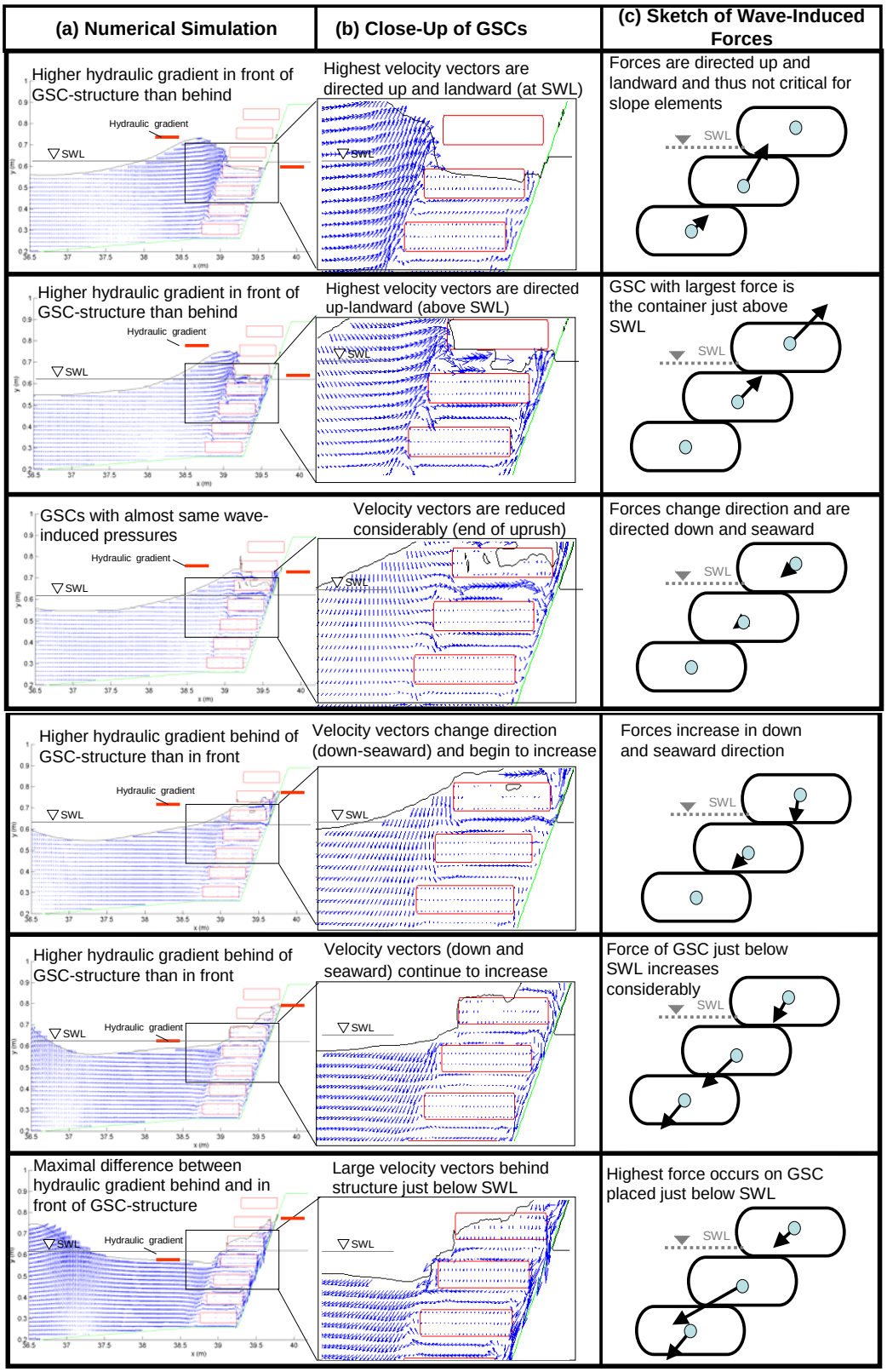

Figure 5- 21: Interaction between Wave-Induced Forces on GSCs

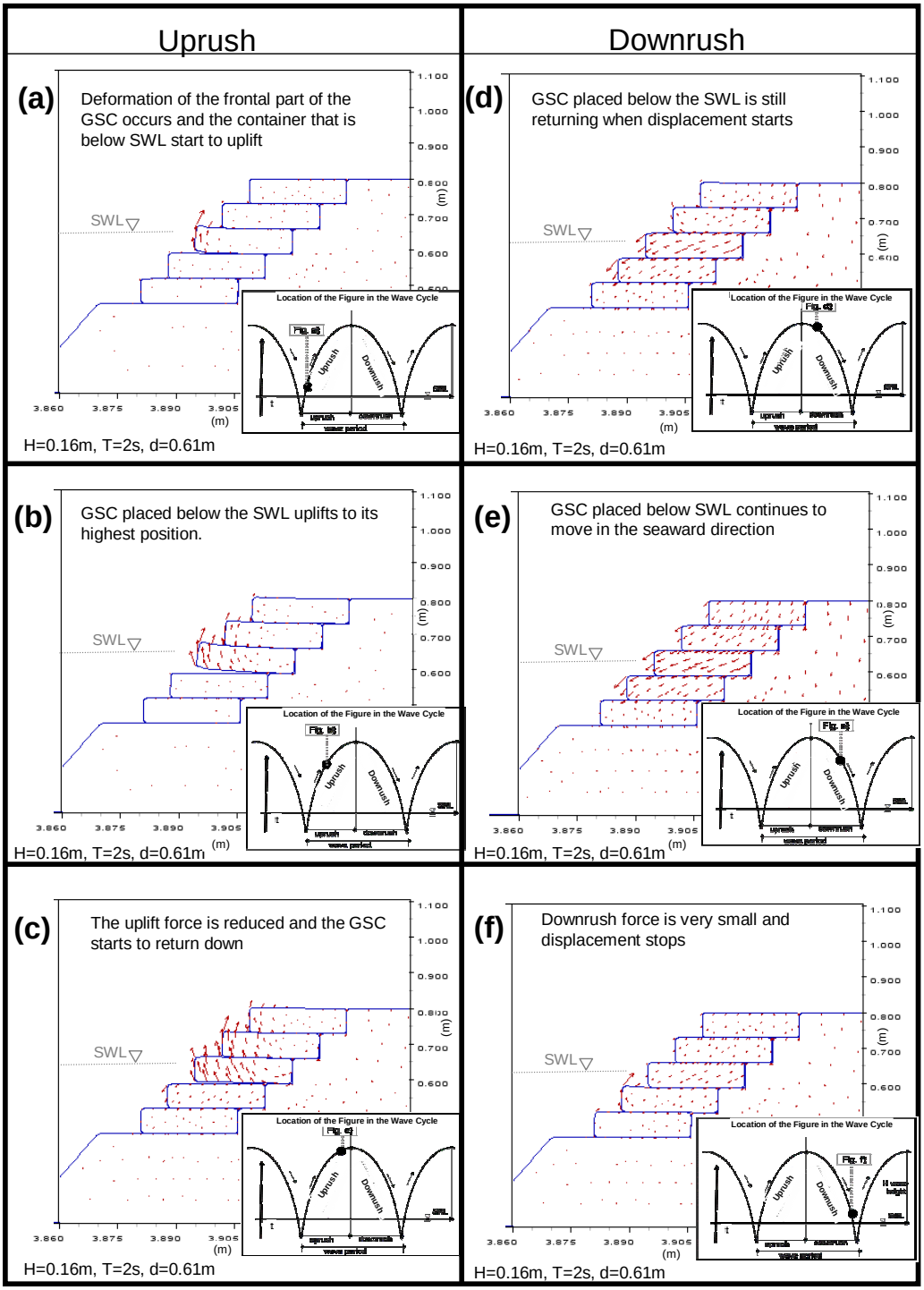

Figure 5- 22: Deformations and Displacements within a Wave Cycle, H=0.16m, T=2s and d=0.61m

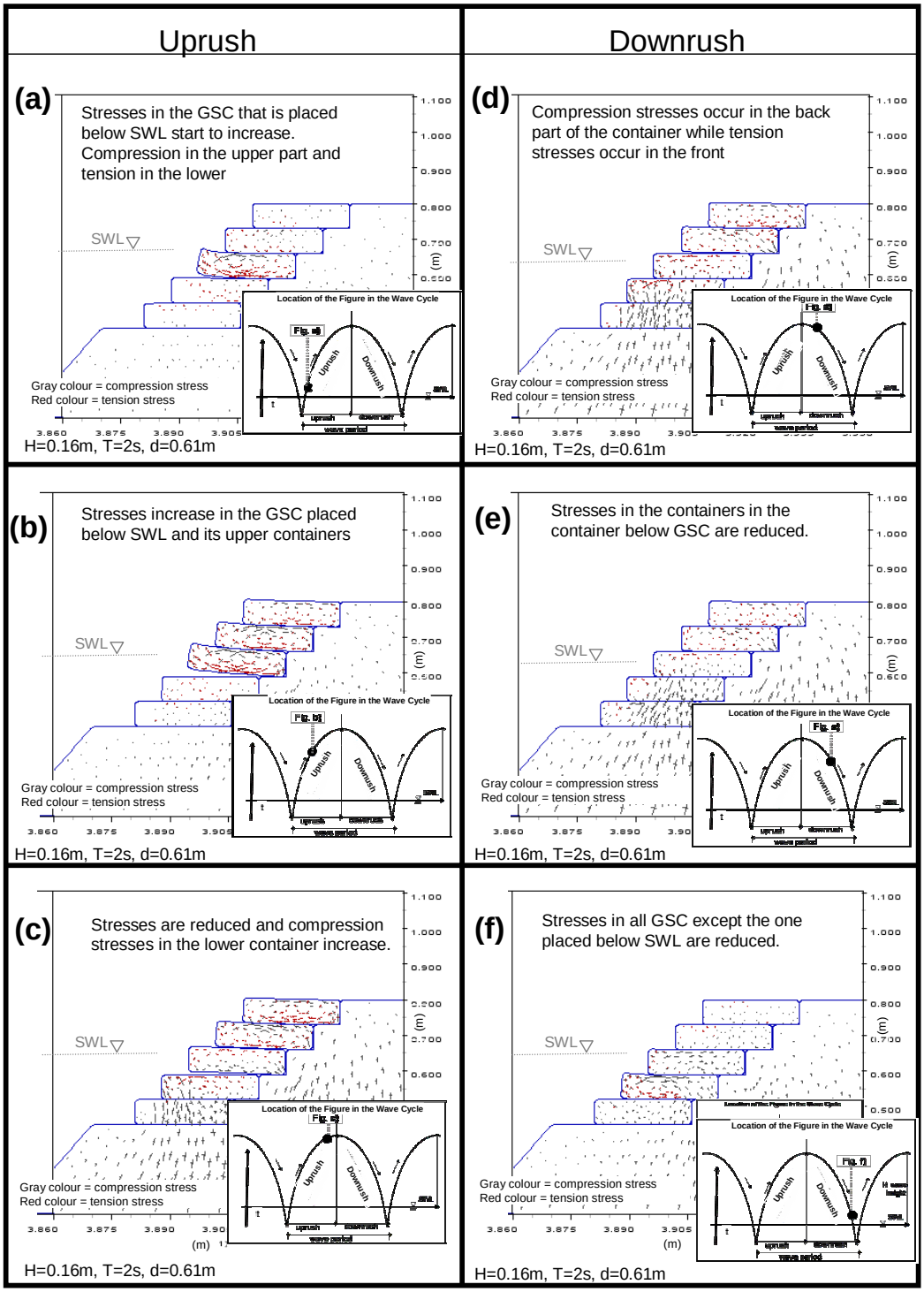

Figure 5- 23: Wave-Induced Stresses within a Wave Cycle, H=0.16m, T=2s and d=0.61m

5.5.6 Wave-Induced Stresses inside GSCs

The wave-induced stresses on GSC are shown in Figure 5-23. However, these results need to be treated with caution with respect to the quantitative prediction, since the COBRAS-UDEC system cannot simulate the sand inside the container. Nevertheless, the numerical simulations are valuable in the sense that they provide together with the

laboratory results an improved insight into the processes involved. The deformations induce large stresses on the containers. In addition, at the time when the GSC just below SWL starts to move, stresses are generated at its rear-upper part, showing that even during the displacement of GSCs, the neighbouring GSCs are transferring part of their weight to the GSC underneath, thus, increasing their hydraulic stability (see Section 6.3 for more details).

5.5.7. Effect of Neighbouring Containers on Hydraulic Stability

The boundary conditions considerably affect the stability of GSCs. Comparison of three structures with the same wave conditions but different boundary conditions were analyzed by the COBRAS-UDEC model system: (i) normal GSC-structure, where critical GSC is just below still water lever with containers above and behind it (Figure 5-24a), (ii) low-crested GSC-structure with considerable overtopping, in which the motion of the critical container is restricted in the horizontal direction by the neighbouring container (Figure 5-24b) and (iii) low-crested GSC-structure, in which the critical GSC has no displacement restriction above or behind (Figure 5-24c).

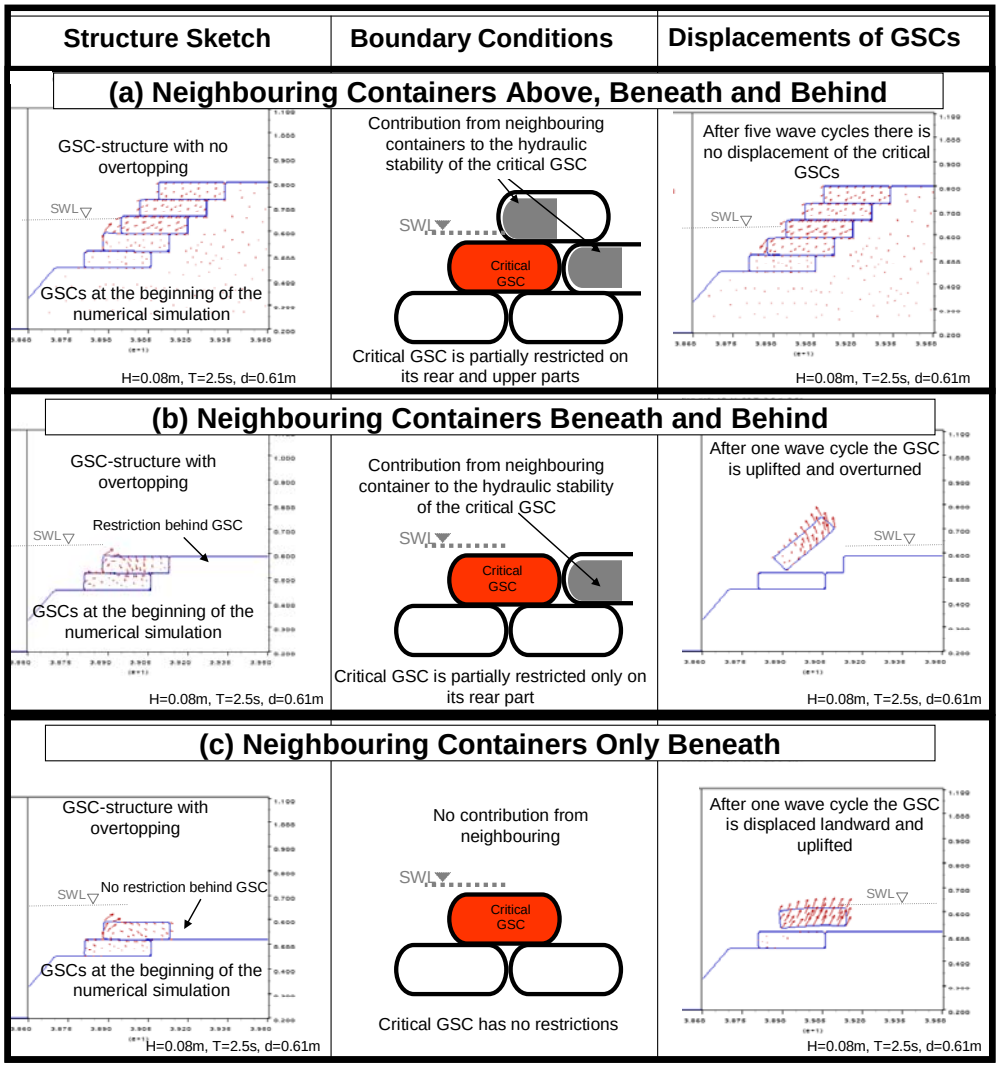

Figure 5- 24: Influence of Neighbouring GSCs on the Hydraulic Stability of GSC-Structures (see also Figures 5-25 and 5-26)

Numerical results showed that the stability of a container depend on the number of neighbouring containers that surround it. Numerical simulations showed that the stability threshold and type of displacement depend on the arrangement of neighbouring containers (Figures 5-24, 5-25 and 5-26).
It was confirmed that if a structure is subject to considerable overtopping, the critical containers are those placed at the crest-edge of the structure (Oumeraci et al, 2002). Crest GSCs consisting of a single layer (cross section) as in Figure 5-26, are considerably less stable than slope and crest GSCs, which have a neighbouring containers behind (Figure 5-25).

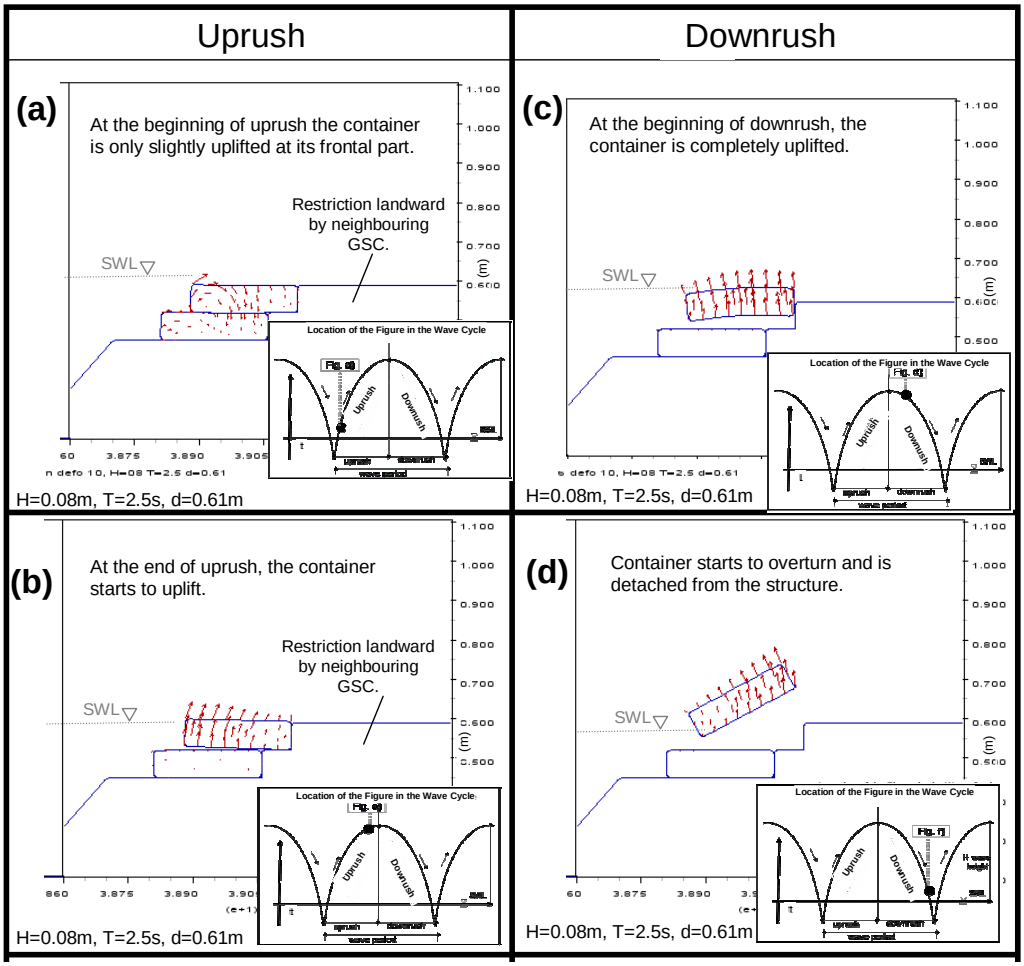

Figure 5- 25: Displacement of Crest GSC with Landward Landward Restrictions

When a single GSC is subject to overtopping, landward sliding might occur during uprush, while a container with a restricted horizontal displacement will be most probably displaced during downrush (see Figure 5-26 and attached DVD for details).
The most stable containers are those placed on the slope, where the neighbouring containers contribute to the stability (Figure 5- 22).

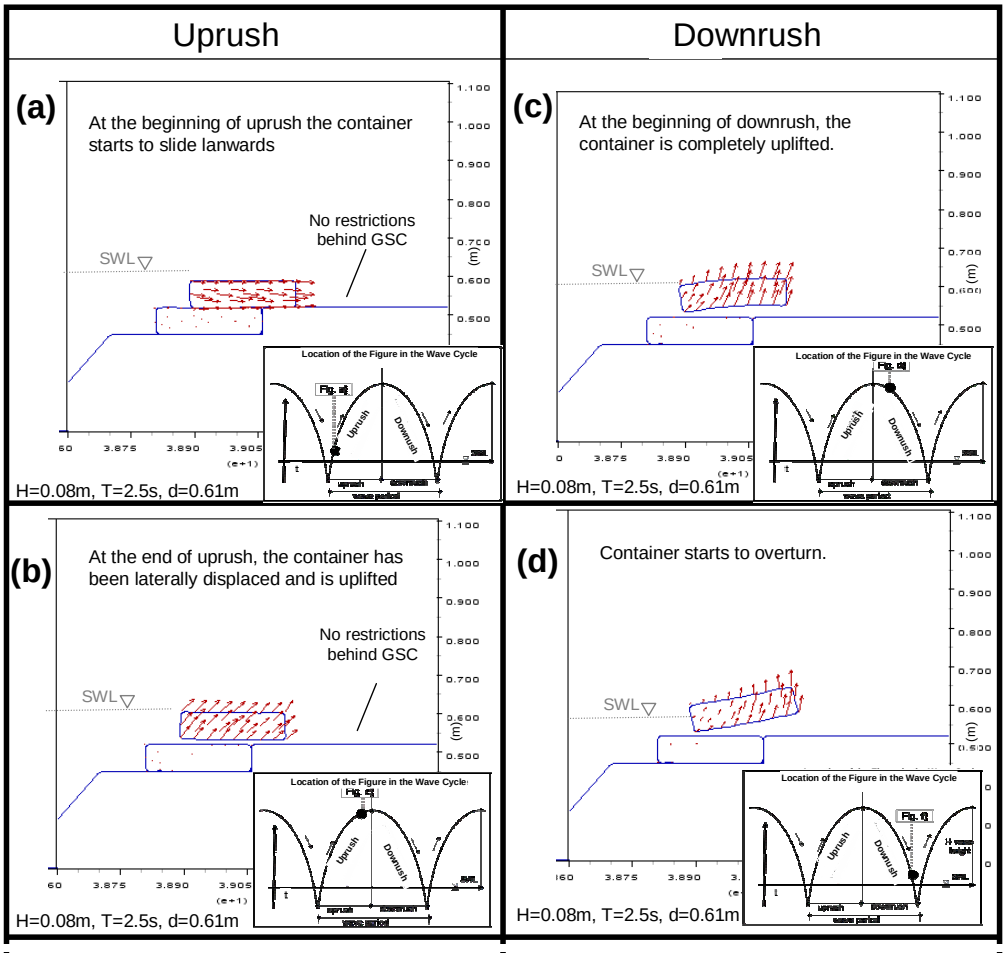

Figure 5- 26: Displacement of Crest GSC without Neighbouring Containers

5.5.8 Friction between Sand Containers

The "COBRAS-UDEC" model system was also used to investigate some relevant parameters that affect the stability of GSC-structures. For instance, the friction between GSCs was found to considerably affect the hydraulic stability.

Consideration of the friction angle between GSCs needs to be considered before selecting the type of geotextile to be used for a prototype GSC-structure. Even small variations in the friction angle may induce completely different displacements of the GSCs as illustrated by Figure 5- 27. The latter shows that a GSC-structure with same geometry and boundary conditions, but different friction angle would result in different stability threshold. Therefore, the friction value should be selected from reliable shear stress tests between two geotextiles.

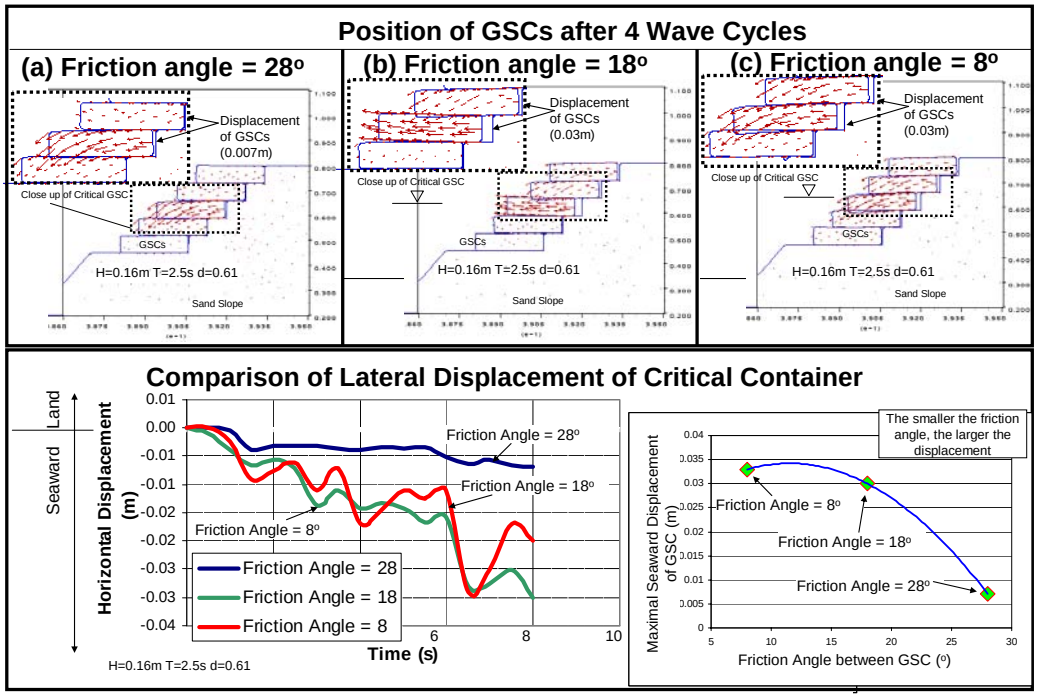

Figure 5- 27: Effect of Friction between GSCs on the Hydraulic Stability of GSC-Structures (H=0.16m, T=2.5s and d=0.61m)

5.6 Summary and Practical Implications of the Results

The main results of the numerical simulations and their implications for the engineering practice may be summarized as follows:

(i) The modified numerical model "COBRAS" can simulate wave action at, on and in a GSC-structure with sufficient accuracy, particularly in terms of surface elevation, particle velocities and wave pressure.

(ii) The "partially coupled" model system "COBRAS-UDEC", used in this study for the simulation of the stability of GSC-structures, has shown surprisingly much better agreement than expected (stability threshold with variations of 10% for surf similarity parameters in the range of $\xi_0 = 4$ to 13).

(iii) The "partially coupled" model system can, however, not describe the internal movement of sand inside the GSC and thus, cannot accurately simulate the frontal deformation of GSCs.

(iv) The extension of "COBRAS" to simulate the flow through a GSC-structure has shown that the wave-induced velocities through the sand fill of the containers are almost 20 times smaller than the velocities outside of the containers, so the flow through the structure is essentially governed by the gaps between GSCs.

(v) The "partially coupled" model system has shown that there is high turbulence at the toe of the structure indicating, where and at which rate erosion might occur.

(vi) The maximal difference of pressure behind and in front of a container generally occurs just after the end of the uprush phase and mainly acts on the containers placed just below the still water level.

(vii) The numerical simulations support the conclusion drawn from the experimental results that the critical slope-container on a GSC-structure is the container placed just below still water level.

(viii) The interaction of wave-induced forces on neighbouring containers was investigated, showing that the resultant forces on each container behave almost independently from the neighbouring containers. The “phase shift” between forces mainly depends on the wave-period and slope of the GSC-structure.

(ix) Friction between GSCs considerably affects the stability of GSC-structures and thus, for prototype GSC-structures, it is necessary to account for this parameter much more than in the past when selecting the type of geotextile to be used for the containers.

(x) Numerical simulations have also shown that the critical areas for the stability of the structure are for the containers placed just below the still water level and at the crest of the structure.

(xi) A coupled RANS-VOF with FEM-DEM has a promising potential as an engineering tool to investigate the stability of coastal structures, including wave-structure interaction. Any coastal structure can be investigated to identify critical areas for the stability, the collapse mechanisms or the response of a coastal structure to dynamic load. However, full coupling of the models is still needed to increase the range of application.

Chapter 6

New Hydraulic Stability Formulae

Based on the new knowledge of the processes associated with the hydraulic stability of geotextile sand containers (GSCs) used for coastal structures, which has been gained in the previous chapters, explicit stability formulae are derived for the two modes of failure of GSCs as described in Chapter 4: sliding and overturning.
In a first step, no account is made of the effect of the deformation on the stability of GSC, so that the drag, inertia and lift coefficients C_D, C_M and C_L can easily be determined.
Due to the lack of reliable results in the literature on the values of C_D, C_M and C_L to be adopted in the stability formulae, systematic laboratory experiments were performed to determine the force coefficients which are appropriate for geotextile sand containers in different locations and configurations.
Finally, corrective factors are introduced in the stability formulae to account for the deformation effects.

6.1 Stability Formulae without Deformation Effects (Stiff GSCs)

Due to the high complexity of the stability problem, the effect of the deformation of GSCs on the hydraulic stability is first neglected by assuming stiff containers (refer to Section 6.3 for deformation effects).
The formulae are based on the dimensions of the GSC commonly applied in many coastal structures such as sea walls, breakwaters and revetments. In such projects, the length of the container l_c is generally twice as large as its width and five times as large as its height (Figure 6- 1). If other dimensions of sand containers are used, the procedure presented in the next sections must be modified accordingly to account for the actual geometry of the GSCs.

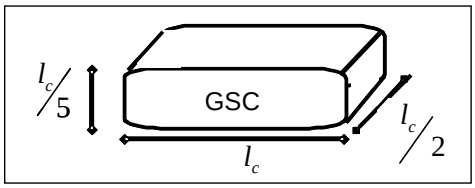

Figure 6- 1: Geometry of Common GSC Used for Coastal Structures

6.1.1 Mobilizing and Resisting Forces on Sand Containers

The wave-induced flow on and around a GSC with horizontal velocity u and associated acceleration $\frac{\partial u}{\partial t}$ results in four types of forces:

Drag force $$F_D = 0.5\rho_w u^2 C_D A_S \qquad (6.\ 1)$$

where ρ_w is the density of water, C_D a drag coefficient which depends on the form and roughness of the container, u the horizontal particle flow velocity and A_S the cross area normal to the flow (see Figure 4-25).

Inertia Force $$F_M = C_M \rho_w V \frac{\partial u}{\partial t} \qquad (6.\ 2)$$

where C_M is the inertia coefficient and V is the volume of the container.

Lift Force $F_L = 0.5 C_L \rho_w A_T u^2$ (6. 3)

where C_L is the lift coefficient, A_T is the plan form area of the container (Areas A_S and A_T are defined in Figure 4-25).

Buoyancy Force $F_B = \rho_w V g$ (6. 4)

where g is the gravity acceleration.

The resisting forces are essentially caused by the weight of the geotextile sand container (GSC) under buoyancy:

Weight of GSC $F_{GSC} = (\rho_s - \rho_w) g V$ (6. 5)

where V is the volume GSC, ρ_s and ρ_w are the density of the sand fill material and water respectively.

6.1.2 Derivation of Stability Formulae

Two failure modes must be considered: sliding and overturning

6.1.2.1 Stability against Sliding

Sliding occurs, when the wave-induced forces pull one of the containers out from the structure (e.g. GSC on seaward or landward slope), or when the container (e.g. GSC on the crest of the structure) simply slides either landwards or seawards (see Figure 6- 2, 4-20 and 4-26).

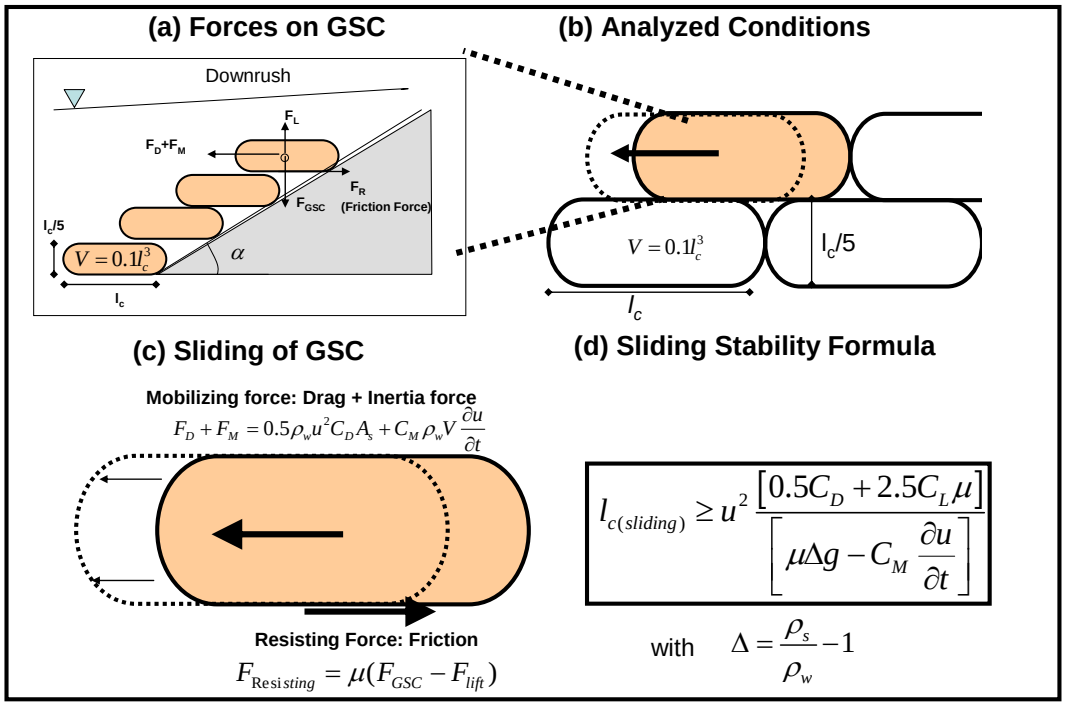

Figure 6- 2: Definition Sketch for Sliding Stability

Considering the assumption that the length of the GSC l_c is twice its width and five times larger as its height, the projected areas A_S, A_T and the volume V of GSC-container can be defined as:

$$V = l_c^{\,3}/10 \tag{6. 6}$$

$$A_S = l_c^{\,2}/10 \tag{6. 7}$$

$$A_T = l_c^{\,2}/2 \tag{6. 8}$$

Considering Figure 6- 2, the container will be stable, when the resisting force is equal or larger than the mobilising forces, thus:

$$\mu\left[F_{GSC} - F_L\right] \geq F_D + F_M \tag{6. 9}$$

where μ is the friction coefficient between GSCs (see Table 2.1 for details on the friction coefficient between GSCs and between GSCs and sand bed).

Substituting equations (6.1), (6.2), (6.3), (6.4) and (6.5) in equation (6.9) and dividing by ρ_w yields:

$$\mu\left[\Delta g \frac{l_c^{\,3}}{10} - 0.5 C_L u^2 \frac{l_c^{\,2}}{2}\right] \geq 0.5 C_D u^2 \frac{l_c^{\,2}}{10} + C_M \frac{\partial u}{\partial t}\frac{l_c^{\,3}}{10} \tag{6. 10}$$

where $\Delta = \frac{\rho_s}{\rho_w} - 1$; ρ_S and ρ_w being the density of the fill (sand) and water, respectively.

To simplify equation (6.10) some transformations are performed. Multiplying both sides of the equation by 10, yields:

$$\mu\left[\Delta g l_c^{\,3} - 2.5 C_L u^2 l_c^{\,2}\right] \geq 0.5 C_D u^2 l_c^{\,2} + C_M \frac{\partial u}{\partial t} l_c^{\,3} \tag{6. 11}$$

Dividing both size of equation (6.11) by $l_c^{\,2}$, yields:

$$\mu\left[\Delta g l_c - 2.5 C_L u^2\right] \geq 0.5 C_D u^2 + C_M \frac{\partial u}{\partial t} l_c \tag{6. 12}$$

Re-arranging the left side yields:

$$\left[\mu\Delta g l_c - \mu 2.5 C_L u^2\right] \geq 0.5 C_D u^2 + C_M \frac{\partial u}{\partial t} l_c \tag{6. 13}$$

Moving the terms with l_c to the left side yields:

$$\left[\mu\Delta g l_c - C_M \frac{\partial u}{\partial t} l_c\right] \geq 0.5 C_D u^2 + \mu 2.5 C_L u^2 \tag{6. 14}$$

Taking l_c as a factor in the left side and u^2 in the right side yields:

$$l_c\left[\mu\Delta g - C_M \frac{\partial u}{\partial t}\right] \geq u^2\left[0.5 C_D + \mu 2.5 C_L\right] \tag{6. 15}$$

Finally, the required length of the container l_c to resist sliding displacement is obtained:

$$l_{c(sliding)} \geq u^2 \frac{\left[0.5 C_D + 2.5 C_L \mu\right]}{\left[\mu\Delta g - C_M \frac{\partial u}{\partial t}\right]} \tag{6. 16}$$

Given the GSC geometry described in Figure 6- 1 and equation 6.6 to 6.8 the required mass of the GSC to ensure stability against sliding is (with $W_{GSC} = 0.1\rho_s l_c^3$):

$$W_{GSC} \geq \rho_s \left(u^2 \frac{\left[0.5C_D + 2.5C_L\mu\right]}{\left[\mu\Delta g - C_M \frac{\partial u}{\partial t}\right]} \right)^3 /10 \qquad (6.\ 17)$$

6.1.2.2 Stability against Overturning

Following the same approach as for sliding, the definition sketch of the overturning stability is shown in Figure 6- 3. Overturning occurs, when the mobilising moments around the rotation point are larger than the resisting moments. The rotation point is defined at the edge of the contact area of the GSC with its neighbouring container underneath (see Figures 6-3, 4-21, 4-22 and 4-29 for more details).

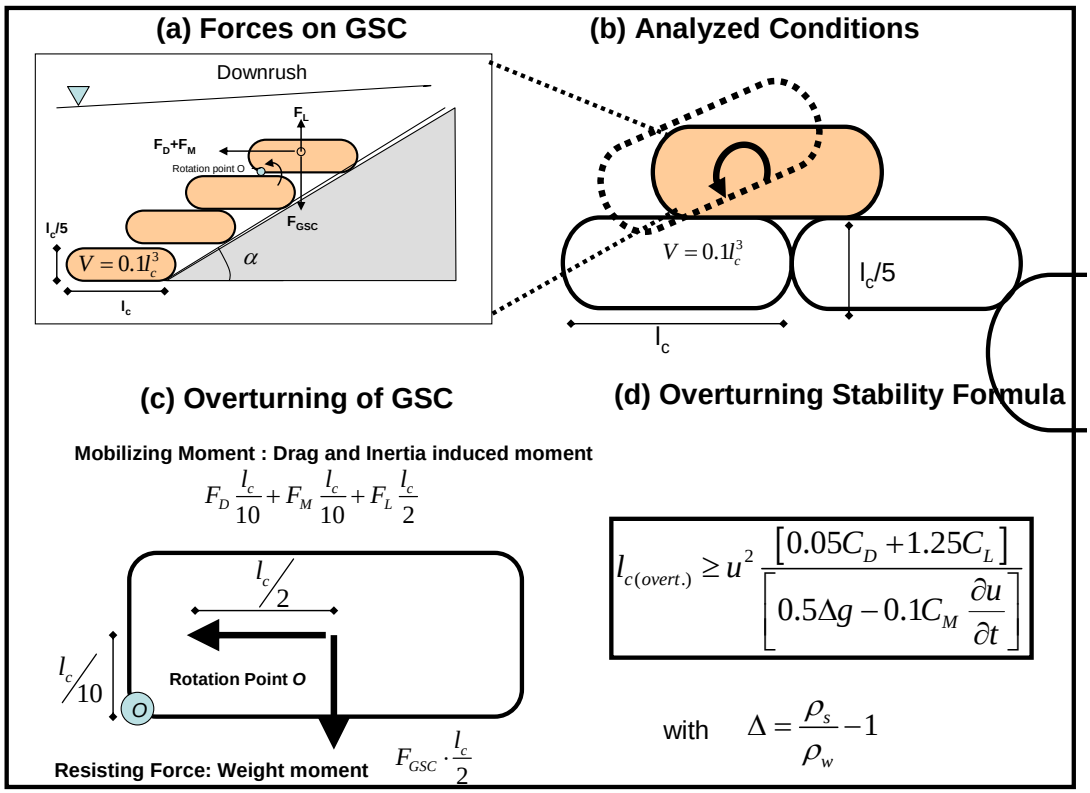

Figure 6- 3: Definition Sketch for Overturning Stability

For the GSC to resist overturning, the resisting moment should be equal or larger than the mobilising moment:

$$F_{GSC}\frac{l_c}{2} \geq F_D\frac{l_c}{10} + F_M\frac{l_c}{10} + F_L\frac{l_c}{2} \qquad (6.\ 18)$$

Substituting equations (6.1), (6.2), (6.3), (6.4) and (6.5) in equation (6.18) yields:

$$5\Delta g\frac{l_c^{\,3}}{10} \geq 0.5C_D u^2\frac{l_c^{\,2}}{10} + C_M\frac{\partial u}{\partial t}\frac{l_c^{\,3}}{10} + 2.5C_L u^2\frac{l_c^{\,2}}{2} \qquad (6.19)$$

Multiplying by 10 both sides of equation (6.19), yields:

$$5\Delta g l_c^{\,3} \geq 0.5C_D u^2 l_c^{\,2} + C_M\frac{\partial u}{\partial t}l_c^{\,3} + 12.5C_L u^2 l_c^{\,2} \qquad (6.20)$$

Dividing both sides of equation (6.20) by $l_c^{\,2}$

$$5\Delta g l_c \geq 0.5C_D u^2 + C_M\frac{\partial u}{\partial t}l_c + 12.5C_L u^2 \qquad (6.21)$$

Putting the terms with l_c into the left side, yields:

$$5\Delta g l_c - C_M\frac{\partial u}{\partial t}l_c \geq 0.5C_D u^2 + 12.5C_L u^2 \qquad (6.22)$$

Taking l_c as a factor in the left side and u^2 on the right side, yields:

$$l_c\left[5\Delta g - C_M\frac{\partial u}{\partial t}\right] \geq u^2\left[0.5C_D + 12.5C_L\right] \qquad (6.23)$$

The required length of the GSC to resist overturning is obtained:

$$l_c \geq u^2\frac{\left[0.5C_D + 12.5C_L\right]}{\left[5\Delta g - C_M\dfrac{\partial u}{\partial t}\right]} \qquad (6.24)$$

Dividing the upper and lower part of the right hand side of equation (6.23) by 10, yields:

$$l_{c(overt.)} \geq u^2\frac{\left[0.05C_D + 1.25C_L\right]}{\left[0.5\Delta g - 0.1C_M\dfrac{\partial u}{\partial t}\right]} \qquad (6.25)$$

Given the GSC geometry described in Figure 6- 1 and equation 6.6 to 6.8, the required mass of the GSC to ensure stability against overturning is (with $W_{GSC} = 0.1\rho_s l_c^3$):

$$W_{GSC} \geq \rho_s\left(u^2\frac{\left[0.05C_D + 1.25C_L\right]}{\left[0.5\Delta g - 0.1C_M\dfrac{\partial u}{\partial t}\right]}\right)^3 /10 \qquad (6.26)$$

6.1.3 Applicability of Stability Formulae

6.1.3.1 Available Force Coefficients and Methods of Analyses

The empirical lift, drag and inertia coefficients C_L, C_D, and C_M are needed to apply the derived stability formulae in equations 6.16 and 6.25.

A review of the force coefficients has shown that data exists particularly for slender pile structures and to some extent for rectangular, circular and other 3D bodies. The most relevant of these data are summarized in Table 6.1, including the method of analysis used to obtain the

drag, inertia and lift coefficients from the forces and wave kinematics measured in the laboratory.
The variation of the coefficients which depend on: the method used, the flow regime and the structure tested, is considerable. To better interpret the differences of the results shown in Table 6.1, the Keulegan-Carpenter *KC* and the Reynolds number *Re* are also provided:

$$KC = \frac{u_m T}{D} \qquad (6.\ 27)$$

$$\mathrm{Re} = \frac{u_m D}{\nu} \qquad (6.\ 28)$$

where u_m is the horizontal water particle velocity, T is the wave period and D is the length scale of the element parallel to the flow direction and ν is the kinematic viscosity of water.

Moreover, three methods of analysis to derive the empirical coefficients from the measurements were used: (i) "Particle Correlation Method", (ii) "Least Square Method" and (iii) "Maximal Correlation Method":

- **The particle correlation method**, correlates forces with water particle kinematics only at times when either the velocity or acceleration is zero ($u=0$ or $\frac{\partial u}{\partial t} = 0$). This corresponds to times of zero or extreme water surface elevation, respectively. At such times, either the drag or inertia term is zero. Therefore, the empirical coefficients can be derived directly (Dean and Dalrymple, 1998, Recio and Oumeraci 2007c).
- **The least square method**, is based on the minimization of the sum of the square errors between the measured force and the predicted force over all or part of the measured data set (Dean and Dalrymple, 1998, Recio and Oumeraci, 2007c and Najafian and Burrows, 1993).
- **The maximum correlation method**, is the most recent and was proposed by Najafian and Burrows (1993). In this method, the coefficients are determined so that: (i) the variances of the observed and predicted forces are equal, and (ii) the correlation coefficients between the observed and the predicted forces are maximized (Najafian and Burrows,1993 and Najafian et al 2003).

For the lift coefficient, only the "particle correlation method" and "least square method" can be implemented since the lift equation (equation 6.3) has only one unknown (C_L).
More details on the comparison between the results of previous studies can be found in Recio and Oumeraci (2007c), while details on the methods of analyses can be found in Najafian and Burrows (1993), Najafian et al (2003) and Recio and Oumeraci (2007c).
Table 6.1 shows that the drag coefficients obtained for horizontal submerged rectangular cylinders are much higher than those of circular structures (i.e. drag coefficients of rectangular elements are up to C_D=22 compared to drag coefficients of circular structures where the drag coefficients are up to C_D=2.5). Another interesting observation is the influence of the roughness on the force coefficients.

6.1.3.2. Practical Implications

Overall, the available results are not appropriate to asses the drag, inertia and lift coefficients C_D, C_M and C_L, which are needed to implement the stability formulae in equations 6.16 and 6.25. In fact, the shape and surface roughness of the GSC as well as the location of the GSC within the structure will strongly affect the flow field around the GSCs and thus, the associated drag, inertia and lift coefficients. Therefore, new systematic laboratory experiments designed for this purpose were performed (Section 6.2).

Table 6.1: Comparison of Available Drag, Inertia and Lift Coefficients C_D, C_M and C_L Including the Method of Analysis

Reference	Type of Structure	Flow Regime	Method of Analysis	Drag Coefficient C_D	Inertia Coefficient C_M	Lift Coefficient C_L	Remarks	
Torum (1994)	Rock unit in a rouble mound berm	*KC* =30~100 *Re*=10^3~10^4	Least square method	0.15~0.40	0.2	-0.1~ 0.1	Rock unit instrumented with a dynamometer, velocities measured very close to the stone	
Rufin (1996)	Steel sphere in a submerged breakwater	*KC* =2~26 *Re* =10^3~10^4	Least square method	0.4-1.8	0.7-1.4	------	Sphere attached to dynamometer, velocities measured very closed to the sphere	
Koether (2002)	Array of very close rectangular cylinders	*KC* < 300 *Re* = 10^4~10^6	Particle correlation	0.1~100	0.1~0.3	------	Reynolds and *KC* number measured between the elements of the filter system	
Vernugopal (2006)	Horizontal submerged rectangular cylinder	*KC* = 0~6 *Re* =10^4~10^5	Particle correlation	1~22	0.7~2	------	Tested a lot of rectangular horizontal "cylinders" with different ratios. Here, results from a ratio of 0.5 (similar to a GSC). See also Section 6.2	
Ikeda (1998)	Horizontal submerged rectangular cylinder	*KC* = 0~8 *Re* =10^4~10^5	Unknown	0.7~19	0.9~2.5	------	Tested a lot of rectangular horizontal "cylinders" with different ratios.	
Dessen (2004)	Submerged stone structures	Max approach velocity 0~1.4 m/s	Regression analysis	0.045~0.14	0.05~5.55	------	Force not measured directly, derived from threshold of movement	
Tromp (2004)	Submerged stone structures	Unknown	Regression analysis	0.25~0.35	0.1~2	0.15~0.22	Force not measured directly, derived form threshold of movement	
Dean (1970)	Slender stiff pile	*KC* =Unknown *Re* = 10^4~10^7	Least square method	0.5~1.8	0.8~1.8	------	Measurement of velocities and accelerations were performed considering the pile as "hydraulic transparent (slender pile)"	
Keulegan (1958)	Slender circular stiff pile	*KC* = 0~125 *Re* =0~10^5	Particle correlation	0.8~2.5	0.7~2.5	------	Measurement of velocities and accelerations were performed considering the pile as "hydraulic transparent (slender pile)"	
CEM (Sarpkaya 1976)	Slender circular pile	*KC* = 0~150 *Re* =0~10^5	Least square method	0.2~1.7	0.5~2	0.1~4	Measurement of velocities and accelerations were performed considering the pile as "hydraulic transparent (slender pile)"	

6.2 Laboratory Experiments for the Determination of Force Coefficients C_D, C_M and C_L

Since the literature review failed to provide the required drag, inertia and lift coefficients for geotextile sand containers used as coastal structures, laboratory experiments are performed with the following objectives:

(i) Derivation of the empirical drag, inertia and lift coefficients C_D, C_M and C_L from measured wave-induced forces on a GSC, instrumented with a force transducer and installed under various boundary conditions and configurations (single and within other containers).

(ii) Quantification of the influence of wave-parameters on the wave-induced forces on GSCs.

(iii) Further clarification of the processes affecting the wave loading of GSC-structures.

6.2.1Experimental Set-Up

The experiments in the LWI-wave-flume consist in testing an instrumented container isolated as well as within a group of containers that are placed in different configurations with other similar containers in the wave-flume and subject to different wave conditions (Figure 6-4). The measuring container is instrumented with a 2D-dynamometer (force transducer) in order to record accurately the longitudinal and transversal components of the wave-induced forces at every time of the wave cycle (Figure 6- 5).

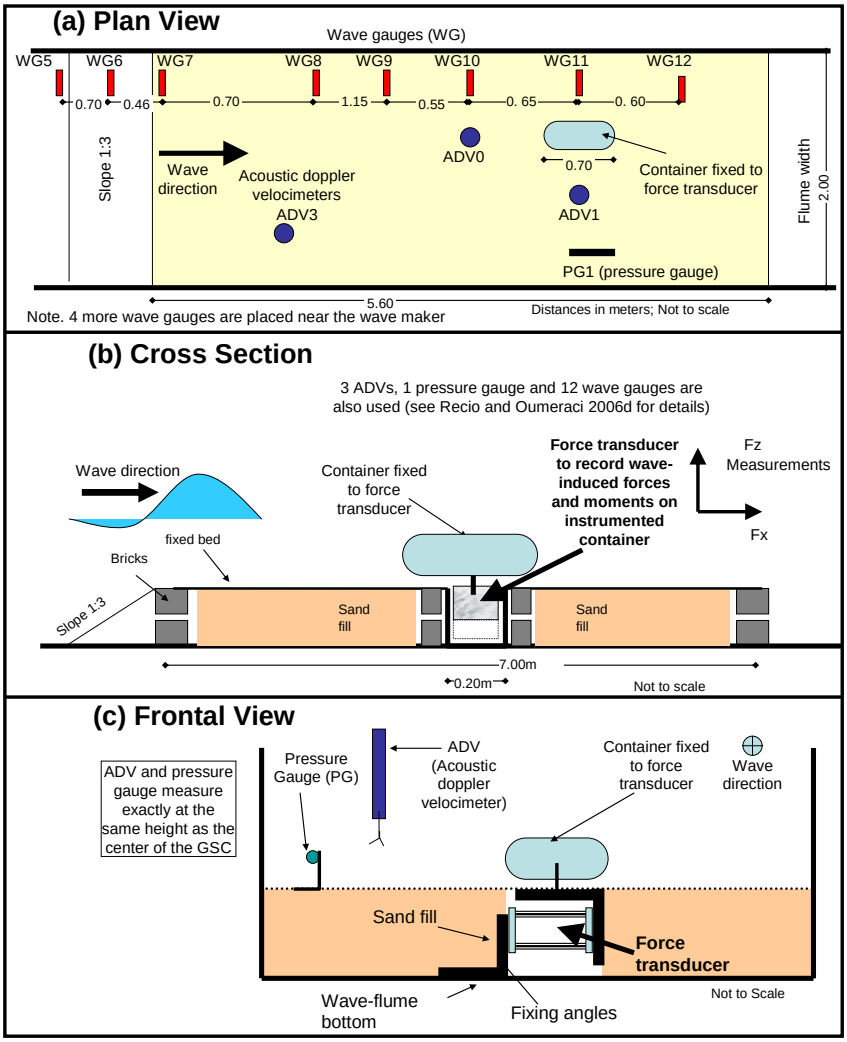

Figure 6-4: Experimental Set-Up and Instrumented Container in the LWI-Wave-Flume

A “false bottom” was constructed on the floor of the flume to create space for installing the force transducer, which is then fixed to a container. The force transducer can record the wave-induced vertical and horizontal forces on the container (Figure 6-4).

The instrumented container is made of mahogany wood. This type of wood is not sensitive to volume change in water even for long periods. Other advantages are that its density is larger than water and that it can be easily shaped to mimic the geometry of a geotextile sand container. Finally, the wood container was covered with the same geotextile as for the GSCs used in the laboratory experiments in Chapter 3 to provide the same roughness as for a prototype (Figure 6- 5).

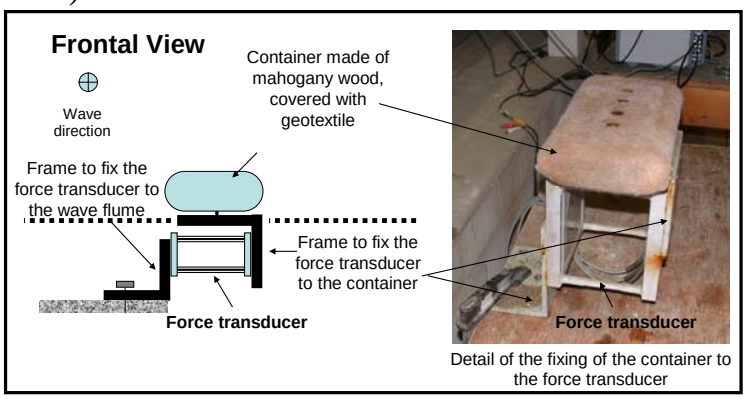

Figure 6- 5: Instrumented Container for Force Measurement

Measurements at and near the instrumented container during the model tests are: (i) vertical and horizontal wave-induced forces on a GSC, recorded by the force transducer, (ii) wave-induced pressures recorded by a pressure gauge, (iii) wave-induced velocities recorded by ADVs (Acoustic Doppler Velocimeters) and (iv) free surface elevations recorded by wave gauges (see also Figure 6-4). For more details on the force transducer and its measurement principle please refer to Recio and Oumeraci (2007c).

The dimensions of the instrumented container are shown in Figure 6- 6. The container has a length of 0.30m, width of 0.15m and a height of 0.06m, which corresponds to the same geometry of the containers considered for the derivation of the stability formula in Section 6.1 (l_c *x* l_c*/2 x* l_c*/5*) (Figure 6-6).

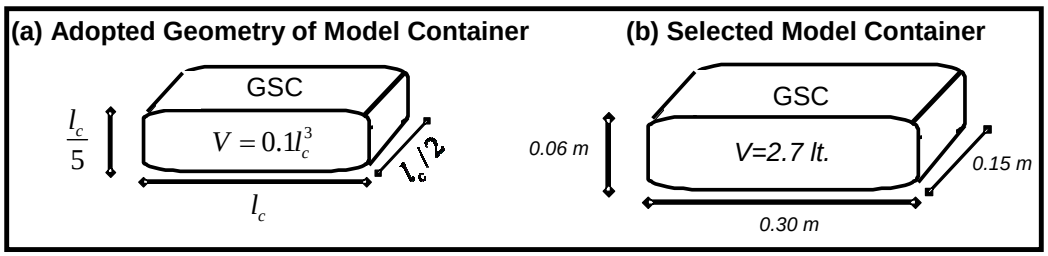

Figure 6- 6: Geometry and Dimensions of Instrumented Container

The following criteria were considered for the selection of the size of the instrumented container:

(i) The scale of the model (relation of size of container and wave conditions) should be geometrically similar to the conditions normally encountered in the field.
(ii) The dimension of the container should be very small as compared to the wave length in order to apply the Morison formula (Dean and Dalrymple 1998).

(iii) The Reynolds number in the model should be large enough to reduce scale effects ($Re > 10^4$).
(iv) The container should be large enough to provide enough space for fixing it to the force transducer.

A geometrical scale in the order of 1:8 was selected for the model tests (details on the scaling of the model can be found in Recio and Oumeraci 2007c).

The **wave conditions** tested include both are regular and irregular waves varying from 0.12m to 30m height with wave periods between 2s and 4.5 seconds with two water depths, 0.61m and 0.70m. Due to the false bottom, which was required to insert the dynamometer (0.25m height), all waves tested are within the range of "shallow water" conditions (*d/L= 0.02 to 0.08*), with *d* being the water depth and *L* the wave length). These correspond to most of the wave conditions encountered for GSC-structures used as seawalls, revetments, breakwaters, artificial reefs, groins, etc. (more details in Recio and Oumeraci, 2007c).

A total of 10 configurations of the model set-up were tested, including a configuration without containers to quantify the wave-induced forces on the dynamometer only (Figure 6- 7). In each configuration, the instrumented container was placed in different configuration and boundary conditions. The systematic test series consist in simple and more complex configurations to investigate the effect of various boundary conditions. Numbering of the configurations in Figure 6-7 follows the order of construction and testing in the wave-flume.

6.2.2 Preliminary Analyses

Preliminary analysis is first performed to validate the recorded data and to quantify the influence of the wave parameters on the wave-induced forces. Only, the most important results are discussed here, more details can be found in Recio and Oumeraci (2007c).
The wave-induced particle velocities, accelerations and total forces on the instrumented container are needed to obtain the drag, inertia and lift coefficients, C_D, C_M and C_L. Since particle accelerations have not been directly measured, they have to be derived either: (i) from wave theories or (ii) from the recorded particle velocities. The latter alternative was adopted and the accelerations were derived from the recorded velocities, following the approach proposed by Torum (1994):

$$\frac{Du}{Dt} = \frac{\partial u}{\partial t} + u\frac{\partial u}{\partial x} + v\frac{\partial v}{\partial z} \qquad (6.29)$$

where the left side of the equation is the total derivative of the velocity *u*, while the right hand is the sum of the local derivative of the horizontal velocity component *u* and the sum of horizontal and vertical velocity gradients, respectively. The local derivative $\left(\frac{\partial u}{\partial t}\right)$ is obtained directly from the measured velocities:

$$\frac{\partial u}{\partial t} = \frac{u_i - u_{i-1}}{\Delta t} = \frac{\Delta u}{\Delta t} \qquad (6.30)$$

where u_i is velocity at time point t_i; u_{i-1} velocity at time point $t_i - \Delta t$ and Δt is the time period between data points.

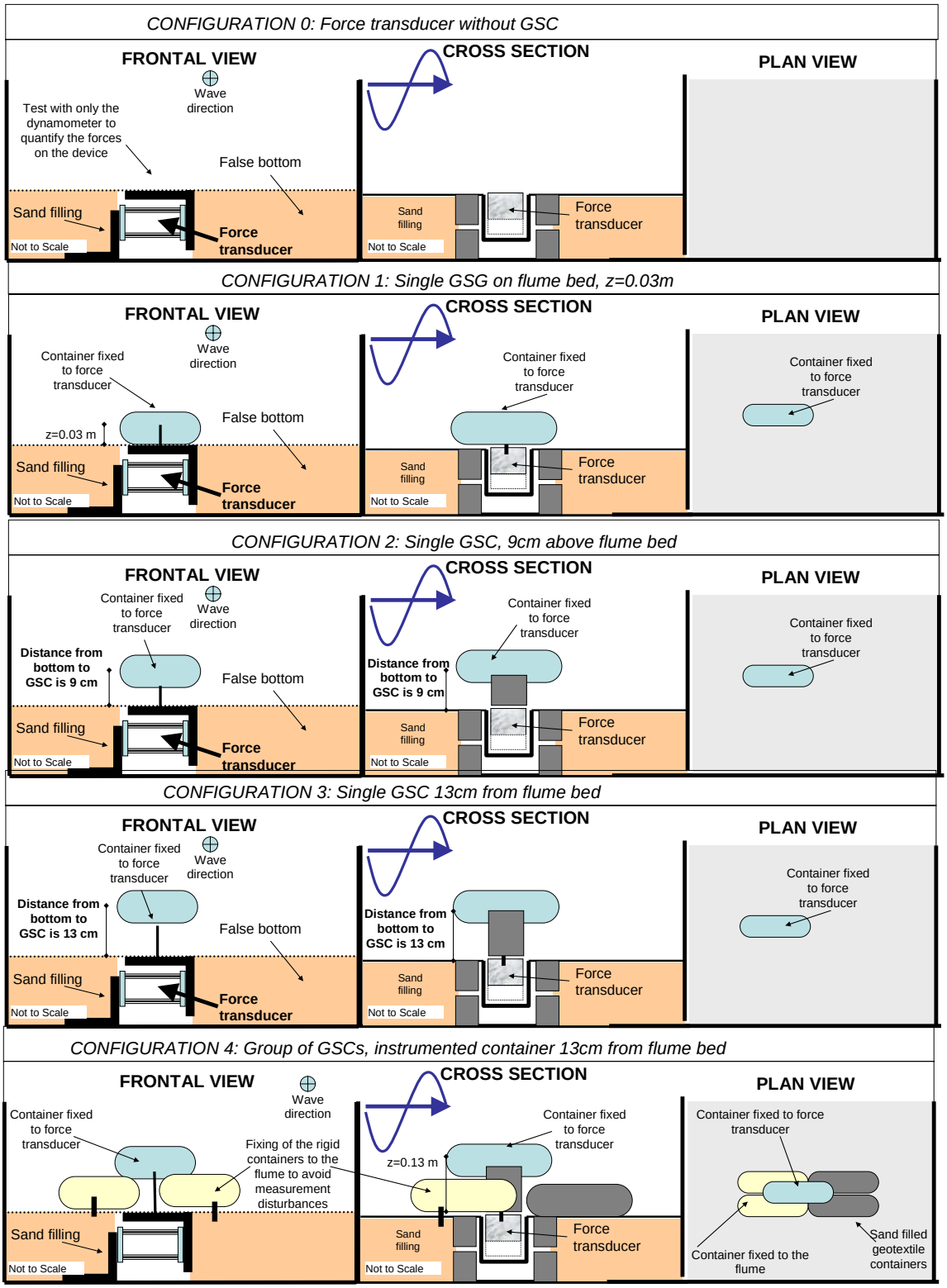

Figure 6- 7: Configurations Tested (continues on next page)

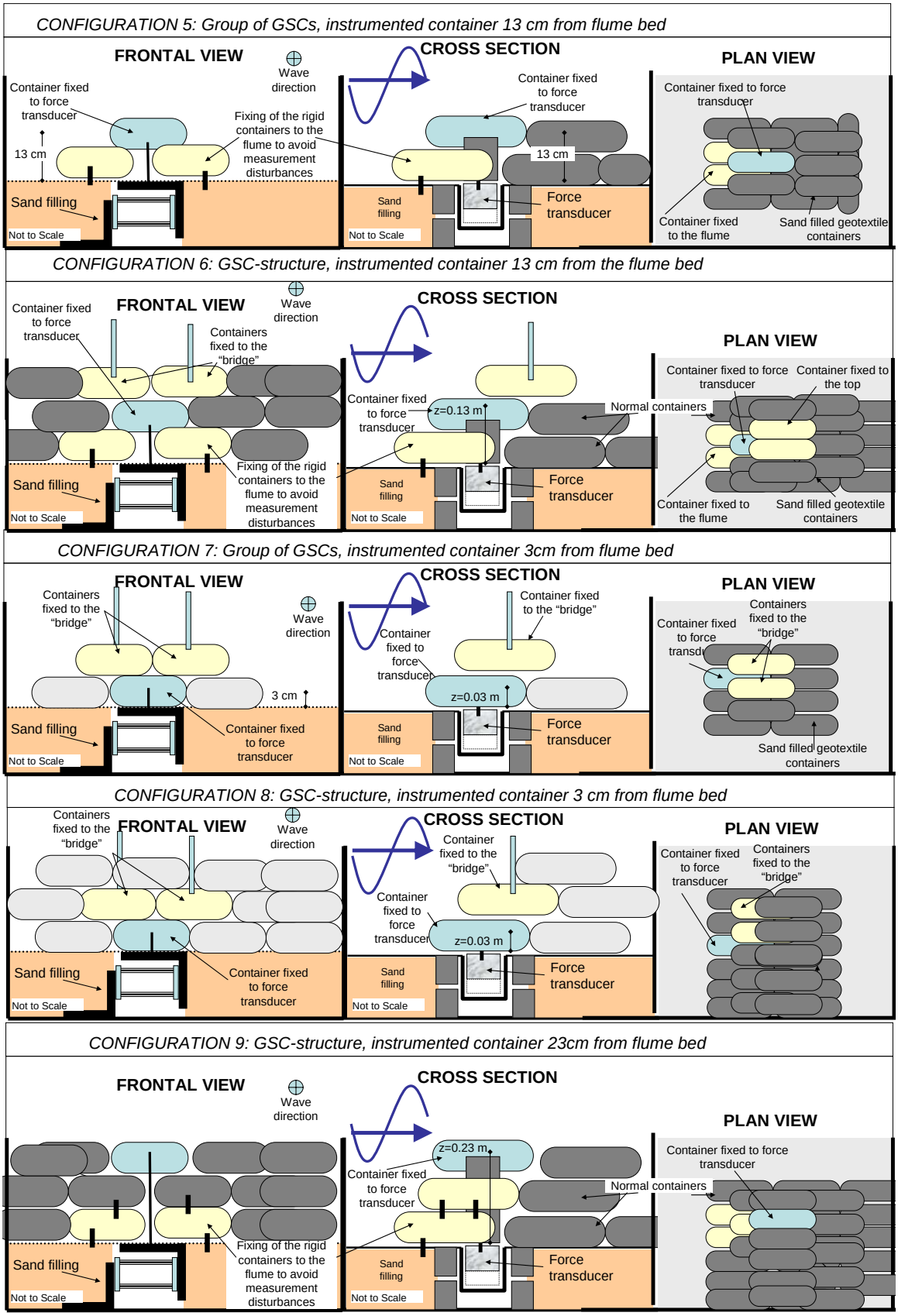

Figure 6- 7: Configurations Tested (continued from previous page; photos of configurations in Recio and Oumeraci, 2007c)

The procedure assumes that the wave at a given measurement point is of permanent form so that the transformation $x = -Ct$ (where C is the wave celerity) can be applied to obtain the velocity gradients. The celerity is set equal to $C = \sqrt{gd}$, (for shallow water as in our model tests), where d is the water depth at the measurement point and g is gravity acceleration.
With this approximation, the following expression for the acceleration can be derived:

$$\frac{Du_i}{Dt} = = \left(1 - \frac{u_i}{C}\right)\frac{u_i - u_{i-1}}{\Delta t} \qquad (6.31)$$

To validate this procedure, the data from one of the velocimeters (ADVs) are used to calculate the acceleration. The derived acceleration was compared with the acceleration calculated by linear wave theory, using the same wave height and period, showing a good agreement (differences within 17%, see Recio and Oumeraci, 2007c for details).
Although all the measuring devices were well-calibrated prior to model testing, some of the model tests were reproduced using the "Cobras-model" (see Chapter 5 and Recio and Oumeraci 2007c) in order to double check the recorded data. The agreement between the experimental data and the numerical simulations was relatively good (differences within 12% for the horizontal forces, 34% for the vertical forces, 22% free surface and 25% for horizontal velocity). Consequently, the adopted approach to determine the particle acceleration from the velocity records and other measurements was found to be within the range of accuracy required (see Recio and Oumeraci 2007c for more details).

Moreover, it is also important to check the relative importance of drag and inertia for the shallow water conditions tested. Dean and Dalrymple (1998) suggested that for shallow water conditions the drag force will predominate over the inertia force. Torum (1994) mentioned that if the peak of the parallel force is close to the peak of the horizontal velocity, then the drag force dominates over the inertia force in the horizontal axis. This assumes that force and velocity are measured in the same "x" and "z" coordinates but different "y" ("hydraulic transparent structure"). Following this approach, the data from some of the model tests, where the dynamometer and the ADV are at same location ("x" and "z"), were examined (Figure 6-8). The peak of the horizontal force matches almost exactly (5% deviation) with the peak of the velocity ($\frac{\Delta t}{T} = \frac{0.1s}{2s} = 0.05$), meaning that a strongly drag-dominant situation is present in the horizontal direction.

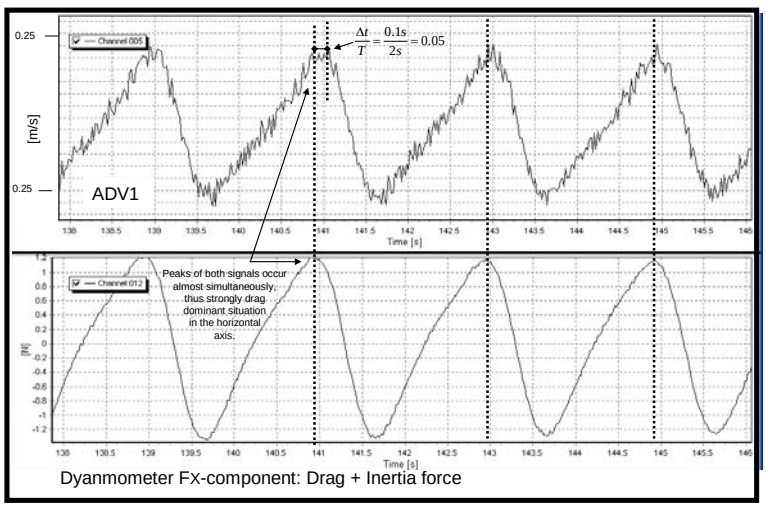

Figure 6- 8: Time Series of Horizontal Force and Horizontal Particle Velocity

6.2.3. Detailed Analysis

6.2.3.1 Effect of Wave Parameters and GSC Configurations on Wave-Induced Forces

The influence of the wave conditions, GSCs configurations and boundary conditions on the wave-induced forces on GSCs was systematically investigated. All the results are reported by Recio and Oumeraci (2007c). The key results may be summarized as follows:

(i) The higher the wave height, the higher the wave-induced forces on the instrumented GSC. The relation is, however, not linear.

(ii) The farther the instrumented GSC is placed from the still water level (z=0), the smaller the wave-induced forces. For example, a container placed close to the still water level ($z=0.23m,\ z/d \approx 0.3$) has much larger wave-induced forces (around 5 times) than a GSC placed near the seabed ($z=0.03m,\ z/d \approx 0.04$).

(iii) The boundary conditions and the location of the instrumented GSC within the structure affect the wave-induced forces. The more containers placed around a specific GSC, the smaller the wave-induced forces. However, the neighbouring containers affect less drastically the wave-induced forces as compared with the elevation of the container above the sea bed. For example, in a structure consisting of three layers of GSCs, the container placed at the second layer will be subject to 40% smaller wave-induced forces than a GSC placed at the same elevation on the crest of a two layer structure. (More details in Recio and Oumeraci, 2007c)

6.2.3.2 Determination of the Drag, Inertia and Lift Coefficients C_D, C_M and C_L

(a) Methods of Analyses and Comparisons: Selection of Appropriate Method

To obtain the force coefficients C_D, C_M, and C_L for each model test, a series of "MatLab" "routines" have been developed. For each model test, the drag, inertia and lift coefficient are derived by three different methods: (i) "Particle Correlation", (ii) "Least Square", (iii) "Maximum Correlation" (refer to Recio and Oumeraci, 2007c for more details on the MatLab routines and algorithms for deriving the force coefficients).

An important remark regarding the derivation of the coefficients is concerned with the location of the velocity probe and the effect of the latter when deriving the coefficients. For all configurations that involved an isolated container or a group of containers, the velocity probe was placed exactly at the same "x" and "z"-coordinates as the instrumented container but different "y"-coordinate (ADV1 in Figure 6-4). Thus, considering the small GSC-structure as "hydraulic transparent"; two other velocity probes were placed before the dynamometer to check that in fact, the structure has a negligibly small influence on the flow (ADV0 and ADV3 in Figure 6-4).

For configurations with a large GSC-structure (e.g. configurations 6, 8 and 9, in Figure 6- 7), the velocity probe was placed about 0.8m seaward from the structure, and then, the signal was synchronized, using the information from the dynamometer and wave gauge above the dynamometer.

In addition, it is also important to clarify the definition of the characteristic length in the direction of the flow D used for deriving the Reynolds and KC-number (equations 6.27 and 6.28). Since in the Reynolds number, D is the characteristic length scale in the main direction of flow, two options were analyzed: (i) to define D as the average diameter of the GSC, thus, $D = \sqrt[3]{l_c \cdot \frac{l_c}{2} \cdot \frac{l_c}{5}} = 0.46 l_c$ and (ii) to define D as the length of the container l_c, thus $D=l_c$. The latter was adopted for the analysis due to the following reasons:

(i) The main objective of the tests is to derive the force coefficients from the experiments involving single, groups and GSC-structures made of sand containers. For all the tests, the containers were placed manually and parallel to the wave direction. Therefore, the length of the container l_c will correspond accurately to the definition of the

characteristic length scale in *Re*, since the main direction of the flow is parallel to the length of the container.

(ii) For single containers, the characteristic length scale corresponds exactly to the length of the container.

(iii) Due to the interlocking and arrangement between elements involved in a small group of containers and GSC-structures, either the length of the container $D=l_c$ or the average diameter $D=0.46l_c$ will not correspond exactly to the length scale of the flow.

As briefly shown Section 6.1.3.1 and in more detail by Recio and Oumeraci (2007c), three methods of analysis have been used in the past to derive the force coefficients C_D, C_M and C_L. In this study, all three methods were comparatively used in order to identify the method providing the best agreement between measured and calculated forces. Some examples of the comparisons are shown in Figure 6- 9. More comparisons are given in Recio and Oumeraci (2007c). The following conclusions can be drawn from the comparative analysis:

(i) The "Particle Kinematics Correlation" method is the least accurate of the three methods: it may under-predict or over-predict the measured forces (calculated results may be as twice as big as the measured results)

(ii) The "Least Square" method agrees very well with the frequency of the signal and seems much better than the particle correlation method. However, it tends to slightly under predict the wave-induced forces (by up to 20%).

(iii) The best agreement between measured and observed forces is achieved by the "Maximum Correlation" method. The maximum absolute values of this method are generally within 80% accuracy. The only drawback is that this method slightly over predicts the calculated forces and thus, is more conservative than the "Least Square" method.

(iv) For the lift coefficient, only the "Particle Correlation" and the "Least Square" method are used since method three is applicable only for the drag and inertia coefficients. The "Least Square" method shows that the agreement for the maximum values is good, but that there are considerable discrepancies in the rest of the data. These discrepancies are due to the influence of the vertical velocity on the vertical force, which are neglected in these analyses. Incorporating the vertical velocities (as other researchers did to improve the agreement) is not feasible, since the velocimeters (ADVs) used in this study cannot record accurately small vertical velocities. ADVs are calibrated for a velocity range of +-1 m/s. Thus, velocities smaller than 0.1m/s cannot be accurately recorded. Since the maximum values are relatively well predicted, neglecting the vertical velocities does not affect the stability analyses for the following reasons: (i) tests are in "shallow water" conditions, thus vertical velocities are small and (ii) when the horizontal velocity is maximal (highest lift force), the vertical velocity is at its minimal value. Thus, by neglecting the vertical velocities, the lift coefficient C_L still predicts accurately the maximal lift force (see also Figure 6-40).

Based on the results of this comparative analysis, the "Maximum Correlation Method" is adopted in this study to determine the drag and inertia coefficient C_D and C_M and the "Least Square Method" to determine the lift coefficients C_L.

(b) Determination of Drag, Inertia and Lift Coefficients C_D, C_M and C_L

Using the "Maximum Correlation Method" for C_D and C_M and the "Least Square Method" for C_L, the results shown in Table 6.2 are obtained and discussed below (a more detailed discussion and a more explicit description of the data and regression functions are given in Recio and Oumeraci, 2007c).

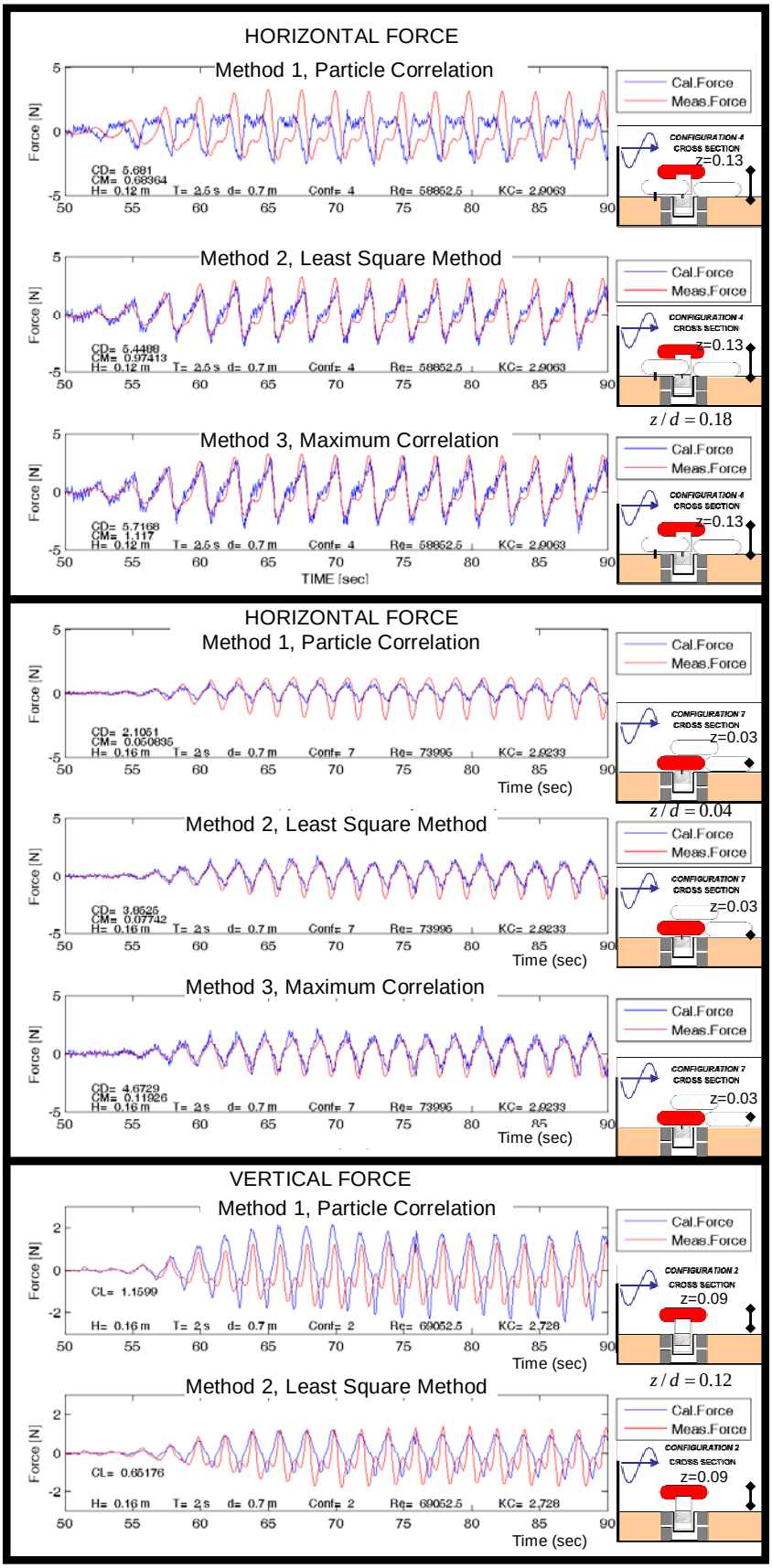

Figure 6- 9: Comparison of Force Coefficients Derived by Different Methods

Table 6.2: Summary of Drag, Inertia and Lift Coefficients C_D, C_M and C_L

Test Configura-tion		C_D	C_M	C_L	***Re*** $\mathrm{Re}=\frac{uD}{\nu}$ with $D=l_c$	**Equation**	**Coeff. of Variation**
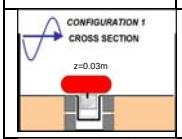	1	1.3~6.5	0.2~0.95	0.2~1.4	$5\text{x}10^4$~ $2.2\ \text{x}10^5$	$C_D=-2x10^{-5}\,\mathrm{Re}+6.81$ $C_M\approx 0.60$ $C_L=1x10^{-5}\,\mathrm{Re}-0.612$	0.18 - 0.48
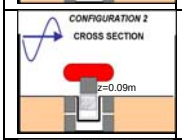	2	2.5~11	0.1~0.6	0.3~1.2	$7\ \text{x}10^4$~ $1.8\ \text{x}10^5$	$C_D=-6x10^{-5}\,\mathrm{Re}+15.01$ $C_M\approx 0.30$ $C_L=1x10^{-5}\,\mathrm{Re}-0.558$	0.23 - 0.45
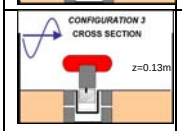	3	4~11.7	0.1~0.8	0.3~1.2	$7\ \text{x}10^4$~ $1.9\ \text{x}10^5$	$C_D=-4x10^{-5}\,\mathrm{Re}+11.54$ $C_M\approx 0.50$ $C_L=2x10^{-5}\,\mathrm{Re}-0.68$	0.24 - 0.43
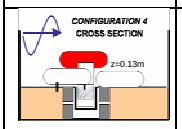	4	2~11	0.05~0.9	0.4~1.5	$8\ \text{x}10^4$~ $1.8\ \text{x}10^5$	$C_D=-2x10^{-5}\,\mathrm{Re}+9.16$ $C_M\approx 0.60$ $C_L=1x10^{-5}\,\mathrm{Re}-0.54$	0.42 - 0.30
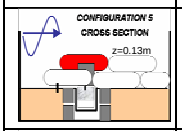	5	4~11	0.15~0.7	0.4~1.3	$8\ \text{x}10^4$~ $1.8\ \text{x}10^5$	$C_D=-6x10^{-5}\,\mathrm{Re}+14.70$ $C_M\approx 0.50$ $C_L=1x10^{-5}\,\mathrm{Re}-0.669$	0.19 - 0.32
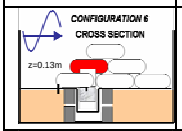	6	2.5~9	0.05~0.55	0.3~1.2	$8\ \text{x}10^4$~ $1.8\ \text{x}10^5$	$C_D=-3x10^{-5}\,\mathrm{Re}+8.9$ $C_M\approx 0.30$ $C_L=1x10^{-5}\,\mathrm{Re}-0.587$	0.42 - 0.31
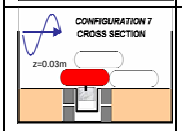	7	2~6	0.05~0.45	0.3~1.2	$8\ \text{x}10^4$~ $1.6\ \text{x}10^5$	$C_D=-1x10^{-5}\,\mathrm{Re}+4.85$ $C_M\approx 0.20$ $C_L=9x10^{-6}\,\mathrm{Re}-0.147$	0.38 - 0.40
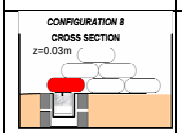	8	0.5~3	0.05~0.2	0.3~1.2	$8\ \text{x}10^4$~ $1.8\ \text{x}10^5$	$C_D=-2\text{x}10^{-5}\,\mathrm{Re}+3.475$ $C_M\approx 0.10$ $C_L=9\text{x}10^{-6}\,\mathrm{Re}-0.222$	0.13 - 0.41
	9	4~15	0.05~0.07	0.3~1.2	$8\ \text{x}10^4$~ $2\ \text{x}10^5$	$C_D=-9\text{x}10^{-5}\,\mathrm{Re}+23.04$ $C_M\approx 0.30$	0.14 -

Note: $D=l_c$. For more details on the results refer to Recio and Oumeraci (2007d). Results showed no clear relation between the Reynolds number and the inertia coefficient C_M, thus, only the averaged value is presented.

(c) Discussion of the Results

The first notice when analyzing the drag and inertia coefficients C_D, C_M and C_L is that the drag coefficients are higher, while the inertia coefficients are smaller than for cylindrical piles (between 0.5 and 2). However, the comparison with the coefficient available for rectangular structures shows a much better agreement. Venugopal (2006) investigated wave-induced forces on horizontally submerged rectangular "cylinders" (under similar *Re* and *KC*-range) and reported large drag coefficients (C_D values up to 22). Ikeda (1988), also in the same range as this study, reported high drag coefficients for rectangular horizontal "cylinders" (C_D values up to 16). The difference of drag coefficients between circular and rectangular elements is, because sharp edged bodies develop a wider wake and shed vortices in oscillatory flow even at very low KC-numbers. As a result of this they experience larger drag coefficients than circular elements. Moreover the "Least Square Method" or "Particle Correlation Method" have been exclusively used in the previous investigations, thus, leading to smaller coefficients than the "Maximum Correlation Method".

The comparison between the drag coefficients obtained in this study with the results of Venugopal is shown in Figure 6- 10. For the comparison the results from configuration 3 are used, since the latter corresponds mostly to the configuration tested by Venugopal (a container 13cm from the bottom *z/d=0.12* and a rectangular horizontal "cylinder" at the mid-water depth *z/d=0.21*). As seen in Figure 6- 10, the coefficients obtained by this study are slightly larger than those obtained by Ikeda and Venugopal (the dependency with the KC number is in relatively good agreement).

Regarding the inertia coefficient, the obtained values are smaller than expected. A possible explanation for these smaller values is that only shallow water conditions have been considered (drag regime dominant *d/L=0.02 to 0.08*) for this study and *d/L=0.07 to 0.2* for Venugopal, 2006). A further possible explanation is the reason suggested by Chaplin (1984). He reported that with sharp edged elements there will be a reduction of inertia force due to a circulation flow (steady vortex motion).

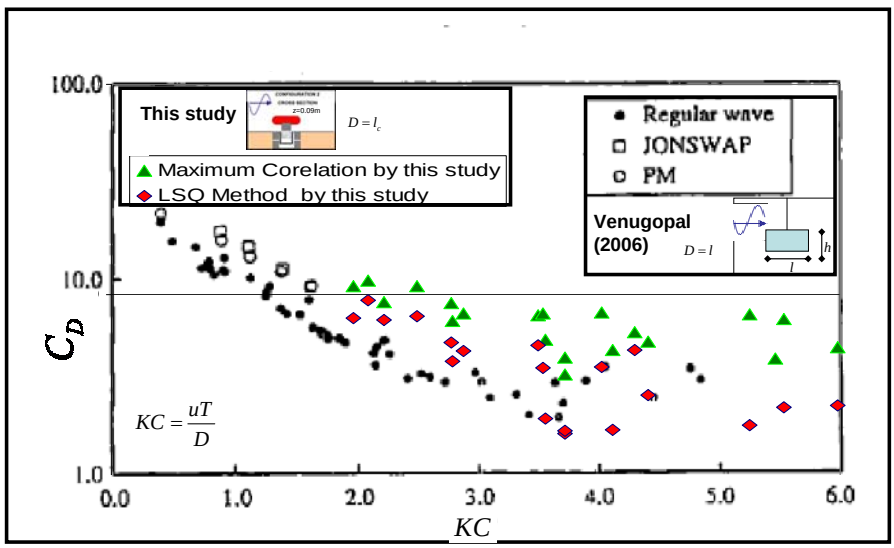

Figure 6- 10: Comparison of Drag Coefficients with the Results of Venugopal (2006)

The drag coefficient C_D is strongly dependent on the Reynolds KC-numbers. The larger the Reynolds number (or KC), the smaller the drag coefficient (Figure 6- 11). The dependency is more pronounced with respect to the Reynolds number than with respect to the KC-number.

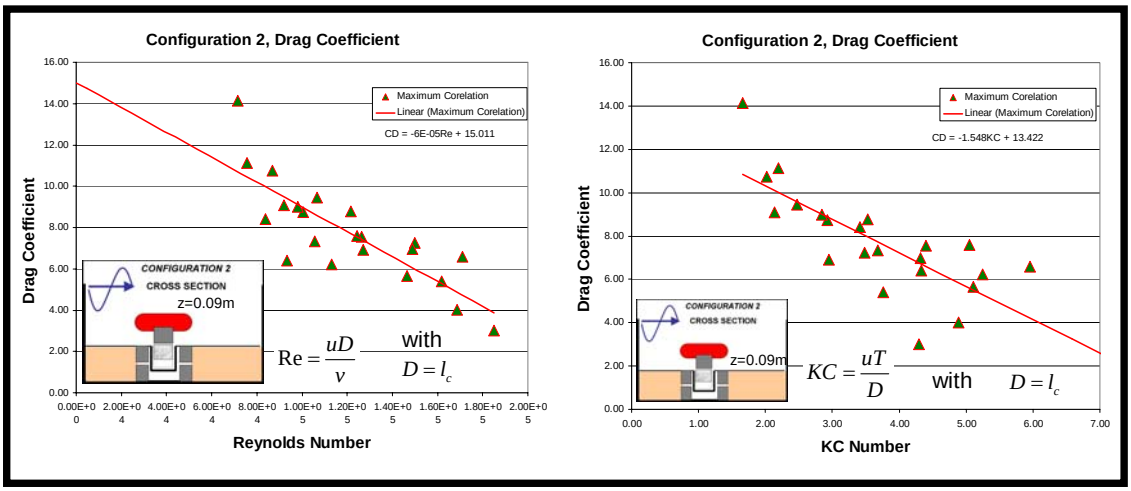

Figure 6- 11: Drag Coefficient Dependency on the Reynolds and KC-number

Regarding the inertia coefficients C_M, there is no clear relation with the Reynolds number or the KC-number, due the dominance of the drag regime for the shallow water conditions investigated (refer to Recio and Oumeraci 2006d for more details).

Regarding the lift coefficient C_L, the effect of the Reynolds number is strong (Figure 6- 12). Contrary to the drag coefficient, however, the larger the Reynolds number, the larger the lift coefficient (there is no clear dependency with KC-number).

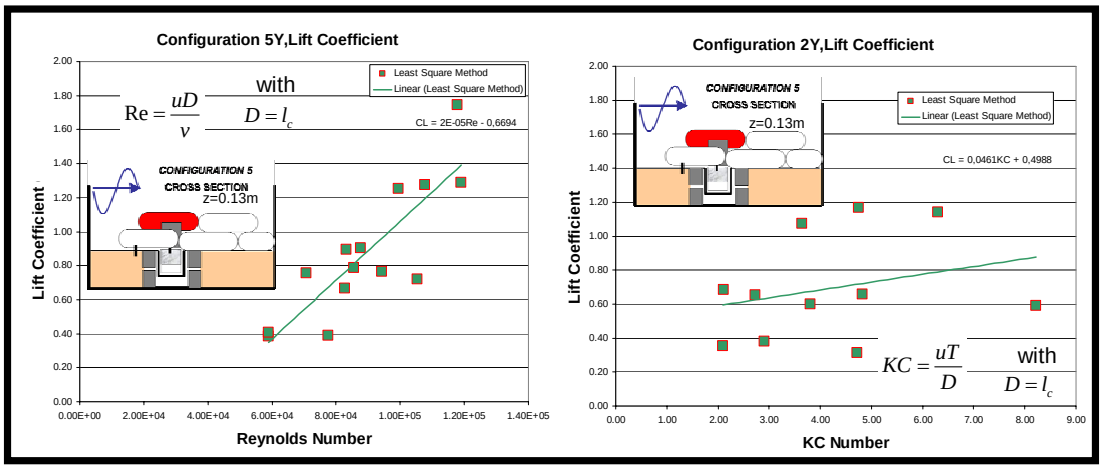

Figure 6- 12: Lift Coefficient Versus the Reynolds and KC-Number

6.2.4 Summary and Implications of the Experimental Results

Previous studies have shown that there are significant discrepancies in the obtained force coefficients C_D, C_M and $C_{L,}$ so that they can not be used for GSC-structures. The main results of the derivation of the force coefficients C_D, C_M and C_L from the laboratory experiments may be summarized as follows:

(i) The numerical model "Cobras" (2D-RANS-VOF) can approximately predict wave-induced forces on submerged elements for "shallow water conditions" (drag predominance).

(ii) The force coefficients C_D, C_M, and C_L have been obtained by means of model tests by applying three different methods of analysis showing that for the tested conditions the "Maximum Correlation Method" predicts more accurately the observed horizontal forces. It tends, however, to slightly over predict the wave-induced horizontal forces by about 10%. For the vertical forces the "Least Square Method" showed a better agreement with respect of the peak values (differences within 20%); however, some discrepancies in the rest of the data can expectedly not be avoided.

(iii) The drag coefficient C_D and lift coefficient C_L depend on the Reynolds number. Drag decreases with higher Reynolds number, while lift coefficient increases with higher Reynolds number. This is however not the case for the inertia coefficient where no clear relation is found.

(iv) The wave-induced forces on the GSCs under the shallow water conditions tested in this study are more influenced by the wave height than by the wave period.

(v) The elevation of the container in the flume and the boundary conditions induced by the neighbouring containers considerably influence the wave-induced loading of the GSC.
The lowest wave-induced forces are recorded for a container placed on the seabed surrounded by neighbouring GSCs and the highest wave-induced forces are recorded for the container placed at the crest of the submerged structure. Chapter 4 showed that for surface piercing structures the critical container will be either the one at the edge of the structure crest or the one placed just below the still water level (SWL).

6.3. Stability Formulae Accounting for Deformation Effects

The deformations of GSCs affect the hydraulic stability of GSC-structures as shown in Chapters 4 and 5. In this section, the influence of the deformations is accounted for by introducing deformation factors into the formulae for the mobilizing and resisting forces. These deformation factors are analytically derived and finally incorporated into the hydraulic stability formulae obtained in Section 6.1.

(a) Effect of Deformations on the Mobilizing and Resisting Forces

As shown in Figure 6-13 the deformations of GSCs affect: (i) the projected areas of the container A_S and A_T and (ii) the force coefficients C_D, C_M and C_L (refer to Section 4.7 for additional details).

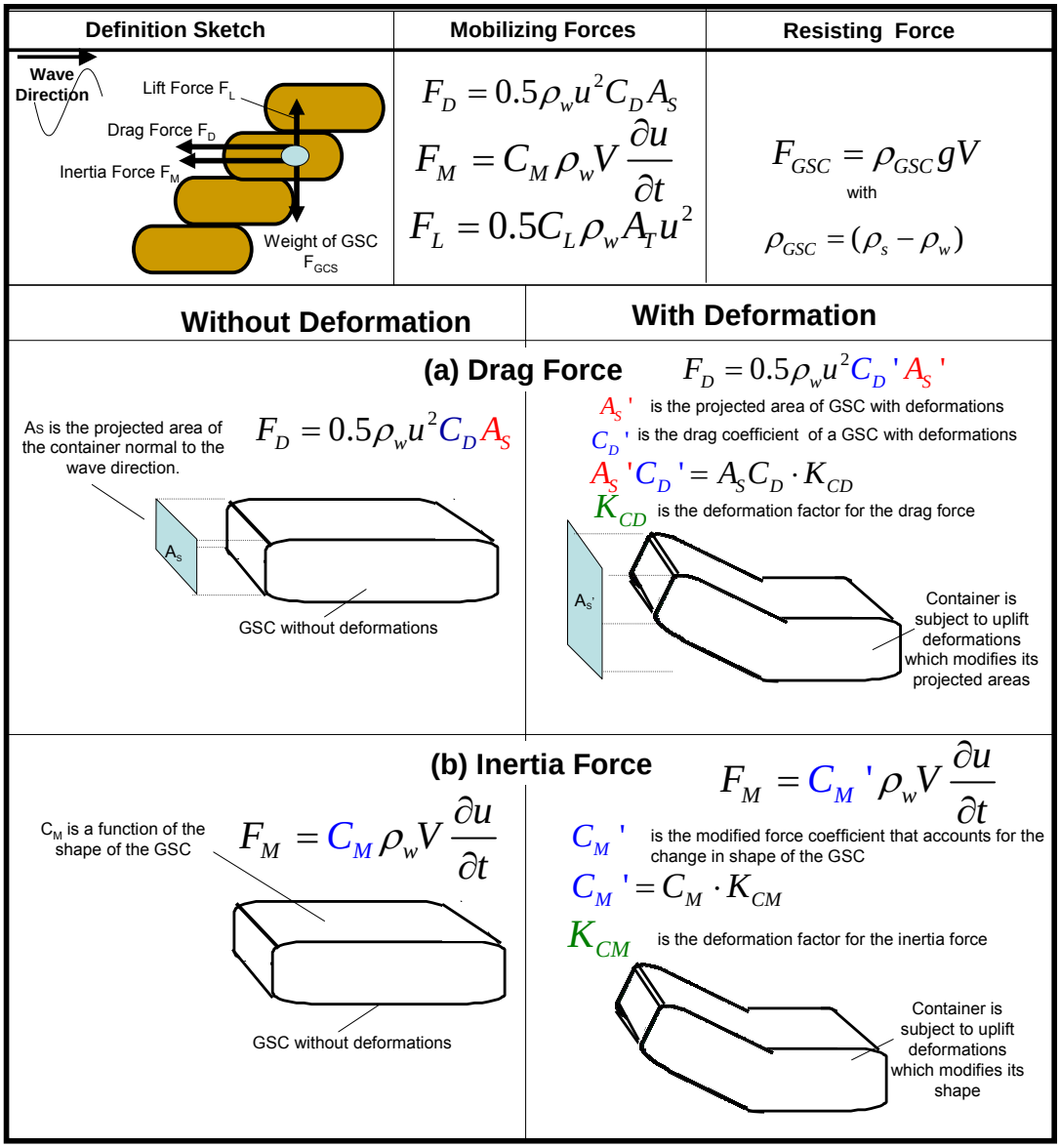

Figure 6- 13: Effect of Deformations on the Mobilizing and Resisting Forces (continues on next page)

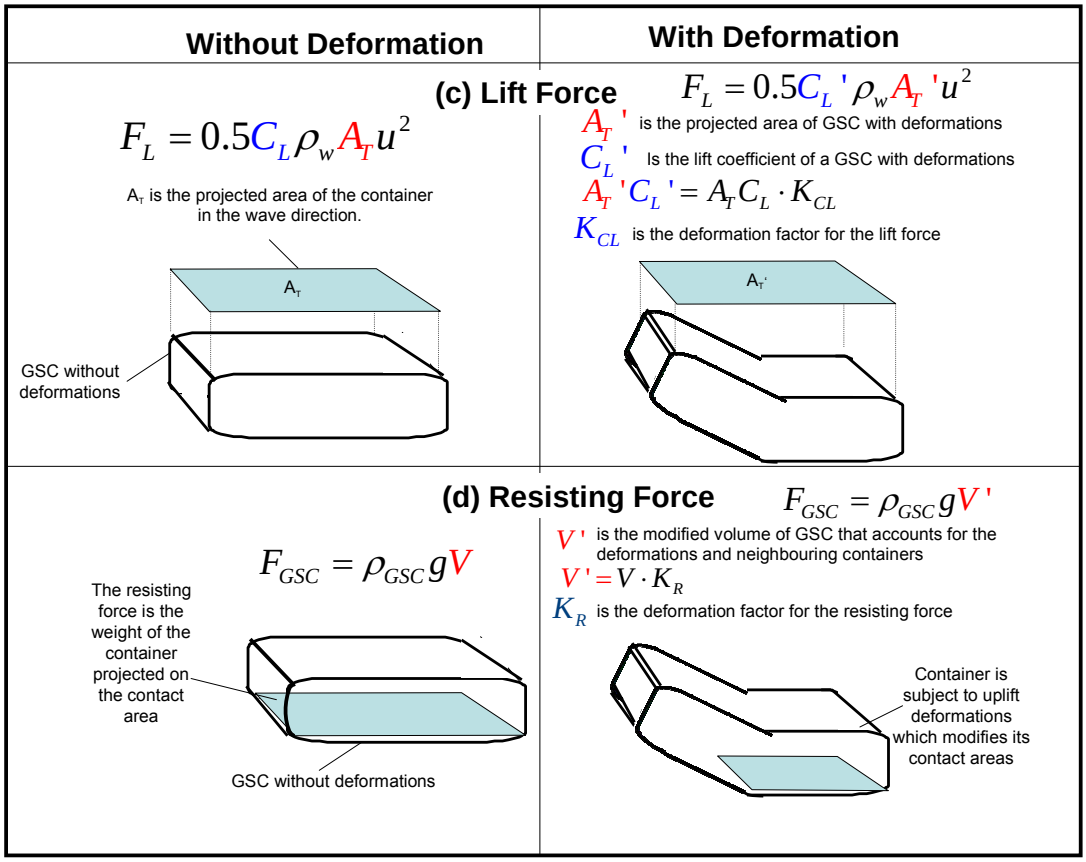

Figure 6- 13: Effect of Deformations on the Mobilizing and Resisting Forces (continued from previous page)

The variation of the projected areas of the containers A_S and A_T due to deformations can be easily derived (see Section 6.3.1 and 6.3.2). However, the drag and lift coefficients C_D and C_L are a function of the Reynolds number *Re* and of the roughness of the container. They are, thus, implicitly influenced by the wave-induced flow and changes of the shape of the container.

Moreover, the only way to derive the drag and lift coefficient for containers with deformations effects C_D' and C_L' is to perform model tests with a deformable container instrumented by a force transducer. Due to serious scaling and further technical problems, this is however not feasible at this stage.

Regarding the inertia coefficient C_M, the change of the shape of the container will explicitly affect the inertia coefficient C_M , since it can be defined as the sum of two terms (Dean and Dalrymple, 1998):

$$C_M = 1 + k_m \qquad (6.33)$$

where the unit *1* represents the pressure gradient component and k_m the added mass, which directly depends on the shape of the body.

For two dimensional flow about a cylinder of elliptical cross section, the added mass coefficient k_m can be shown to be (Figure 6- 14a):

$$k_m = \frac{a}{b} \qquad (6.\ 34)$$

where *a* and *b* are the semi-axes aligned with and transverse to the line of acceleration, respectively.

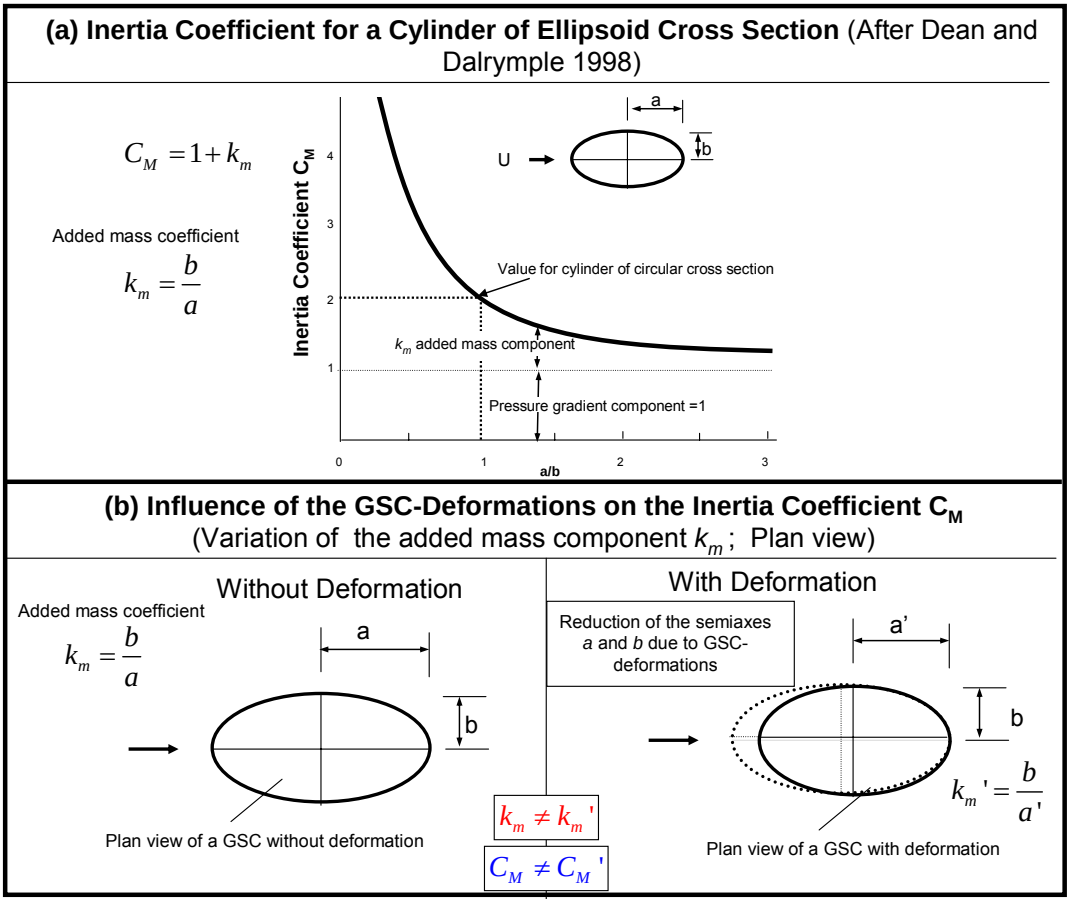

Figure 6- 14: Effect of the Deformations on Inertia Coefficients C_M

In the case of GSCs, deformations induce variations of shape of the container. Therefore, the added mass component k_m of the inertia coefficient C_M will be subject to variations as shown in Figure 6- 14b. For two dimensional flow on a slender pile, the influence of the change of the shape on the inertia coefficient can be accounted for by implementing equation (6.34). However, for three dimensional flow about a GSC, the influence of the change of shape due to deformations on the inertia coefficient can only be determined by laboratory experiments specially designed for this purpose.

Regarding the resisting force F_{GSC}, the GSC-deformations will affect the projected weight of the container on the GSC beneath, thus, also affecting its stability. The derivation of the variation of the projected weight is straightforward (see Sections 6.3.1 and 6.3.2).
Considering the afore-mentioned, it can be summarized that the GSCs-deformations affect: (i) the projected areas of the containers A_S and A_T, (ii) the force coefficients C_D, C_M and C_L and (iii) the projected weight of the container on the container beneath. Therefore, a generic stability formula for GSCs that account for the deformations should also include deformation factors that account for these variations.

Generic deformation factors for the drag, inertia and resisting forces (K_{CD}, K_{CM}, K_{CL} and K_R) will depend on the magnitude of the deformations suffered by the container which is affected by: (i) sand fill ratio of GSC, (ii) slope angle of the structure, (iii) wave conditions, (iv) stiffness of the geotextile and (v) properties of the fill material (Table 6.3).

Table 6.3: Deformation Factors

Deformation Factor	Definition	Influencing Factors
K_{CD}	Deformation factor for the drag force	Sand fill ratio of GSC, wave conditions, properties of the fill material and stiffness of geotextile
K_{CM}	Deformation factor for the inertia force	
K_{CL}	Deformation factor for the lift force	
K_R	Deformation factor for the resisting force	Sand fill ratio of GSC, properties of the fill material wave conditions, steepness of the structure and position and number of neighbouring GSCs

(b) Assumptions for the Derivation of the Deformations Factors

In the next sections, the deformation factors K_{CD}, K_{CM}, K_{CL}, and K_R for the correction of the mobilizing and resisting forces on GSC are analytically derived and implemented in the hydraulic stability formulae for the two common failure modes of GSCs: sliding and overturning. For this purpose, the following assumptions are made which are derived from laboratory observations:

(i) The deformation factors are based on the geometry of the GSC as commonly applied in most coastal structures, in which the length of the container l_c is twice as large as its width and five times as large as its height (Figure 6- 15). If other geometry of GSCs is used, the procedure presented in the next sections must be modified accordingly, to account for the actual geometry of the GSCs.

(ii) The deformations are accounted for GSCs with a sand fill ratio of 80%. Therefore, if the GSCs have a sand fill ratio different than 80%, the deformation factors should be modified accordingly (Figure 6- 15).

(iii) It is initially assumed that the angle of the front slope of the structure with the horizontal is 45^o (Figure 6- 15). Based on model test observations, deformation factors for other slope angles are additionally derived, but they should be used with caution since all of the studies of this thesis are performed for sloped GSC-structures with 45^o.

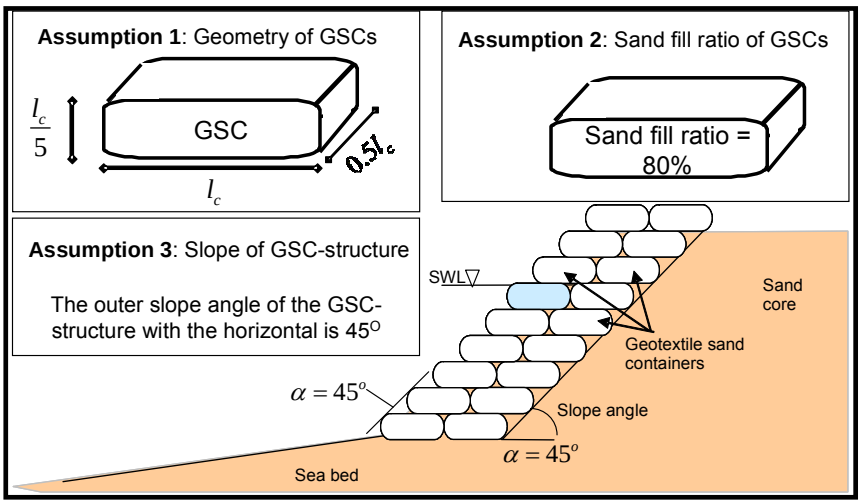

Figure 6- 15: Initial Assumptions for the Derivation of the Deformation Factors

(iv) During the model tests (refer to Chapter 4 for details), it was observed that during uprush and depending on the wave conditions, different types of uplift deformations on the GSCs occured (Figure 6- 16a): (a) only one GSC in the GSC-structure is subject to uplift deformation, (b) several GSCs are uplifted or (c) all GSCs suffer uplift deformation. However, in order to derive the deformation factors, it is assumed that: (a)

the uplift deformation of the GSCs is independent of the wave conditions, (b) all GSCs in the GSC-structure suffer uplift deformations and (c) the uplift deformations on GSC are independent of the position of the container in the GSC-structure (Figure 6- 16b).

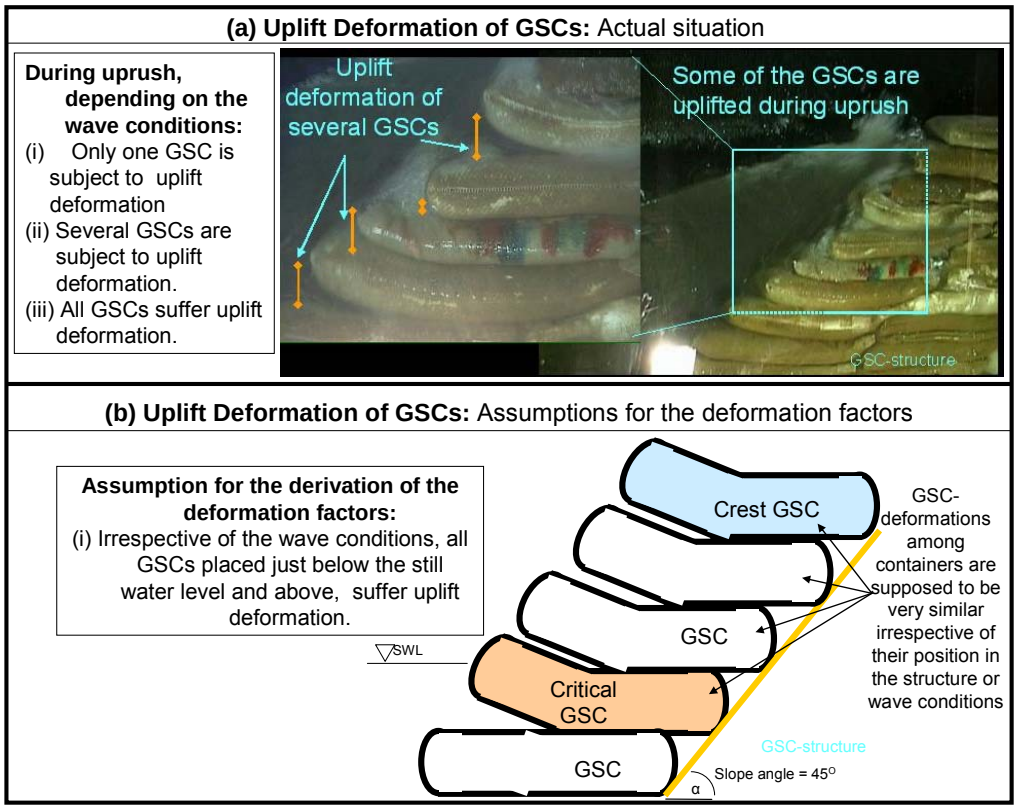

Figure 6- 16: Further Assumptions for the Derivation of the Deformation Factors Associated with the Uplift of GSCs

(v) In addition, depending of the wave conditions, the uplift deformation of the containers varies in the following ways: (a) the angle between the lower part of the uplifted container with the horizontal varies from 15 to 45°, while (b) the non-uplifted length of the container varies from $0.65l_c$ to $0.95l_c$ (Figure 6- 17a). However, the most common uplift deformation observed in GSC-structures was a reduction of the length of the GSC by 20% (non-uplifted length of the container $l_{Aeff}=0.8l_c$), showing that there is a relation between the steepness of the structure and the uplift deformation of the GSCs (refer to Section 4.5 for more details). Therefore, it is assumed that: (a) the angle of the uplifted part of the container with the horizontal direction is 45° and (b) the non-uplifted length of the container during deformations is $0.8l_c$ (Figure 6- 17b). The afore-mentioned assumption represents a more realistic maximal deformation of the GSCs.

(vi) The previous section showed that the GSC-deformations also affect the force coefficients C_D, C_M and C_L. However, the only procedure to accurately quantify the influence of the deformations on the force coefficients is to perform specific model tests properly scaled with deformable GSCs which at present are not practicable. On the other hand, since the variation of the projected areas is considered, the influence of the shape variations of the GSC on the flow field (Reynolds and KC numbers) is expected to be small. Flow separation and vortices are expected to be very similar to those of non-deformed containers and therefore, the influence of the deformations on the force coefficients are neglected (Figure 6-18), thus:

$$C_D = C_D' \ ; \ C_M = C_M' \text{ and } C_L = C_L' \qquad (6.\ 35)$$

where C_D', C_M' and C_L' are the force coefficients that account for the GSC-deformations.

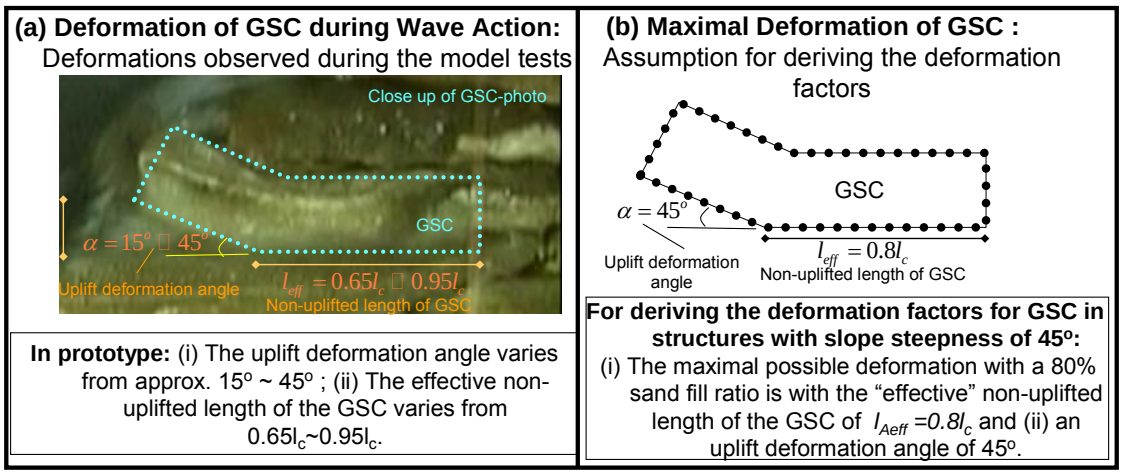

Figure 6- 17: Assumption for the Derivation of the Deformation Factors Associated with the Maximal Deformation of GSCs

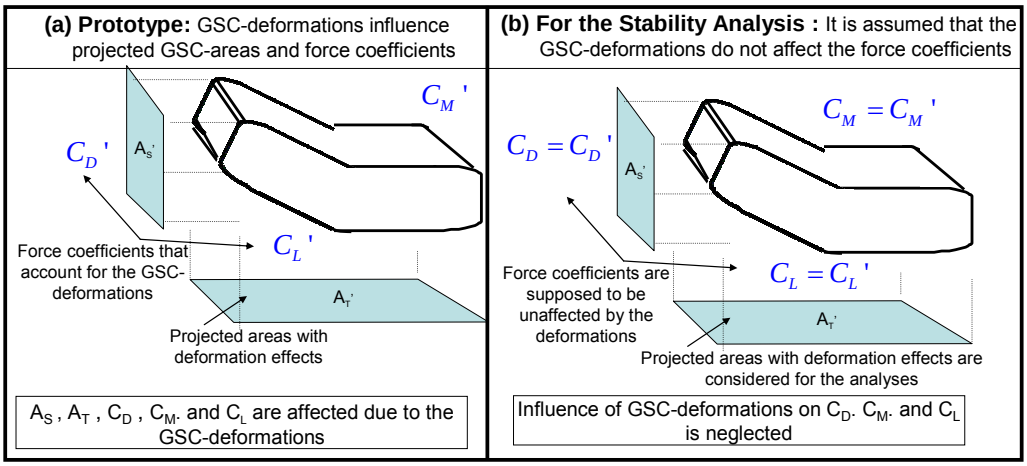

Figure 6- 18: Assumption for the Derivation of the Deformation Factors Associated with the Force Coefficients C_D, C_M and C_L

Considering the afore-mentioned assumptions, the deformation factors K_{CD}, K_{CM}, K_{CL} and K_R are derived in the next sections.

6.3.1 Stability against Sliding

Due to the differences in wave loading and boundary conditions a distinction is made between slope and crest containers constituting the GSC-structure.

6.3.1.1 Slope Containers

The most complex displacement of a GSC in a surface piercing structure is the sliding of containers that are placed just below SWL (see Chapter 4). The exact time, when the displacement of slope containers occurs, is illustrated by Figure 6- 19, while the time series of wave-induced forces on GSCs between neighbouring containers is shown in Figure 6- 20. When the resultant horizontal force on the critical container is maximum (GSC below SWL), the resultant horizontal force of the container above is almost zero (Figure 6- 20). Wave-

induced vertical forces behave similarly. Sliding of slope GSCs occur when large wave-induced horizontal forces are applied on a container, while the container above is subject to extremely small wave-induced horizontal forces. Therefore, the following two assumptions have been made: (i) only the wave-induced forces on the critical container are considered and (ii) only the weight of neighbouring GSCs is considered to contribute to the stability of the GSC.

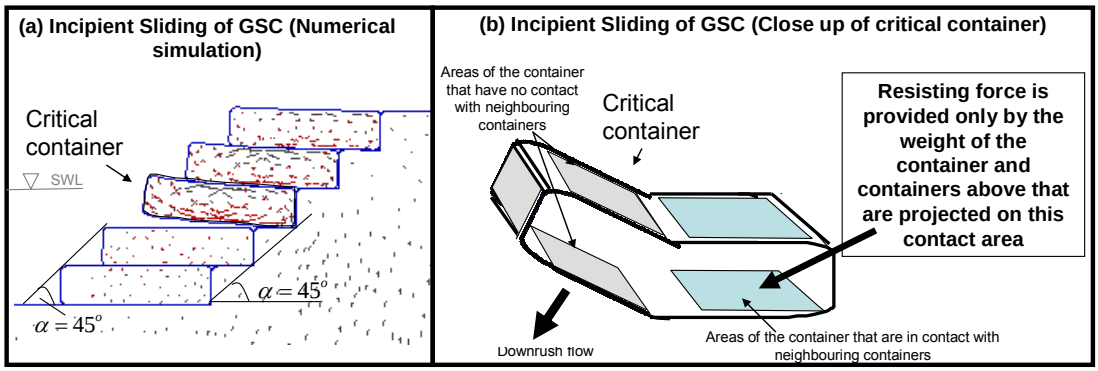

Figure 6- 19: Deformation of Critical Container at the Time of Incipient Sliding

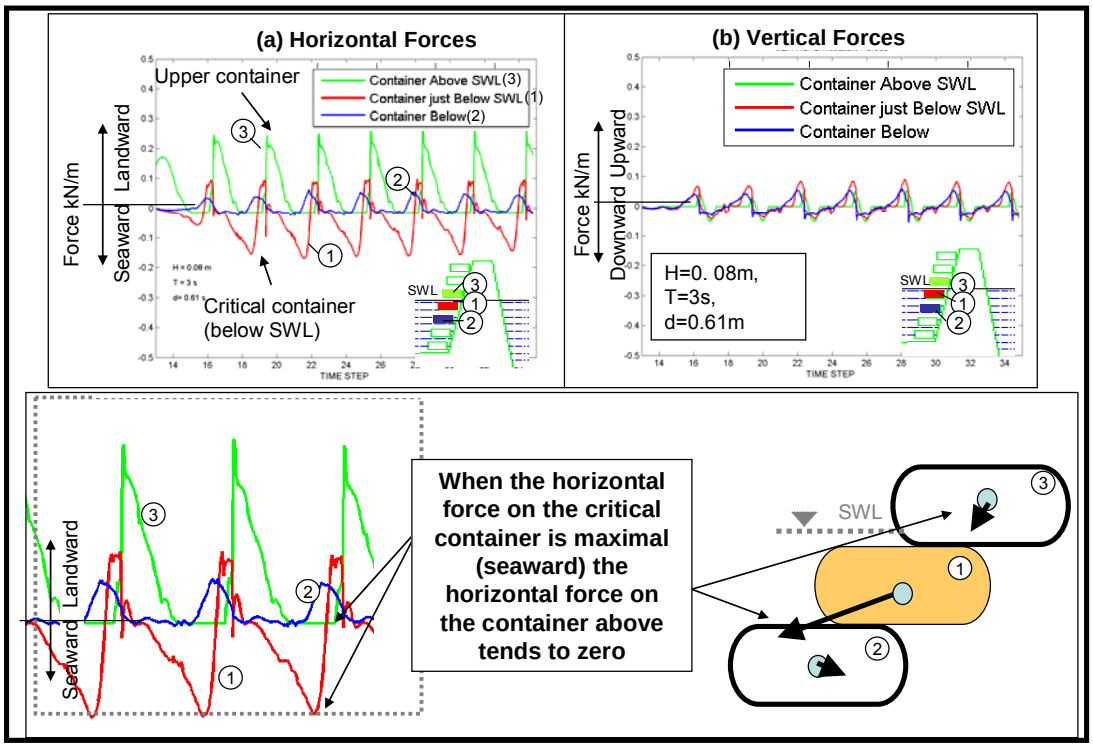

Figure 6- 20: Interaction of Wave-Induced Forces on Containers Placed near SWL (numerical simulation)

(a) Drag Force: Deformation Factor KS_{CD}

Recalling the GSC-geometry (Figure 6-15) and the following assumptions: (i) only the deformation of a GSC with 80% sand fill ratio is considered (Figure 6- 16 and 6-18b) and (ii) the influence of the deformations on the drag coefficient C_D is neglected (Figure 6- 19), the deformation factor KS_{CD} should account only for the variation of the projected area normal to the wave direction A_S' , which can be defined as (Figure 6- 21):

$$A_S' = 0.28 l_c \frac{l_c}{2} = 0.14 l_c^2 \qquad (6.\ 36)$$

Considering that the projected area normal to the flow before deformation A_S can be described as:

$$A_S = \frac{l_c^2}{10} = 0.1 l_c^2 \qquad (6.\ 37)$$

Thus, the deformed projected area normal to the flow can be defined as:

$$A_S' = KS_{CD} A_S \qquad (6.\ 38)$$

where KS_{CD} is the deformation factor for sliding that affects the drag force:

$$KS_{CD} = \frac{A_S'}{A_S} = 1.4 \qquad (6.\ 39)$$

Showing that the drag force is increased by about 40% due to the deformations of the GSC.

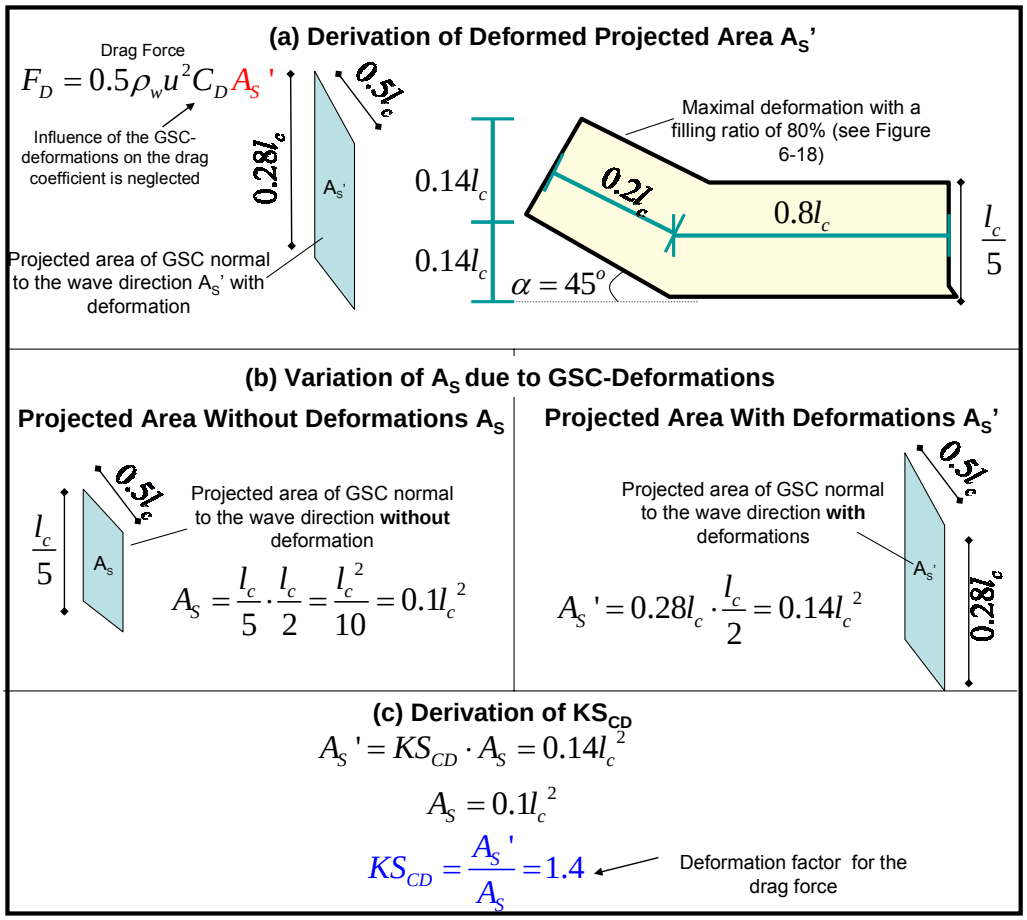

Figure 6- 21: Deformation Factor KS_{CD} for Drag Force

(b) Inertia Force: Deformation Factor KS_{CM}

The deformation of the container will result in a change of its shape and subsequently also in the change of the inertia coefficient C_M (Figure 6- 14). However, as mentioned in the previous sections (Figure 6- 18), the influence of the GSC-deformations on the force coefficients is neglected.

Other considerations that support the assumption of neglecting this effect of the GSC-deformations on the inertia force F_M are: (i) the volume of the container is assumed to remain

constant, thus the influence of shape is small (variation in the added mass component k_m is small) and (ii) inertia forces are considerable smaller than drag forces as shown in Section 6.2. Therefore, until more specific information on the influence of the GSC-deformations on the inertia force F_M is available, the deformation factor for the inertia force KS_{CM} can be defined as:

$$KS_{CM} = 1.00 \qquad (6.\ 40)$$

(c) Lift Force: Deformation Factor KS_{CL}

Recalling the assumptions presented in the previous section, the deformation factor for the lift force KS_{CL} should account for the variation of the projected area in the wave direction due to the deformations A_T' , which can be defined as (Figure 6- 22):

$$A_T' = 0.94 l_c \frac{l_c}{2} = 0.47 l_c^{\,2} \qquad (6.\ 41)$$

Considering that the projected area parallel to the flow can be obtained as:

$$A_T = 0.5 l_c^{\,2} \qquad (6.\ 42)$$

Thus, the deformed projected area parallel to the flow A_T' can be expressed as:

$$A_T' = KS_{CL} A_T \qquad (6.\ 43)$$

where KS_{CL} is the deformation factor for sliding that affects the lift force, defined as:

$$KS_{CL} = \frac{A_T'}{A_T} = 0.94 \qquad (6.\ 44)$$

Showing that there is a reduction of about 6% in the lift force due to the deformations of the GSC.

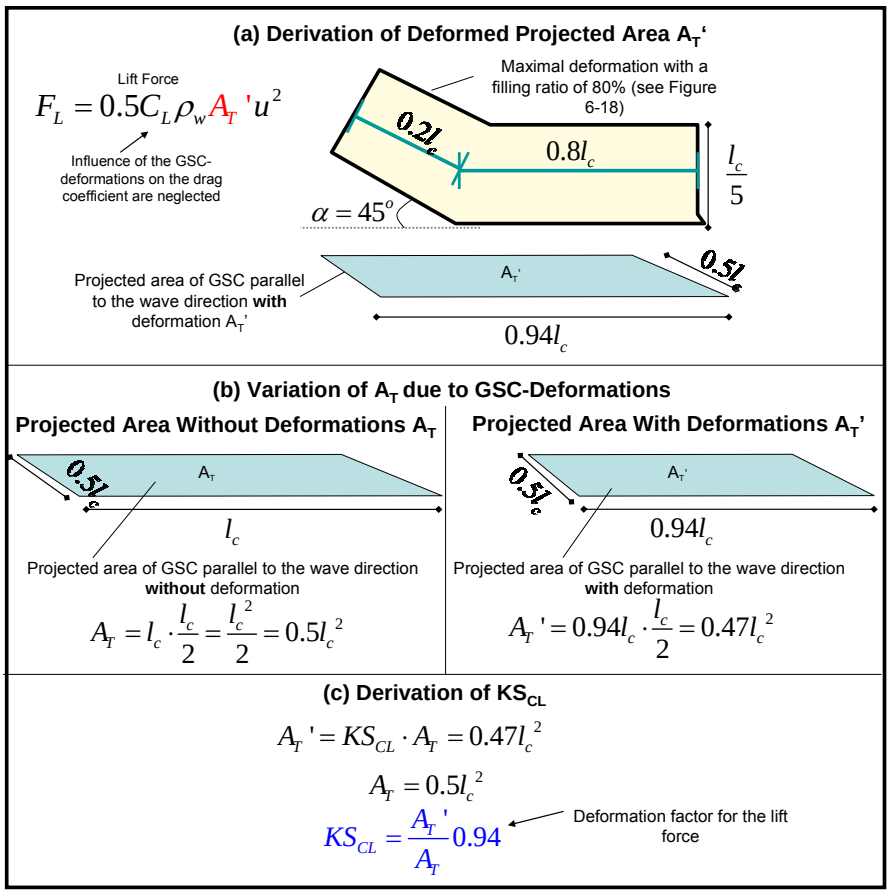

Figure 6- 22: Deformation Factor KS_{CL} for the Lift Force

(d) Resisting Force: Deformation Factor KS_R

Sliding of slope containers occurs, when the container returns from uplift deformation during downrush (Section 4.6). At incipient sliding, the sand particles in the frontal part of the container are subject only to very small stresses. Moreover, the contact areas between containers are reduced due to uplift deformation (Figure 6- 23).

In addition, the following assumptions must be recalled: (i) the deformations of all containers above the critical GSC are very similar and independent of their position in the GSC-structure (Figure 6- 16), (ii) the contact areas between neighbouring containers that are never uplifted are a function of the slope angle of the front of the GSC-structure with the sea bed (Section 4.5) and (iii) the maximal reduction of the contact area of a container in a GSC-structure with 45^o slope steepness is about 20% (Figure 6- 23).

Therefore, the deformation factor KS_R should account for: (i) the reduction of resisting force due to the deformations and (ii) the increase of the resisting force due to the contribution of upper containers (Figure 6- 23 and 6-24).

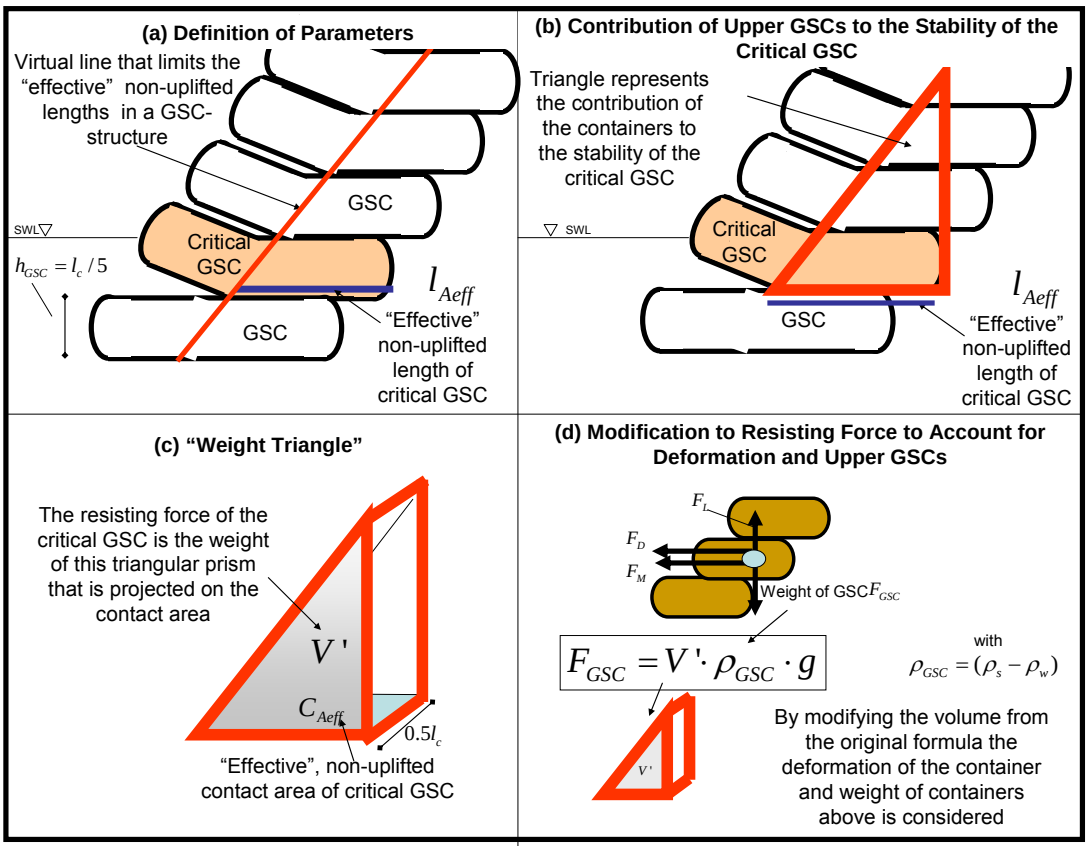

Figure 6- 23: Conceptual Model for the Resisting Force of Slope Containers that Account for the Deformation and Weight of Upper Containers

Therefore, to derive the deformation factor KS_R, the equation of the resisting force is recalled:

$$F_{GSC} = \rho_{GSC} V g \qquad (6.\ 45)$$

Equation 6.45 does neither account for: (i) the contribution of the weight of the neighbouring containers nor for (ii) the reduction of stability due to the GSC-deformations.

Modifying equation (6.45), the resisting force of the critical slope container against sliding displacement becomes:

$$F_{GSC} = \rho_{GSC} V' g \quad (6.46)$$

where V' is the volume of containers after deformation that is projected on the contact area underneath (Figure 6- 23c) and can be defined as:

$$V' = V \cdot KS_R \quad (6.47)$$

where KS_R is the resisting force deformation factor.

KS_R, is a function of the "effective" non-uplifted length of the container l_{Aeff}, and the slope steepness of the structure α, thus (Figure 6- 24):

$$l_{Aeff} = l_c - l_{Aupl} \quad (6.48)$$

The effective non-uplifted length of the container l_{Aeff} (see Figure 6- 24 and 6-25) is equal to the length of container l_c minus the uplifted length of the container l_{Aupl}. Considering that the uplifted part is a function of the slope steepness of the structure (Section 4.5), thus, the uplifted length of the container l_{Aupl} can be described as:

$$l_{Aupl} = \frac{l_c / 5}{\tan \alpha} \quad (6.49)$$

With a slope angle α of 45° (K_R factors for other slope angles are provided at the end of the section), thus,

$$l_{Aupl} = \frac{l_c}{5} \quad (6.50)$$

Therefore, the effective resisting contact area of the critical container is:

$$l_{Aeff} = l_c - \frac{l_c}{5} = 0.8 l_c \quad (6.51)$$

which also corresponds to the initial assumption for GSC-structures with slope steepness of 45°, stating that only 20% of the length of the container is uplifted.

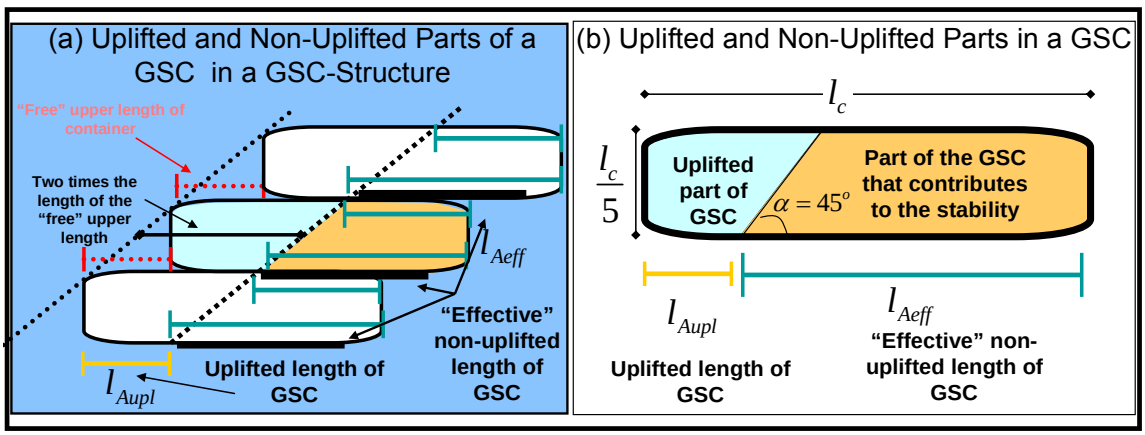

Figure 6- 24: Definition of Parameters for the Derivation of the Resisting Force of Containers (see also Figures 6-23 and 6-25)

In addition, the area of the triangle A_{tri} can be described as (Figure 6- 25):

$$A_{tri} = \left[\frac{1}{2}\right]\left[l_c - \frac{l_c}{5\tan\alpha}\right]\left[l_c \tan\alpha - \frac{l_c}{5}\right] \quad (6.52)$$

Considering again the slope angle of the structure $\alpha = 45^o$, yields:

$$A_{tr} = \left[\frac{1}{2}\right]\left[l_c - \frac{l_c}{5}\right]\left[l_c - \frac{l_c}{5}\right] \quad (6.53),$$

$$A_{tri} = \frac{8}{25} l_c^{\,2} = 0.32 l_c^{\,2} \quad (6.54)$$

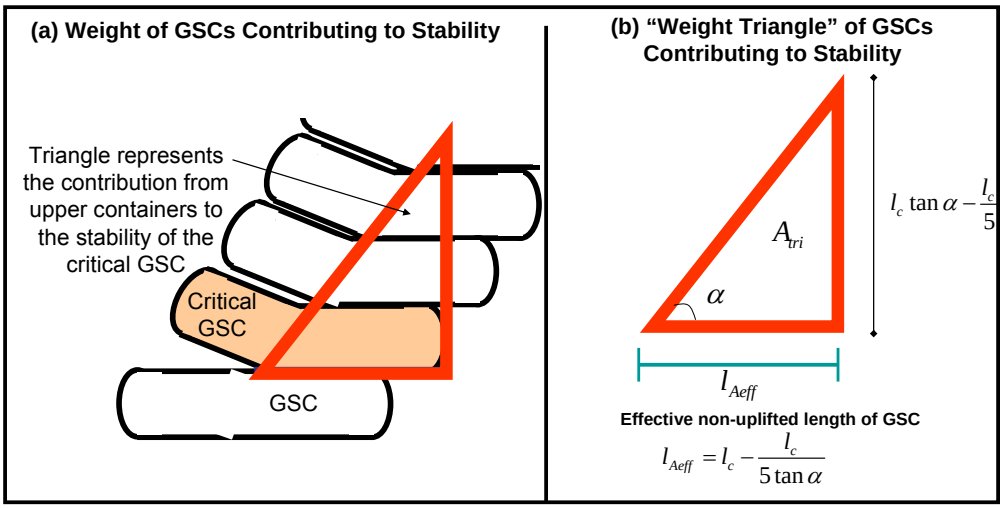

Figure 6- 25: Parameterisation of the Weight of Containers Contributing to the Stability

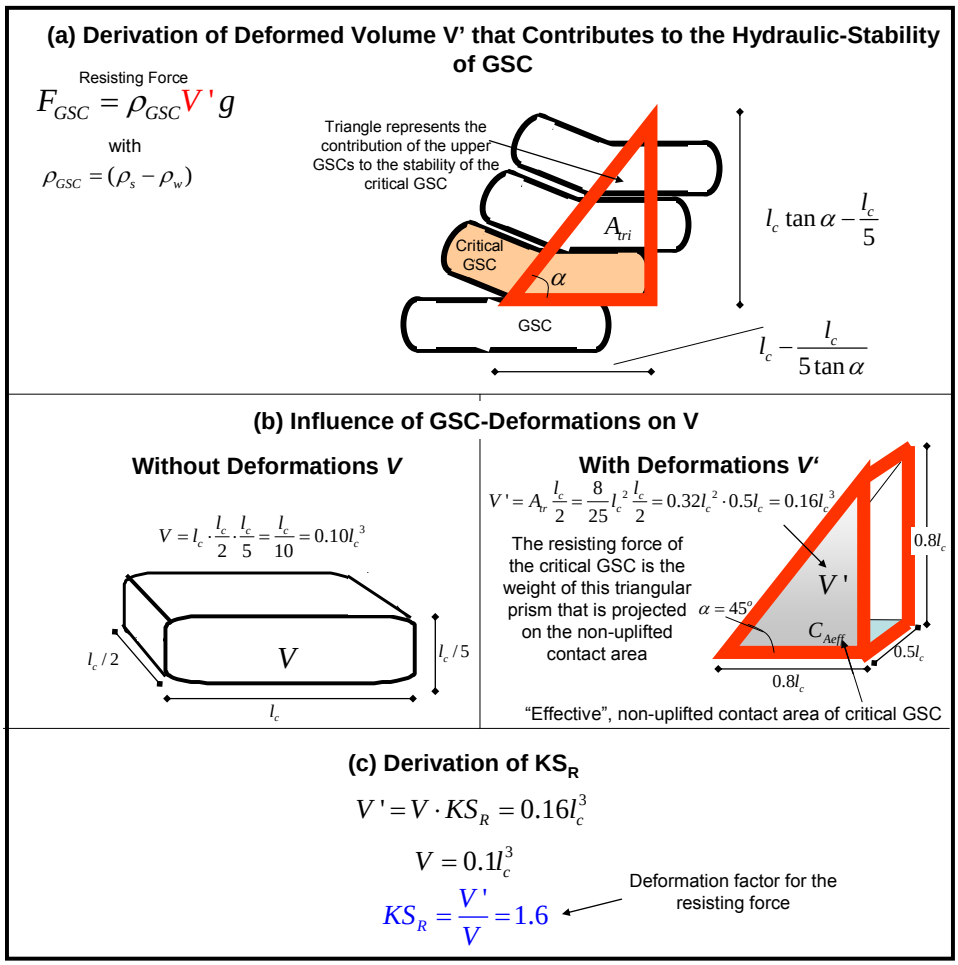

Figure 6- 26: Deformation Factor for the Resisting Force

Therefore, the volume *V'* is obtained from the area of the "weight triangle" A_{tri} multiplied by the width of the container $l_c/2$:

$$V' = A_{tr}\frac{l_c}{2} = \frac{8}{25}l_c{}^2\frac{l_c}{2} = 0.32l_c{}^2 \cdot 0.5l_c = 0.16l_c{}^3 \qquad (6.\ 55)$$

Considering that $V' = V \cdot K_R = 0.16l_c^3$, and $V = \frac{l_c^3}{10} = 0.1l_c^3$, then KS_R for slope containers in a 45^o sloped structure can be defined as (derivation procedure is summarized in Figure 6- 26):

$$KS_R = 1.6 \qquad (6.\ 56)$$

This means that the contribution of the upper containers is higher than the reduction due to the deformations and thus, the resisting force of a slope container is increased by 60%.

Moreover, following the same approach, the resisting factors for other slope angles have been derived (Table 6.4).

Table 6.4: KS_R for Sliding of Slope Containers

Deformation Factor	Slope Angle	Value
KS_{R30}	30^o	0.61
KS_{R45}	45^o	1.6
KS_{R60}	60^o	6.7
KS_{R75}	75^o	8.3
KS_{R90}	90^o	10 (*)

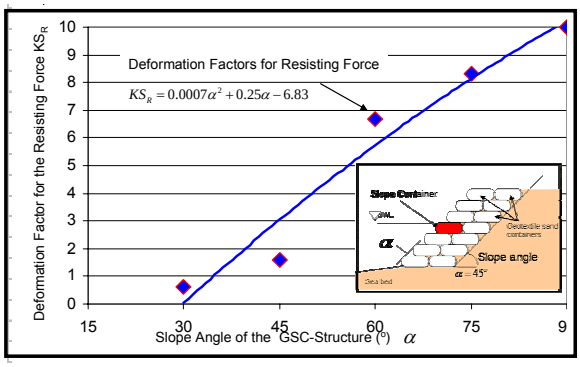

(*) with 90^o there is no uplift deformation and the whole weight of upper containers contributes to the stability

For GSC-structures with 30^o, if the free board R_c (vertical distance from SWL to crest of the structure) is smaller than $0.23l_c$, then, the deformation factors for crest containers need to be used (see Section 6.3.1.2) or the procedure presented here has to be adapted to account exactly for the number of upper containers that contribute to the stability. For other slope angles, the proposed deformation factors are valid for the following conditions:

- For $\alpha = 45^o$, $R_c > 0.5l_c$.
- For $\alpha = 60^o$, $R_c > 1.5l_c$.
- For $\alpha = 75^o$, $R_c > 3.5l_c$.

6.3.1.2 Crest Containers

The procedure adopted to derive the deformation factors for crest containers is very similar to the procedure described in Section 6.3.1.1. for slope containers.

Since similar deformations occur for slope and crest containers, it is reasonable to assume that the deformation factors will be similar for the drag inertia and lift forces F_D, F_M and F_L, thus:

$$KS_{CD} = 1.40 \qquad (6.\ 57)$$

$$KS_{CM} = 1.00 \qquad (6.\ 58)$$

$$KS_{CL} = 0.94 \qquad (6.\ 59)$$

However, the deformation factor for the resisting force KS_R will be different as there is no contribution from the weight of upper containers. For crest containers, the resisting volume of

the container *V'* is a trapezoidal prism, which also depends on the slope angle α of the GSC-structure (see Figure 6- 27).
The uplifted frontal part does not contribute to the stability of the GSC, because at time of incipient sliding, the frontal part is returning back from uplift deformation. Thus, the frontal part of the GSC is subject to very small stresses and therefore, the frontal uplifted part of the GSCs does not contribute to the stability.

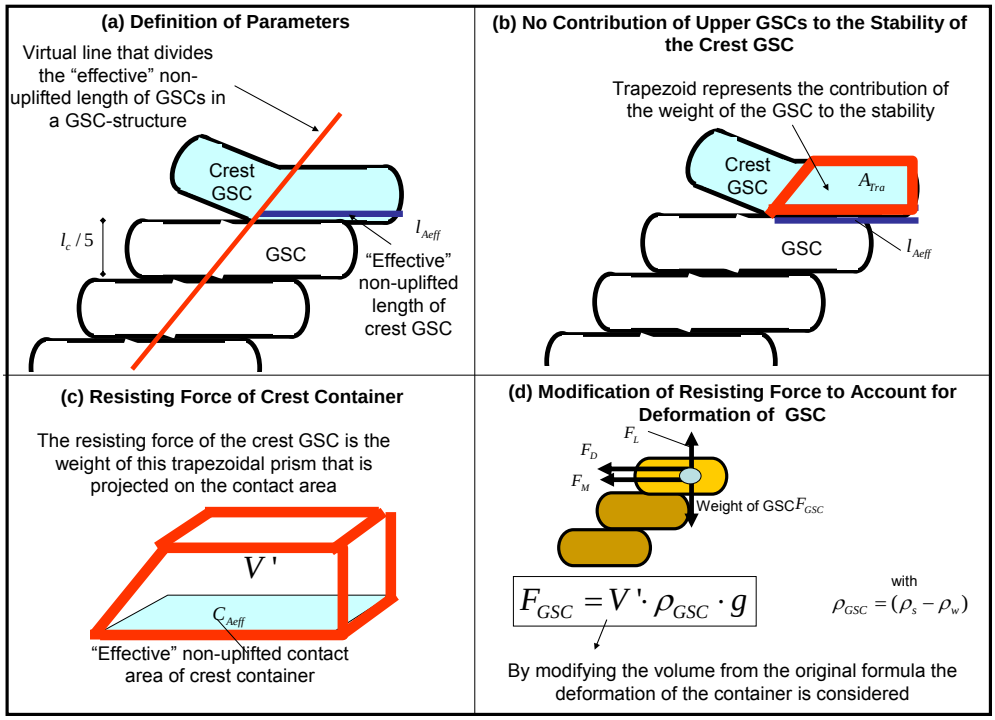

Figure 6- 27: Definition of Effective Volume *V'* of Deformed Crest Container

Defining again the "effective" non-uplifted length of the crest container l_{Aeff}:

$$l_{Aeff} = l_c - \frac{l_c/5}{\tan\alpha} \qquad (6.\ 60)$$

The area of the trapezoid A_{Tra} (Figure 6- 28) can be described as:

$$A_{Tra} = \left[\frac{1}{2}\right]\left[\frac{l_c}{5}\right]\left(\left[l_c - \frac{2l_c}{5\tan\alpha}\right] + \left[l_c - \frac{l_c}{5\tan\alpha}\right]\right) \qquad (6.\ 61)$$

The volume of the trapezoid *V'* can be described as (Figure 6- 28):

$$V' = \left[\frac{1}{2}\right]\left[\frac{l_c}{5}\right]\cdot\left[\frac{l_c}{2}\right]\left(\left[l_c - \frac{2l_c}{5\tan\alpha}\right] + \left[l_c - \frac{l_c}{5\tan\alpha}\right]\right) \qquad (6.\ 62)$$

Recalling a structure with a slope angle of 45°:

$$V' = \left[\frac{1}{2}\right]\left[\frac{l_c}{5}\right]\cdot\left[\frac{l_c}{2}\right]\left(\left[l_c - \frac{2l_c}{5}\right] + \left[l_c - \frac{l_c}{5}\right]\right) \qquad (6.\ 63)$$

Thus,

$$V' = 0.07 l_c^{\ 3} \qquad (6.\ 64)$$

Considering,

$$V' = V \cdot KS_R = 0.07 l_c^3 \qquad (6.\ 65)$$

$$V = 0.1 l_c^3 \qquad (6.\ 66)$$

The resisting force deformation factor for crest containers KS_R can be defined as:

$$KS_R = \frac{V'}{V} = 0.7 \qquad (6.\ 67),$$

showing that the resisting force of crest containers is reduced by 30% due to the deformations.

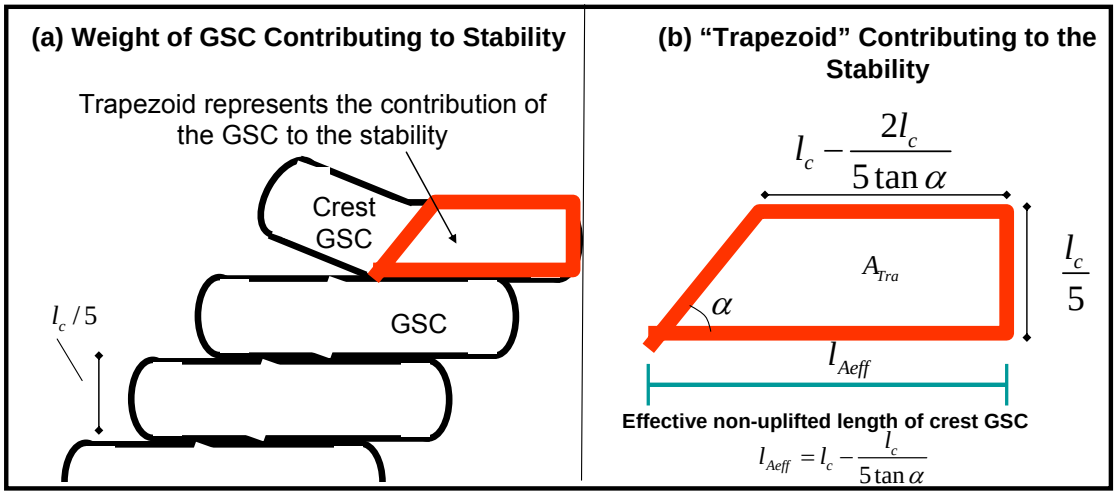

Figure 6- 28: Parameterization of the Weight of the Crest Container Contributing to the Stability

Moreover, following the same approach, the resisting factors KS_R for other slope angles have been derived (Table 6.5).

Table 6.5: KS_R for Sliding of Crest Containers

Deformation Factor	Slope Angle	KS_R
KS_{R30}	30°	0.48
KS_{R45}	45°	0.70
KS_{R60}	60°	0.82
KS_{R75}	75°	0.91
KS_{R90}	90°	1

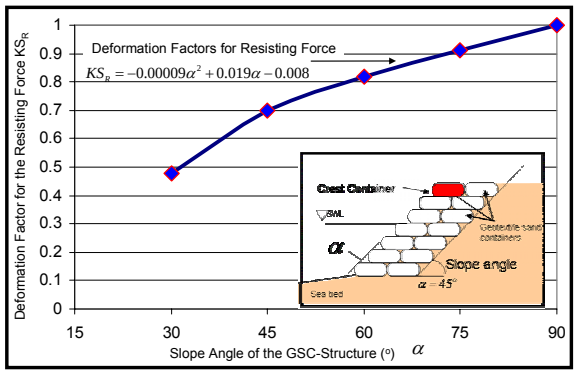

6.3.2 Stability against Overturning

Overturning of GSCs occurs when the mobilizing moments are higher than the resisting moments (Sections 6.1 and 4.7). Due to the deformations, the horizontal and vertical projection of the distance between the forces and the rotation point will move to a different location, thus, affecting the wave-induced moments (see Figure 6- 29). The rotation point *O* is defined as the rear-bottom-edge of the container as observed during the numerical simulations and as defined by Wouters (1998) (Section 5.5.7 and Figure 5-23). Therefore, by deriving the exact location of the gravity centre of the deformed container *G'*, the deformation factors *KO* for the overturning formula can be obtained (Figure 6- 29).

Considering the assumptions of these analyses (Figures 6-16 to 6-18), the most critical deformation that a container can suffer (considering a sand fill ratio of at least 80%) consists

in a reduction of the contact area of 20% and an uplift deformation with an angle of 45° degrees as shown in Figure 6- 30.

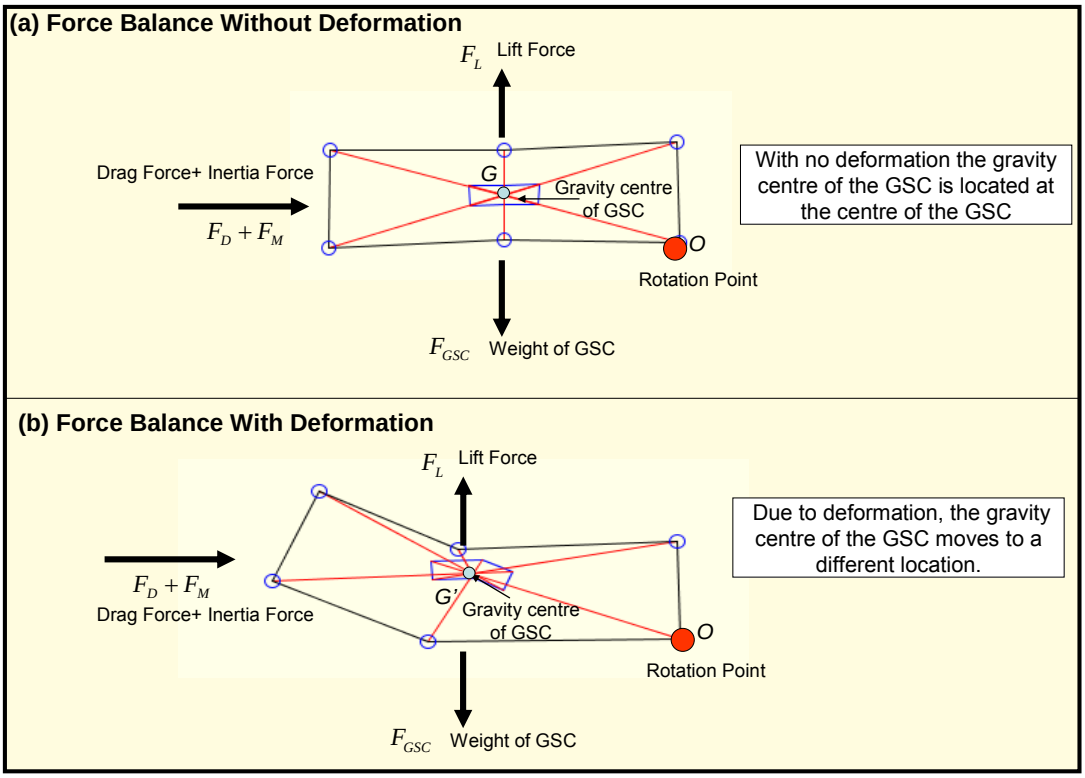

Figure 6- 29: Variation of the Gravity Centre of a Deformed Geotextile Sand Container

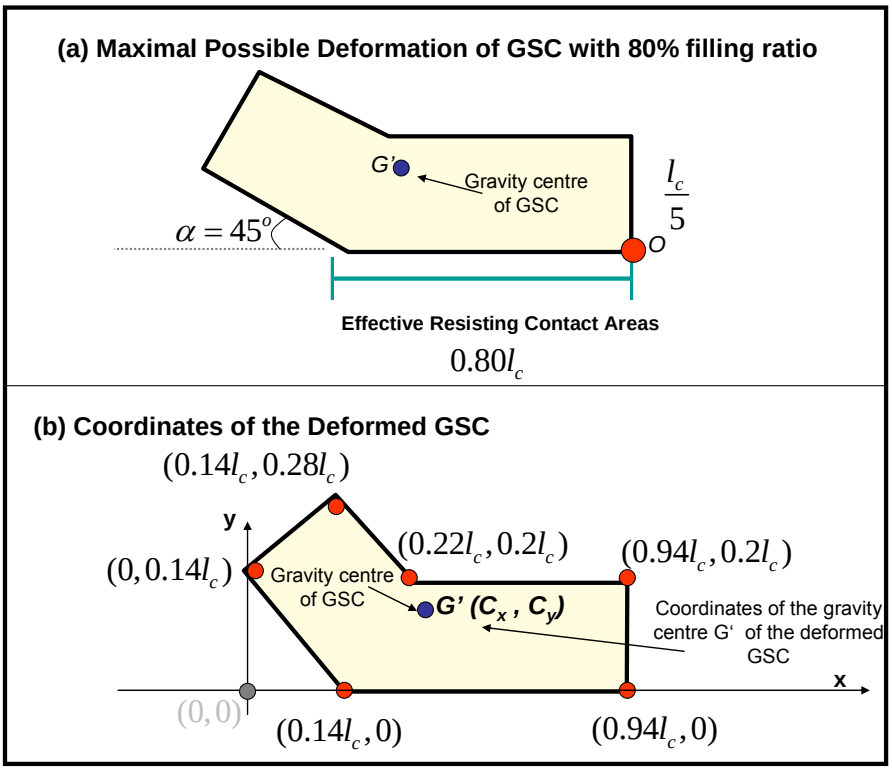

Figure 6- 30: Deformation Sketch for the Derivation of the Gravity Centre of a Deformed Crest Container (see also Figure 6- 29 and 4-28)

Therefore, the gravity centre of the deformed container can be calculated by using the following equations:

$$C_x = \frac{1}{6A_p}\sum_{i=0}^{N-1}(x_i + x_{i+1})(x_i y_{i+1} - x_{i+1} y_1) \quad (6.\ 68)$$

$$C_y = \frac{1}{6A_p}\sum_{i=0}^{N-1}(y_i + y_{i+1})(x_i y_{i+1} - x_{i+1} y_1) \quad (6.\ 69)$$

where C_x and C_y are the coordinates in "*x*" and "*y*" of the gravity centre of the polygon; x and y are the coordinates of each of the points in the polygon, A_p is the polygon area and N is the number of sides of the polygon.

Thus, the coordinates of the gravity centre of the polygon (deformed GSC) with respect to the coordinate system shown in Figure 6- 30 are:

$C_x = 0.48 l_c$ (6. 70)
$C_y = 0.11 l_c$ (6. 71)

Therefore, the horizontal projection of the distance between the vertical forces and the point of rotation is $r_s' = 0.46 l_c$ (horizontal projection of the distance between C_x to O).
On the other hand, the vertical projection of the distance between the horizontal forces and the point of rotation is $m_s' = 0.11 l_c$

6.3.2.1 Slope Containers

The overturning of slope containers in a GSC-structure occurs only if the wave-induced forces applied on the critical container are much larger than the resisting forces as explained in Section 4.7.

Since the forces required to generate overturning of slope containers are much larger than the forces required to induce sliding, deriving the stability formula for slope containers against overturning is not required.

However, to illustrate the overturning of slope containers, numerical simulations using the "partially coupled" model (see Chapter 5) were performed (Figure 6-31), showing that the wave-induced forces needed to induce overturning of slope containers are at least 5 times larger than the required forces to induce sliding.

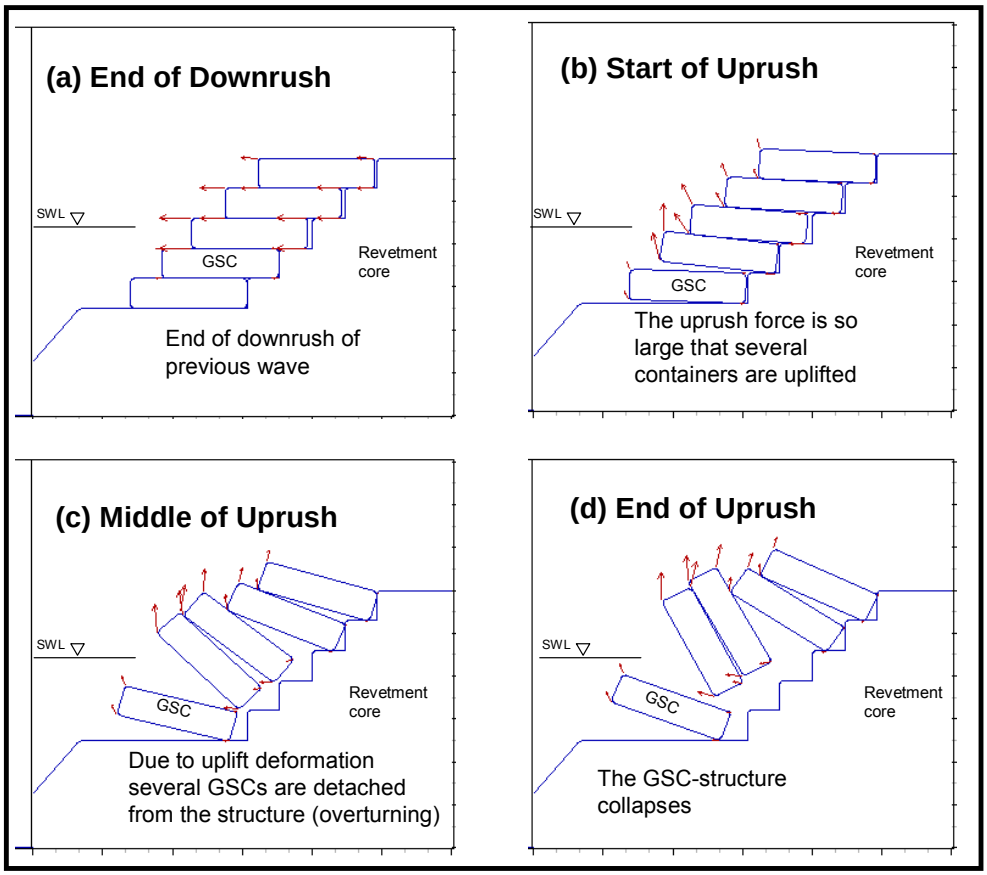

Figure 6- 31: Overturning of Slope Containers: Results of Numerical Simulation (GSCs simulated as rigid to reduce computational time)

6.3.2.2 Crest Containers

The deformations factors for overturning of crest containers *KO* should account for: (i) the variation in forces as explained in Section 6.3.1 and (ii) the variations of the moment due to the new location of the gravity centre of the GSC after deformation *G'*.

(a) Deformation Factor KO_{CD} for the Moment Induced by the Drag Force

The moment induced by the drag force M_{CD} on a crest container can be described as (see also Section 4.7):

$$M_{CD} = F_{CD} \cdot m_s = 0.5u^2 C_D \rho_w A_S m_s \qquad (6.\ 72)$$

where m_s is the vertical projection of the distance between the centre of gravity of the non-deformed container *G* and the rotation point *O* (Figures 6-13, 6-27 and 4-28).

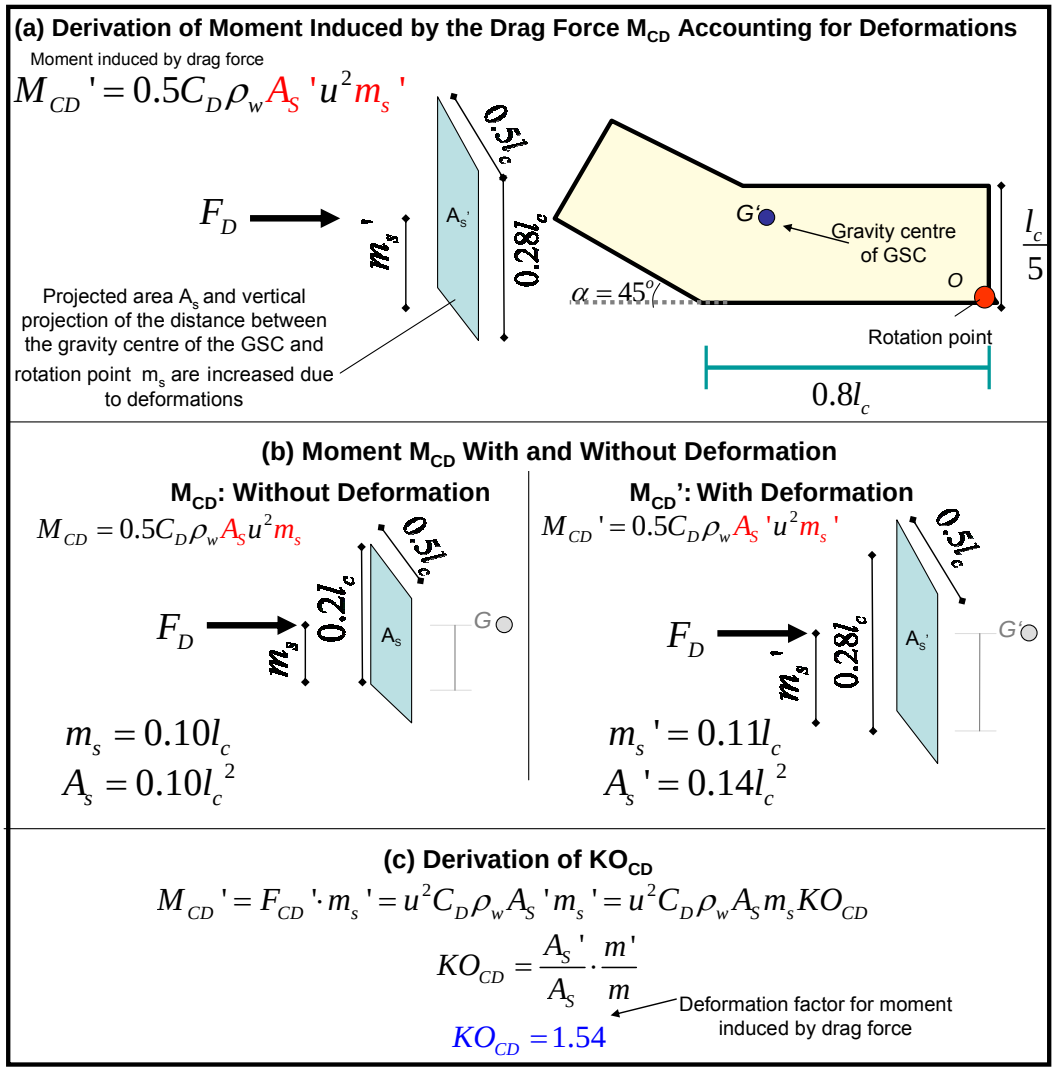

Figure 6- 32: Deformation Factor KO_{CD} for the Moment Induced by the Drag Force

However, deformation affects both m_s and A_S thus, the moment induced by the drag force that account for the deformations can be obtained as:

$$M_{CD}' = F_{CD}' \cdot m_s' = 0.5 u^2 C_D \rho_w A_S' m_s' \quad (6.\ 73)$$

where m_s' is the vertical projection of the distance between the centre of gravity of the deformed container G' and the rotation point O; A_S' is the projected area of the deformed container normal to the flow. Considering the following relations:

$$m_s = 0.1 l_c \quad (6.\ 74)$$

$$m_s' = 0.11 l_c \quad (6.\ 75)$$

$$A_s' = 1.4 A_S \quad (6.\ 76)$$

The drag moment that account for the deformation is:

$$M_{CD}' = F_{CD}' \cdot m_s' = 0.5 u^2 C_D \rho_w A_S' m_s' = 0.5 u^2 C_D \rho_w A_S m_s KO_{CD} \quad (6.\ 77)$$

where KO_{CD} is the deformation factor for the moment induced by the drag force and defined as (derivation summarized in Figure 6- 32):

$$KO_{CD} = \frac{A_S'}{A_S} \cdot \frac{m'}{m} = 1.54 \qquad (6.\ 78),$$

showing that the moment induced by the drag force is increased by about 54% due to the deformations of the crest container.

(b) Deformation Factor KO_{CM} for the Moment Induced by the Inertia Force

Following the same approach as for the drag moment, the moment induced by the inertia force can be defined as:

$$M_{CM} = F_M \cdot m_s = C_M V \rho_w \frac{\partial u}{\partial t} \cdot m_s \qquad (6.\ 79)$$

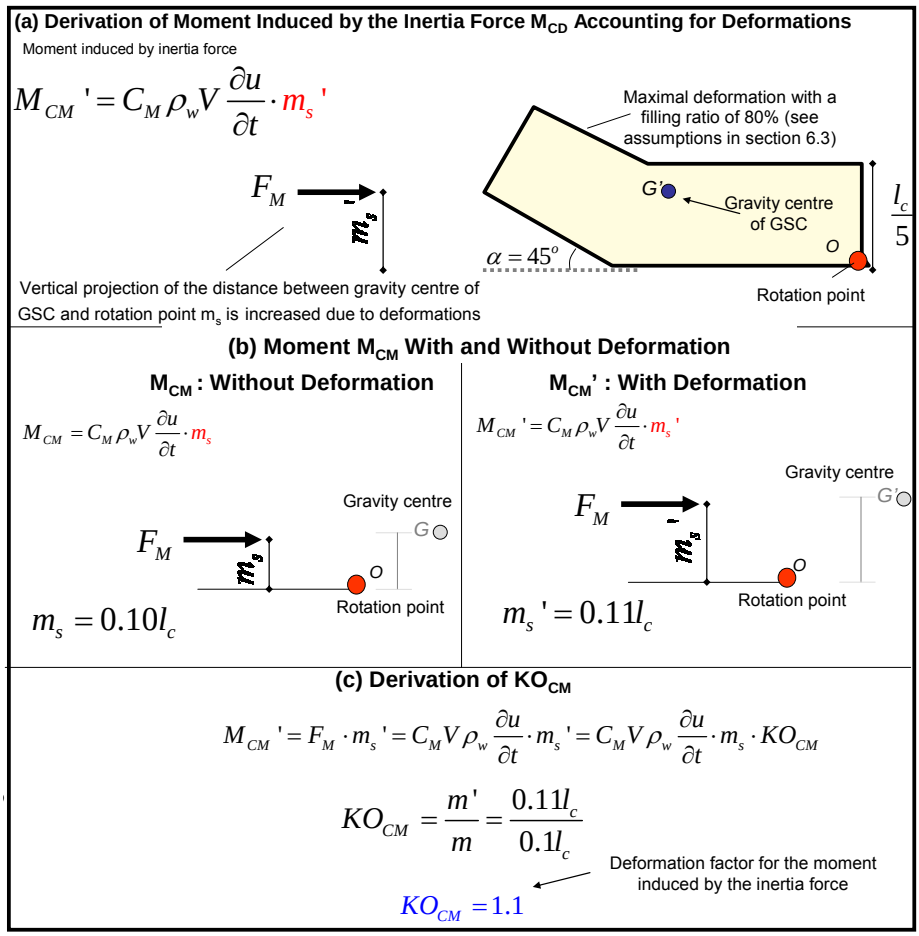

Figure 6- 33: Deformation Factor KO_{CM} for the Moment Induced by the Inertia Force

However, as with the moment induced by the drag force M_{CD}, the vertical projection of the distance between the centre of gravity of the container and the rotation point is increased due to the deformations. Thus, the moment induced by the inertia force that account for the deformation, is obtained as:

$$M_{CM}' = F_M \cdot m_s' = C_M V \rho_w \frac{\partial u}{\partial t} \cdot m_s' \qquad (6.\ 80)$$

where m_s' is the increased vertical projection of the gravity centre of GSC *G'* and the rotation point *O* due to deformations:

$$m_s' = 0.11 l_c \quad (6.\ 81)$$

The moment induced by the inertia force that accounts for the deformation M_{CM}' can be defined as:

$$M_{CM}' = F_M \cdot m_s' = C_M V \rho_w \frac{\partial u}{\partial t} \cdot m_s' = C_M V \rho_w \frac{\partial u}{\partial t} \cdot m_s \cdot KO_{CM} \quad (6.\ 82)$$

where KO_{CM} is the deformation factor that accounts for the influence of the GSC-deformations on the moment induced by the inertia force and described as (derivation summarized in Figure 6- 33) :

$$KO_{CM} = \frac{m'}{m} = \frac{0.11 l_c}{0.1 l_c} = 1.1 \quad (6.\ 83)$$

showing that the moment induced by the inertia force is increased by 10% due to the deformations of the crest container.

(c) Deformation Factor KO_{CL} for the Moment Induced by the Lift Force

Following the same approach as in previous sections, the lift moment can be defined as:

$$M_{CL} = F_L \cdot r_S = 0.5 u^2 C_L \rho_w A_T \cdot r_S \quad (6.\ 84)$$

where r_s is the horizontal projection of the distance between the centre of gravity *G* of the container and the rotation point *O* (Figures 6-13 and 4-28).

However, deformation affects A_T and r_s, therefore, the moment induced by the lift force that account for the deformations can be obtained as:

$$M_{CL}' = F_L' \cdot r_S' = 0.5 u^2 C_L \rho_w A_T' \cdot r_s' \quad (6.\ 85)$$

where A_T' is the projected area of the deformed container parallel to the flow and r_s' the projection of the distance between the centre of gravity of the deformed container *G'* and the rotation point *O*.

Thus, the moment induced by the lift force that account for the deformation is:

$$M_{CL}' = F_L' \cdot r_S' = 0.5 u^2 C_L \rho_w A_T' \cdot r_s' = 0.5 u^2 C_L \rho_w A_T \cdot r_s \cdot KO_{CL} \quad (6.\ 86)$$

where KO_{CL} is the deformation factor for the moment induced by the lift force and defined as (procedure summarized in Figure 6- 34):

$$KO_{CL} = \frac{A_T'}{A_T} \cdot \frac{r_s'}{r_s} = \frac{0.47 l_c^2}{0.54 l_c^2} \cdot \frac{0.46 l_c}{0.5 l_c} = 0.80 \quad (6.\ 87)$$

showing that the deformation reduces the lift moment by approximately 20%.

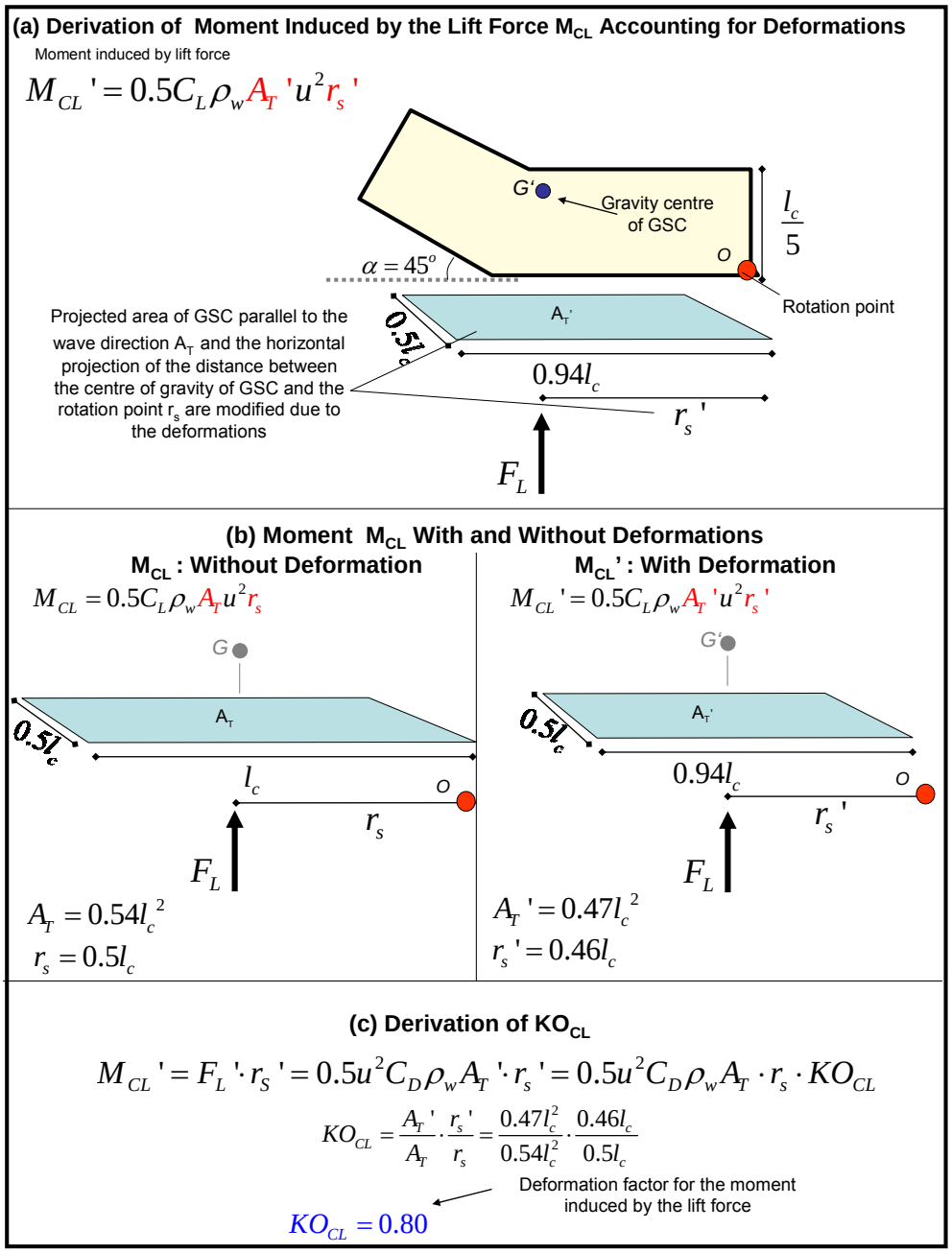

Figure 6- 34: Deformation Factor KO_{CL} for the Moment Induced by the Lift Force

(d) Deformation Factor M_{GSC} for the Moment Induced by the Resisting Force

The moment induced by the resisting force M_{GSC} can de described as:

$$M_{GSC} = \rho_{GSC} V g \cdot r_s \qquad (6.\ 88)$$

where r_s is the horizontal projection of the distance between the centre of gravity of the container G and the rotation point O. Unlike sliding, overturning occurs when all the sand particles inside the container are subject to compression stresses, thus, the whole weight of the container contributes to the stability.

Moreover, deformation affects r_s, thus, the moment induced by the resisting force that accounts for the GSC-deformations can be obtained as:

$$M_{GSC}' = \rho_{GSC} Vg \cdot r_s' \quad (6.\ 89)$$

where r_s' is the projection of the distance between the centre of gravity of the deformed container G' and the rotation point O.

Thus, the resisting moment that accounts for the deformation is:

$$M_{GSC}' = \rho_{GSC} Vg \cdot r_s' = \rho_{GSC} Vg \cdot r_s \cdot KO_R \quad (6.\ 90)$$

where KO_R is the deformation factor for the resisting moment defined as (procedure summarized in Figure 6- 35):

$$KO_R = \frac{r_s'}{r_s} = \frac{0.46 l_c}{0.5 l_c} = 0.92 \quad (6.\ 91),$$

indicating that the deformation reduces the resisting moment M_{GSC} by approximately 8%.

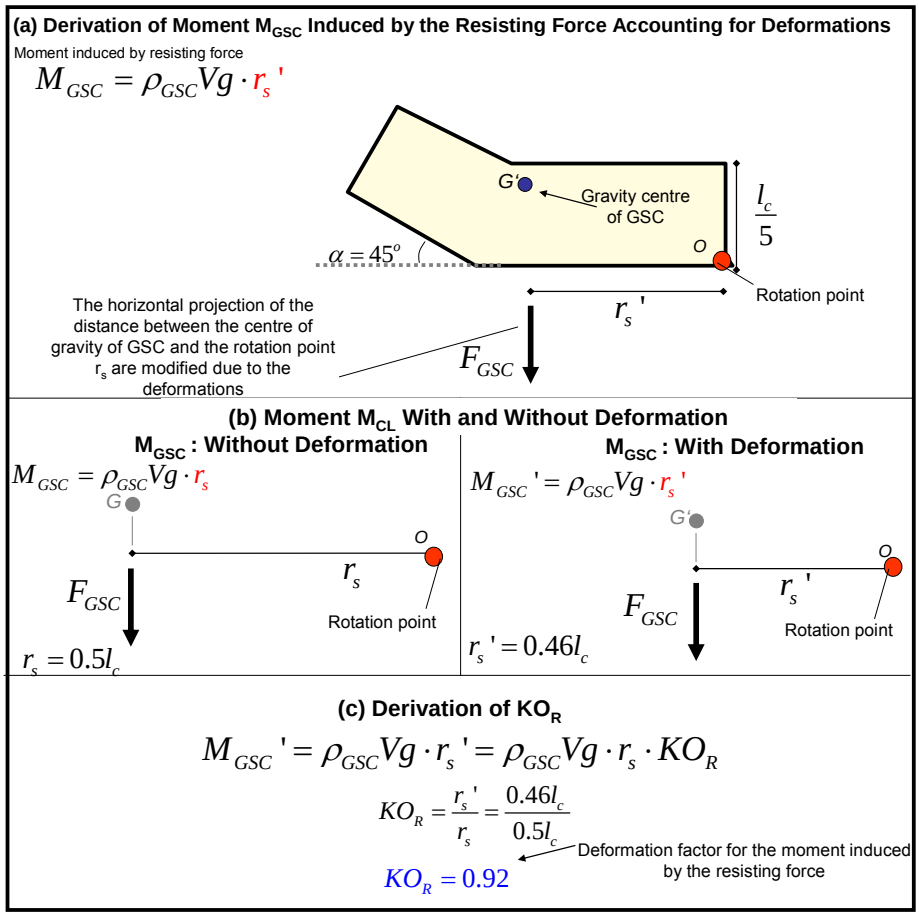

Figure 6- 35: Deformation Factor KO_R for the Moment Induced by the Resisting Force

6.3.3 Discussion on the Deformation Factors KS_i and KO_i

In this section, the deformation factors that account for the deformations of GSC have been derived, showing that the deformation strongly affects the mobilizing and resisting forces on GSCs. The deformation factors also clarify the influence of boundary conditions such as neighbouring containers on the stability of GSCs. Slope containers have much higher stability than crest containers due to the contribution of the upper containers (given the same wave-loading, crest containers must be at least 8 times heavier than slope containers; in terms of incident wave, if crest and slope containers are subjected to same wave condition, crest container must be 4 to 8 times heavier than slope containers to achieve the same stability).

The deformation of GSCs may increase the drag force by approximately 40%, while for the resisting forces may be reduced about 30%, thus, illustrating the influence of the deformations on the stability of GSC-structures (see Section 6.4 for the effect on the stability).
The stability formulae with the corresponding deformation factors and force coefficients C_D, C_M and C_L are summarized and discussed Section 6.5 with respect to their validation.

6.4 Comparative Analysis of New Stability Formulae with and without Deformation Effect and Available Formulae

The new stability formulae with and without deformation effects and the available formulae are compared and illustrated in Figure 6-36. However, the comparative analysis of the available stability formulae for GSCs (Section 2.4) and the proposed new stability formulae from this study is not straightforward. In fact, the formula proposed by Hinz and Oumeraci (2002) and Wouters (1998) depend mainly on the wave height H and the surf similarity parameter $\frac{\tan\alpha}{\sqrt{H_s / L_o}}$, while the water depth d is not explicitly considered. On the other hand, the formula proposed by Bouyze and Schram (1990) and the formulae presented in this study depend mainly on the wave induced horizontal velocity and are thus also sensitive to the wave period and water depth. Therefore, for the initial comparison, the water depth, wave period and freeboard should be kept constant, while the wave height should be varied (Figure 6-36).
In addition, the formulae proposed in this study (equations 6.16 and 6.25) require the wave induced horizontal velocity u and the associated acceleration $\frac{\partial u}{\partial t}$. The maximal wave-induced horizontal velocity and only the 10% of the acceleration were implemented in the formulae, since the maximal wave-induced velocity occurs when the associated acceleration tends to zero (Figure 6-40). Moreover, the recommendations for the construction of GSC-structures presented by Naue (2003) which are based on existing GSC-structures were also included in the comparison (Figure 6-36). Finally, the formulae were compared in terms of the required length (m) instead of the required mass (kg) due to the following reasons: (i) all available formulae are only valid for a specific geometry of the container, (ii) the stability formulae explicitly provide the required length: e. g. from the length, together with the prescribed geometry, the mass is derived and (iii) since the mass of the containers is proportional to l_c^3 (l_c being the length of the container) comparison between the mass does not necessary clarify the relations between the formulae.

The results of the comparative analysis are summarized in Figure 6-36:

(i) The formulae with deformation effects presented in this study (Section 6.3) provide larger required lengths than the formulae without deformation effects. Differences are more noticeable for the crest containers (up to 60% in terms of required length) than for the slope containers (up to 28% in terms of required length), since the latter have stability contribution from neighbouring containers (refer to Section 6.3.1.1).

(ii) The required mass provided by the formulae with and without deformation is very different (mass proportional to l_c^3). For example, for the wave conditions *H=2m T=6s* and *d=4m* as illustrated in Figure 6-36a the formula with deformation effects provides a required mass of 1916kg while the formulae without deformation effects requires a mass of only 395kg, thus illustrating the strong influence of the deformations on the stability of GSCs.

(iii) Regarding the comparative analysis including available formulae; the formula from Bouyze and Schram (1990) provides the smallest required length. The reason is that the formula was derived from model tests using geotubes and therefore cannot be applied for GSCs with a finite length (refer to Section 2.4 for more details).

(iv) The formula for slope containers of Hinz and Oumeraci (2002) and the formula from Wouters (1998) provide similar results (variations within 8% in terms of required length). Variation between the two formulae are probably only due to the empirical parameter derived from model tests (2.75 derived from Hinz and Oumeraci, 2002 instead of 2.5 from Wouters, 1998). On the other hand, the formula for crest containers proposed by Hinz and Oumeraci (2002) provides slightly higher required lengths (up to 16% in terms of required length) than the formulae presented by Wouters (1998). In fact, Hinz and Oumeraci (2002) were the first to quantify the differences in wave loading and boundary conditions between slope and crest containers.

(v) Moreover, the shape of the function of the formulae developed in this study is different as compared with the other formulae. The reason is that according to the new formulae the required container length is a function of u^2 (parabolic function), thus, are very sensitive to the wave height ($l_c \propto u^2 \propto H^2$), while in the formulae proposed by Hinz and Oumeraci (2002) and Wouters (1998) l_c is approximately proportional to $H^{3/4}$ ($l_c \propto H^{3/4}$). In addition, the stability formulae developed in this study are more sensitive to wave period and water depth than the other formulae (i. e. Hinz and Oumeraci, 2002 and Wouters, 1998). Generally, the new formulae provides smaller lengths for smaller wave heights ($H<1.5m$) and larger container lengths for higher waves ($H>4m$). Since the new formulae are much more sensitive to the wave period T and water depth d, it is however, impossible to conclude under which wave conditions the formulae presented in this study will provide smaller or larger lengths. For example, in Figure 6-36a ($H=0\sim4m$, $d=4m$ $T=6s$), the new formula for sliding provides smaller container lengths for $H<2.5m$ and larger container lengths for $H>2.5m$ when compared with the formulae of Hinz and Oumeraci (2002). However, as soon as the wave period or water depth changes a different situation will result.

(vi) All available formulae including the new formulae of this study provide very different required values of mass of the containers, since the mass is proportional to l_c^3. For example, with a wave height of $H=2m$, wave period of $T=6s$ and water depth of $d=4m$, the required mass provided by the new stability formula for slope containers is *1916kg*, while the formula proposed by Hinz and Oumeraci (2002) provides *3542kg* and Wouters' formula *4860kg*. However, with a higher wave height of $H=3m$, the required mass provided by the new formulae is *19500kg*; Wouters' formula (1998) provides *16400kg* and Hinz and Oumeraci (2002) *11500kg*, thus, illustrating the influence of the wave height H on the required mass. A difference in 1 meter in the wave height H results in at least 3 to 10 times larger required mass.

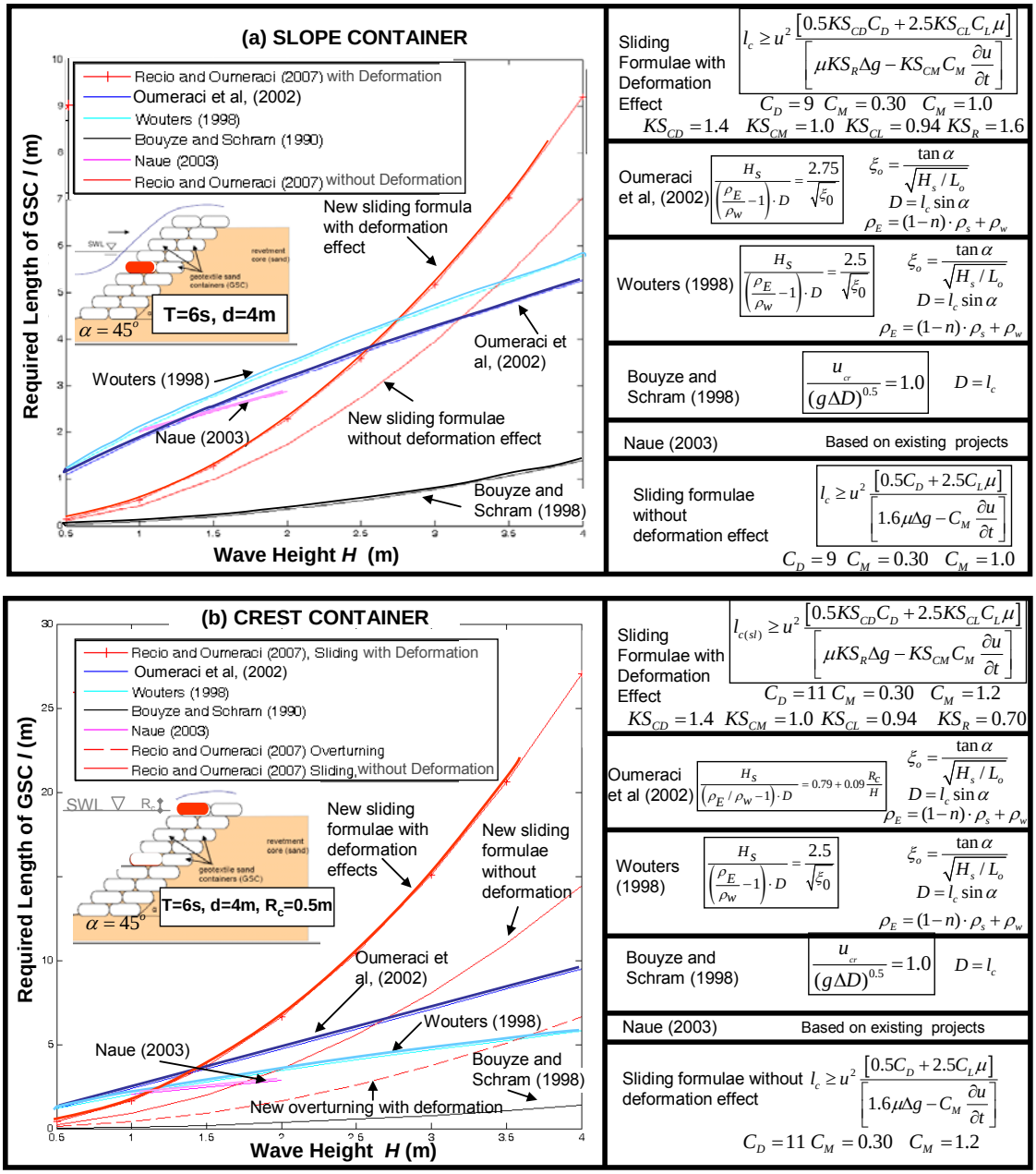

Figure 6- 36: Comparison between New Stability Formulae with and without Deformation Effects Including Further Available Formulae

6.5 Validity of Proposed Stability Formulae, Force Coefficients and Deformation Factors

The proposed generic methodology for deriving the stability formulae, force coefficients and deformation factors for GSCs against sliding and overturning of GSCs has been proposed in Sections 6.1 to 6.3. The presented approach is valid for GSCs with the following properties: (i) container made with non-woven geotextile, (ii) with a sand fill ratio of 80%, (iii) with a geometry, for which the containers' length is twice as large as its width and five times as large as its height and (iv) GSC-structure with slope angle of $\alpha = 45^o$ (Section 6.3).

Force coefficients C_D, C_M and C_L for the stability formulae are derived by means of specially designed experimental studies for several boundary conditions and configurations (Section 6.2). The approach and methodology are valid for any type of GSC-structure. However, the validity of the force coefficients corresponds to the tested conditions and is, therefore subject to some limitations (see Section 6.5.2 for details).

Finally, the influence of the deformations on GSCs is accounted for by introducing deformation factors into the stability formulae for GSCs (Section 6.3), which are based on several assumptions. Assumptions are made based on model tests results (Chapters 4 and 5, more details also in Sections 6.3 and 6.5.3).

6.5.1 Stability Formulae, Force Coefficients and Deformation Factors

The proposed stability formulae, force coefficients C_D, C_M and C_L and deformation factors K_{CD}, K_{CM}, K_{CL} and K_R derived in this Chapter are summarized in Figure 6- 37. The definition of parameters and typical values to be used in the stability formulae are presented in Figure 6-38.

To apply the hydraulic stability formulae, the following parameters are needed: (i) the wave-induced horizontal velocity at the depth of the critical container u, (ii) the wave-induced horizontal acceleration at same location $\frac{\partial u}{\partial t}$, (iii) the friction factor between GSCs μ and (iv) the force and deformation coefficients.

Wave-induced horizontal velocities and accelerations can be derived from wave theories (see also Section 6.5.2 for validity and suggestions). The friction factor can be derived from Table 2.2 (or from shear stress tests between geotextiles) and the force coefficients C_D, C_M and C_L as well as and the deformation factors KS_i and KO_i from the relations and values provided Figure 6- 37 (validity in Section 6.5.2).

(a) Stability Formulae for GSCs Including the Effect of Deformation

Sliding Stability

Required container length

$$l_{c(sl)} \geq u^2 \frac{\left[0.5KS_{CD}C_D + 2.5KS_{CL}C_L\mu\right]}{\left[\mu KS_R\Delta g - KS_{CM}C_M\frac{\partial u}{\partial t}\right]}$$

Required container mass

$$W_{GSC} \geq \rho_s \left(u^2 \frac{\left[0.5KS_{CD}C_D + 2.5KS_{CL}C_L\mu\right]}{\left[\mu\Delta KS_R g - KS_{CM}C_M\frac{\partial u}{\partial t}\right]} \right)^3 /10$$

Overturning Stability

Required container length

$$l_{c(ov)} \geq u^2 \frac{\left[0.05KO_{CD}C_D + 1.25KO_{CL}C_L\right]}{\left[0.5\Delta KO_R g - 0.1KO_{CM}C_M\frac{\partial u}{\partial t}\right]}$$

Required container mass

$$W_{GSC} \geq \rho_s \left(u^2 \frac{\left[0.05KO_{CD}C_D + 1.25KO_{CL}C_L\right]}{\left[0.5\Delta KO_R g - 0.1KO_{CM}C_M\frac{\partial u}{\partial t}\right]} \right)^3 /10$$

(b) Deformation Factors and Force Coefficients for the Stability Formulae

GSC-Structure	Sliding	Overturning	Force Coefficients
Single GSC on Sea Bed 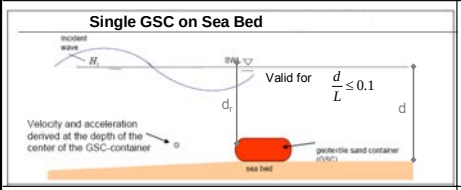	$KS_{CD} = 1.40$ $KS_{CM} = 1.00$ $KS_{CL} = 0.94$ $KS_R = 0.70$	$KO_{CD} = 1.54$ $KO_{CM} = 1.1$ $KO_{CL} = 0.80$ $KO_R = 0.92$	$C_D = -2x10^{-5}\,\mathrm{Re} + 6.81$ with $1.3 \leq C_D \leq 6.5$ $C_M = 0.60$ $C_L = 1x10^{-5}\,\mathrm{Re} - 0.612$ with $0.2 \leq C_L \leq 1.4$
Group of GSCs on Sea Bed (i. e. Scour Protection) 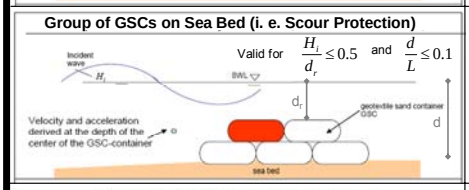	$KS_{CD} = 1.40$ $KS_{CM} = 1.00$ $KS_{CL} = 0.94$ $KS_R = 0.70$	$KO_{CD} = 1.54$ $KO_{CM} = 1.1$ $KO_{CL} = 0.80$ $KO_R = 0.92$	$C_D = -6x10^{-5}\,\mathrm{Re} + 14.70$ with $4 \leq C_D \leq 11$ $C_M = 0.50$ $C_L = 1x10^{-5}\,\mathrm{Re} - 0.669$ with $0.4 \leq C_L \leq 1.3$
Submerged GSC-Breakwaters (Artificial Reef) 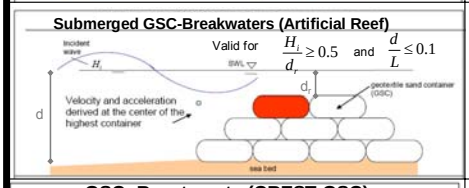	$KS_{CD} = 1.40$ $KS_{CM} = 1.00$ $KS_{CL} = 0.94$ $KS_R = 0.70$	$KO_{CD} = 1.54$ $KO_{CM} = 1.1$ $KO_{CL} = 0.80$ $KO_R = 0.92$	$C_D = -9x10^{-5}\,\mathrm{Re} + 23.04$ with $4 \leq C_D \leq 15$ $C_M = 0.30$ $C_L = 1x10^{-5}\,\mathrm{Re} - 0.587$ with $0.3 \leq C_L \leq 1.2$
GSC- Revetments (CREST GSC) 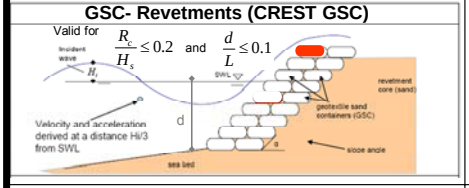	$KS_{CD} = 1.40$ $KS_{CM} = 1.00$ $KS_{CL} = 0.94$ $KS_R = 0.70$	$KO_{CD} = 1.54$ $KO_{CM} = 1.1$ $KO_{CL} = 0.80$ $KO_R = 0.92$	$C_D = -2x10^{-5}\,\mathrm{Re} + 6.81$ with $1.3 \leq C_D \leq 6.5$ $C_M = 0.60$ $C_L = 1x10^{-5}\,\mathrm{Re} - 0.612$ with $0.2 \leq C_L \leq 1.4$
GSC- Revetments (SLOPE GSC) 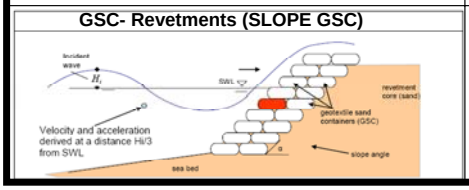	$KS_{CD} = 1.40$ $KS_{CM} = 1.00$ $KS_{CL} = 0.94$ $KS_R = 1.60$	Not applicable (GSC pulled out seaward)	$C_D = -3x10^{-5}\,\mathrm{Re} + 8.9$ with $2.5 \leq C_D \leq 9$ $C_M = 0.30$ $C_L = 1x10^{-5}\,\mathrm{Re} - 0.587$ with $0.3 \leq C_L \leq 1.2$

Note: Determined for shallow water conditions $d/L<0.10$ and $Re=10^4$-10^6

Figure 6- 37: Stability Formulae, Deformation Factors and Force Coefficients (slope angle 45° and sand fill ratio of GSC of 80%, refer to Tables 6.4 and 6.5 for other slope angles)

Definition of Parameters and Typical Values

Definition of parameters:

l_c is the required length of the container in m

W_{GSC} is the required mass of the container in kg

u is the horizontal velocity derived at the depth of the critical container in m/s

$\frac{\partial u}{\partial t}$ is the horizontal acceleration derived from the obtained velocity in m/s²

μ is the friction factor between geotextiles

g is the gravity acceleration in m/s²

$\Delta = \left(\frac{\rho_s}{\rho_w} - 1\right)$ *where*

ρ_S is the density of the sand fill in the GSC in kg/m³

ρ_w is the density of the water in the GSC in kg/m³

$\mathrm{Re} = \left(\frac{uD}{\nu}\right)$ is the Reynolds number

D is the length scale of GSC in the flow direction $D = l_c$ in meters

ν is the kinematic viscosity of water in m²/s

KS_i is the deformation factor for sliding

KO_i is the deformation factor for overturning

Typical values of parameters:

u and $\frac{\partial u}{\partial t}$ can be obtained from wave theories in m/s and m/s^2 respectively

$\mu = 0.57$ for non-woven geotextiles and sea bed of sand

$\mu = 0.48$ for non-woven geotextiles

g = 9.81 in m/s^2

$\Delta = 0.76$ If $\rho_S = 1800 kg/m^3$ and $\rho_w = 1025 kg/m^3$

$\nu = 10^{-6} m^2/s$

Remarks and Limitations

If the local Reynolds number is higher than 10^6 and/or the wave conditions do not correspond to "shallow water" conditions (d/L<0.10), the results should be interpreted with caution, since only Re<10^6 and shallow conditions were tested in this study.

The force coefficients are a function of the Reynolds number and thus of the length of the container. Calculation of the desired length is an iterative process. The length is calculated with approximate force coefficients and then the coefficients are adjusted to match the corresponding Reynolds number.

Refer to section 6.5 for more details on the validity and limitations

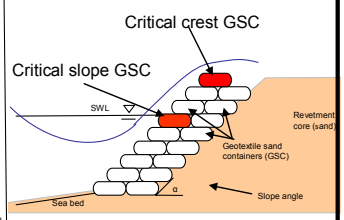

Considered Geometry

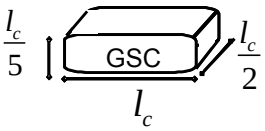

Formulae valid only for this geometry of the geotextile sand containers. However, formulae, coefficients and deformation factors can be adapted to any other geometry

Figure 6- 38: Definition of Parameters and Typical Values to be Used in the Stability Formulae

However, the force coefficients C_D, C_M and C_L are a function of the Reynolds number which also depends on the unknown size of the container. Thus, the procedure as illustrated in the flow chart in Figure 6- 39 is proposed to apply the developed formulae:

(i) Calculate the horizontal wave-induced flow velocity and acceleration at the elevation of the critical container using an appropriate wave theory. The stability formulae are very sensitive to the wave-induced horizontal velocities (u^2 in the formulae), thus, deriving the horizontal velocities and accelerations for other elevations would result in unrealistic dimensions of the containers.

(ii) From the corresponding range of force coefficients C_D, C_M and C_L , select a value of each coefficient.

(iii) Select the appropriate deformation factors K_{CD}, K_{CM}, K_{CL} and K_R (refer to Section 6.5.2 for more details).

(iv) Calculate the characteristic length l_c (or mass W_{GSC}), using the stability formulae.

(v) Using the characteristic length in the direction of the flow l_c, calculate the Reynolds number, calculate the force coefficients C_D, C_M, and C_L using the relations shown in Figure 6- 37.

(vi) Using the new calculated force coefficients C_D, C_M, and C_L (obtained in (iv)), re-calculate the required length l_c.

(vii) Repeat steps (iii) to (v) until the input force coefficients are similar to the obtained coefficients from step (v). Steps (i) to (vii) should be performed for the sliding and overturning formulae to determine which formulae gives the largest required length l_c.

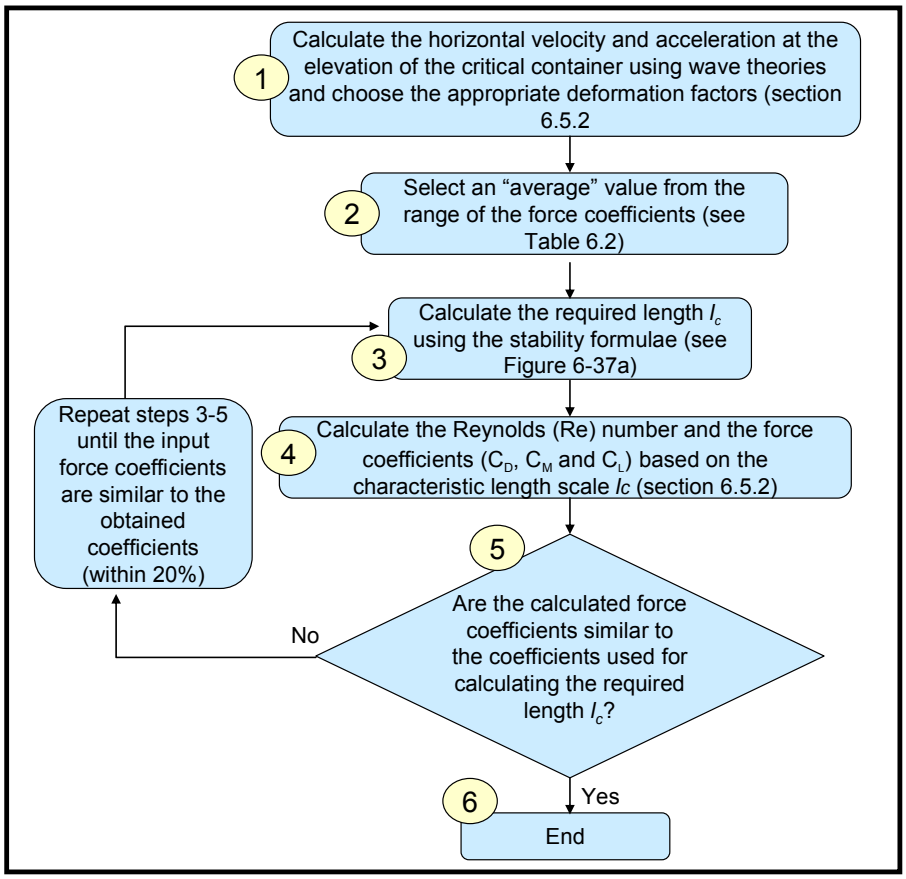

Figure 6- 39: Flow Chart for the Application of the Proposed Stability Formulae

6.5.2 Validity of the Proposed Approach and Formulae

(a) Validity of the Proposed Stability Formulae

The methodology proposed in Section 6.3.1 for the hydraulic stability can be applied to any GSC-structure, irrespective of the properties and geometry of the GSCs. However, the stability formulae given in Figure 6-37 are valid only for GSCs for which the length of the container is twice as large as its width and five times as large as its height (see Figure 6-15).

In addition, the formulae requires as main input parameters: (i) the wave-induced horizontal velocity at the location of the critical container *u*, (ii) the wave-induced horizontal acceleration at the same location $\frac{\partial u}{\partial t}$. The formulae are very sensitive to the horizontal flow velocity (u^2 in the formula), thus, velocity is much more critical than the acceleration. Moreover, it would be extremely conservative to use the maximum velocity *u* and maximum acceleration $\frac{\partial u}{\partial t}$ when determining the dimensions of GSCs. In theory, when the maximal drag force ($F_D \propto u^2$) acts on the container (function of u^2), the inertia force ($F_D \propto \frac{\partial u}{\partial t}$) tends to zero, due to the phase shift of $\pi/2$ between velocity and acceleration (Figure 6- 40). On the other hand, for "shallow water conditions" ($\frac{d}{L} \leq 0.10$), the drag force dominates over the inertia force. Therefore, for such conditions, the inertia force is much smaller than the drag force.

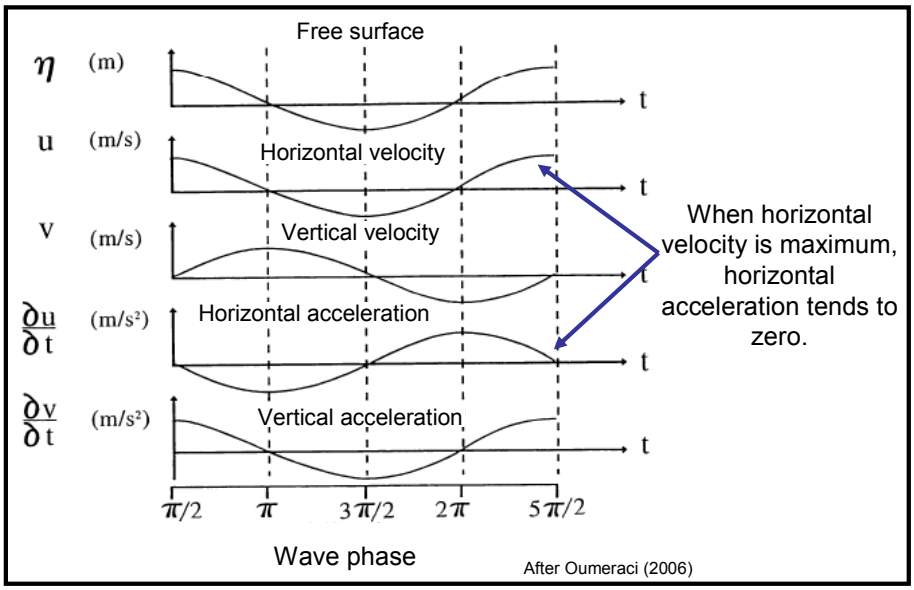

Figure 6- 40: Wave-Induced Particle Kinematics (Definition Sketch)

There are additional factors that could influence the selection of the value of the wave particle kinematics to be used in the formulae, including uncertainties associated with: (i) the input parameters such as design wave, (ii) the specific site conditions, (iii) the materials used for the GSC-structure and (iv) the expected quality control during the construction of the structure.

Therefore, it is recommended to use the formulae by accounting for all of the above-mentioned considerations before selecting the input values of the horizontal wave-induced particle velocity u and acceleration $\frac{\partial u}{\partial t}$.

(b) Validity of the Derived Force Coefficients C_D, C_M and C_L

Similar to the validity of the proposed stability formulae, the approach proposed to derive the force coefficients C_D, C_M and C_L can be applied to any type of coastal structure made of elements such as geotextile sand containers, rocks and concrete elements. However, the force coefficients C_D, C_M and C_L are derived specifically for geotextile sand containers under the following conditions: (i) shallow water ($\frac{d}{L} \le 0.10$), (ii) Reynolds numbers in the range of $Re=10^4 to 10^6$, (iii) roughness of the GSCs is for a mechanical non-woven geotextile, (iv) GSC-structures with slope angle of $\alpha = 45^o$ and (v) non-deformable GSCs.

The force coefficients C_D, C_M and C_L are strongly affected by the relation between depth and wave length (d / L) (Dean and Dalrymple, 1998). Therefore, the force coefficients derived in Section 6.2 are valid for shallow water conditions ($\frac{d}{L} \le 0.10$).

On the other hand, only Reynolds numbers in the range of $10^4 < Re < 10^6$ were tested.

In addition, the roughness of the container will affect the force coefficients C_D, C_M and C_L (i. e. Dean and Dalrymple, 1998, Sarpkaya, 1976, Oumeraci, 2006). Therefore, if a geotextile other than a mechanical non-woven is used, the accuracy of the force coefficients might be

affected. The influence is expected to be small, but until reliable results are available, it is recommended to use with caution the force coefficients on GSCs with a different roughness.

Moreover, the force coefficients C_D, C_M and C_L were derived for structures with a slope angle of $\alpha = 45^o$. Since the coefficients were derived as a function of the horizontal flow velocity or considering the structure as "hydraulically transparent", it is expected that the force coefficients will suffer variations, depending on the slope of the structure. The force coefficients C_D, C_M and C_L can be applied to other GSC-structures with slope angle different from 45^o. However, results should be interpreted considering the possible variations due to the slope angle.

The force coefficients were derived by introduction a wave-induced force on a non-deformable GSC, while in prototype, the container is subject to deformations. Therefore, force coefficients for deformable GSCs might be different from those for non-deformable containers. However, since the variations of the projected areas are considered, the flow-variations due to the deformations are expected to be small.

(c) Validity of the Derived Deformation Factors K_{CD}, K_{CM}, K_{CL} and K_R

As mentioned in previous paragraphs, the approach proposed to derive the deformation factors is valid for any type of geotextile sand container. However, the deformation factors are derived for possible deformations, which are most critical for the stability. The latter are based in the following assumptions: (i) sand fill ratio of the GSCs of 80%, (ii) GSCs made of mechanical non-woven geotextile and (iii) GSC-structure with a steepness of 45^o.

The smaller the sand fill ratio, the more unstable the container will behave (Section 4.4), and therefore, the deformation factors are expected to be inversely proportional to the sand fill ratio of the container. If other sand fill ratios are used, the deformation factors should be modified to account for the additional deformations. No information is available regarding the relation between the sand fill ratio and the deformation factors. However, it can be assumed that the variation of the deformation factors is proportional to the sand fill ratio and thus, the deformation factors can be adjusted (i. e. a GSC with 70% fill ratio will need 10% larger deformation factors to account for the deformations). On the other hand, the stiffness of the geotextile affects the deformation factors, since deformation is inversely proportional to the stiffness of the geotextile. It is impossible to quantify the influence of the stiffness of the geotextile on the deformation. However, it is expected that the influence is very small and thus, the deformation factors may also be used for other types of geotextiles.

Regarding the slope angle, it was found during the model tests (Section 4.5) that the deformations also depend on the slope angle and based on this assumption, deformation factors for other GSCs in structures with various angles have been derived. Since the assumption was based on model tests results, it is expected that the deformation factors for other slope angles are as accurate as for the factors derived for structures with a slope angle of $\alpha = 45^o$.

Finally, the deformation factors derived in Section 6.3.3 clearly illustrate the difference regarding the stability of slope and crest containers. Deformation factors show that the required length of a crest container needs to be approximately twice longer than a slope container (i.e. crest GSC must be approx. 8 times heavier than a slope container) to withstand the same wave-loading.

Therefore, the deformation factors might be conservative for the following conditions: (i) the sand fill ratio is strictly controlled and higher than 90% and (ii) the stiffness of the geotextile is higher than the one used during the model tests (deformation by penetration tests equal to 35%, DIN EN ISO 12956, after Naue, 2004).

It is recommended to use the formulae, force coefficients and deformation factors taking into account the above-mentioned considerations.

Chapter 7

Summary, Conclusions, Recommendations and Outlook

New shore protection structures such as seawalls, groins, breakwaters, revetments and artificial reefs are increasingly being developed. Softer and low cost protection alternatives, such as structures made of geotextile sand containers (GSC), are often used instead of more expensive and hard coastal structures made of concrete or rubble material.

Although the effect of the deformations of the sand containers on the hydraulic stability is significant, no stability formulae are available to account for those deformations and the associated processes leading to the observed failures. Therefore, the main contributions of this thesis are: (i) improvement of the understanding of the processes related to the hydraulic stability of coastal GSC-structures, including the effect of the deformations of the GSCs and (ii) development of stability formulae that account for the deformations.

To achieve an improved understanding of the processes that affect the stability of GSC-structures, experimental and numerical studies were performed focusing on the following issues: (i) permeability of GSC-structures and its influence on the stability, (ii) wave-induced loads on the sand containers, (iii) wave-induced flow on GSC-structures, (iv) internal movement of sand in the containers and its effect on the stability, (v) variation of contact areas among neighbouring GSCs during wave action, (vi) types of displacement of GSCs within a coastal structure (vii) influence of geotextile-friction between neighbouring containers, (viii) influence of boundary conditions on the stability and finally (ix) the effect of the deformations on the stability of GSC-structures.

Based on the results of several types of experimental and numerical studies, analytical stability formulae including the associated factors, that account for the deformations of GSCs for each type of observed displacement, were developed. In addition, the required drag, inertia and lift coefficients C_D, C_M and C_L were determined experimentally. Stability formulae that account for the deformations for each type of coastal structures made of geotextile sand containers such as breakwaters, revetments, dune reinforcement and scour protection systems are proposed.

Therefore, the main results and conclusions drawn from this study are first summarized. Secondly, recommendations are given with respect to the practical application of the proposed hydraulic stability formulae, including their limitations. Finally, the priority tasks for future research are suggested.

7.1 Summary of Main Results and Conclusions

(a) Hydraulic Permeability of GSC-Structures

Comprehensive hydraulic model tests are performed for the first time to determine the permeability of several types of GSC-structures. Moreover, the stability of GSC-structures having the same geometry, but different permeability and different arrangements of the sand containers was investigated in the wave-flume of Leichtweiss Institute (LWI). In addition, a conceptual model for the permeability of GSC-structures is proposed. The main results from these studies can be summarized as follows:

(i) The hydraulic permeability of a GSC-structure depends mainly on the size of the gaps between neighbouring containers. The flow through a GSC-structure is governed by the flow through the gaps and thus, the flow through the sand container can be neglected.
(ii) If no further data are available, a permeability coefficient for GSC-structures of $k = 10^{-2}$ m/s might be adopted.
(iii) The mode of placement of the sand containers in a GSC-structure considerably affects the permeability of the structure, random placing has the highest permeability, but less hydraulic stability than longitudinally placed containers of a surface piercing GSC-structure.
(iv) A simple conceptual model is proposed (Section 3.5), which can be used to approximately estimate the permeability of GSC-structures.

(b) Experimental Studies on the Processes Affecting the Stability of GSC-Structures

The processes that affect the deformations and stability of GSC-structures were investigated by means of several types of hydraulic model tests. The model tests were performed in the wave flume of Leichtweiss Institute. Based on the experimental results, a better understanding of the processes which affect the hydraulic stability of the structure has been achieved, including the effect of the deformations of the sand containers and their mutual interaction, showing that:

(i) The most critical location on the seaward slope with respect to the hydraulic stability is for the containers placed just below the still water level.
(ii) The deformations of the containers strongly affect the stability of GSC-structures. Deformations reduce the resisting contact areas between the containers and thus, the resisting forces on the containers
(iii) The internal movement of sand inside the container induces deformation of the container and therefore substantially affects the stability of the GSC-structure. Internal movement of sand depends on the sand fill ratio of the container which should thus, be strictly controlled to ensure the stability of any GSC-structure. The sand fill ratio of GSCs should be optimal (equal or higher than 80%, depending on the elongation properties of the geotextile used for the containers).
(iv) Breaking waves are not as critical as originally expected for the hydraulic stability of GSC-structures. This is probably due to the flexibility and damping properties of the GSCs which contribute to attenuate the propagation of pressure inside the GSC-structure.

(c) Numerical Studies on the Processes Affecting the Stability of GSC-Structures

A computational fluid dynamic model (RANS-VOF) and two computational structural dynamic models (FEM-DEM) are further improved, partially coupled and validated to extend the range of the hydraulic model tests performed towards an improved understanding of the processes that affect the stability of structures made of geotextile sand containers (GSC). The main results might be summarized as follows:

(i) The modified fluid dynamic model (RANS-VOF) used in this study can simulate wave action at, on and in a GSC-structure with sufficient accuracy, particularly in terms of surface elevation, particle velocities and wave pressure.
(ii) The “partially coupled” model system used in this study for the simulation of the stability of GSC-structures has shown surprisingly much better agreement than expected (stability threshold with variations of 10% for a range of the surf similarity parameter of $\xi_o = 4 \sim 13$).
(iii) The extension of the fluid dynamic model to simulate the flow through the containers has shown that the wave-induced velocities through the sand fill of the containers are almost 20 times smaller than the velocities in front of the containers, therefore

confirming that the flow through the structure is essentially governed by the gaps between the sand containers.

(iv) The interaction of wave-induced forces on neighbouring containers was also investigated, showing that the resultant forces on each container behave almost independently of the neighbouring containers. The "phase shift" between forces depends on the wave-period and slope of the GSC-structure.

(v) The friction between the sand containers considerably affects the stability of GSC-structures and thus, for prototype GSC-structures, it is necessary to account for this parameter more than in the past.

(d) New Hydraulic Stability Formulae for GSC-Structures

Based on the new knowledge of the processes associated with the hydraulic stability of GSCs used for coastal structures, which was gained from the experimental and numerical investigations, explicit stability formulae were derived for the two common modes of failure of GSCs: sliding and overturning. The derived stability formulae require the knowledge of the force coefficients C_D, C_M and C_L. The force coefficients were derived from specially designed laboratory tests involving several types of configurations and boundary conditions. Results have shown that drag coefficient C_D and lift coefficient C_L mainly depend on the Reynolds number. In addition, wave-induced forces on GSCs are more affected by the wave height than by the wave period. The number and position of neighbouring containers strongly affect the wave loading of a sand container.

Deformation factors that account for the deformation of GSCs were analytically derived and incorporated into the hydraulic stability formulae. Deformation factors also illustrate the influence of the deformation on the mobilizing and resisting forces. Due to the deformations, the drag force is increased by up to 40%, while the resisting force is reduced by up to 30%. Deformations affect considerably the stability of GSCs (up to approximately 50% in terms of required length of the container).

7.2 Applicability and Limitations of the Proposed Stability Formulae

The stability formulae, force coefficients and deformation factors are summarized in Figure 7-1 and should be used by considering the site specific conditions and properties of the geotextiles (refer to Section 6.5 for more details).

The methodology and approach used to derive the hydraulic stability formulae can be applied to any GSC-structure independently of the properties or geometry of the GSCs. However, the derived formulae (Figure 7-1) are valid only for GSCs for which the length of the container is twice as large as its width and five times as large as its height (Figure 6-16). Modifications of the formulae to adapt them to other geometries are straight forward and thus, stability formulae for any geometry of GSCs can easily be derived following the approach proposed in this study (refer to Section 6.5 for more details on the application of the formulae).

The force coefficients C_D, C_M and C_L, were derived from specially designed laboratory tests involving several types of configurations and boundary conditions (Figure 7-1).

(a) Stability Formulae for GSCs Including the Effect of Deformation

Sliding

Required container length

$$l_{c(sl)} \geq u^2 \frac{\left[0.5KS_{CD}C_D + 2.5KS_{CL}C_L\mu\right]}{\left[\mu KS_R\Delta g - KS_{CM}C_M\frac{\partial u}{\partial t}\right]}$$

Required container mass

$$W_{GSC} \geq \rho_s \left(u^2 \frac{\left[0.5KS_{CD}C_D + 2.5KS_{CL}C_L\mu\right]}{\left[\mu\Delta KS_R g - KS_{CM}C_M\frac{\partial u}{\partial t}\right]} \right)^3 /10$$

Overturning

Required container length

$$l_{c(ov)} \geq u^2 \frac{\left[0.05KO_{CD}C_D + 1.25KO_{CL}C_L\right]}{\left[0.5\Delta KO_R g - 0.1KO_{CM}C_M\frac{\partial u}{\partial t}\right]}$$

Required container mass

$$W_{GSC} \geq \rho_s \left(u^2 \frac{\left[0.05KO_{CD}C_D + 1.25KO_{CL}C_L\right]}{\left[0.5\Delta KO_R g - 0.1KO_{CM}C_M\frac{\partial u}{\partial t}\right]} \right)^3 /10$$

(b) Deformation Factors and Force Coefficients for the Stability Formulae

GSC-Structure	Sliding	Overturning	Force Coefficients
Single GSC on Sea Bed 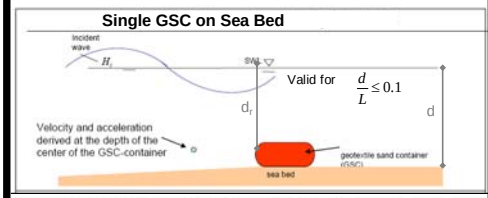	$KS_{CD} = 1.40$ $KS_{CM} = 1.00$ $KS_{CL} = 0.94$ $KS_R = 0.70$	$KO_{CD} = 1.54$ $KO_{CM} = 1.1$ $KO_{CL} = 0.80$ $KO_R = 0.92$	$C_D = -2x10^{-5}\,\mathrm{Re} + 6.81$ with $1.3 \leq C_D \leq 6.5$ $C_M = 0.60$ $C_L = 1x10^{-5}\,\mathrm{Re} - 0.612$ with $0.2 \leq C_L \leq 1.4$
Group of GSCs on Sea Bed (i. e. Scour Protection) 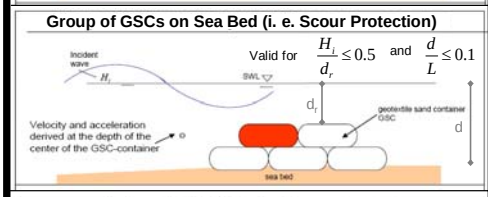	$KS_{CD} = 1.40$ $KS_{CM} = 1.00$ $KS_{CL} = 0.94$ $KS_R = 0.70$	$KO_{CD} = 1.54$ $KO_{CM} = 1.1$ $KO_{CL} = 0.80$ $KO_R = 0.92$	$C_D = -6x10^{-5}\,\mathrm{Re} + 14.70$ with $4 \leq C_D \leq 11$ $C_M = 0.50$ $C_L = 1x10^{-5}\,\mathrm{Re} - 0.669$ with $0.4 \leq C_L \leq 1.3$
Submerged GSC-Breakwaters (Artificial Reef) 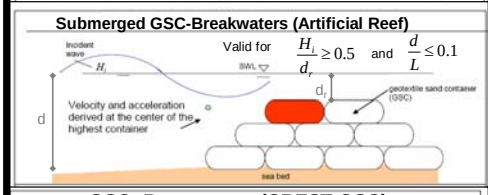	$KS_{CD} = 1.40$ $KS_{CM} = 1.00$ $KS_{CL} = 0.94$ $KS_R = 0.70$	$KO_{CD} = 1.54$ $KO_{CM} = 1.1$ $KO_{CL} = 0.80$ $KO_R = 0.92$	$C_D = -9x10^{-5}\,\mathrm{Re} + 23.04$ with $4 \leq C_D \leq 15$ $C_M = 0.30$ $C_L = 1x10^{-5}\,\mathrm{Re} - 0.587$ with $0.3 \leq C_L \leq 1.2$
GSC- Revetments (CREST GSC) 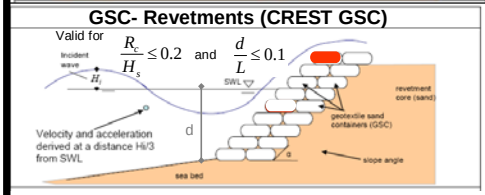	$KS_{CD} = 1.40$ $KS_{CM} = 1.00$ $KS_{CL} = 0.94$ $KS_R = 0.70$	$KO_{CD} = 1.54$ $KO_{CM} = 1.1$ $KO_{CL} = 0.80$ $KO_R = 0.92$	$C_D = -2x10^{-5}\,\mathrm{Re} + 6.81$ with $1.3 \leq C_D \leq 6.5$ $C_M = 0.60$ $C_L = 1x10^{-5}\,\mathrm{Re} - 0.612$ with $0.2 \leq C_L \leq 1.4$
GSC- Revetments (SLOPE GSC) 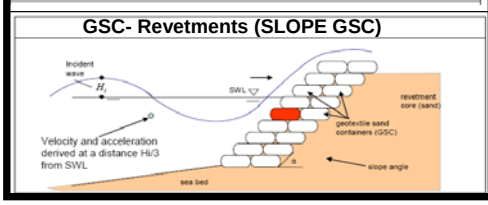	$KS_{CD} = 1.40$ $KS_{CM} = 1.00$ $KS_{CL} = 0.94$ $KS_R = 1.60$	Not applicable (GSC pulled out seaward)	$C_D = -3x10^{-5}\,\mathrm{Re} + 8.9$ with $2.5 \leq C_D \leq 9$ $C_M = 0.30$ $C_L = 1x10^{-5}\,\mathrm{Re} - 0.587$ with $0.3 \leq C_L \leq 1.2$

Note: Determined for shallow water conditions $d/L<0.10$ and $Re=10^4$-10^6

Figure 7- 1: Stability Formulae, Deformation Factors and Force Coefficients (slope angle 45° and sand fill ratio of GSC of 80%, refer to Tables 6.4 and 6.5 for other slope angles, refer to Section 6.5 for details on the application of the formulae)

Similar to the validity of the stability formulae, the approach and methodology used to derive the force coefficients C_D, C_M and C_L can be applied to any type of coastal structure made of elements such as geotextile sand containers, rocks and concrete-elements. However, the force coefficients C_D, C_M and C_L are derived for geotextile sand containers under the following conditions: (i) shallow water waves ($\frac{d}{L} \leq 0.10$), (ii) Reynolds numbers in the range of

$Re=10^4 \sim 10^6$, (iii) roughness of the GSCs is for a non-woven geotextile, (iv) GSC-structures with slope steepness of 45^o and (v) non-deformable GSCs.

Moreover, only differences in the relation between depth and wave length (d/L) are expected to affect considerably the values of the force coefficients. Thus, the force coefficients C_D, C_M and C_L derived in this study are only valid for shallow water wave conditions ($\frac{d}{L} \leq 0.10$). Higher Reynolds numbers $Re>10^6$, roughness of a woven-geotextile and different slope angles are supposed to only slightly affect the force coefficients C_D, C_M and C_L. Therefore, the force coefficients presented in this study can be used for these situations (refer to Section 6.5.2 for detailed discussion on the possible influence of these factors on the force coefficients).

Deformation factors that account for the deformation of GSCs were analytically derived (Figure 7-1). As with the force coefficients, the approach and methodology used to derive the deformation factors is valid for any type of geotextile sand container. However, the deformation factors were derived for the most critical deformation with respect to the stability that the container can suffer and were based in the following factors: (i) sand fill ratio of the GSCs of 80%, (ii) GSCs made of mechanical non-woven geotextile and (iii) sloping GSC-structure with a steepness of 45^o.

The deformations of a sand container strongly depend on the fill ratio of the container. The smaller the sand fill ratio, the less stable that the GSC will behave. If other sand fill ratios are used, the deformation factors should be modified to account for the additional deformations. However, it can be assumed that the variation of the deformation factors is proportional to the sand fill ratio and thus, the deformation factors can be adjusted (i. e. a GSC with 70% fill ratio will need 10% higher deformation factors to account for the deformations).

On the other hand, the stiffness of the geotextile affects the deformation factors. However, this influence is expected to be so small that the deformation factors can be applied to any type of GSCs.

The deformations also depend on the slope angle of the GSC-structure (Section 4.5). Based on this relation, deformation factors for other GSCs in structures with various slope angles have been derived. Since the assumption was made based on laboratory observations, it is expected that the deformation factors for other slope angles are as accurate as for the factors derived for sloping structures with a steepness of 45^o (refer to Section 6.5.2 for more details).

Finally, the proposed stability formulae and numerical analyses performed in this study show that the friction between GSCs plays an important role for the stability of GSC-structures. Therefore among the durability, tensile strength and abrasion resistance, the friction between geotextile should also be considered when designing or building GSC-structures.

7.3 Future Research Issues

This study has significantly improved the knowledge available on the stability of GSC-structures. However, considerable research still needs to be performed.

The permeability of GSC-structures was investigated in this thesis and a new conceptual model to derive the permeability of sand container has led to reasonable results. However, the conceptual model needs to be further developed to improve its range of applicability.

On the other hand, the influence of the following parameters on the hydraulic stability of GSC-structures needs to be systematically investigated: (i) sand fill ratio of the sand container, (ii) steepness of the GSC-structure, (iii) type of geotextile, and (iv) type of sand fill material in GSCs.

Moreover, the numerical models used in this study need to be fully coupled to extend the knowledge of the following processes associated with the stability of GSC-structures:

- Collapse mechanisms of GSC-structures.
- Further clarification on the types of displacements of GSCs.
- Performance of detailed and systematic parameter studies on: (a) friction between geotextiles, (b) slope angle of the structure, (c) wave-induced stresses of GSCs and (d) sand fill ratio of GSCs. The main and most difficult remaining task regarding the numerical model system is to extend the models to simulate the internal movement of sand inside the containers. This extension will allow a more realistic and accurate simulation of the deformation of the GSCs.

The following topics, although outside the scope of this thesis must also be addressed:

- Rate of growth of marine life on GSCs depending on climate conditions and its influence on the stability of the GSC-structure (influence on friction and tensile strength of the GSC due to marine grow).
- Effect of the collapse of an individual sand container on the overall stability of GSC-structures.
- Stresses on the geotextile of GSC and possible damage during the fabrication of the sand containers and placement in GSC-structures.
- Influence of the type of fill material, including non-permeable materials such as clay, on the stability of GSCs.

References

Abaqus 2000, *Introduction to the Finite Element Method*, Hibbitt, Karlsoon & Sorensen, Abaqus Manual, U.S.

Aberg B. 1992, *Hydraulic Conductivity of Noncohesive Soils*, Journal of Geotechnical Engineering, 118(9) pages 1335-1347.

Bleck, M. and Oumeraci, H. 2004, *Hydraulic Performance of Artificial Reefs: Global and Local Description*, Proceedings of the 28th ICCE 2002, pages 1778-1790, Cardiff, Wales.

Bourzaev A. 2003, *Hydraulische Prozesse an und in einem Deckwerk aus Geotextilen Sandcontainern*, Diplom-Arbeit (Master Student Project Report), Leicthweiss Institute for Hydraulic Engineering and Water Resources, TU Braunschweig, Germany (in German).

Boutt D, Cook B, 2002, *Application of a Directly Coupled numerical Model of Fluid-Solid Mechanics*, Massachusetts Institute of Technology, Lecture Notes.

Bouyze J. G. and Schram A. R. 1990, *Stabiliteit van Grondkribben en Onderwatergolbrekers Opgebouwd uit Zandworsten*, TU-Delf, Studentarbeit (Master Student Project Report) (in Dutch).

Burg, S. 2006, *Untersuchung zur hydraulischen Stabilität geotextiler Sandcontainer in einer Böschung unter Verwendung von MatLab (Investigation on the Hydraulic Stability of a Revetment made with Geotextile Sand Containers by Using Matlab)*, Studentarbeit (Master Student Project Report), Leichtweiss Institute for Hydraulic Engineering and Water Resources (in German).

CEM, *Coastal Engineering Manual* 2004, U.S. Army Corps of Engineering, U.S.

Chao-Lung T. Ming-Chung L. and Chih-Yuan, 2004, *Porosity Effects on Non-breaking Surface Waves over Permeable Submerged Breakwaters*. Coastal Engineering Journal, Elsevier, Vol. 50 Issue 4, pages 213-224.

Chaplin 1994, *Nonlinear Forces on a Horizontal Cylinder beneath Waves*, Journal of Fluid Mechanics 147, pages 449-464.

Cundall P.A. 1979, *A Discrete Numerical Model for Granular Assemblies*, Geotechnique 29, pages 47-65.

DaVis 1999, *PIV-software and Manual*, La Vision Company, Göttingen, Germany.

Dean R. G. and P. M. Aagard. 1970, *Wave Forces, Data Analysis and Engineering Calculation Method*, Journal of Petrol. Technology.

Dean, R. G., and Dalrymple R. A. 1998, *Water Wave Mechanics for Engineers and Scientists*, World Scientific, Advanced Series on Ocean Engineering, Singapore.

Dessen M. 2004, *The Influence of Flow Acceleration on Stone Stability*, Master Thesis, University of Delft, the Netherlands.

Eberhardt E. 2003, *Discontinue Analysis and the Distinct Element Method*, Lecture Notes, Earth and Ocean Sciences at UBC.

Engelund F. 1953, *On the Laminar and Turbulent flows of Groundwater Through Homogeneous Sand*. Trans Danish Academy of Technical Sciences, Vol. 3.

Fuerboeter, A, 1991, *Wave Loads on Sea Dykes*, In: M.B. Abbott and W.A. Price Coastal, Estuarial and Port Engineer's.

Gemme D., 2005, *Application of PIV to Determine Wave Induced Velocities on a GSC-Revetment*, Studentarbeit (Master Student Project Report), Leichtweiss Institute for Hydraulic Engineering and Water Resources.

Grett H. 1984, *Das reibungsverhalten von Geotextilien in bindigem und nichtbindigem Boden*, Mitteilungen des Franzius-Instituts für Wasserbau und Küsteningenieurwese der Universität Hannover (in German).

Grüne J., Sparboom U., Schmidt-Koppenhagen R., Wang Z., Oumeraci H., 2007, *Stability Tests of Geotextile Sand Containers for Monopile Scour Protection*, Proceedings of the 30th International Conference of Coastal Engineering, Sand Diego, U.S. pages 145-153.

Harvie D. and Fletcher D, 2000, *Volume of Fluid Advection Algorithm*, ANZIAM Journal, Australian Mathematical Soc. pages 690-711, Australia.

Hendar P. A. 1960, *Stability of Rock-fill Breakwaters*, PhD Thesis, Chalmers Univ. of Technology, Dept. of Hydr. Göteborg, Sweden.

Heerten G., Jackson A., Restall S. and Saathoff F., 2000, *New Developments with Mega Sand Containers of Nonwoven Needle-Puncture Geotextile for the Construction of Coastal Structures*, Proceedings International Conference on Coastal Engineering 2000, pages 32-38, Australia.

Heerten G., Saathof F., Stelljes K., 2000, *Geotextile Bauweisen ermöglichen neue Stratefien im Küstenschutz*. Geotechnik, Heft 2, Glücklaur Verlag Essen, pages 80-86 (in German).

Hudson, R. 1956, *Laboratory Investigation of Rubble-Mound Breakwaters*. Journal of the Waterways and Harbour Division, pages 93-118.

Hudson R. 1961, *Laboratory Investigation of Rubble Mound Breakwater*, Trans. ASCE 126, pages 492-541.

Hughes S. A. 1993, *Physical Models and Laboratory Techniques in Coastal Engineering*, World Scientific.

Ikeda Y., Otsuka k., Tanaka N. 1998, *Wave Forces Acting on Horizontally Submerged Cylinders in Regular Waves at Low KC Number*. Report No. 00410, Department of Naval Architecture, University of Osaka, Japan.

IPCC, 1996 *Climate Change 1995, Impacts, Adaptations and Mitigation of Climate Changes*, Cambridge University Press, pages 365-398.

Isbash S. V. and Khaldre K.Y. 1976, *Hydraulics of River Channel Closures*, Butterworths, London.

Itasca Consultants 2004, *UDEC Manual*, Volumes 1 to 5, Minneapolis U.S..

Jacobs, B.K. and Kobayashi, N. 1983, *Sandbag Stability and Wave Runup on Beach Slopes*, University of Delaware , Research Report No. CE-83-36.

Jacobs, B.K. and Kobayashi, N., 1985, *Experimental Study on Sandbag Stability and Runup*, Proceedings Coastal Zone pages 127-133.

Keulegan G.H. and Carpenter L.H. 1958, *Forces on Cylinders and Plates in an Oscillating Fluid*, Journal of Res. Nat. Bur. Stand., Vol. 60, No. 5.

Kim H. T. Yoo D and Park S. S. 2004, *A Fundamental Approach for an Investigation of Behaviour Characteristics of the Vegetation Structures Using Sandbags*, Proceedings of GeoAsia 2004, pages 225-232.

Koether G. 2002, *Hydraulische Wirksamkeit Getauchter Einzelfilter und Filtersysteme*, PhD Thesis, Braunschweig University.

Kübler; S. 2002, *Hydraulische Stabilität von geotextilen Sandcontainern unter Seegangseinwirkung*. Diplomarbeit (Master Research Project Report) am Leichtweiss Institute for Hydraulic Engineering and Water Resources.

Lambe T. W. and Whitman R.V., 1979, *Soil Mechanics*, John Wiley & Sohns, MIT, U.S..

Lin P. and P.L.-F. Liu, 1998, *A Numerical Study of Breaking Waves in the Surf Zone*, Journal of Fluid Mechanics 359, pages 239-264.

Liu P. 2004, *A Finite Volume of Fluid Method for Solving the Navier-Stokes-Equation with Application to Water-Wave Problems*, Lecture Notes of the 3 Days Compact Course, Leichtweiss Institute for Hydraulic Engineering and Water Resources, Germany.

Liu, P.L.-F. and Lin P. 2002, *Cobras Manual, Cornell Breaking Wave and Structures*, Cobras Manual a VOF- based RANS-model. Cornell University U.S.

Liu, P.L.-F. and Lin P., 1997. *A Numerical Model for Breaking Wave: the Volume of Fluid Method*. Research Report. No. CACR-97-02, Centre for Applied Coastal Research, Ocean Engineering Laboratory, University of Delaware, U.S.

Liu, P.L.-F., Lin P., Chang K.A. and Sakakiyama T., 1999. *Numerical Modelling of Wave Interaction with Porous Structures*. J. Waterway, Port, Coastal and Ocean Engineering, ASCE 125 (6), pages 322-330.

Maricopa 2004, *Flood Prot*ection, Brochure, County Department of Emergency Management, U.S.

Marth R., Mueller G. and Wolters G., 2005. *Damages of Blockwork Coastal Structures due to Internal Wave Impact Induced Pressures*, Proceedings of the International Coastal Symposium, Ireland.

Matsuoka H., Sihong L. and Yamaguchi K. 2001, *Mechanical Properties of Soilbags and their Application to Earth Reinforcement*, Proceedings of the International Symposium on Earth Reinforcement, Fukuoka, Japan, pages 587-592.

Matsuoka H., 2002, *A Surprising Strength of "Soil Bag"*, Concrete Journal Vol.40, No.3, Mar. 2002 Japan Concrete Institute (JCI No.438)

McConnell Kirsty, 1998, *Revetment Systems Against Wave Attack, A Design Manual*, ASCE Press, U.S..

Michioku K., Maeno S., Furuzawa T. and Haneda M., 2005, *Discharge through a Permeable Rubble Mound Weir*, Journal of Hydraulic Engineering ASCE, January 2005, pages 1-10.

Mirafi 2004, *Physical Properties of Geosynthetics*, Technical Brochure.

Morison, J. R., M. P. O'Brien, J. W. Johnson, and S. A. Schaaf, 1950 , *The Force Exerted by Surface Waves on Piles Petrol*. Trans., AIME, Vol. 189.

Muttray M. and Oumeraci H., 2002, *Wave Transformation at Sloping Perforated Walls*, Proceedings of the International Conference on Coastal Engineering 2002, pages 2031-2043.

Najafian G., and Burrows R. 1993, *Critical Assesment of the Least Square Error Method Used in Derivation of Morison's Force Coefficients*, Journal of Offshore Mechanics and Artic Engineering, Vol. 116, 1.

Najafian G., Burrows R. and Tickell R.G. 2003, *Geometric Interpretation of the Least Square Method Used in Derivation of Morison Force Coefficients*, Journal JRC, Vol. 2003-1 pages 1-7.

Naue and Soil Filters Australia 2003, *Designing with Geotextile Sand Containers*, Technical Brochure.

Naue Fasetechnik 2004, *Direct Shear Stress Results*, Internal Communication

Naue Fasetechnik 2004, *Secutex GRX, Technical Brochure* (in German).

Oumeraci 1999, *Hydromechanik*, Vorlesungsumdruck für das Grundfach „Hydromechanik", TU-Braunschweig (in German).

Oumeraci H. 1999 and 2006., *Vorlesungsumruck für das Vertiefungsfach "Hydromechanik und Küsteningenieurwesen"* Leichtweiß Institute for Hydraulic Engineering (in German).

Oumeraci H. and Bleck M.. 2001, *Hydraulische Wirksamkeit von künstlichen Riffen unter besonderer Berücksichtigung des Energietransfers im Wellenspektrum* -Zwischenbericht zum gleichnamigen DFG-Projekt. LWI Bericht Nr. 863 (in German).

Oumeraci H., M. Bleck, Hinz M. and Kuebler S., *Großmaßstabliche Untersuchungen zur Hydraulischen Stabilität geotextiler Sandcontainer unter Wellenbelastun (Large-scale Model Tests for the Hydraulic Stability of Geotextile Sand Containers under Wave Attack*. Research Report no. 878. Leichtweiss Intitute for Hydraulic Engineering and Water Resources, 62 pages (in German).

Oumeraci H and Hinz, M. 2004, *Geotextile Sand-filled Container as Innovative Measures for Shore Protection*, Technical paper, Proc. EuroGeo 2004, Vol 1, pages 175-180.

Oumeraci, H. 2003, *Review and Analysis of Vertical Breakwater Failures - Lessons learned*. Coastal Engineering, Special Issue on "Vertical Breakwaters", Amsterdam, The Netherlands: Elsevier Science Publishers B.V., vol. 22, nos. 1/2, pages 3- 29.

Oumeraci, H., Bleck M., Hinz M. and Möller, J. 2002a *Theoretische Untersuchungen geotextiler Sancontainer im Küstenschutz*. Bericht des Leichtweiß-Instituts Nr. 866, Braunschweig (in German).

Oumeraci, H. 2004, *Sustainable Coastal Flood Defenses: Scientific and Modeling Challenges Towards an Integrated Risk-based Design Concept*, Keynote Lecture, Proceedings of the International Conference on Flood Risk Assesment, University of Bath, UK September 2004, pages 9-24.

Oumeraci H, Kortenhaus A. and Werth K. 2007 *Hydraulic Performance and Armour Stability of Rubble Mound Breakwaters with Core Made of Geotextile Sand Containers: Comparison with Conventional Breakwaters*, Abstract submitted to the Conference of Coastal Structures, Venice, Italy

Pilarczyk K. 1998, *Dikes and Revetments, Design, Maintenance and Safety Assessment*, A.A. Balkema, Rotterdam, the Netherlands.

Pilarczyk, K. W. 2000, *Geosynthetics and Geosystems in Hydraulic and Coastal Engineering*. A.A. Balkema, Rotterdam, the Netherlands.

Porraz M.J.L., Masa A. J. A. and Medina, R.R. 1979, *Mortar-filled Containers, Lab and Ocean Experiences*, Proceedings Coastal Structures, pages 270-289.

Raffel, M., Willert C. and Kompenhans J. 1998, *Particle Image Velocimetry –A Practical Guide-*, Springer Verlag.

Ray, R. 1977, *A Laboratory Study of the Stability of Sand-filled Nylon Bag Breakwater Structures*.

Recio J., Yasuhara K. and Murakami S. 2001, *Model Tests of Reinforced Sand Revetment under Assailing Ocean Waves*, Geosynthetics Engineering Journal (Japan) Vol.16, pages 235-243.

Recio J., 2004. *Considerations for Simulating a GSC-revetment using a Numerical Model*, Short Progress Report, Leichtweiss Institute for Hydraulic Engineering and Water Resources (internal report).

Recio J. and Oumeraci H. 2005a, *Analyse der Stabilitätsgefährdenden Prozesse von Deckwerken aus Geotextilen Sandcontainer*, 5. FZK Kolloquium „Seegang, Küstenschutz und Offshorebauwerke“ Hannover, pages 83-87 (in German).

Recio J. and Oumeraci H. 2005b, *Processes Affecting the Hydraulic Stability of Geotextile Sand Containers -Experimental Studies-*, Leichtweiss Institute for Hydraulic Engineering and Water Resources, Research Report No 944, 78 pages.

Recio J. and Oumeraci H. 2005c, *Effect of the Deformation on the Hydraulic Stability of Revetments made of Geotextile Sand Containers*, Proceedings of the International Symposium, “Tsunami Reconstruction with Geosynthetics”, Bangkok, Thailand pages 53-68.

Recio J. and Oumeraci H. 2006a, *Hydraulic Processes Associated with the Instability of GSC-Structures -A Numerical Study Using the “Cobras-Model”*, Leichtweiss Institute for Hydraulic Engineering and Water Resources, Research Report No 941, 61 pages.

Recio J. and Oumeraci H. 2006b, *Processes Affecting the Stability of Revetments made with Geotextile Sand Containers*. Proceedings of the International Conference of Coastal Engineering, ICCE 2006, San Diego, U.S. pages 356-374.

Recio J. and Oumeraci H. 2006c, *Preliminary Experiments and Numerical Simulations of Solitary Wave Acting on a Submerged-Filter-Reef*, Leichtweiss Institute for Hydraulic Engineering and Water Resources, Research Report No 945, 16 pages.

Recio J. and Oumeraci H. 2007a, *Permeability of GSC-Structures -Laboratory Tests and Results-*, Leichtweiß Institute for Hydraulic Engineering and Water Resources, Research Report No 943, 45 pages.

Recio J. and Oumeraci H. 2007b, *“Numerical Simulations on the Stability of Coastal Structures made of Geotextile Sand Containers (GSC)*, Leichtweiss Institute for Hydraulic Engineering and Water Resources, Research Report No 942, 42 pages.

Recio J. and Oumeraci H. 2007c, Geotextile Sand Containers for Coastal Structures, *Geotextile Sand Containers for Coastal Structures -Hydraulic Stability Formula and Tests for Drag, Inertia and Lift Coefficients-*, Leichtweiss Institute for Hydraulic Engineering and Water Resources, Research Report No 936, 97 pages.

Recio J. and Oumeraci H. 2007d, *Enflussfaktoren zur Stabilität von Küstenbauwerke aus geotextilen Sandcontainern*, 6. FZK Kolloquium „Küstenschutz und Seebau“ Hannover (in German).

Recio J. and Oumeraci H. 2007e, *Effect of Deformations on the Hydraulic Stability of Coastal Structures made of Geotextile Sand Containers*. Geotextile and Geomembrane Journal, Elsevier, Vol. 25, pp. 278-292.

Restall S., Hornsey W., Oumeraci H., Hinz M., Saathoff F., and Werth K., 2004, *Australian and German Experiences with Geotextile Containers for Coastal Protection*, proceedings Eurogeo 2004

Restall S. and Saathoff J., 2002 *Australian and German Experiences with Geotextile Containers for Coastal Protections*, EuroGeo 2002.

Ripple, 1980, *Ripple, A Computer Program for Incompressible Flows with Free Surfaces*. Los Alamos National Laboratory Report LA-12007-MS.

Rufin T., Mizutani N. and Iwata K. 1996, *Estimation Method of Stable Eeight of Spherical Armour Unit of a Submerged Wide-Crown Breakwater*, Journal of Coastal Engineering, Elsevier, Vol. 28, pages 183-228.

Saadawi H. 2001, *Improving the Finite Element Method using Cell-DEVS*, Dept. of Systems and Computer Engineering, Carleton University, U.S.

Sarpkaya, T. 1976a. *Vortex Shedding and Resistance in Harmonic Flow About Smooth and Rough Circular Cylinders at High Reynolds Numbers*, Report No. NPS-59SL76021, Naval Postgraduate School, Monterey, CA.

Sarpkaya, T. 1976b. *In-Line and Transverse Forces on Cylinders in Oscillatory Flow at High Reynolds Number*, Proceedings of the Eighth Offshore Technology Conference, Houston, TX, Paper No. OTC 2533, Vol 2, pp 95-108.

Sawaragi T., Deguchi I., 1992, *Waves on Permeable Layers*, Proceedings of the International Conference on Coastal Engineering, pages 1531-1544.

Schäfer C. 1999, *Analysis and Implementation of the Discrete Element Method using a Dedicated Highly Parallel Architecture in reconfigurable Computing*. Research Report, Queens University, Canada.

Scheidegger A.E. 1974, *The Physics of Flow Through Porous Media*, University of Toronto Press, Toronto.

Sellers R. 2000, *Fluid Mechanics*, On-line Lecture Notes, Queen University, Canada.

Sitharam T. 2002, *Numerical Simulation using Discrete Element Modelling*, Research Articles, Current Science, Vol 78, No 7.

Smid 2001, *Untersuchungen zur Ermittlung der mittleren Wellenüberlaufrate an einer senkrechten Wand und einer 1:1.5 geneigten Böschung für Versuche mit und ohne Freibord*, Studienarbeit Leichtweiss Institute for Hydraulic Engineering and Water Resources, (Master Research Project Report) (in German).

Sulisz W., 1995, *Effect of Permeability on Stability of rubble Bases*. Journal of Waterway, Port, Coastal and Ocean Engineering, May/June 1995 pages 162-170.

Tekmarine Inc. 1982, *Large-scale Model Studies of Artic Island Slope Protection*. Sierra California.

Torum A. 1994, *Wave Induced Forces on Armour Unit on Berm Breakwaters*, Journal of Waterway, Port, Coastal and ocean Engineering. Vol. 120, No. 3.

Tromp 2004, *Influences of Fluid Accelerations on the Threshold of Motion*, Master Thesis, University of Delft, the Netherlands.

U.S. Army Engineer Research and Development Center, 2004, *Coastal Engineering Manual. CEM*, Vicksburg, MS, U.S..

Vafai K. 2000, *Handbook of Porous Media*, Marcel Dekker, New York.

Van Der Mer 1987, *Stability of Breakwater Armour Layers –Design Formulae*. Coastal Engineering Journal Vol 11, pages 219-239.

Van Gent M. R. A., Tönjes P., Petit H., van den Bosch P. 1994, *Wave Action on and in Permeable Structures*. Proceedings of the international Conference of Coastal Engineering 1994. pages 1739-1753.

Venis W.A. 1967, *Closure of Estuarine Channels in Tidal Regions, Behaviour of Dumping Material when Exposed to Currents and Wave action*. De Ingenieur Vol. 50.

Vernugopal V., Varyani K., Barltrop N. 2006, *Wave Force Coefficients for Horizontally Submerged Rectangular Cylinders*. Journal of Coastal Engineering, Elsevier, Vol. 33, pages 1669-1704.

Weck O. 2004, *Finite Element Method*, Massachusetts Institute of Technology (MIT) 2004 Lecture 16.810. U.S.

Williams AF Burcharth H. F. and Adel H, 1992, *The Permeability of Rubble Mound Breakwaters. New Measurements and New Ideas*, Proceedings of the international Conference of Coastal , Engineering 1992.

Wouters, J. 1998, *Open Taludbekledingen; stabiliteit van geosystems (Stability of Geosystems)* Deftt Hydraulics Report H1930, Annex 7 (in Dutch).

Nomenclature

a : linear empirical coefficient for the Forcheimer equation
A : total cross area
A_p : area of polygon
A_S : projected area of the containers normal to the wave direction
A_S' : projected are of the deformed container normal to the wave direction
A_T : projected area in wave direction
A_T' : projected area of the deformed containers in wave direction
A_{tri}: area of the triangle of containers in cross section with deformation effects
A_{Tra}: area of the trapezoid of containers in cross section with deformation effects
b : nonlinear empirical coefficient for the Forcheimer equation
B_{sb}: width of sandbag
C : wave celerity
c: cohesion of soil material
C_{Aupt} : uplifted contact area of container
C_{Aeff} : effective non-uplifted contact area of container
C_D : drag coefficient
C_L : lift coefficient
C_M : inertia coefficient
C_D': drag coefficient with deformation effects
C_L': lift coefficient with deformation effects
C_M': inertia coefficient with deformation effects
cm: centimetre
C_w : empirical coefficient for Oumeraci's formula
C_x : "x" coordinate of the centre of gravity of a polygon
C_y : "y" coordinate of the centre of gravity of a polygon
D : length scale in the direction of flow.
D_g : diameter of the geotextile tube.
D_{eq} : equivalent diameter of the gap-pipe between GSCs.
d : water depth
D_{50} : thickness of armour layer
D_g : the diameter of the grain
Dn : armour unit volume
e : error term in least square method
E : mathematical expectation (average)
E_d : dissipated energy
E_i : incident energy
E_r : reflected energy
E_t : transmitted energy
F_D: drag force
F_G: gravitational force
F_L : lift force
F_M: inertia force
F_{GSC}: resisting force of container
F_p : total predicted horizontal force
F_T : total measured horizontal force
g : acceleration due to gravity
G : centre of gravity of container
G' : centre of gravity of container with deformation effects
h_1 : water level in front of structure
h_2 : water level behind of structure
h_{cont} : height of soil container
h_{GSC} : the height of sand container
H_i : significant wave height of incident wave
H_o: deep water wave height
h_r : friction head loss
H_r : significant wave heights of reflected wave
Hs : significant wave
H_{sb}: height of sandbag
i : hydraulic gradient
k : Darcy's coefficient of permeability
K : stability coefficient
k_{fric} : roughness of geotextile in gap-pipe
kg : kilogram
k_m: added mass coefficient for C_M
kN : kilonewton
KO_{CD} : deformation factor for the drag coefficient during overturning of container
KO_{CM} : deformation factor for the inertia force during overturning of container
KO_{CL} : deformation factor for the lift force during overturning of container
KO_R : deformation factor for the resisting force during overturning of container
kPa : kilopascal
KS_{CD} : deformation factor for the drag coefficient during sliding of container
KS_{CM} : deformation factor for the inertia force during sliding of container
KS_{CL} : deformation factor for the lift force during sliding of container
KS_R : deformation factor for the resisting force during sliding of container
l_c : length of container
l_{Aupt} : length of uplifted part of container
l_{Aeff} : length of effective non-uplifted part of container
M_{CD} : moment induced by the drag force
M_{CM} : moment induced by the inertia force
M_{CL} : moment induced by the lift force
M_{GSC} : moment induced by the resisting force
M_{CD}' : moment induced by the drag force with

deformation effects

M_{CM}' : moment induced by the inertia force with deformation effects

M_{CL}' : moment induced by the lift force with deformation effects

M_{GSC}' : moment induced by the resisting force with deformation effects

m : meter

mm : millimetre

m_s : vertical projection of the distance between the centre of GSC and rotation point

m_s': vertical projection of the distance between the centre of a deformed GSC and rotation point

N : Newton

n : porosity of filling material

Ns : stability parameter (known also as stability number

O : rotation point of container during overturning

P : perimeter

Pa : Pascal

p_n : pressure at point n

Q : flow rate

Q^*:relative overtopping rate

q: overtopping discharge per unit length of structure

Rc : structure freeboard

R_d : run down

Re: Reynolds number

R_h: Hydraulic radius of gap-pipe between GSCs

r_s : horizontal projection of the distance between the centre of gravity of a container and a rotation point

r_s' : horizontal projection of the distance between the centre of gravity of a deformed container and a rotation point

R_u : run up

$R_{u2\%}$: run-up level which is exceeded by two per cent of the incoming waves.

s : second

T : wave period

$T_{tension}$: tension of geotextile

u : wave-induced horizontal particle velocity

u_{cr} : critical velocity

u_i : velocity at time point i

v: characteristic flow velocity

V : volume of the container

V' : volume of the container with deformation effects

v_n : velocity at point n

W : weight of the armour layer

W_{50} : average weight of the cover-layer element

z_n : measurement point in the direction of gravity

ξ_o : Iribarren number (surf similarity parameter)

δ : distance of displacement of element

μ : friction coefficient

λ : friction factor

ν : kinematic viscosity of water

γ_{fGSC} : reduction factor for GSC-revetments

$\frac{\partial u}{\partial t}$: wave induced horizontal particle acceleration

α is the angle of repose of the armour

$\frac{\partial v}{\partial t}$: wave induced vertical particle acceleration

ϕ : friction angle of soil material

α : angle of the slope of the structure

α_f : empirical coefficient the Forcheimer equation

β : empirical coefficient the Forcheimer equation

η : free surface elevation

Δl : length of filter sample

σ_1 : principal stresses

σ_3 : principal stresses normal to the load

γ_b : reduction factor for a berm

γ_β : reduction factor for oblique wave attack

γ_f : reduction factor for slope roughness

Δ_t : relative density of the geotextile tube

ρ_E : sand container elements

Δ : submerged density of armour element

ρ_s : the density of the sand

Δt : time period between data points.

$\frac{Du}{Dt}$: total derivative of wave induced velocity

ε : turbulence dissipation parameter

Δh : water head difference

β : angle of incidence of wave

σ : spreading of short-crested waves

Abbreviations

ADV : acoustic doppler velocimeter
GSC : geotextile sand container
GWK: large wave flume at Hannover
i. e. : in example
LWI : Leichtweiss Institute
PG : pressure gauge
PIV : particle image velocimetry
RANS : Reynolds Averaged Navier Stokes
SWL: still water level
UDEC : Universal Distinct Element Code
VOF : Volume of Fluid
WG : wave gauge